Ultra high energy gamma ray point sources and cosmic ray anisotropy

Lilian Joan Graham

ULTRA HIGH ENERGY GAMMA RAY POINT SOURCES AND COSMIC RAY ANISOTROPY

by

Lilian Joan Graham, B.Sc.

A thesis submitted to the University of Durham in accordance with the regulations for admittance to the degree of Doctor of Philosophy

Department of Physics

University of Durham

August 1994

TABLE OF CONTENTS

ABSTRACT

ACKNOWLEDGEMENTS

CHAPTER 1: INTRODUCTION 1-1

1.1 Introduction 1-1

1.2 History 1-2

1.3 Extensive Air Showers 1-3

1.4 Acceleration Mechanisms 1-6

1.4.1 Shocks Associated with SNR 1-7

1.4.2 Compact Sources 1-12

1.4.3 Quasars and AGN 1-17

1.5 Present Status of γ-Ray Observations 1-18

1.5.1 Cyg X-3 1-18

1.5.2 Her X-1 1-21

1.5.3 4U 0115+63 1-23

1.5.4 Cyg X-1 1-24

1.5.5 1E2259+586 1-25

1.5.6 V0332+53 1-26

1.5.7 Cen X-3 1-26

1.5.8 Sco X-1 1-27

1.5.9 Vela X-1 1-28

1.5.10 The Crab 1-29

1.5.11 Geminga 1-32

1.5.12 PSR0355+54 1-34

1.5.13 PSR0655+64 1-34
1.5.14 PSR1913+16 1-35
1.5.15 PSR1937+21 1-35
1.5.16 PSR1953+29 1-35
1.5.17 Markarian 421 1-36
1.5.18 M31 1-37
1.5.19 GRO J0422+32 1-38
1.5.20 GRO J1837+59 1-39
1.5.21 AE Aquarii 1-39

1.6 The Muon Question 1-40

References . . . . .

CHAPTER 2: BAKSAN AIR SHOWER ARRAY 2-1

2.1 Introduction 2-1

2.2 Constant Fraction Discriminator 2-6

2.3 The Least Squares Method of Arrival Direction Evaluation . . 2-8

2.4 Curvature Effect 2-9

2.5 Estimation of Angular Resolution Using M-C Simulations . . 2-11

References . . . . .

CHAPTER 3: DATA ANALYSIS 3-1

3.1 Introduction 3-1

3.2 Count Rate 3-1

3.3 Anomalous Time Delays 3-2

3.4 Zenith Angle 3-6

3.5 Difference of Differences 3-8

CHAPTER 4: SOLAR AND LUNAR SHADOWING 4-1

4.1 Introduction 4-1

4.2 Data Analysis 4-3

4.2.1 Solar Coordinates 4-3

4.2.2 Lunar Coordinates 4-5

4.3 Annuli of Equal Solid Angle 4-7

4.4 Angular Resolution 4-9

4.5 Predicted Distribution For a Given σ 4-10

4.6 Maximum-Likelihood Method 4-14

4.7 Results 4-15

4.8 Angular Resolution from Crab Burst 4-18

References . . . . .

CHAPTER 5: POINT SOURCES 5-1

5.1 Introduction 5-1

5.2 On Source and Background Evaluation 5-2

5.3 Results 5-5

5.4 Periodicity Analysis 5-7

5.5 Cyg X-3 Radio Bursts 5-20

5.6 The Crab Burst of 1989 5-23

References . . . . . .

CHAPTER 6: COSMIC RAY ANISOTROPY 6-1

6.1 Introduction 6-1

6.1.1 Galactic Plane Enhancement 6-2

6.1.2 Sidereal Anisotropy 6-5

6.1.3 The Magellanic Clouds 6-9

6.2 Origin of Solar and Sidereal Variations 6-10

6.2.1 Anisotropy from Beyond the Earth's Atmosphere 6-10

6.2.2 Anisotropies from Within the Earth's Atmosphere 6-11

6.3 Harmonic Analysis 6-11

6.4 Anisotropy Analysis 6-16

6.4.1 Data Selection 6-16

6.4.2 Observed Maps 6-17

6.4.3 Pressure and Temperature Effects 6-17

6.4.4 Predicted Maps 6-17

6.4.5 Comparison of the Predicted Map with those Observed 6-22

6.4.6 Harmonic Analysis 6-25

6.4.7 Galactic Plane Enhancement. 6-30

References . . . . . .

CHAPTER 7: CONCLUSIONS 7-1

7.1 Synopsis of Results 7-1

7.1.1 Angular Resolution 7-1

7.1.2 Point Sources 7-1

7.1.3 Cosmic Ray Anisotropy 7-2

7.2 Future Developments at BASA 7-3

7.2.1 Detector Temperature 7-3

7.2.2 Pressure Data 7-4

7.2.3 Particle Densities 7-4

7.2.4 GPS System 7-5

7.2.5 Muon Detector 7-5

References . . . . . .

APPENDIX 1: Time Delay Plots . . . . . .

APPENDIX 2: Point Source Results . . . . . .

ABSTRACT

The experimental set-up at the Baksan Air Shower Array, used to detect air showers above $\sim 0.2 \times 10^{14}$eV, is described.

An estimation of the angular resolution using the cosmic ray shadow of the Sun and the Moon gives a value of $\sim 2.5°$ which is consistent with previous estimates from Monte-Carlo simulations.

Using data from this array covering 1985-1992, a search is made for γ-ray emission from 18 candidate sources. Upper limits to the flux from these sources are stated in all cases. A periodicity search is made on data for which the excess for a single transit of a particular source is above 3σ. The results of this periodicity analysis on such days points to 4 possible observations of pulsed emission at the 95% confidence level. These are 4U0115+63 on 19.03.89, PSR1953+29 on 12.02.85, 1E2259+586 on 01.08.91 and PSR0655+64 on 12.08.89. Without confirmation from other groups however the findings are not significant enough to stand alone.

A harmonic analysis has been performed on the 8 years of data and after pressure corrections and a Farley & Storey analysis to eradicate any spurious sidereal variations we find negligible evidence of 2nd or 3rd harmonic but a 1st harmonic amplitude and phase of $(12.7 \pm 1.2) \times 10^{-4}$ at 23.1 ± 0.3hr right ascension. When one takes into account the $\cos\delta$ effect on the sidereal anisotropy this value becomes $17.4 \pm 1.6 \times 10^{-4}$.

Future developments and improvements to be undertaken at BASA, including the building of a muon detector, are outlined.

ACKNOWLEDGEMENTS

I would like to thank Professor A.D. Martin for the provision of the facilities of the Department of Physics at the University of Durham during the course of my studies and the Science and Engineering Research Council for the award of my research studentship. I am also extremely grateful to my supervisor, Dr. John Osborne, for his encouragement, help and above all patience. I would also like to acknowledge the work done by Alan Lotts in running the Starlink facilities at Durham.

Thanks are due to Paula Chadwick, Nigel Dipper and Steve Rayner at the Observatory for their unflinching help with barycentring procedures. I would also like to thank Professor A.E. Chudakov, Dr Yu. Andreyev, Dr V.V. Alexeenko and Dr V. Tizengauzen for their many helpful discussions and their warm hospitality. A mention must also go to Nuanwan Sanguansak who has managed to keep our office cheerful even through the writing up days. A special thanks goes to Paul Young whose help has been invaluable.

I would also like to mention members of the YTA both past and present - they are too numerous to mention but they know who I mean. I strongly suspect I shall not come across their particular brand of humour again. To Janine and Sam, a special thank you for never talking to me about astronomy and never telling me your star signs. I am very grateful for the support of my family who have tolerated with great stoicism my attempts to be a perpetual student. Finally, thanks to Omar Almaini without whom this thesis would have been completed ages ago.

1 INTRODUCTION

1.1 Introduction

The first chapter of the thesis provides a brief background in γ-ray and CR astronomy and discusses the present status of point source observations. Chapter 2 outlines the experimental apparatus at the Baksan Air Shower Array (BASA) and Chapter 3 goes on to describe the routine data analysis performed on the data taken at BASA. Chapter 4 describes a method for obtaining the angular resolution of the array using the CR shadow of the Sun and the Moon and presents an estimate of BASA's angular resolution using this method. Point sources are investigated in Chapter 5 and a periodicity search performed on selected data. A harmonic analysis is performed in Chapter 6 and an upper limit to the ratio of γ-rays to CR from the Galactic plane obtained. The final chapter summarises the main results and outlines the future experimental developments and improvements which are to be carried out at BASA.

1.2 History

In this thesis a search is made, using data from the Baksan Air Shower Array at an energy of $\sim 10^{14}$eV, for γ-ray point sources and cosmic ray anisotropy. Both have implications for the origins of cosmic rays (CR). Because CR are charged particles they do not trace back to their source directions due to their interactions with magnetic fields. However interactions of CR near the source can produce neutral γ-rays which *will* point back to their origin. Thus γ-rays and γ-ray sources can be used as tracers of cosmic rays. The cosmic ray anisotropy can go some way to answering the question of whether CR are of Galactic or extra-Galactic origin. This will be described in more detail in Chapter 6.

The history of cosmic rays can be traced back to the turn of the century. Initial experiments by Wilson, Elster & Geitel (eg Wilson 1901) involved samples of air in ionisation chambers. Despite careful shielding, significant conductivity remained due to radiation from outside the chamber. It was initially thought that this radiation was terrestrial in origin. Balloon borne experiments performed by Hess however indicated that after a decrease from sea level to 700m the ionisation increased with altitude up to the maximum altitude attained which was 5km (Hess 1911,1912). Kolhörster (1913) confirmed this result with data from balloon flights up to 9km. It was found that the intensity of radiation increased 10fold from sea level to 9km above sea level. Furthermore the radiation was not of solar origin because the ionisation did not vary significantly between night and day.

Because of their penetrating nature it was thought that the ionisation might be due to γ-rays. However there was an observed variation of intensity with geomagnetic latitude. This led Clay (1927) to conclude that the particles had to be charged.

The theoretical explanation of the latitude effect came from LeMaître & Vallarta (1933) using calculations from Stomer (1930). The result depends on the fact that neutral particles would not be affected by the geomagnetic field whereas charged particles would be.

For charged particles entering the Earth's atmosphere vertically and parallel to the magnetic lines of force there is no interaction. Slight interaction will occur if the particles deviate from the parallel. Therefore at the magnetic poles there will be little deflection of the particles. At the equator the magnetic field is perpendicular to the direction of the CR thus the CR are strongly deflected. This leads to the observed latitude effect whereby the CR flux depends on the latitude of the observation. Because CR were seen to display this effect it was concluded that they were charged particles and not γ-rays as previously thought.

A further consequence of this theory was that a measurement of the intensity could be used to determine the ratio of the momentum to the charge of particles. At a particular point on the Earth's surface there are allowed and forbidden directions of incidence for each magnetic rigidity considered. It was predicted that if the particles were mostly positive then there should be an excess from the West and if they were predominantly negative then there should be an excess from the East.

This East-West effect led Johnson (1933) to conclude that the particles were positively charged and make the suggestion that these were protons. Higher altitude balloon flights led to the discovery that below 10^{12}eV approximately 90% of primary CR are indeed protons.

1.3 Extensive Air Showers

Given that even for detectors at mountain altitudes the Earth's atmosphere constitutes more than 20 radiation lengths, there is no hope of observing directly the primary cosmic rays or γ-rays which impinge upon the top of the atmosphere. However when the incident

primary is of energy above $\sim$ 0.1TeV it produces a cascade of secondary particles and when the primary is $>$ 50TeV sufficient of these secondaries survive to mountain altitudes to comprise a viable signal. This 'swarm' of secondary particles moves through the atmosphere near the speed of light and is approximately 1-2m thick at detector level.

In most cases when the primary is a CR (hadron) the resulting shower will have an electromagnetic (e-m), muon and hadron component. The incident primary interacts with the nucleus of an atmospheric particle producing secondary nucleons and mesons (mainly pions). These nucleons themselves initiate further cascades and the nuclear core comprises $\sim$1% of the shower particles at detector level.

On average there are equally many π°, π^{+} and π^{-} produced. The π^{+} and π^{-} interact with atmospheric nuclei forming further secondaries until they have energy less than $\sim 3\times10^{10}$ eV at which point they decay to form muons. Because of their long interaction lengths μ are unlikely to interact with atmospheric nuclei nor are they likely to decay due to the large Lorentz factor governing their half life. Thus the number of μ rises steadily as the nuclear component of the shower develops and once the nuclear cascade decays, and the shower has reached its maximum development, the number of μ remains fairly constant. Above 10^{14} eV $\sim$10% of the shower particles at detector level are μ.

The neutral pions, having a very short half-life, $t_{\frac{1}{2}} \sim 10^{-16}$s, decay to form γ-rays which initiate e-m cascades which develop by alternate pair production and bremsstrahlung. The e-m cascades are better understood than the hadronic cascades. As energy is fed in from the nuclear cascade the e-m shower continues to grow with the number of electron-positron pairs increasing almost exponentially to begin with. This continues until the mean energy of the electron-positron pairs is less than $\sim$ 100MeV at which stage the energy loss by ionization is greater than that by bremsstrahlung. For all but the highest energy primaries ($> 10^{17}$eV) this maximum is attained well above detector level. The lateral spread of EAS

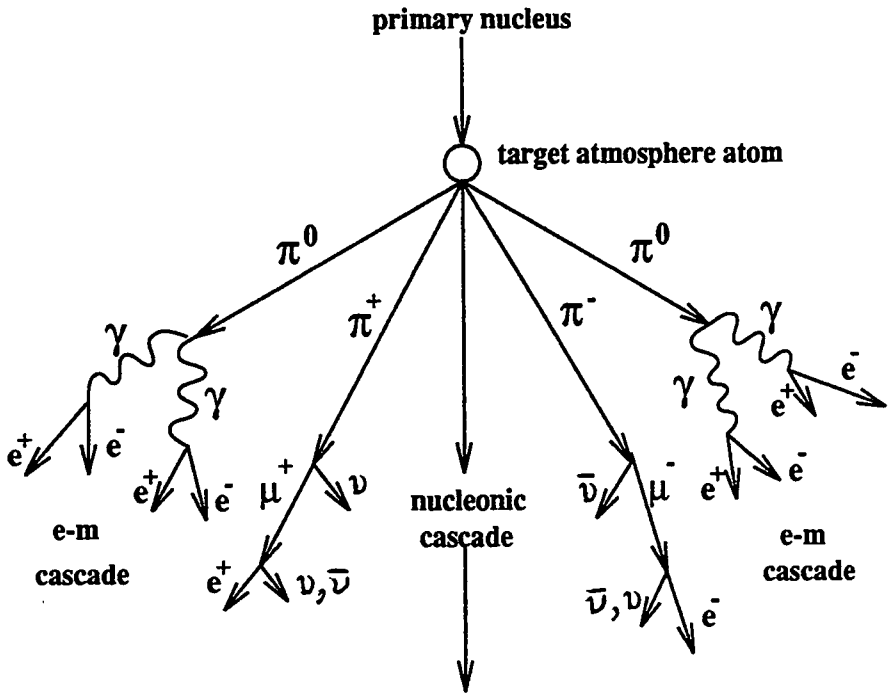

Figure 1.1 The development of a CR initiated extensive air shower (after Weekes 1988.)

at detector level, which can be approximately 150m, is mainly due to multiple Coulomb scattering of the e-m component. Above 10^{14} eV ~90% of the shower particles at detector level are electrons. It is worth bearing in mind however that at lower energies the e-m component is absorbed in the atmosphere before reaching detector level so that over all energies μ are the most abundant CR secondaries.

When the primary is a γ-ray an e-m cascade is initiated. Only occasionally does a secondary γ-ray interact hadronically rather than electromagnetically (this occurs with a probability of $\sim$ 0.3%.) In this case the charged pions which result can decay to give μ as in the hadron initiated showers. However this occurs far more rarely than the processes which produce μ in CR initiated showers. Thus theoretically it should be possible to differentiate between CR and γ-ray initiated showers by the relative number of μ in each. However present cascade theories rely on the extrapolation of particle physics data at much lower energies and it is not yet clear whether this extrapolation is in fact an accurate one. Indeed as will be discussed later certain γ-ray observations appear to contradict the theory.

1.4 Acceleration Mechanisms

It was originally suggested by Baade & Zwicky (1934) that supernovae (SN) and the subsequent formation of neutron stars (NS) were the main sources of CR. This was a popular theory until the late 1970's when it became widely accepted that it was the supernova remnant (SNR) and associated shock rather than the initial stellar explosion itself that caused the CR (eg Axford *et al* 1977). While this mechanism can explain acceleration of particles up to ~10^{15}eV it is difficult to obtain particles much above this. It is generally thought that above this energy it is either necessary to re-accelerate the

particles in some way or to have a new source of acceleration. Other suggestions involve compact objects with the power either being supplied by rotational energy of a NS or by accretion from a companion onto a NS.

At the highest energies, where CR are thought to be extragalactic, it is thought that shock acceleration may produce energetic particles in AGN, possibly at a shock in an accretion flow onto a super-massive black hole (Protheroe & Szabo 1992). Possible problems with this theory are that they over-predict the total flux of γ-rays.

We look now at the possibilities in some more detail.

1.4.1 Shocks Associated with SNR

A brief description of a shock is as follows (eg Drury 1991). Consider a volume filled with gas, the uniform state of which is disturbed locally (eg density or pressure increased) by injecting mass or energy into the system. Information about this local excess spreads out as the system relaxes back to a uniform state. If inertial effects are important then the disturbance typically propagates in one or more waves with characteristic velocities. For gas dynamics the characteristic velocity is the speed of sound. However what gives rise to a shock is the fact that the characteristic velocities are not constant, usually they increase as the system is compressed. The situation can be likened to a piston being pushed into a closed tube. As one pushes the piston into the tube the initial disturbances travel slower than subsequent ones as the latter are propagating in an already compressed medium. This means that all the waves pile up as the later propagations 'catch up' with the earlier ones. This concentration of the entire disturbance into a very thin layer is termed a shock/shock front or shock wave.

A strong shock is one in which the kinetic energy density >> internal energy density upstream and the ram pressure >> internal pressure. Spacecraft have observed acceleration

of particles to MeV energies by interplanetary shock waves eg at Earth's bow shock and in other shocks associated with the solar wind. The local energy density of CR is ρ_E $\sim$ 1eV/cm^3. If this is typical of Galactic values then the power required to produce the observed flux of Galactic CR is

$$L_{CR} = \frac{V\rho_E}{\tau_R}$$
$$\sim 5 \times 10^{40} erg/sec$$

where $V =$ is the Galactic volume

$$= \pi R^2 d$$
$$\sim \pi(15kpc)^2(200pc)$$

and $\tau_R =$ residence time of CR in Galactic disk (where the sources are assumed to be)

Given that SN provide $\sim 10^{51}$ ergs every $\sim$ 30 years then this is approximately 50 times the power output required for the observed CR spectrum (Völk H.J. 1987). The energy which is available from gravitational contraction can be shown to be $E_{grav} = \frac{3}{5}\frac{GM^2}{R}$. A simple non-linear treatment of SNR shocks shows that the efficiency is of the order of 1 (a more detailed treatment would give a lower value). While, as we have seen, such a high efficiency is not necessary to account for the power requirements of CR on the basis of the observed power output and frequency of SN (eg Axford *et al* 1982) it must be to the good if any mechanism which must account for the production of such highly energetic particles is highly efficient. The discovery of quasars generating γ-rays with efficiency perhaps $> 50\%$ (Hartmann *et al* 1992) is consistent with this high efficiency predicted by shock acceleration.

Also if SNRs were the source of CR up to $\sim 10^{14}$eV then this would naturally account for the lack of significant anisotropies at these energies since contributions from nearby sources would overlap.

The original Fermi acceleration mechanism (Fermi 1949) is known as 2nd order Fermi acceleration (because the momentum gain rate is proportional to the square of the turbulent velocity) . Particles can either gain or lose energy in a given encounter depending on the angles but after many encounters there is a net gain. It is generally thought that 2nd order acceleration at parallel shock waves can only play a role in weak shocks (eg Ostrowski M. 1984). Later Fermi proposed a 1st order mechanism whereby the geometry of an infinite plane shock is such that the result of an encounter is always an energy gain (Fermi 1954). The basic mechanism is the transfer of macroscopic kinetic energy of moving magnetised plasma to individual charged particles. The resulting energy distribution is nonthermal.

There are two characteristic features of Fermi acceleration :

1 The highest energy particles tend to be those which have undergone acceleration for the longest time. These particles also have a tendency to escape most easily from the shock (Berezhko *et al* 1987).

2 If the accelerator has a finite lifetime them there is a maximum energy to which it can accelerate particles.

The mechanism of diffusive 1st order particle acceleration in shock waves was proposed some 25 years ago (for a review see eg Blandford & Eichler 1987). The fractional momentum gain in each crossing/recrossing cycle is proportional to the difference between the upstream and downstream velocities in the rest frame of the shock. Linear theory of shock acceleration (eg Blandford & Ostriker 1978) predicts a power law with index dependent on the shock compression ratio, ξ (the ratio of the upstream to downstream velocities) . The index γ is given by

$$\gamma = -\frac{\xi + 2}{\xi - 1}$$

For a strong shock $\xi = 4$ and so γ = -2. A flatter spectrum is obtained for relativistic shocks or any shock whose compression ratio is >4. Non-linear effects create some curvature in the spectrum but for a general compression ratio the differential index of ~-2 is preserved (Ellison & Eichler 1985). This prediction of a power law index of -2.0 fits with the observational data as many high energy sources have a spectra $\sim E^{-2}$. However the observed radio spectra for a number of shell-like SNR exhibit quite flat behaviour (Green 1992) which is incompatible with the standard diffusive shock acceleration model.

Ejected material from a SN explosion will move out through the ISM driving a shock wave at which acceleration can occur. As long as the characteristic length for diffusion is much less than the radius of curvature of the shock one can approximate the shock front as a plane.

The limiting factor to the maximum energy possible for particles accelerated in this way comes from the finite lifetime of the SN blast wave. This can be estimated from the time it takes the expanding shell to sweep through its own mass of the ISM after which it begins to slow down. For a 10 solar mass remnant expanding at v = 5×10^8 cm/sec into a medium of average density 1 proton/cm^3 this is ~ 1000 years (Gaisser T.K. 1990). If the magnetic field in the ISM is ~ 3μGauss then this sets a limit to the maximum energy to which a particle can be accelerated of Z $\times$ 3×10^{13}eV. Lagage & Cesarsky using slightly different values for the parameters involved put the figure at Z $\times$ 10^{15}eV (Lagage & Cesarsky 1983).

Synchrotron losses are given by

$$(-\frac{dE}{dt})_{\text{synch}} \sim 1.6 \times 10^{-3} \, (\frac{Zm_e}{Am})^4 \, E^2 \, B^2 erg/sec$$

where E = total energy of particles

m = mass of particle

and the other symbols have their usual meaning

(eg Longair 1981) Because of the $(\frac{Zm_e}{Am})^4$ term, this loss mechanism is much more significant for electrons (where the mass ratio is small) than for protons and heavier nuclei except in extreme B fields eg near the surface of a NS.

Such a shock mechanism could achieve higher energies for accelerated particles if either the B field or the time scale for acceleration were increased. In fact SN probably do not explode into average ISM conditions. For example SN1987A exploded into an environment formed by the wind of the progenitor. This could increase the upper limit by one or two orders of magnitude (Völk & Biermann 1988). The rate of acceleration could also be increased if the field has a component perpendicular to the direction of propagation rather than parallel as previously assumed (Jokipii J.R. 1987). Alternatively there is some indication that relativistic shocks are more efficient that non-relativistic shocks (Kirk & Schneider 1987).

It is generally thought however that this SNR mechanism only works unaided up to around the knee of the CR spectrum (this cut-off is of course rigidity dependent, heavier species such as iron could be accelerated up to $\sim 10^{16}$ eV.) Below the knee the observed differential energy spectra have exponents $\sim$ 2.6 - 2.7. Because of the fact previously stated that the highest energy particles tend to be those which have undergone acceleration for the longest time also have a tendency to escape most easily from the shock, the source spectrum need not be a power law right up to the knee - it could flatten before finally cutting off at the knee. It should be remembered of course that the source spectrum must be combined with eg a leaky box model of particle propagation. This means that the CR spectrum is steeper than that at source since the highest energy particles escape more readily from the Galaxy.

In order to accelerate CR to above $\sim 10^{14}$eV it has been suggested that either a new source mechanism is required or that there need be some re-acceleration. The latter could occur

in encounters with other shocks. The power law spectrum is not affected by interactions involving weak shocks but can be affected by strong shocks. As the observed secondaries do not appear to have been affected with this way it is possible to put a limit on the probability of encountering a strong shock (eg Cesarsky 1987). Weak shocks are of no use here as the acceleration is almost exactly balanced by adiabatic energy losses (Blandford & Ostriker 1978).

Further re-acceleration mechanisms and possible new source mechanisms are discussed further in the next sections.

1.4.2 Compact Sources

After the first pulsar was detected (Hewish *et al* 1968) Ostriker & Gunn started work on the dynamics of electrically charged particles and showed that rotating magnetic fields are capable of accelerating particles to considerable energies (Gunn & Ostriker 1969, 1971). Calculations showed that rotating magnets are basically monoenergetic sources of particles and do not display the differential energy spectrum as is observed for CR (eg Thielheim K.O. 1993). Accelerating particles to observed energies requires very strong magnetic fields changing rapidly with time. In the final stages of stellar evolution the gravitational collapse of a star of mass 6 - 40 solar masses can result in an extremely dense NS of radius ~10km. It is believed that considerable angular momentum and angular flux remains with the NS and thus there is very high angular velocity and a very high magnetic field especially near the magnetic poles. Thus rotating NS are good candidates as sources of high energy particles and pulsed e-m radiation. The first pulsar was therefore interpreted as a NS.

Many NS manifesting themselves as pulsars (PSRs) are part of binary systems (ie they are gravitationally bound to a companion). The Roche potential is the gravitational potential

in a co-ordinate system rotating at the same rate as the axis joining the two stellar centres. The critical Roche surface is the equipotential surface which passes through the inner Lagrangian point.

An accretion powered NS is one in which the mass transfer from the companion has a large effect on the NS dynamics. This mass transfer can occur if there is enough kinetic energy so that the total energy exceeds the potential energy of the critical Roche surface. This can be achieved if the companion has a stellar wind. Alternatively mass transfer can occur if the companion expands due to stellar evolution so that its surface exceeds the critical surface. Matter which has crossed the inner Lagrangian point into the Roche lobe of the compact object has angular momentum and settles into an accretion disk where it loses this angular momentum gradually as it works its way closer to the compact object. For a companion overflowing the Roche lobe the disk should be steady but for the stellar wind case the disk is expected to be transient and reversing in direction (eg Fryxell & Toam 1989). Accretion powered NS known are observed preferentially by the X-rays they emit and are known as X-ray binaries (XRB). The magnetic fields of NS in such XRB are of the order of $1\text{-}4\times10^{12}$ Gauss as deduced from X-ray spectra (Makashima 1990). At the Alfven radius (r_A) the magnetic pressure equals the ram pressure of the accreting matter. It is this which determines the inner edge of the accretion disk. Outside r_A material pressure dominates so the accretion disk is not intact. Inside r_A the magnetic field dominates forcing matter to flow along magnetic field lines towards the NS (eg Ghosh & Lamb 1979). This region is known as the magnetosphere. Rotation powered NS occur when mass transfer is small or absent. These are observed preferentially by radio frequency signals.

The rate of accretion is limited by the Eddington luminosity which is obtained by equating the outward force per electron due to accretion-induced radiation to the inward gravita-

tional force per proton.

$$\frac{L_{Edd}}{4\pi R^2 c}\sigma_T = \frac{GMm_p}{R^2}$$

$$where\ \sigma_T = \text{ Thomson cross} - \text{section}$$

$$\text{gives } L_{Edd} \sim 1.4 \times 10^{38}\frac{M}{M_\odot} \text{ erg s}^{-1}$$

If the accretion is highly anisotropic or if the material is being expelled along preferred directions eg jets then it is possible to exceed the Eddington luminosity.

Models involving compact sources assume the power source is either accretion or NS rotation. In the former the kinetic energy of infalling material is released through some dissipative mechanism in the accretion disk or magnetosphere. The Eddington limit for NS is $\sim 10^{38}$ erg s^{-1}. If most of this energy went in to particle acceleration power requirements for the bulk of CR would require ~500 such sources continually active in the Galaxy (Joss & Rappaport 1984).

In the case of rotation powered NS, energy is released through magnetic dipole radiation. If a large fraction of this rotational energy is available to accelerate particles and all SN formed NS with a period <10ms then this could account for the bulk of CR with $\sim 2\times 10^{50}$ ergs released every 30 years (Gaisser T.K. 1990) However the distribution of initial periods of NS are uncertain and many may have a slow initial rate.

Shock in Accretion Flow

The shock must occur beyond the Alfven radius otherwise the field irregularities necessary for scattering the CR particles back and forth across the shock are not frozen into the converging flow of plasma into the shock. Since acceleration must take place beyond r_A the full energy of accretion is not available for particle acceleration. The maximum energy available is $\sim 10^{16}$eV per particle (Kazanas & Ellison 1986). The magnetic field required

is so high that even for ions the limiting loss is synchrotron. This mechanism works best for relatively low B fields $\sim 10^8$ Gauss. For example it would not work for Her X-1 since B $\sim 4\times10^{12}$ Gauss (Nagle *et al* 1988).

Pulsar Wind Shock

The light radius of a pulsar characterises the state of rotation of the magnet within and is given by $r_L = \frac{c}{\omega}$ where ω is the angular frequency of rotation.

If the Alfven radius lies beyond the light cylinder then the pulsar will form a wind the ram pressure of which will prevent accretion. If however the Alfven radius is inside then the wind is stifled by accretion as the accretion disk penetrates into the magnetosphere. The pulsar wind will be shocked by the interaction with the atmosphere or wind of the companion and could be the site of UHE acceleration (Harding & Gaisser 1989).

In this case there is such a strong B field that the acceleration rate can now be many orders of magnitude faster than for acceleration at an exterior SN blast shock. The limiting size is now the size of the accelerating region rather than the age of the SN. We have

$$E_{max} \sim eB_sR_s = \frac{eB_*R_*^3\Omega^2}{\sqrt{3}c^2}$$

whereB_*, R_* are values at the NS surface

whereB_s, R_s are values at the shock

and$\Omega =$ angular frequency

For a 10ms pulsar with a magnetic field of $\sim10^{12}$ Gauss this is nearly 10^{17}eV (Gaisser 1990). Because of the high B field involved synchrotron losses limit the energy to which electrons can be accelerated.

For this model we require (Nagle *et al* 1988) that

$$\frac{P_{ms}\dot{M}_{18}^{\frac{2}{7}}}{B_{12}^{\frac{4}{7}}} < 30$$

where $\dot{M}_{18} =$ *the accretion rate in* $10^{18} g/sec$

B_{12} = the magnetic field in $10^{12} G$

and $P_m s$ = the rotation period in ms

Thus Her X-1 is too slow for this to work but Cyg X-3 could if the 12.6ms periodicity is true.

Disk Dynamo

Accretion disk dynamos can convert mechanical energy of accretion power into particle acceleration by inducing large-scale electric fields through rotation of plasma in the disk (Lovelace 1976). In an accreting NS with a strong B field the field lines from the NS will intersect the accretion disk giving rise to a $\mathbf{v} \times \mathbf{B}$ electric field starting at the inner edge of the accretion disk. The maximum energy is given by E $\sim 3.5\times10^{14}$eV $B_{12}^{\frac{-3}{7}} L_{38}^{\frac{5}{7}}$ (Chanmugam & Brecher 1985). For accretion near the Eddington limit this gives E $\sim$ 2.6×10^{16}eV. The maximum energy is obtained for a low B field so one wants the Alfven radius to be just above the surface of the NS. For higher fields only a portion of the gravitational energy has been released by matter that has reached the inner edge of the accretion disk. (Nagle *et al* 1988).

A variation in the model is that in which the difference between the Keplerian velocity at the inner edge of the disk and the velocity of NS magnetosphere causes a potential drop near the disk-magnetosphere boundary (Cheng & Ruderman 1989). This model was partially motivated to account for the shift of some Her X-1 signals relative to the known X-ray period. These observations will be discussed in more detail later in the chapter.

The expected spectrum of accelerated particles is monoenergetic if all the particles are initially at or near rest and traverse the same potential drop at once. However pair production cascades initiated by the accelerated primaries could produce a power law spectrum of secondary particles (eg Daugherty & Harding 1982).

Turbulent Reconnection

The sporadic nature of some γ-ray sources is reminiscent of solar flares. Flares are caused by the release of energy built up as the magnetic fields are stressed by turbulent motions of the solar plasma. When the magnetic fields 'reconnect' in a turbulent magnetohydrodynamic plasma electric fields are formed which can accelerate particles. (Matthaeus *et al* 1984, Sorrell 1984).

A similar situation may take place in XRB which have strong B fields which may thread accreting plasma. Differential rotation together with uneven rates of accretion are likely to stress the magnetic fields. Reconnection can occur along neutral sheets where oppositely directed field lines are brought together. The potential drops maintained by the induced E fields along neutral sheets can accelerate particles. The maximum energy to which a proton can be accelerated is given by

$$E_{max} \sim e\eta\frac{v_A}{c}BR$$

where η = efficiency factor < 0.1

$R =$ distance over which the potential is maintained

and v_A = Alfven velocity

The maximum energy is then $\sim 10^{14}$eV (Harding 1990). This mechanism has been proposed to explain UHE bursts in accreting XRB (Wang 1986).

1.4.3 Quasars and AGN

The γ spectra of 3C279 and related objects have been observed to show no pion decay curvature (Eichler 1994) suggesting that γ-rays could be made primarily from electrons or positrons (which themselves could of course be secondary particles). The energy spectra of γ-rays from quasars in the EGRET range is consistent with shock acceleration and reported TeV γ-rays from Mrk421 imply a similar energy spectrum between EGRET and TeV energies.

It has been suggested that shock acceleration may produce energetic particles in AGN. Protheroe & Szabo (1992) conclude that AGN may be an important source of CR at the knee of the spectrum and may cause the observed enhancement. It is pointed out that although heavier nuclei will also be produced they will not escape from the central accelerating region as they will be broken up in interactions with photons. Thus the extragalactic component in the region of the knee will be 100% protons and one should expect an enhancement in the number of protons in CR at $\sim 10^{16}$eV. As mentioned before however this theory over-predicts the total γ-ray flux.

1.5 Present Status of γ-Ray Observations

Here we review the current situation in VHE ($\geq 10^{12}$eV)and UHE ($\geq 10^{14}$eV) γ-ray observations. In the former energy range the atmospheric Čerenkov technique is applied whereas in the latter extensive air shower arrays are utilised. The reader is directed to excellent reviews by Nagle *et al* (1988), Weekes (1988,1992), Chadwick *et al* (1990), Rao & Sreekantan (1992) and Lorenz (1993).

1.5.1 Cyg X-3

Cygnus X-3 is often thought of as a close binary (young pulsar) surrounded by an envelope of thick matter (Weekes 1988). The 4.8hr variation which is seen in the IR and X-ray (but not in the radio region) could then be explained by the eclipse of the emission region by the companion star in the course of its orbital motion. During its spectacular radio flares Cyg X-3's radio flux can increase by a factor of 10^3 making it for several days one of the brightest radio sources. Its variability in IR - radio emission is reflected too in the X-ray emission which displays an asymmetric 4.8h sine wave which doesn't display a complete eclipse, varies from cycle to cycle and has both quasi- periodic and long term variations. At the peak of its X-ray emission it is one of the brightest X-ray sources in the sky. A balloon experiment in 1976 first observed Cyg X-3 in the 100MeV region. This was subsequently confirmed by SAS-II although COS-B saw no significant signal.

The first VHE observation came in 1972 from the Crimean Astrophysics Observatory and occurred just after a known radio outburst. Over 8 years they subsequently observed a 4.8hr period with a strong peak at phase 0.15-0.2 and a weaker peak at 0.6-0.8 phase (Vladimirskii *et al* 1973, Neshpor *et al* 1980). The Whipple group observed 4.8hr periodicity in 1980 and 1981 but the light curve was found to be variable over a timescale of months. For 1988-1990 however they saw no steady dc flux or 4.8hr period (O'Flaherty K.S. *et al* 1991). The Durham group in data covering 1981-1989 found evidence for 4.8hr modulation (Brazier K.T.S. *et al* 1990b) as did the Sandia Čerenkov group who found a 4.4σ excess in phase 0.6-0.8 for August-September 1981 (Weekes 1988) and the Gulmarg group who saw a 6σ excess at phase 0.6 in data covering January 1976 - December 1977. However Gulmarg's 1984 data showed no such modulation nor did the Utah Čerenkov data of 1988-1989 (Cassidy G.L. *et al* 1990, Corbato S.C. *et al* 1991).

In September 1983 Durham observed a 7 minute outburst at phase 0.625 of the 4.8hr period which displayed a 12.5908ms periodicity. Reanalysis of 1981 and 1982 data gave weak evidence of this also. Further evidence came with their October-November 1985 and June-Sept 1988 data at La Palma. However they found no evidence for such a periodicity in their data of October 1988 or after a known radio outburst in 1989 (Bowden C.C.G. *et al* 1991a). The only other group to have found such a periodicity is the Adelaide Čerenkov group who in July-September 1989 found a 12.6ms pulsed burst following a radio outburst. However this was in a 600s window 1050s before the time predicted from the 1988 La Palma observation and at a period 1μs shorter (Gregory *et al* 1990). Whipple (O'Flaherty K.S. *et al* 1990) and Pachmarhi found no evidence of such a periodicity although there is some controversy over the method of analysis of some of the Whipple data. Initial evidence in a 60s burst of a 12ms pulsar in Haleakala data of October 12th 1985 proved not to be significant.

The first PeV observation of Cyg X-3, indeed the first PeV observation of any source, was made by the Kiel group in 1976-1980 data (Samorski and Stamm 1983a,1983b). A 4.4σ dc excess was seen as was some evidence of a 4.8hr period. A point of some controversy was that their signal came from EAS showers which were not μ-poor . Haverah Park confirmed the detection in their 1978-1982 data with a 5σ peak at phase 0.225 - 0.250 (Lloyd-Evans *et al* 1983). Unfortunately they had no data on either μ-content or shower age. Fly's Eye in 1983 and Plateau Rosa in 1982-1987 found evidence of 4.8hr modulation with a peak around 0.2 - 0.3 in phase as did Ohya in their data January 1986 - April 1981 which was selected to be μ-poor. However the 1980-1983 Plateau Rosa data , the KGF April - May 1985 data (Sinha S. *et al* 1990b) and Akeno's μ-poor data for 1981- 1984 found significant excesses at phase $\sim$ 0.5-0.6 (Kifune T. *et al* 1986). The Kobe experiment found evidence of 4.8hr modulation in their large age parameter data (Asakimori K. *et al* 1990). EAS-TOP data covering February 1989 - January 1993 (Aglietta M. *et al* 1990,

Aglietta M. *et al* 1993a) and the Mitsuishi Array and μ-detector data covering June 1988 - December 1992 found no evidence for orbital modulation (Fujita K. *et al* 1993). Akeno found a 3.5σ excess coming from a direction about 2° - 3° from Cyg X-3. The reason for the shift is unknown (Teshima M *et al* 1990).

There are few recent reports of dc emission being detected in either all data or μ-poor data. In particular CASA/MIA μ-poor data from April 1991 - March 1993 (Cronin J.W. *et al* 1992, Borione A. *et al* 1993b), CYGNUS data (both raw and μ-poor) from 1986-1993 (Alexandreas D.E. *et al* 1993a) and the Nottingham μ-detector data from 1987-1992 (Blake P.R. *et al* 1993) and later Akeno data from 1990-1993 (Chiba N. *et al* 1993) show no dc excess.

1.5.2 Her X-1

Her X-1 is almost certainly a nearby low mass X-ray binary (LMXRB) containing a pulsar thought to be at a distance of about 5kpc (Weekes 1988). Unlike many XRB it is not a radio or 100 MeV source (Weekes T.C. 1992). Her X-1 was first discovered to be an X-ray source in 1971 by the UHURU satellite. A periodicity of 1.24s was observed in the signal believed to be the period of the NS in the X-ray binary. Her X-1 displays also a 1.7 day and a 35 day periodicity in the X-ray region. The former is believed to be the orbital period around the companion star but the latter is less well understood. Theories of its origin include the precession of the NS or the precession of the actual accretion disk. Above 50MeV GAMMA-1 has observed pulsed emission in data taken in December 1990 with a periodicity of 1.24s at phase 0.6-0.7 of the orbital period (Chuikin E.I. *et al* 1993).

As with most γ-ray sources there are many conflicting reports of observations of Her X-1. The first positive observation in the VHE region came from the Durham group at Dugway who observed a 3 minute outburst in April of 1983 displaying the 1.24s X-ray

period. Subsequent observations in 1984 confirmed this find but observations in July 1983 only gave weak evidence of such emission. Further observations by the Durham group this time at La Palma on July 16th 1988 gave very similar results to the April 1983 observation (Chadwick P.M. *et al* 1990). It is perhaps significant that both the April 1983 and July 1988 observations occurred at the onset of the 35 day period as have many of the subsequent positive claims. For example the Gulmarg Čerenkov telescope (Rawat H.S. *et al* 1990) observed a 15 minute burst at the X-ray period consistent with the Durham value on June 12th 1988 which was also at the start of the 35 day period. The Pachmarhi Čerenkov group claimed to have observed a 42σ effect during a 14 minute burst on April 11th 1986 but unfortunately problems with the recording equipment meant that a periodicity search was impossible.

In the PeV region Fly's Eye II were the first to claim a positive detection of the pulsar periodicity with their data covering 10th - 14th July 1983 although later data gave no such evidence (Ko S. *et al* 1990). Ohya confirmed the pulsar periodicity in their 1989-1991 data set (Muraki Y. *et al* 1991) and Ooty observed evidence of such a pulsar signal on July 1st, August 8th and 9th and November 21st of 1986 (Sreekantan B.V. *et al* 1990).

Both KGF (Sinha S. *et al* 1990a, Acharaya B.S. *et al* 1991) and Ohya (Muraki Y. *et al* 1991) claimed to observe the 1.7 day modulation with KGF also observing excesses on both days when the source was at the phase of the peak in the light curve. Both these days were just around the onset of the 'high on' state in the 35 day cycle.

An interesting phenomenon has come to light with the report by the CYGNUS group of two 30 minute bursts on the 24th of July 1986 which were not only at a period about 0.15% lower than the X-ray period but were also μ-rich showers (Alexandreas D.E. *et al* 1991). Evidence for such a blue-shifted period was also given by the Whipple group with an observed 1.23575s periodicity in the signal from Her X-1 on June 11th 1986

(Gillanders G.H. *et al* 1990) and from Haleakala (Austin R. *et al* 1990) who found a consistent periodicity in a 15 minute burst observed on the 13th of May 1986 and again on the 23rd of May 1987. It is interesting to note that Ohya observed a 2.5σ excess from Her X-1 on the day of the CYGNUS bursts (Muraki Y. *et al* 1990). Why there should be such a blue-shift in the observed period is not yet clear. It is worth noting that the *combined* significance of the pulsed emission with the daily dc excess for the CYGNUS data for that day gives a result which is consistent with a random distribution (Alexandreas *et al* 1993c). The CASA/MIA group report no significant pulsed emission from their 1989 data either at the 1.24s, 1.7day or 35 day period (Cronin J.W. *et al* 1992).

There have been few reports of a DC excess from Her X-1 either in the TeV or PeV range. Even groups who claim to have observed periodic emission find no steady DC flux. KGF did report a 2.8σ dc excess in their 1985 - 1987 data mainly in their μ-rich data (Acharaya B.S. *et al* 1991) but later data covering 1990-1991 gave no such excess. The CASA/MIA group did see a slight excess in their 1988 - 1989 data but this disappeared when a selection cut to reject hadron-initiated showers was made. All other groups, including CYGNUS (Alexandreas D.E. *et al* 1993a) , HEGRA (Bloomer S.D. *et al* 1990, Merck M. *et al* 1991, Merck M. *et al* 1993), Tien Shan (Kirov I.N. *et al* 1992), EAS-TOP (Aglietta M. *et al* 1990,1991,1993a) and the Nottingham μ-detector (Blake P.R. *et al* 1993) have found no evidence for dc emission.

1.5.3 4U 0115+63

4U 0115+63 is thought to be one of the dozen or so massive Be star XRB. An X-ray period of 3.61s has been detected and a 24.31 day orbital period deduced with a highly eccentric orbit. As with most of such objects, emission from 4U 0115+63 is of a transient nature possibly due to episodic accretion due to the large orbits.

4U 0115+63 was first observed as a variable discrete source by the Crimean Čerenkov group in September/October of 1971 during drift scans centred on $\delta = +62°$. They named the source Cas γ-1. Further observations were made in 1972 and 1973 with the only positive detections being made in December 1972. No periodicity search was possible (Stepanian *et al* 1972).

Within the $\pm$ 1° Crimean error box Uhuru found a variable X-ray source from which an outburst was observed during December 1970 - March 1971. Further X-ray observations by, for example, OSO-7 and SAS-3 confirmed its transient nature observing outbursts where the X-ray intensity increased by as much as a factor of 10^4. During these outbursts the emission was found to be pulsed with a period of 3.61s.

In the 100 MeV region a positive signal was observed in the Crimean error box by SAS-II in March 1973 but not by COS-B indicating a transient nature in this energy range also.

In the TeV region the Durham group are the only ones as yet to have found evidence of continuous pulsed emission - this in the September 21st - 29th data of 1984 taken at their Dugway installation (Chadwick P.M. *et al* 1985). Further observations at La Palma in September - October 1988 revealed two 7 day periods with evidence of continuous pulsed emission (Brazier *et al* 1990a). Haleakala (Resvanis *et al* 1987) and Whipple (Lamb *et al* 1987) have reported a few episodes of pulsed emission varying from 400-1000s to 3 days but found no steady pulsed emission and indeed the Whipple confirmation was later withdrawn after reanalysis of a larger database (Macomb *et al* 1991). Gulmarg found one episode of pulsed emission lasting $\sim$ 1950s on November 14th 1987 from $\sim$ 40 hours of data (Rannot *et al* 1990) but Pachmarhi found no evidence for a period of about 3.6s in their 1987 - 1988 data (Achrya B.S. *et al* 1990).

In the UHE region the Tien Shan group reported a 4.7σ peak in the 24.309 day period for their 1974 - 1982 data (Kirov I.N. *et al* 1992) and Akeno found a 2.5σ excess above 10^{17} eV

for February 1990 - July 1991, the second highest excess of 52 candidate sources (Hayashida N. *et al* 1991). However further data from Jan 1990-Feb 1993 gave only an upper limit. No other EAS array group has reported a dc excess with CYGNUS (Alexandreas D.E. *et al* 1991a, 1993a), EAS-TOP (Aglietta M. *et al* 1991,1993a) and Plateau Rosa' (Morello C. *et al* 1990) finding no significant dc or daily signal in data ranging from 1982 - 1993. Also CYGNUS found no evidence for pulsed emission from April 1986 - Jan 1993 (Alexandreas D.E. *et al* 1991b).

1.5.4 Cyg X-1

Cygnus X-1 is a typical massive early-type binary. It has been suggested that one of the components is a black hole. Cyg X-1 is one of only 2 XRB sources found yet in the COMPTEL data set which covers 0.75-30 MeV.

There are no positive VHE reports, with Fly's Eye II Čerenkov telescope finding no steady, transient or sporadic emission from November 1987 - August 1991 (Cooper R.G. *et al* 1991) and Whipple finding no dc or daily excess in 1987 - 1988 (Gillanders G.H. *et al* 1990).

In the UHE regime the Moscow State University EAS array found a 2.0σ excess in all their showers from October 1985 - September 1986 and a 2.5σ excess in their old showers (Khristiansen G.B. *et al* 1990). It is not clear why γ- initiated showers should be older than hadron initiated ones. (The age parameter of a shower, s, is indicative of the number of particles in the shower. When $s<1$, the number of particles increases as the shower develops until it contains a maximum number of particles when $s = 1$. Then the number of particles falls as the shower continues to develop and $s>1$.) Tien Shan (Kirov I.N. *et al* 1992) found for 1974-1982 a 3.9σ broad peak in the 5.6 day period which was not caused by μ-poor events only. They found no dc excess however. CYGNUS (Alexandreas D.E. *et al* 1993a), Fly's Eye (Ko S. *et al* 1990), the Tibet EAS array (Amenomori *et al* 1993a)

and Hegra (Merck M. *et al* 1991,1993) reported no dc or daily emission for data covering 1986-1993. The Mitsuishi array and μ-detector found no evidence for a dc excess from 1988 - December 1992 (Fujita *et al* 1993) and the Nottingham μ-detector found no dc (either long term or daily) emission in data taken from 1987 - 1992 (Blake *et al* 1993).

1.5.5 1E2259+586

1E2259+586 is an X-ray pulsar (period 6.98s) which is coincident with a SNR. It is thought to be a LMXRB although as yet there is no clear evidence of orbital motion despite initial indications in X-ray and IR data of a 2300s orbital period.

In the TeV region Whipple failed to find any persistent emission at the pulsar period in its 1985-1988 data (Cawley *et al* 1989). Subsequent observations in 1990 using the 'supercuts' analysis failed to indicate any dc excess (Reynolds P.T. *et al* 1991). Haleakala also reported only upper limits (Chadwick *et al* 1990). Data taken by the Durham group at La Palma in 1988 gave some evidence of periodic emission at the second harmonic of the X-ray period but later observations in 1989 failed to confirm this (Chadwick P.M. *et al* 1990).

There have been no positive observations of 1E2259+586 in the PeV regime. GREX found no significant excess from 1986 -1990 (Beaman J. *et al* 1991) , HEGRA found no dc or daily emission from 1989 - 1992 (Merck *et al* 1993) and nor did CYGNUS in their data covering 1986 - 1993 (Alexandreas D.E. *et al* 1991a, 1991c, 1993a).

1.5.6 V0332+53

V0332+53 is a HMXRB with pulsar period 4.38s and orbital period 34.25 days. There have been no positive TeV or PeV detections of this object. Whipple applied their 'supercuts'

analysis to data taken in 1988 but found no significant dc excess (Reynolds P.T. *et al* 1991).

1.5.7 Cen X-3

Cen X-3 is a HMXRB at a distance of 10kpc. It has been observed in the X-ray region by Ginga and Mir-Kvant. Unpredictable variations in its period make periodicity searches difficult.

Cen X-3 was first observed in the VHE regime by the Durham group. 200 hours of data from 1987 - 1989 showed emission at the X-ray period confined to the phase band 0.75 - 0.85 (Brazier K.T.S. *et al* 1990c). Potchefstroom confirmed this with 71 hours of data from 1986 - 1989 (North A.R. *et al* 1990). Only orbital phase interval 0.7 - 0.8 showed any significant evidence of pulsed emission. However the Woomera group (Thornton G.J. *et al* 1991) found no evidence of such emission in 70 hours of observations taken in 1991. In their 1988 - 1989 data JANZOS found no dc or daily emission nor any evidence of emission pulsed at the X-ray period (Allen W.H. *et al* 1991).

In the PeV regime Mt. Chacaltaya found no evidence of dc or pulsed emission either in their raw data or in μ-poor events from 1987 - 1990 (Kakimoto F. *et al* 1990).

1.5.8 Sco X-1

Sco X-1 is a LMXRB with orbital period $\sim$ 18.9 hours. It is thought to contain a millisecond pulsar but as yet there is no confirmation of early X-ray indications of a 4.53ms or 2.93ms periodicity.

This source has been detected in the TeV region by Potchefstroom and the Durham group at Narrabri found a 3.1σ dc excess in their 1988 - 1989 data with each individual

night displaying an excess (Chadwick P.M. *et al* 1990). They found some evidence of orbital modulation but no evidence of any ms periodicity near the X-ray candidate values. Whipple failed to detect a dc signal from Sco X-1 in 1990 using their 'supercuts' analysis (Reynolds P.T. *et al* 1991).

In the PeV regime Mt. Chacaltaya reported an excess of hadronless showers from Sco X-1 in May 1986 modulated with the orbital period (Matano T. *et al* 1990) and the Ooty group reported a 5σ excess from Sco X-1 from March - May 1986 (Gupta S.K. *et al* 1991). Neither group found a long term dc excess (Kakimoto F. *et al* 1990).

1.5.9 Vela X-1

Vela X-1 is a HMXRB at a distance of 1.4kpc with a pulsar period of 283s and an orbital period of 8.96 days. X-ray measurements by SAS-3 and Ginga indicate that the X-ray emission is highly variable and Vela X-1 has a complicated pulse period history showing both spin up and spin down activity. It is believed to be a NS paired with a massive companion. Vela X-1 has not been detected in the radio region nor has it been detected by SAS-II or COS-B in the 100MeV region (Mattox 1989) so it is not the most likely candidate for VHE or UHE emission.

Despite this Vela X-1 has been observed in the TeV regime. The first detection came from data taken in 1986 by the Potchefstroom group who found evidence of pulsed emission throughout the binary orbits and strong bursts with the same period. However this period was inconsistent with later γ and X-ray periods. Later observations in 1987 and 1988 confirmed the burst activity and persistent emission but at a period agreeing with the Ginga value (North A.R. *et al* 1991). Durham data taken at Narrabri between 1986 and 1989 confirmed the persistent emission but found no evidence of any bursts (Brazier K.T.S. *et al* 1990d). In 1991 they detected one burst similar to that of Potchefstroom but

this Durham burst was at a phase different to either value quoted for the Potchefstroom bursts. Woomera found no evidence for X-ray periodicity in 100 hours of data in early 1991 (Thornton G.L. *et al* 1991) and JANZOS also failed to find any dc signal in 24 hours of data taken in 1989 (Bond I.A. *et al* 1990, Allen W.H. *et al* 1991).

The first UHE observation came from Adelaide (Protheroe *et al* 1984). However the effect was only seen when showers with s > 1.3 were selected and there is no theoretical motivation for such a selection criterion. Furthermore subsequent observations by the group failed to confirm the result (Clay *et al* 1987). The Mt. Chacaltaya array found no evidence of a dc excess or orbital period modulation in either their raw data or in μ-poor events in data spanning 1986 - 1989 (Matano T. *et al* 1990, Inoue N. *et al* 1991).

1.5.10 The Crab

The Crab Nebula is a remnant of a SN explosion in 1054 and has a fast spinning central magnetised neutron star. It is a good candidate to produce at least VHE γ-rays. The reason for this is that its high degree of polarisation in the optical tends to suggest that synchrotron processes are occurring that would require electrons above 10^{12}eV in a magnetic field of $\sim 10^{-4}$ Gauss. Since nuclear decay cannot produce such energetic particles some kind of acceleration process would seem to be indicated. Such a mechanism could also accelerate protons which, on interacting with the SNR filamentary material, could produce neutral pions which in turn could decay to give γ-rays.

In 1963 the first hard X-ray source Tau X-1 was discovered and associated with the Crab Nebula. In 1968 a radio pulsar was found in the Crab showing it to be a spinning NS. Similar pulsations at 33ms have been observed in the IR, optical, UV, X-ray and MeV γ-ray regimes. Observations by SAS-II and COS-B confirmed the Crab as a 100MeV source.

In the VHE range the Whipple team have had much success in observing unpulsed emission from the Crab to the extent that they claim it can now be treated as a VHE standard candle. The first observation in 1972 yielded a 3σ result with subsequent improvements in the telescope and the use of imaging techniques culminating in a 45σ detection in their 1988 - 1991 data. Other groups have also utilised various γ-ray selection techniques successfully. Michigan and California University found 5.8σ and 4.2σ dc signals respectively (Weekes 1988). The ASGAT Čerenkov telescope in 150 hours of data from 1991 - 1992 found a 5.7σ signal from the Crab. The BIGRAT low elevation Čerenkov telescope have found no dc excess in 18 hours of data taken in 1992-1993 but they still have to apply their imaging techniques to the data (Edwards *et al* 1993). The THEMISTOCLE air Čerenkov experiment (Baillon P. *et al* 1993) has detected high energy photons from the Crab up to 15 TeV. This goes some way to bridging the gap between the standard Čerenkov measurements and the EAS measurements.

Despite finding a dc excess, ASGAT found no evidence for pulsed emission and Whipple also have found no evidence for the 33ms pulsar period in their data. The first pulsed observation of the Crab came in 1972 from the Smithsonian Čerenkov Telescope group who found a 3.4σ and 5.4σ signal in the main and interpulse region (Fazio *et al* 1972). Pachmarhi, Durham, Haleakala and others have seen bursts of pulsed emission but the only instance of continuous pulsed emission has been seen by the Durham group in 103 hours of data from September 1982 - November 1983 (Weekes 1988).

In the UHE region the Lodz EAS array found from 1975 - 1982 a 5.4σ signal in the general direction of the Crab (a bin of 37.5° in RA and 10.0° in declination was used). The muon content was found to be not much lower than the background but there were large errors in the muon measurements. Tien Shan found a signal in μ-poor showers only for their 1974 - 1982 data. However no other EAS array group has found a dc signal from the Crab including CYGNUS (Alexandreas *et al* 1993a), CASA/MIA (Borione A. *et al*

1993a), Hegra (Merck *et al* 1993) , Akeno (Chiba *et al* 1993) and Haverah Park (Lawrence M.A. *et al* 1990).

As for pulsed emission, Ooty found a 3.9σ excess at the interpulse from June 1984 - May 1987. Selecting showers with s > 1.4 improved their signal although, as stated earlier, there is no reason from Monte-Carlo simulations why γ-initiated showers should be older than CR-initiated ones. Plateau Rosa' found a 1.4σ excess at the main pulse of their February 1982 - December 1987 data. However CYGNUS (Alexandreas *et al* 1993a), CASA/MIA and EAS-TOP all found no evidence of pulsed emission with data taken at overlapping times to the above positive findings .

A burst of UHE γ-rays from the Crab in February 1989 was first noted by BASA. On February 23rd 1989 KGF observed a 3.4σ excess from the Crab of almost normal muon content (Acharya *et al* 1990). They also observed pulsed emission finding a 5.7σ excess in the first half of the period which includes the main pulse at zero phase an the interpulse at phase 0.42 observed at other wavelengths. EAS-TOP saw a 2.1σ effect with some evidence that the source events were somewhat older than normal CR showers. When only showers with Ne > 10^5 were selected the signal rose to 3.4σ. Tien Shan observed a 2.4σ excess. CYGNUS however found no emission on the day preceding or following the Baksan burst (the Crab was not overhead during burst time) (Alexandreas *et al* 1993a). Ohya using a μ-poor selection criteria found no evidence of emission on this day either (Muraki Y. *et al* 1990). The Crab burst and in particular the Baksan result will be discussed further in Chapter 5.

1.5.11 Geminga

Geminga was first observed in 1972-1973 by SAS-II at the 7σ level and named γ-195 (Thompson D.J. *et al* 1977) . Its existence was confirmed by the COS-B satellite with data from August 1975 - December 1981 (Bennet K. *et al* 1977). A subsequent search in the COS-B error box by the X-ray satellite Einstein found 4 sources the strongest of which was 1E0630+178 (Bignami G.F. *et al* 1983).

Initially it appeared that this new source might have a 59s periodicity. This was first postulated by the SAS-II team who said themselves that their evidence was not compelling (Thompson D.J. *et al* 1977). Such a period was first confirmed and then denied, once all their data had been analysed, by the COS-B team (Masnou J.L. *et al* 1981). Further confirmation seemed to come from Tien Shan (Zyskin Yu. & Mukanov D.B. 1983,1985), Exosat and Einstein (Bignami G.F. *et al* 1984) and the Gulmarg Čerenkov group (Kaul R.K. *et al* 1985). Whipple though found no such evidence in 15 hours of data from November 1983 - February 1984.

A Fast Fourier Transform procedure on ROSAT's March 14th - 17th 1991 data on the soft X-ray source 1E0630+178 discovered a period of 237.097s (Halpern J.P. & Holt S.S. 1992). This was promptly confirmed by 3 EGRET observations of γ-195 in April - June 1991 (Bertsch D.L. *et al* 1992). A reanalysis of the 1975-1982 COS-B data above 100meV also confirmed that γ-195 had such a period (Hermsen W. *et al* 1992). The matching of the X-ray and γ-ray period meant that the counterpart for Geminga had been found - Geminga was undoubtedly an X-ray pulsar. As yet no emission from Geminga has been detected by COMPTEL at EGRET phases but Geminga has been relatively poorly covered by COMPTEL (Bennet *et al* 1993).

Archive Dugway data of the Durham group taken on October 4th - 11th 1983 was analysed with no search in period or epoch (Bowden C.C.G. *et al* 1993). The resulting light curve

correlated well with EGRET. Data taken by the same group at Narrabri in 1992 only gave an upper limit (the fact that the energy threshold at Narrabri was 3 times that at Dugway is perhaps significant.) Archive data from the Tata Čerenkov telescope taken in 1984 - 1985 was reanalysed. There are two sites separated by 11km. They found no strong evidence for periodicity in the the combined data from simultaneous runs at the two sites but there were a few pulsed bursts of duration one minute during which pulsed emission was observed at both sites. Mt. Hopkins (Gillanders G.H. *et al* 1990) and Whipple (Cawley M.F. *et al* 1985) have found no significant unpulsed emission (February 1987 - June 1988 and November 1983 - February 1984 plus 1989-1991 respectively) The Whipple group found no pulsed emission in data from 1989-1990 (Akerlof *et al* 1993).

In the UHE region there has been less success. EAS-TOP data from 1985-1993 showed no significant effect in the μ-poor data or Ne $> 10^5$ data (angular resolution improves for larger showers) (Aglietta M. *et al* 1993a). CYGNUS (Alexandreas D.E. *et al* 1993a), HEGRA (Merck *et al* 1993), Plateau Rosa' (Morello C. *et al* 1990) and the Tibet array (Amenomori *et al* 1993a) have thus far found no daily or dc excess in data from 1986-1993 nor have CYGNUS found any evidence of a 273ms periodicity in data from 1989-1993 (Alexandreas *et al* 1993).

The EAS-TOP data from 1991-1993 while giving no overall dc excess does give some evidence of an EGRET-like light curve in the external high energy subset of data (Aglietta *et al* 1993b). The GRAPES (Gamma Ray Astronomy at PeV Energies) installation at Ooty found no overall excess from 1984-1987 but found evidence of emission lasting one week with 83 events observed compared to an expected 44.1 (Gupta *et al* 1993).

Interestingly Geminga has yet to be observed in the radio regime. The Westerbork Synthesis Radio Telescope found no radio pulsar in the 0.4 ° COS-B error box at 21cm in 1980-1982 (Spelstra & Hermsen 1984) A search made in 1990 (Hermsen & Spelstra 1990)

at 90cm, 49cm and 21cm yielded no signal either (pulsar models predict wider beaming for longer radio wavelengths and thus at 90cm the beam would have a the observer's line of sight.) Once the 273ms period was discovered the Effelsburg radio telescope was used to search at 21cm and 18cm for about 80 and 85 minutes respectively (Seiradakis J.H. 1992). No periodicity was found.

Geminga is the first neutron star (NS) observed in X-rays and γ-rays but not radio. This could be explained easily of course if Geminga's radio beam simply did not intersect our line of sight - the γ-rays and X-rays being more widely beamed and having a higher probability of being observed.

1.5.12 PSR0355+54

PSR0355+54 is a radio pulsar which displays large glitches in its radio period.

The Pachmarhi group observed pulsed emission in their 1989-1991 data above 2TeV. (Lorenz 1993) Whipple found no dc excess from 1988 -1991 using their 'supercuts' method (Reynolds P.T. *et al* 1991).

In the PeV regime GREX found no dc excess from 1986-1990 (Beaman J. *et al* 1991) and CYGNUS found no dc or daily emission from 1986-1993 (Alexandreas D.E. *et al* 1991a, 1991b, 1993a).

1.5.13 PSR0655+64

This pulsar has a period of 196ms. There have been no positive detections of PSR0655+64 in the VHE or UHE energy regions. Whipple found no evidence for a dc excess in 84 minutes of data taken from 1988-1991 (Lang M.J. *et al* 1991).

1.5.14 PSR1913+16

PSR1913+16 is a double pulsar with an orbital period of 7.75 hours. There have been no positive detections of PSR1913+16 in the VHE or UHE energy regions. Tien Shan found no significant dc excess in their data covering 1974-1982 (Kirov I.N. *et al* 1992) .

1.5.15 PSR1937+21

This pulsar has a period of 1.6ms. There is only one VHE report of emission from PSR1937+21 and that is from the Durham group. From 129 hours of observations they report evidence of a signal lasting 7-8 days with a period 1.56ms (Weekes 1988). There have been no reports of emission in the UHE region with CYGNUS (Alexandreas D.E. *et al* 1993a), EAS-TOP (Aglietta M. *et al* 1990,1991), HEGRA and Plateau Rosa (Morello C. *et al* 1991) all failing to find a dc or daily excess.

1.5.16 PSR1953+29

PSR1953+29 is unusual in two main ways : it is one of the few known pulsars with periodicity less than 10ms and although it is a radio pulsar it is part of a binary system (Weekes T.C. 1988). Its 6.1ms periodicity was discovered during a systematic search of the error boxes of the 100MeV COS-B data. These error boxes had dimensions $\pm$ 2° and thus a pulsar found within it need not necessarily be the γ-ray source unless the γ-rays are found to show pulsed emission or the pulsar is in some way unusual. PSR1953+29 is certainly that with a pulsar period of 6.1ms and an orbital period of 117.3 days.

It was subsequently observed in the TeV region by the Durham group in 1983 and then again in 1984. The sinusoidal light curve they obtained was very different to that expected from a 'normal' radio source.

There has been no report of a positive signal in the UHE region with CYGNUS (Alexandreas D.E. *et al* 1993a), EAS-TOP (Aglietta M. *et al* 1991) , HEGRA and Plateau Rosa' (Morello C. *et al* 1990) all finding no significant dc or daily emission from 1982 - 1993.

1.5.17 Markarian 421

Markarian 421 is a BL Lac object which displays compact radio emission, strong optical polarisation and displays rapid variability in the optical, IR and X-ray regimes. It is the weakest of the 20 AGN observed by EGRET in the energy range $10^6 - 10^9$eV and in this energy range it showed no time variability. Markarian 421 is at a redshift of about 0.031 , about 100Mpc away.

Mrk421 is one of the two sources which the Whipple team can consistently detect using their "supercuts' analysis . (Punch M. *et al* 1992) 7.5 hours of data taken in early 1992 resulted in a 6.3σ signal being seen. This is the equivalent of about 0.28 of the Crab flux measured by the Whipple team. Subsequent observations in winter 1993 gave a flux of 0.25 of the Crab flux indicating some degree of time variability. Whipple searched for 18 AGN objects in all including 7 detected at GeV by EGRET but only detected a signal from Mrk421 (Kerrick *et al* 1993, Schubnell *et al* 1993).

It is perhaps due to Mrk421's close proximity that we are able to see in in the TeV region at all. This is because the difficulty with observing TeV and PeV photons from extra-galactic objects is that at these energies the γ-rays undergo absorption with the 2.7° microwave background or with starlight and IR photons in extragalactic space. Clearly this effect becomes more important with increasing energy and distance traversed by the γ-rays. It is possible that the reason Whipple can only observe Mrk421 is not due to some intrinsic property of Mrk421 itself but rather merely due to the fact that it is close enough for a measurable flux of γ-rays to reach us. In fact recent work has attempted to put limits

on the cosmic infrared background radiation from the measurements of Mrk421. It would appear that there is indeed a high energy cut of at $\sim 10^{13}$eV in which case one would not expect to be able to observe Mrk421 in the PeV region.

In the PeV region CASA/MIA searched their 1990-1992 data for EGRET extragalactic sources (including Mrk421) but report only upper limits.(Lorenz 1993) CYGNUS found no signal from Mrk421 or 12 other AGN in their data covering 1986-1993 (Alexandreas *et al* 1993b). Negative results were also obtained by HEGRA (Merck *et al* 1993), EAS-TOP (Aglietta *et al* 1993a) and the Tibet array (Amenomori *et al* 1993b).

1.5.18 M31

At present it is believed that all but the highest energy cosmic rays are of Galactic origin. It is thus of great interest to examine M31 for evidence of UHE γ-ray emission.

M31 contains many discrete X-ray sources but has not yet been detected at 100MeV. Up until recently the only extragalactic object observed above 30MeV was 3C273. Now the EGRET facility on the Compton GRO satellite (20MeV-30GeV) has observed 20AGN.

M31 is difficult to study using the Čerenkov technique due to its optical brightness. However, the Durham group observed some evidence for emission from it in September - November 1983 perhaps from a single discrete source within M31 (Weekes 1988). Other Čerenkov experiments including the Smithsonian group (1969-1970) and Whipple (October - November 1984) found no evidence of emission from M31.

There has been no report of a positive signal in the UHE region with CYGNUS (Alexandreas D.E. *et al* 1993a), EAS-TOP (Aglietta M. *et al* 1991) and Plateau Rosa' (Morello C. *et al* 1990) all finding no significant dc or daily emission from 1982 - 1993.

1.5.19 GRO J0422+32

GRO J0422+32 (Nova Persei) is a hard X-ray transient first detected by BATSE on the 5th of August 1992 (Paciesas *et al* 1992). BATSE and OSSE found it to emit about 3 times the Crab flux in the range 40-230 keV. The telescope was repointed so that all 4 GRO instruments could observe the source (Harman B.A. *et al* 1992) and it was found that there is significant emission up to about 600keV with the source displaying a hard spectrum. GRO J0422+32 showed variability on all time scales and BATSE reported quasiperiodic oscillation (QPO) activity centred and ν = 0.04Hz and ν=0.2Hz (Koureliotou C. *et al* 1992). OSSE found it to have a spectrum similar to and 3 times brighter than the BH candidate Cyg X-1 as observed by them in June 1991. Like the only other XRB source found so far in the COMPTEL database GRO J0422+32 is a BH candidate.

This detection prompted other groups to look in this direction and the SIGMA detector on GRANAT (Vikhlinin A *et al* 1992) detected it in the 40-150keV range on August 15th,16th and 17th finding the daily averaged flux to be remarkably constant at around 2.9 times the Crab flux. They also observed QPO activity on August 22nd at 0.28Hz and 0.035Hz. The former was seen in the full 40-150keV range while the latter was mainly in the 40-70keV range. The flux was seen to decrease monotonically from 2.91 Crab to 1.85 Crab from August 15th - September 6th (Goldwurm A. *et al* 1992) . The WATCH all sky monitor on GRANAT also observed GRO J0422+32 finding a flux 2.5 times that of the Crab >20keV on August 11th. (Cameron R.A. *et al* 1992)

An optical counterpart was suggested by the Crimean Astrophysical Observatory (CAO) from CCD images taken (Castro-Tirado A.J. *et al* 1992). This candidate was observed by the Perkins 1.8m telescope who found spectral features characteristic of optical counterparts of various other X-ray sources and so confirmed the identification (Wagner R.M. *et L* 1992). The optical counterpart was observed for more than 20 nights since August

28th by the Wise and Oak Ridge Observatory. (Mazeh T. *et al* 1992) Each night the star displayed erratic eruptions on timescales of 1-2 hours typically of an amplitude 0.1 magnitude resulting in a QPO like feature close to ν=0.5hr^{-1}. Kyoto University observations of the optical counterpart revealed periodic modulation with period 5.208 hours of amplitude 0.10 magnitude in V.

The International UV Explorer detected a source on August 16th with slightly discrepant source coordinates to those given by the CAO (Shrader C.R. *et al* 1992). The Special Astrophysics Observatory 6m telescope observed considerable variations in the continuum of this source in the UV region on timescales of days.

The IUVE coordinates were confirmed by the VLA which observed the radio counterpart of GRO J0422+32 increasing in flux from 4mJy at 4.9GHz on August 16th to about 8mJy on August 17th at 1.49 and 4.9GHz.

GRO J0422+32 has also been detected in the infrared at 10.8 microns by the 3m telescope on Mauna Kea (Telesco C. *et al* 1992).

1.5.20 GRO J1837+59

This bright source was observed by EGRET in 1992 coincident with one seen in earlier observations in May - June the previous year. No counterpart is known from catalogued sources at any other wavelength.

1.5.21 AE Aquarii

AE Aquarii is a DQ Her type cataclysmic variable at a distance of 84pc. Cataclysmic variables are semidetached binaries which contain a WD accreting matter from its companion. It has an orbital period of 9.88 hours and the optical and X-ray emission is pulsed at 33s

which is attributed to WD rotation. Most of the power lies in the second harmonic. It shows optical and radio flares on timescales of > 1 hour as well as flickering on timescales of about 20 minutes during which QPO activity dominates the precise spin periodicity.

AE Aquarii was first observed in the VHE region by Potchefstroom. Between 1988 and 1990 they found evidence of pulsed emission at a period 0.15s greater than the optical and X-ray period with most of the power in the second harmonic (Brink C. *et al* 1990). In 38 hours of data taken in 1990 Durham found no evidence of emission at the fundamental period but 7 consecutive datasets suggested emission at the second harmonic. (Bowden C.C.G. *et al* 1991b)

In the PeV regime the air shower array at Mt. Chacaltaya found no significant dc excess between 1986 and 1990 either in the raw or hadron-less data (Inoue N. *et al* 1991).

1.6 The Muon Question

As stated previously it is predicted that γ-ray-initiated showers should have approximately an order of magnitude less muons in them than hadron-initiated showers. Although this is the result of extrapolation of present accelerator data from energies presently attainable, the DESY e-p collider experiment shows no strong increase of the γ-p cross-section at high energies (Muraki Y. *et al* 1993). and HERA results imply that at 100TeV at least γ-ray initiated showers should indeed be μ-poor (Derrick *et al* 1992).

However several experimental results have brought this into question. In fact the first PeV detection, which was of Cyg X-3 (Samorski & Stamm 1983a,b), showed that the signal came from showers which were not μ-poor. Another example is the proposed burst from Her X-1 in which the CYGNUS collaboration observed two 30 minute bursts on the 24th

of July 1986 which were not only at a period about 0.15% lower than the X-ray period but were also μ-rich showers (Alexandreas D.E. *et al* 1991). Searches by CASA/MIA and the Nottingham μ-detector for an excess from the Galactic Plane have shown no increase in the ratio $\frac{I_\gamma}{I_{CR}}$ when selecting μ-poor showers as might be expected if the neutral radiation were γ-rays.

In order for a signal to point back to source it is necessary for it to be neutral - otherwise its direction would be altered by the interstellar magnetic fields. It is assumed that these neutral signals are γ-rays. Neutrons are ruled out because they would decay before arriving at the Earth. Only above $\sim 10^{18}$eV could relativistic effects prolong their half-lives sufficiently for them to provide a signal (Mikhailov 1994). It is of course possible that the signal could be some new exotic neutral particle but one would be well advised to eliminate all other possibilities before invoking such a radical solution. Certainly one would want more substantiated observations before coming to any conclusion.

REFERENCES : CHAPTER 1

Acharaya B.S. *et al* 21^{st} I.C.R.C. **2** 319 (1990)

Acharaya B.S. *et al* 22^{nd} I.C.R.C. **1** 237 (1991)

Aglietta M. *et al* 21^{st} I.C.R.C. **2** 345 (1990)

Aglietta M. *et al* 22^{nd} I.C.R.C. **2** 277 (1991)

Aglietta M. *et al* 23^{rd} I.C.R.C. **1** 216 (1993a)

Aglietta M. *et al* 23^{rd} I.C.R.C. **1** 309 (1993b)

Aglietta M. *et al* Geneva Cosmic Ray Conference (1993)

Akerlof C.W. *et al* Proc GRO Science Workshop 4 (1989)

Akerlof C.W. *et al* 23^{rd} I.C.R.C. **1** 305 (1993)

Alexandreas D.E. *et al* 22^{nd} I.C.R.C. **1** 249 (1991)

Alexandreas D.E. *et al* 22^{nd} I.C.R.C. **1** 301 (1991a)

Alexandreas D.E. *et al* 22^{nd} I.C.R.C. **1** 352 (1991b)

Alexandreas D.E. *et al* 22^{nd} I.C.R.C. **1** 436 (1991c)

Alexandreas D.E. *et al* Ap J **405** 353 (1993a)

Alexandreas D.E. *et al* 23^{rd} I.C.R.C. **1** 416 (1993b)

Alexandreas D.E. *et al* 23^{rd} I.C.R.C. **1** 326 (1993c)

Alexandreas D.E. *et al* 23^{rd} I.C.R.C. **1** 223 (1993d)

Allen W.H. *et al* 22^{nd} I.C.R.C. **1** 344 (1991)

Amenomori M *et al* 23^{rd} I.C.R.C. **1** 342 (1993a)

Amenomori M *et al* 23^{rd} I.C.R.C. **1** 412 (1993b)

Austin R. *et al* 21^{st} I.C.R.C. **2** 110 (1990)

Asakimori K. *et al* 21^{st} I.C.R.C. **2** 18 (1990)

Axford W.I. *et al* 15^{th} I.C.R.C. **11** 32 (1977)

Axford W.I. *et al* A&A **11** 317 (1982)

Baade W. & Zwicky F. Proc. Nat. Acad. Sci. **20** 239 (1934)

Baillon P. *et al* 23^{rd} I.C.R.C. **1** 271 (1993)

Beaman J. *et al* 22^{nd} I.C.R.C. **1** 297 (1991)

Bennet K. *et al* A&A **56** 469 (1977)

Bennet K. *et al* 23^{rd} I.C.R.C. **1** 172 (1993)

Berezhko E.G. *et al* 20^{th} I.C.R.C. **2** 171 (1987)

Bertsch D.L. *et al* Nature **357** (1992)

Bignami G.F. *et al* Ap J **272** L9 (1983)

Bignami G.F. *et al* Nature **310** 464 (1984)

Blake P.R. *et al* 23^{rd} I.C.R.C. **1** 402 (1993)

Blandford R.D. & Eichler D. Phys Rep **154** 1 (1987)

Blandford R.D. & Ostriker J.P. Ap J **221** L29 (1978)

Bloomer S.D. *et al* 21^{st} I.C.R.C. **2** 334 (1990)

Bond I.A. *et al* 21^{st} I.C.R.C. **2** 271 (1990)

Borione A. *et al* 23^{rd} I.C.R.C. **1** 286 (1993a)

Borione A. *et al* 23^{rd} I.C.R.C. **1** 385 (1993b)

Borione A. *et al* 23^{rd} I.C.R.C. **1** 425 (1993c)

Borione A. *et al* 23^{rd} I.C.R.C. **1** 220 (1993d)

Bowden C.C.G. *et al* 22^{nd} I.C.R.C. **1** 253 (1991a)

Bowden C.C.G. *et al* 22^{nd} I.C.R.C. **1** 356 (1991b)

Bowden C.C.G. *et al* 23^{nd} I.C.R.C. **1** 294 (1993)

Brazier K.T.S. *et al* 21^{st} I.C.R.C. **2** 379 (1990a)

Brazier K.T.S. *et al* 21^{st} I.C.R.C. **2** 91 (1990b)

Brazier K.T.S. *et al* 21^{st} I.C.R.C. **2** 296 (1990c)

Brazier K.T.S. *et al* 21^{st} I.C.R.C. **2** 292 (1990d)

Brink C. *et al* 21^{st} I.C.R.C. **2** 283 (1990)

Cameron R.A. *et al* IAU Circular 5587 (1992)

Cassidy G.L. *et al* 21^{st} I.C.R.C. **2** 14 (1990)

Castro-Tirado A.J. *et al* IAU Circular 5588 (1992)

Cawley M.F. *et al* 19^{th} I.C.R.C. **1** 173 (1985)

Cawley M.F. *et al* Proc Int Workshop on VHE Gamma ray Astronomy ed A.A. Stepanian *et al* 165 (1989)

Cesarsky C.J. *et al* 20^{th} I.C.R.C. **8** 87 (1987)

Chadwick P.M. *et al* Nature **318** 642 (1985)

Chadwick P.M. *et al* J Phys G:Nucl Part Phys **16** 1773 (1990)

Chanmugam G. & Brecher K. Nature **313** 767 (1985)

Cheng K.S. & Ruderman M.A. Ap J **337** L77 (1989)

Chiba N. *et al* 23^{rd} I.C.R.C. **1** 365 (1993)

Chuikin E.I. *et al* 23^{rd} I.C.R.C. **1** 184 (1993)

Clay J. *et al* Proc Royal Acad, Amsterdam **30** 115 (1927)

Clay R.W. *et al* 20^{th} I.C.R.C. **1** 250 (1987)

Cooper R.G. *et al* 22^{nd} I.C.R.C. **1** 265 (1991)

Corbato S.C. *et al* 22^{nd} I.C.R.C. **1** 281 (1991)

Cronin J.W. *et al* Phys Rev D **45** 4385 (1992)

Daugherty J.K. & Harding A.K. Ap J **252** 337 (1982)

Derrick *et al* Phys Lett B **293** 465 (1992)

Drury L.O'C. Cosmic Rays, SN and the ISM Ed. M.M. Shapiro (1987)

Edwards P.G. *et al* 23^{rd} I.C.R.C. **1** 259 (1993)

Eichler D. Ap J Suppl Ser **90** 877 (1994)

Ellison D.C. & Eichler D. Phys Rev Lett **55** 2735 (1985)

Fazio G.G. *et al* Ap J **175** L117 (1972)

Fermi E. Phys rev **75** 1169 (1949)

Fermi E. Ap J **119** 1 (1954)

Fryxell & Toam Ap J **335** 862 (1989)

Fujita K. *et al* 23^{rd} I.C.R.C. **1** 376 (1993)

Gaisser T.K. *et al* Cosmic Rays and Particle Physics 1990

Ghosh & Lamb Ap J **234** 296 (1979)

Gillanders G.H. *et al* 21^{st} I.C.R.C. **2** 23 (1990)

Goldwurm A. *et al* IAU Circular 5589 (1992)

Green D.A. A Caltalogue of Galactic SNR (1992)

Gregory A.A. *et al* A&A **237** L5 (1990)

Gunn J.E. & Ostriker J.P. Phys Rev Lett **22** 728 (1969)

Gunn J.E. & Ostriker J.P. Ap J **165** 523 (1971)

Gupta S.K. *et al* 22^{nd} I.C.R.C. **1** 316 (1991)

Halpern J.P. & Holt S.S. Nature **357** 222 (1992)

Harding A.K. Frontier Objects in Astrophysics and Particle Physics eds. F. Giovannelli & G. Mannochi (1990)

Harding A.K. & Gaisser T.K. Ap J (1989) check in ap j files

Harman B.A. *et al* IAU Circular 5584 (1992)

Hartmann R.C. *et al* Ap J **385** L1 (1992)

Hayashida N. *et al* 22^{nd} I.C.R.C. **1** 309 (1991)

Hermsen W. *et al* IAU Circular 5541 (1992)

Hermsen W. & Spelstra T. 21^{st} I.C.R.C. **1** 208 (1990)

Hess V.F. Physik Z **13** 1084 (1912)

Hess V.F. Physik Z **13** 1084 (1912)

Hewish A. *et al* Nature **217** 709 (1968)

Inoue N. *et al* 22^{nd} I.C.R.C. **1** 380 (1991)

Johnson T.H. Phys Rev **43** 834 (1933)

Jokipii J.R. Ap J **313** 842 (1987)

Joss P.C. & Rappaport S.A. Ann Rev A&A **22** 537 (1984)

Kakimoto F. *et al* 21^{st} I.C.R.C. **2** 358 (1990)

Kaul R.K. *et al* 19^{th} I.C.R.C. **1** 365 (1985)

Kazanas D. & Ellsion D.C. Nature **319** 380 (1986)

Kerrick A.D. *et al* 23^{rd} I.C.R.C. **1** 405 (1993)

Khristiansen G.B. *et al* 21^{st} I.C.R.C. **2** 362 (1990)

Kifune T. *et al* Ap J **301** 320 or 230 (1986)

Kirk J.G. & Schneider P. Ap J **315** 425 (1987)

Kirov I.N. *et al* J. Phys. G: Nucl Part Phys **18** 12 2027 (1992)

Ko S. *et al* 21^{st} I.C.R.C. **2** 131 (1990)

Koureliotou C. *et al* IAU Circular 5592 (1992)

Lagage & Cesarsky A&A **125** 249 (1983)

Lamb R.C. *et al* Very High Energy Gamma-Ray Astronomy Ed K.E. Turver 139 (1987)

Lang M.J. *et al* 22^{nd} I.C.R.C. **1** 204 (1991)

Lawrence M.A. *et al* 21^{st} I.C.R.C. **2** 67 (1990)

LeMaitre G. & Vallarta M.S. Phys Rev **43** 87 (1933)

Lloyd-Evans J. *et al* Nature **305** 784 (1983)

Longair High Energy Astrophysics (1981)

Lorenz E. Nuclear Physics B (Proc Suppl) 33A,B 93 (1993)

Lovelace R.V.E. Nature **262** 649 (1976)

Macomb D.B. *et al* Ap J (1991)
Makashima K. Proc of Structure & Evolution of Neutron Stars (1990)

Masnou J.L. *et al* 17^{th} I.C.R.C. **1** 177 (1981)

Matano T. *et al* 21^{st} I.C.R.C. **2** 266 (1990)

Matthaeus *et al* Phys rev lett **53** 1449 (1984)

Mattox J. Proc. GRO Workshop ed. W.N. Johnson 4 (1989)

Mazeh T. *et al* IAU Circular (1992)

Merck M. *et al* 22^{nd} I.C.R.C. **1** 261 (1991)

Merck M. *et al* 23^{rd} I.C.R.C. **1** 361 (1993)

Mikhailov A.A. *et al* J Phys G: Nucl Part Phys **20** 841 (1994)

Morello C. *et al* 21^{st} I.C.R.C. **2** 349 (1990)

Muraki Y. *et al* 21^{st} I.C.R.C. **2** 56 (1990)

Muraki Y. *et al* 22^{nd} I.C.R.C. **2** 245 (1991)

Nagle D.E. *et al* Ann Rev Nucl Part Sci **38** 609 57 (1988)

Neshpor Yu.I. *et al* Izv. Krymsk. Astrofiz. Obs. **61** 61 (1980)

North A.R. *et al* 21^{st} I.C.R.C. **2** 275 (1990)

North A.R. *et al* 22^{nd} I.C.R.C. **1** 328 (1991)

O'Flaherty K.S. *et al* 21^{st} I.C.R.C. **2** 2 (1990)

O'Flaherty K.S. *et al* 22^{nd} I.C.R.C. 257 (1991)

Ostrowski M. A&A **283** 344 (1984)

Paciesas *et al* IAU Circular 5580 (1992)

Protheroe R.J. *et al* Ap J **280** L47 (1984)

Protheroe R.J. & Szabo A.P. Particle Astrophysics & Cosmology Eds. Shapiro M.M., Silbeberg R. & Wefel J. (1992)

Punch M. *et al* Nature **358** 477 (1992)

Rannot R.C. *et al* 21^{st} I.C.R.C. **2** 315 (1990)

Rao M.V.S. & Sreekantan B.V. Current Science **62** 9 617 (1992)

Rawat H.S. *et al* 21^{st} I.C.R.C. **2** 104 (1990)

Resvanis L. *et al* Very High Energy Gamma-Ray Astronomy Ed K.E. Turver 135 (1987)

Reynolds P.T. *et al* 22^{nd} I.C.R.C. **1** 392 (1991)

Samorski M. & Stamm W. Ap J **268** L17 (1983a)

Samorski M. & Stamm W. 18^{th} I.C.R.C. **11** 244 (1983b)

Schubnell M. *et al* 23^{rd} I.C.R.C. **1** 409 (1993)

Seiradakis J.H. *et al* IAU Circular 5532 (1992)

Shrader C.R. *et al* IAU Circular 5591 (1992)

Sinha S. *et al* 21^{st} I.C.R.C. **2** 126 (1990a)

Sinha S. *et al* 21^{st} I.C.R.C. **2** 51 (1990b)

Sorrell W.H. *et al* Cosmic Radiation in Contemporary Astrophysics ed. M.M. Shapiro (1984)

Spelstra T. & Hermsen W. A&A **135** 135 (1984)

Sreekantan B.V. *et al* 21^{st} I.C.R.C. **2** 340 (1990)

Stepanian *et al* Nature **239** 40 (1972)

Stomer C. Z. Astrophys **1** 237 (1930)

Telesco C. *et al* IAU Circular (1992)

Teshima M. *et al* 21^{st} I.C.R.C. **2** 71 (1990)

Thielheim K.O. *et al* Nucl Phys B (Proc Suppl) 33A,B 181 (1993)

Thompson D.J. *et al* Ap J **213** 252 (1977)

Thornton G.J. *et al* 22^{nd} I.C.R.C. **1** 336 (1991)

Toptygin I.N. Space Sci Rev **26** 157 (1980)

Tumer O.T. *et al* 21^{st} I.C.R.C. **2** 155 (1990)

Vikhlinin A *et al* IAU Circular 5606

Vladimirskii B.M. *et al* 14^{th} I.C.R.C. **1** 118 (1973)

Völk H.J. 20^{th} I.C.R.C. **7** 157 (1987)

Völk H.J. & Biermann P.L. Ap J **333** L65 (1988)

Wagner R.M *et al* IAU Circular (1992)

Wang Y-M. Astrophys & Space Sci **121** 193 (1986)

Weekes T.C. Phys Rep **160** 1 (1988)

Weekes T.C. Space Sci Rev **59** 315 (1992)

Wilson C.T.R. Proc Royal Soc **68** 151 (1901)

Zyskin Yu. & Mukanov D.B. 18^{th} I.C.R.C. **1** 122 (1983)

Zyskin Yu. & Mukanov D.B. 19^{th} I.C.R.C. **1** 177 (1985)

2 BAKSAN AIR SHOWER ARRAY

2.1 Introduction

The Baksan Air Shower Array (BASA) is situated in the North Caucasus mountains (43°N, 43°E) at an altitude of 1700m above sea level. It is composed of two main sections, an inner array of 400 liquid scintillators known as the Carpet array, and 6 smaller arrays of detectors situated as shown in Figure 2.1. The central Carpet is divided into 4 subsections A - D each consisting of 100 liquid scintillators of dimensions 0.7 × 0.7 × 0.3 m^3, that is each subsection has an area of 49m^2 and the Carpet itself has dimensions 14 × 14 m^2. The 6 outer detectors each have 18 similar scintillators amounting to an area of 9m^2. The scintillators themselves are filled with white spirit somewhat heavier than benzene but lighter than kerosene. Its formula is C_nH_{2n+2} with n ~ 10. The scintillator material itself $C_{15}H_{11}NO$ has a concentration of 1 gram per litre. This emits light most efficiently in the region about 3800Å however the photomultipliers (PM) are most efficient at about 4200Å . Thus a shifter is used to absorb light in the region 3700Å - 4100Å and re-emit it in the region 4200Å - 4300Å nearer the PM efficiency maximum. This shifter $C_{24}H_{16}N_2O_2$ has a concentration of 0.03 grams per litre.

Each of the 4 Carpet subsections and the 6 outlying detectors are connected to a linear divider which splits the summed pulse from the 100 or 18 scintillators into 2 analogue

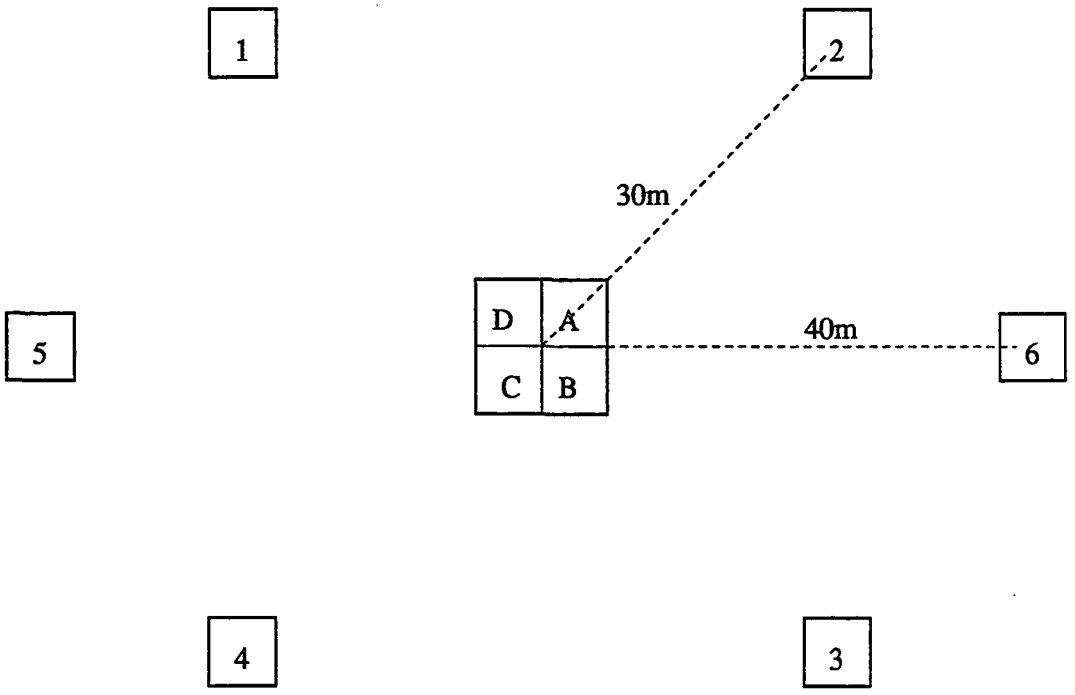

Figure 2.1 The geometry of the Baksan Extensive Air Shower Array.

pulses. The first of these is passed through an integral discriminator. For a signal to be accepted as real the pulse height must be greater than that of a penetrating particle on the area of the scintillator array in question for each of the 6 outer detectors. For the 4 parts of the Carpet detector the criterion is >0.3 of a penetrating particle. It is expected that 1 meson will lose 50MeV energy so that the threshold for the 6 outer detectors is 50MeV and for the 4 parts of the Carpet it is 15MeV. If the 0.3 particle height condition is satisfied for all 4 elements of the Carpet then the timing system is started. This happens with a rate of approximately $50s^{-1}$. If further the 1 particle height condition is satisfied in outlying detectors 1 - 4 also then the signal is considered to have originated from a real shower and the recording system is started. The number of such events is recorded as a master count.

The second discriminator (see Figure 2.2) is used for the event stop times. This is a constant fraction discriminator and for a signal to be considered real an event must have a pulse height at least equal to 0.8 that of a penetrating particle on the area of the scintillator array in question. This value is taken so that the stop signals will be slightly more sensitive than the master count so that theoretically there would always be a stop trigger for each start trigger. Ideally both would have a value of 1 but due to the jitter of the constant fraction discriminator it was decided to use a value of 0.8. The constant fraction is taken to be $\frac{1}{20}$. This constant fraction discriminator is used in an attempt to minimise the dependency of the time recorded on the amplitude of the pulse registered and will be described in greater detail later. Provided that the constant fraction discriminator conditions are satisfied for the 4 components of the Carpet and detectors 1 - 4, the time delays will be recorded. This occurs at a rate of about $1s^{-1}$. Thus 49 times out of 50 the timing electronics are started but not stopped. The reason for using 2 discriminators is

more historical than physical. The central Carpet installation with its integral discriminator was in use before the outlying detectors were built and it was decided to utilise the electronics already in place as a start signal.

In practice the pulses from each of channels 1 - 6 are relayed through a 120m cable at a speed of about 1 metre in 5 nanoseconds. The start pulse from the Carpet is delayed by a 68m cable. Thus the 6 stop pulses are delayed by 600ns and the start pulse by 344ns (including natural delays in the Carpet electronic cables). The difference in artificial delays imposed on the pulses is sufficient that the Carpet pulse is always the first to be registered and can be used as a measure of the start of the timing. The maximum distance between an outlying detector and the Carpet is 40m and with light travelling about 1 metre in 3ns this means that a near horizontal shower hitting an outlying detector first would hit it about 120ns before the Carpet. Similarly this event would hit the opposite outlying detector 120ns after it hit the Carpet. Thus the delayed pulses from the 6 detectors give a stop signal resulting in time delays measured between 256-120 and 256+120. This neatly allows storage in integer*1 format from -128 to +128.

The details of the delays and the time of the event are stored in the memory of an on-line computer the output of which is made every 20 minutes. Thus a day's data comprises 72 such 20 minute runs. The event relative arrival times are recorded with millisecond accuracy. The drift rate of the clock is of the order of 3-5 ms per day. There is no absolute timing information thus any periodicity results must give only relative phases.

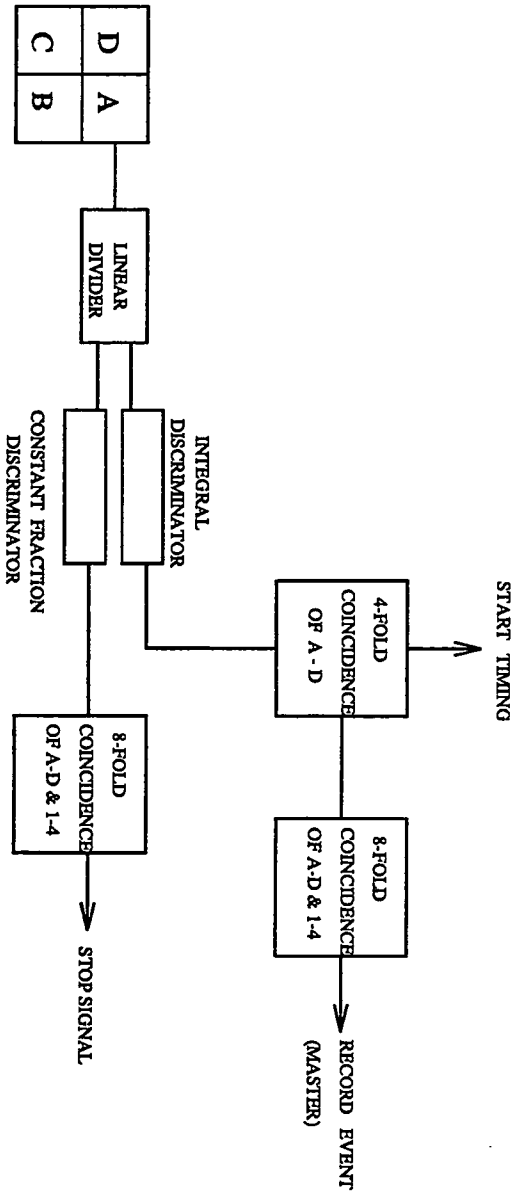

Figure 2.2 The triggering conditions for shower events at BASA. Each of the 4 Carpet subsections and each of the 6 outlying detectors are connected to 2 discriminators as demonstrated here for section A of the Carpet array.

2.2 Constant Fraction Discriminator

As mentioned previously, the arrival time of an EAS measured by a scintillator depends on the number of EAS particles hitting the particular scintillator. This is due partly to the response dependency of the discriminator on the amplitude of the PM signal.

The upper figure in Figure 2.3 shows 3 pulses of different amplitude approximated as triangular for clarity. If the trigger of the scintillator is set to a fixed value, say as shown by the dashed line, then the time delay measured will be dependent on the pulse size. The varying energy pulses will trigger at t_1, t_2 and t_3 respectively. The maximum effect occurs for a pulse which just triggers at its peak. This effect was a particular worry to the BASA experiment due to the PM used. Most experiments use plastic scintillators with very good PM - often two separate PM for the timing and amplitude measurements so that each can be optimised for its specific task. However BASA has a universal PM to record time and amplitude meaning that the time properties are rather poor. This is compounded by the fact that the pulses from many scintillators are summed to obtain one time delay and the summed pulse is obviously distorted.

The solution, or at least partial remedy, lies in using constant fraction discriminators. Here the trigger level is not set at a fixed value but rather at a fixed fraction of the summed pulse height. Provided that all the pulses are the same shape then this should give a constant registering time.

In practice this constant fraction is obtained by a zero-crossing method. Each incoming pulse is inverted and there is also obtained a delayed pulse. The incoming pulse is multiplied by the chosen fraction δ and summed with the delayed full size pulse. The timing is started when the signal crosses the zero point. This should give a time delay independent of the pulse height. The method is illustrated in the lower figure in Figure 2.3 with the pulses approximated as triangular for clarity.

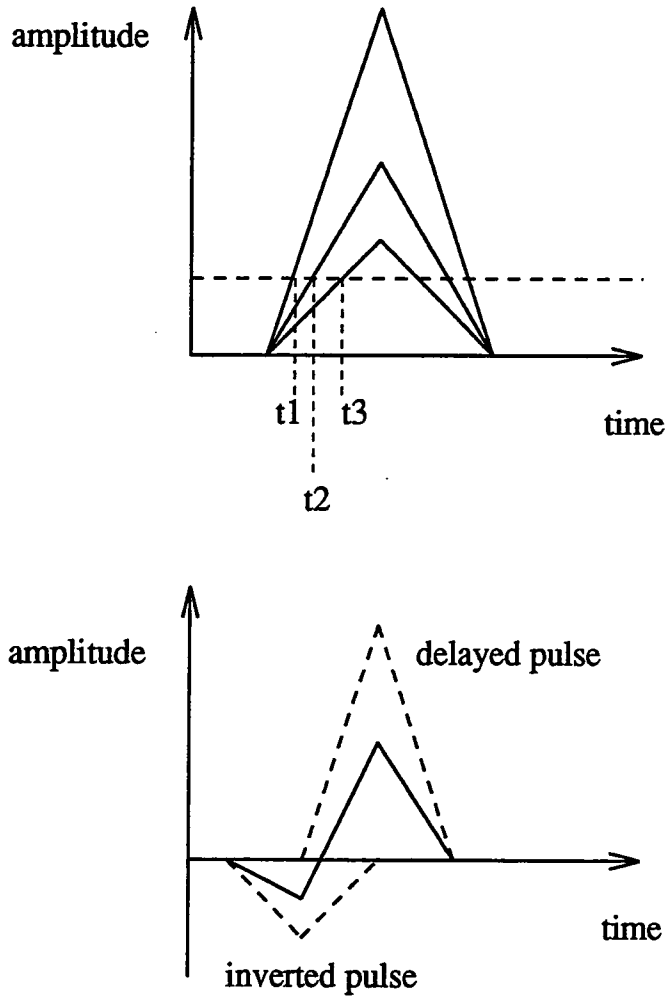

Figure 2.3 3 pulses of different energy triggering at t1,t2,t3 and the zero crossing method of constant fraction discrimination.

Initially the value of the constant fraction used was $\frac{1}{3}$ but subsequent Monte-Carlo simulations indicated that the optimum value of δ tended to zero. There is a limit of course to how low you can take δ due to background pulses and noise so in 1990 the value of δ was changed to $\frac{1}{20}$.

2.3 The Least Squares Method of Arrival Direction Evaluation

Given the time delays of shower events at each of the 6 detectors it is possible knowing the detector locations to apply a least squares fit to obtain the event arrival direction. This assumes a plane wave shower front as no corrections are made to the time delays dependent on the density of particles at each detector to allow for a curved shower front.

The shower axis can be defined by the direction cosines

$$l = \sin\theta \sin\phi$$

$$m = \sin\theta \cos\phi$$

$$n = \cos\theta$$

For a horizontal array the z coordinate is zero and we have that for a plane front

$$ct_i = lx_i + my_i$$

for the i^{th} event. The least squares line minimises the sum of the squares of the distances between the observed and fitted points. Thus we require to minimise

$$\sum_{i=1}^{n} [\, ct_i - (\, lx_i + my_i)]^2$$

Having evaluated l and m it is then possible to evaluate the zenith and azimuth angles (θ, ϕ) of the incoming shower using

$$\phi = \tan^{-1} \frac{l}{m}$$
$$\theta = \sin^{-1} \sqrt{(l^2 + m^2)}$$

In practice rather than using the actual time delay we use the time delay with respect to the mean time delay evaluated over 20 minutes.

2.4 Curvature Effect

The calculations made at BASA are based on the assumption that an incoming EAS presents a plane front to the detectors. In fact this is not the case, shower fronts are known to be curved. Figure 2.4 shows a grossly exaggerated curved wave front and the effect which it can have. The effect shown here is for the worst case when the shower axis lies outside the array.

Monte-Carlo simulations (Alexeenko et al 1990a) indicated that the radius of curvature is well described by a sphere of radius about 3km up to 300m from the shower axis for electrons and a radius of about 4.5km for γ-rays. It is estimated that such an effect would give rise to an error of about 1ns in the time delays. It is possible make a correction for this effect by utilising the fact that the number of particles in the front decreases the further one goes from the shower axis. Because of this, if one measures the number of particles in each detector it is possible to locate the shower core and apply a correction to each time delay based on that detector's distance from the shower core. However this is not possible at present as BASA has no information on the amplitude of the pulses

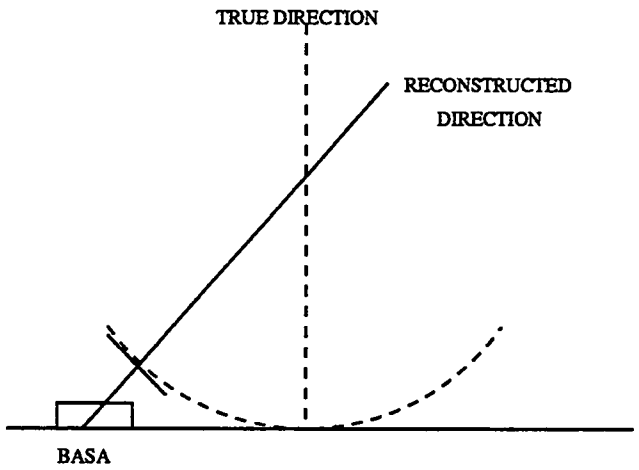

Figure 2.4 The effect of approximating a curved wave front by a plane wave. The effect is greatly exaggerated for clarity.

at each detector. This will be discussed further in Chapter 7 where improvements and developments to BASA are described.

2.5 Estimation of Angular Resolution Using Monte-Carlo Simulations.

Monte-Carlo simulations were carried out (Alexeenko et al 1990b) to obtain the time and energy details of charged particles in EAS taking into account experimental details such as detector layout, trigger conditions and the method of fast timing. The simple cascades generated had corrections in them for the generation of pairs by photons, the Compton effect, the photon effect, ionisation losses of electrons, Bremsstrahlung and diffusion. Only electrons and only vertical showers simulated. The timing of the air shower was folded in with a jitter of σ = 2ns to allow for the particle entering a different part of the detector. The passing of this through the constant fraction discriminator was then simulated.

The best angular resolution occurred as expected for the minimum constant fraction δ although the dependence was not as strong as anticipated. Furthermore it was found that excluding events where the difference of differences (see Chapter 3 for details) were anomalous did not improve the angular resolution. This reflects the fact that this is indeed a difference of differences and the individual t_i could deviate badly but their difference of differences remain normal. However the difference of difference value is a good indicator of detector electronic instabilities and as such is a worthwhile indicator of dubious data.

A method often used to estimate the angular resolution of a detector is to divide the array into 2 sub-arrays and perform 2 separate calculations to find 2 values of a single shower. The difference between the two values should give an idea of the angular resolution. This method works if the two sub-arrays are independent and if one considers only instrumental

effects then indeed they are. However as stated above the main contributions to the errors arise from the shower structure and particle statistics. Thus if the 2 detectors are symmetric with respect to the shower front (as is the case here since most shower axes lie outside the array and there is no selection on events dependent on where their shower axis lies) then the 2 sub-arrays are not independent and will be subject to similar physical effects. Thus the two array method here only directly shows the instrumental effects.

Further numerical simulations (Alexeenko et al 1990a) indicated that 62% of source events will lie within a cell of radius 2.5°. The relationship between source cell size and angular resolution will be discussed in more detail in Chapter 4.

3 DATA ANALYSIS

3.1 Introduction

In total 8 years of data, 1985 - 1992, were analysed. The raw data were subjected to certain tests in an attempt to use only data of a high quality. These were the exclusion of

1. days where the count rate was abnormally low
2. days with anomalous 24 hour time delays
3. events with zenith angle greater than 40°
4. events failing a 'difference of difference' cut in the time delays

3.2 Count Rate

The daily mean count in a 20 minute run was evaluated for each data file. There is no genuine physical effect which could cause for example a drastic fall in pressure to account for the drops of the magnitude observed in the count rate for a single day. (See Figures 3.1 and 3.2) The fall in count rate during 1987 - 1988 is due to a change in the detector

conditions. Previously there were 2 high voltage supplies connected to the detector : one to the 'Carpet' array and another higher voltage supply to the outside detectors. This latter supply ceased to function early in 1987 at which time both the 'Carpet' array and the outer detectors were both connected to the lower voltage supply. This effective decrease in voltage for the outer detectors meant that with the threshold for triggering an event unchanged the threshold was nearer the maximum of the pulse and hence there were greater instabilities in the count rate and less events triggered the detector. It was not until late 1988 that the higher voltage supply was restored to the outer detectors.

It was also decided to exclude any runs within a day which had less than 70% of that day's mean 20 minute count. In this way one could exclude bad runs which had not been numerous enough to contaminate an entire day's data to a noticeable degree.

3.3 Anomalous Time Delays

In parallel with the count rate criteria, the mean time delays over 24 hours were evaluated for each of the 6 detector channels. Zero time delays in channels 5 or 6 are perfectly acceptable as event arrival direction reconstruction is still then possible. An electronic fault resulted in zero time delays (ie the absence of a time delay) occasionally being erroneously registered as one or two ns. To overcome this a time delay of < 8ns was deemed non-physical (with the average time delay being ~ 120 ns there is no way in which such a small time delay could be meaningful) and the time delay set to zero.

The above two tests marked days in which there was clearly a problem. There was still however the hope that some of the data from such days was salvageable. To this end the run by run count rates and time delays were examined (See Appendix 1) to see if the

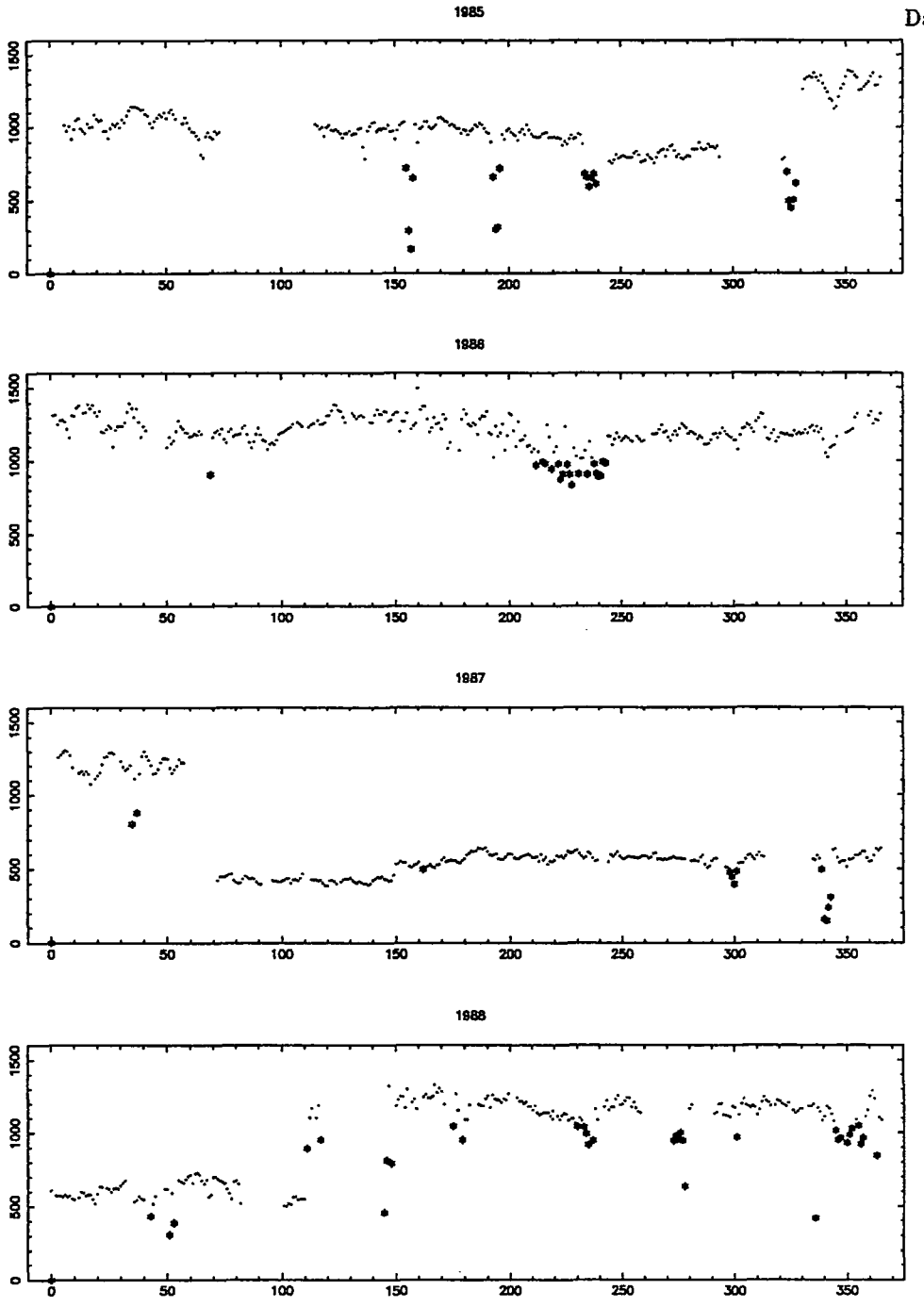

Figure 3.1 The mean 20 minute counts for each day of 1985 - 1988. The day number starting from the 1st of January is plotted on the x-axis and the corresponding count is on the y-axis. The filled stars denote days excluded due to anomalous count rates.

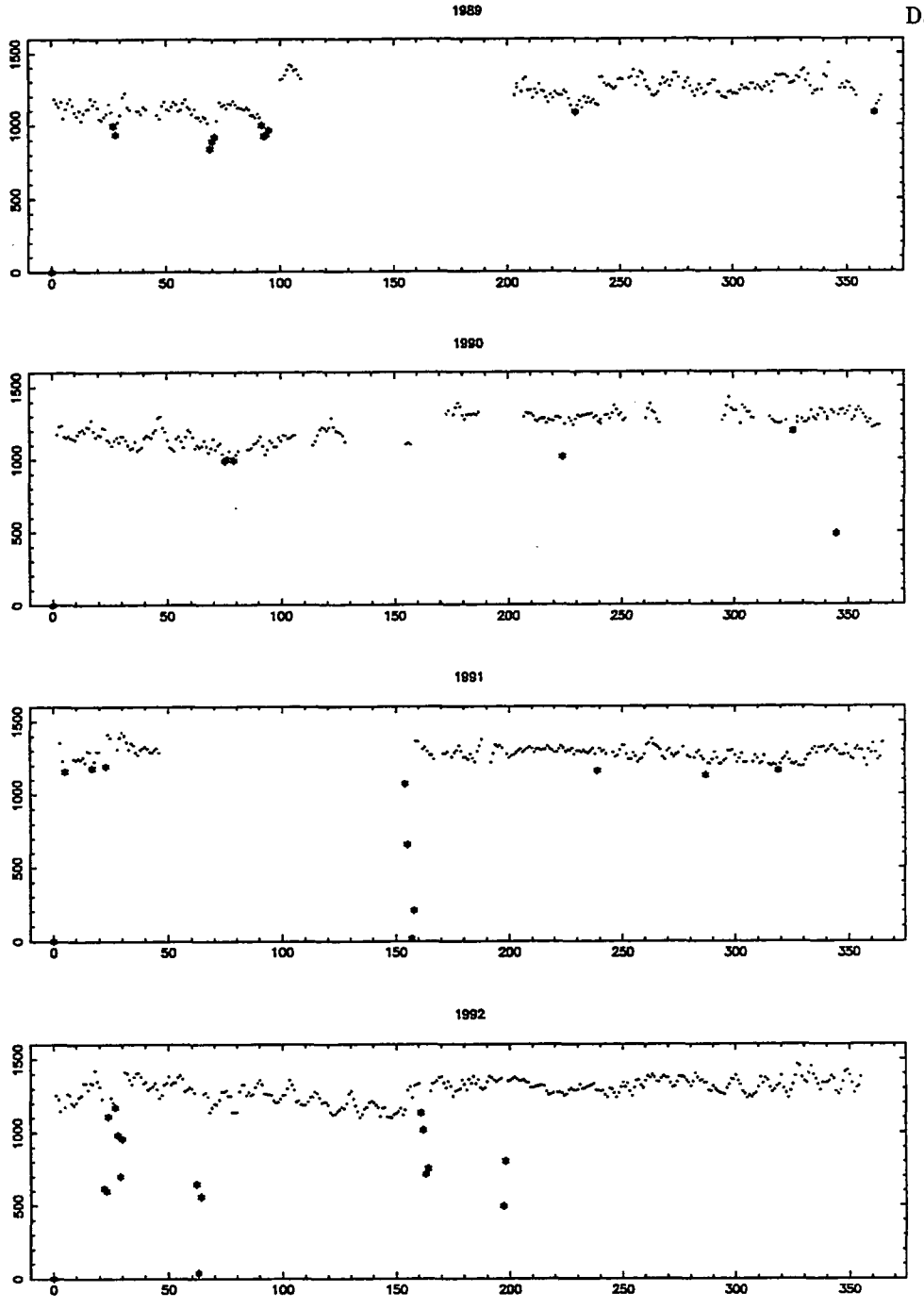

Figure 3.2 The mean 20 minute counts for each day of 1989 - 1992. The day number starting from the 1st of January is plotted on the x-axis and the corresponding count is on the y-axis. The filled stars denote days excluded due to anomalous count rates.

exclusion of a number of runs' data would render the day fit for inclusion. A file was created of all such runs.

From 20 minute results a list of runs in which there is a large step change in the time delays was compiled to be added to the above file for exclusion from further work. As a rough guide to the order of magnitude of step change to be excluded the change in arrival direction of a given event for different time delays was calculated where the separation between events with RA and dec (α_1, δ_1) and (α_2, δ_2) is

$\cos^{-1}(\cos\delta_1 \cos\delta_2 \cos(\alpha_1 - \alpha_2) + \sin\delta_1 \sin\delta_2)$ This indicated that a difference of 1° was not exceeded provided the time delay increment was

- $\leq$ 4ns for channel 1 (and therefore presumably 2, 3, 4 also.)
- $\leq$ 6ns for channel 6 (this simply being indicative of the fact that channels 5 and 6 are $\frac{3}{2}$ times as far as the other channels, hence their time delays are larger and a given increment will have less effect.

These runs could then be excluded from any further analysis as could a now diminished set of pathological days. Below are shown the number of days for which data files existed and those which were selected for the final analysis :

Year	Days with data files	Days used
1985	283	257
1986	330	274
1987	305	270
1988	260	206
1989	246	223
1990	246	231
1991	232	212
1992	353	311
1985-1992	2255	1984

3.4 Zenith Angle

A shower which has a large zenith angle has to traverse a greater depth of atmosphere and will upon arriving at the detector have a smaller shower size than a low zenith angle shower of comparable energy. (See Figure 3.3)

Hence such a shower has a lower probability of triggering the array than a like energy low zenith angle shower. The exact relation is :

$$N_e(z) = N_{max} \exp\left(\frac{-h \sec z}{\lambda}\right)$$

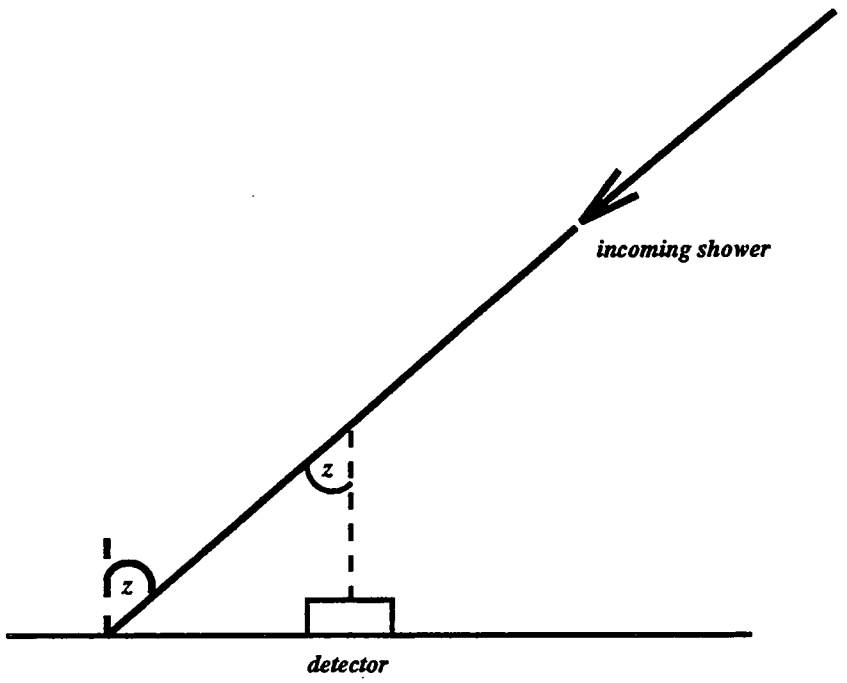

Figure 3.3 An incoming shower of zenith angle z.

where

- N_e is the size of the shower at sea level
- N_{max} is the size of the shower at its maximum development
- h is the depth of atmosphere traversed in gm cm^{-2}
- z is the zenith angle
- λ is the attenuation length.

Given the geographical location of BASA in a mountainous region it is unlikely that a shower could penetrate the amount of atmosphere required at a zenith angle of greater than 40°. Therefore all such showers are likely to be spurious and are omitted.

3.5 Difference of Differences

Due to the geometry of the array for any azimuthal direction of the incident shower two parallel pairs of outside detectors present the same overall detector to the shower. Thus the difference between the pairs $\Delta t = (t_1 - t_2) - (t_3 - t_4)$ where t_i is the time delay of an event recorded in channel i, characterises the uncertainty in the arrival direction evaluation. (The nonstability of the start signal, which is in fact quite large due to the large linear dimensions of the Carpet, is excluded from this value.) That theoretically Δt should be zero can be seen from the following: Here we assume a plane wavefront with velocity V and let the pulse starting time be T_1 to T_4 for each of the 4 outer detectors and T_0 for the central 'Carpet' detector (see Figure 3.4).

Clearly $d_1 + d_2 = \alpha$ and $d_3 + d_4 = \alpha$.

$$\text{Distance } AC = V(T_3 - T_0)$$

$$BC = V(T_4 - T_0)$$

$$DC = V(T_2 - T_0)$$

$$EC = V(T_1 - T_0)$$

$$\text{Thus } t_1 - t_2 = \frac{ED}{V}$$

$$\text{and } t_3 - t_4 = \frac{AB}{V}$$

Now the sine rule gives

$$\frac{D_i}{\sin\phi} = \frac{d_i}{\sin\theta} \quad i = 1,4$$

$$\text{thus } D_1 + D_2 = \frac{d_1 \sin\phi}{\sin\theta} + \frac{d_2 \sin\phi}{\sin\theta} = (d_1 + d_2)\frac{\sin\phi}{\sin\theta}$$

$$\text{and } D_3 + D_4 = \frac{d_3 \sin\phi}{\sin\theta} + \frac{d_4 \sin\phi}{\sin\theta} = (d_3 + d_4)\frac{\sin\phi}{\sin\theta}$$

$$\text{giving } D_1 + D_2 = D_3 + D_4 \text{ since } d_1 + d_2 = \alpha = d_3 + d_4$$

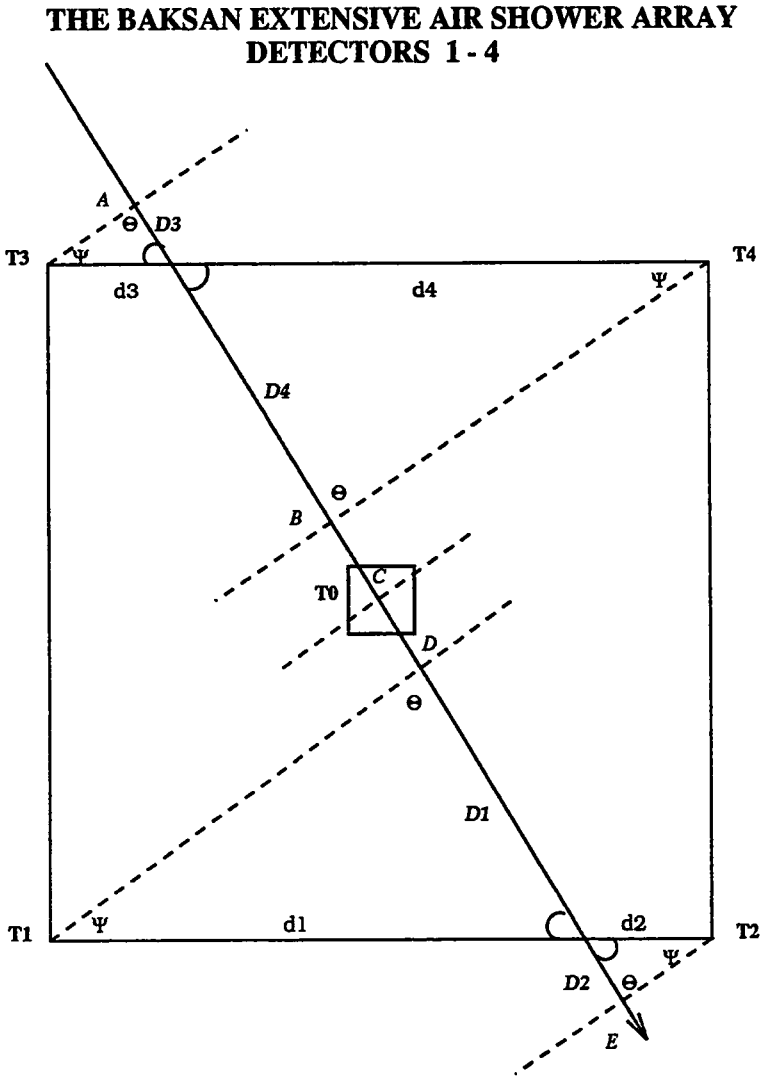

Figure 3.4 The geometry of the inner 4 detectors of BASA - the so called 'Carpet' detector.

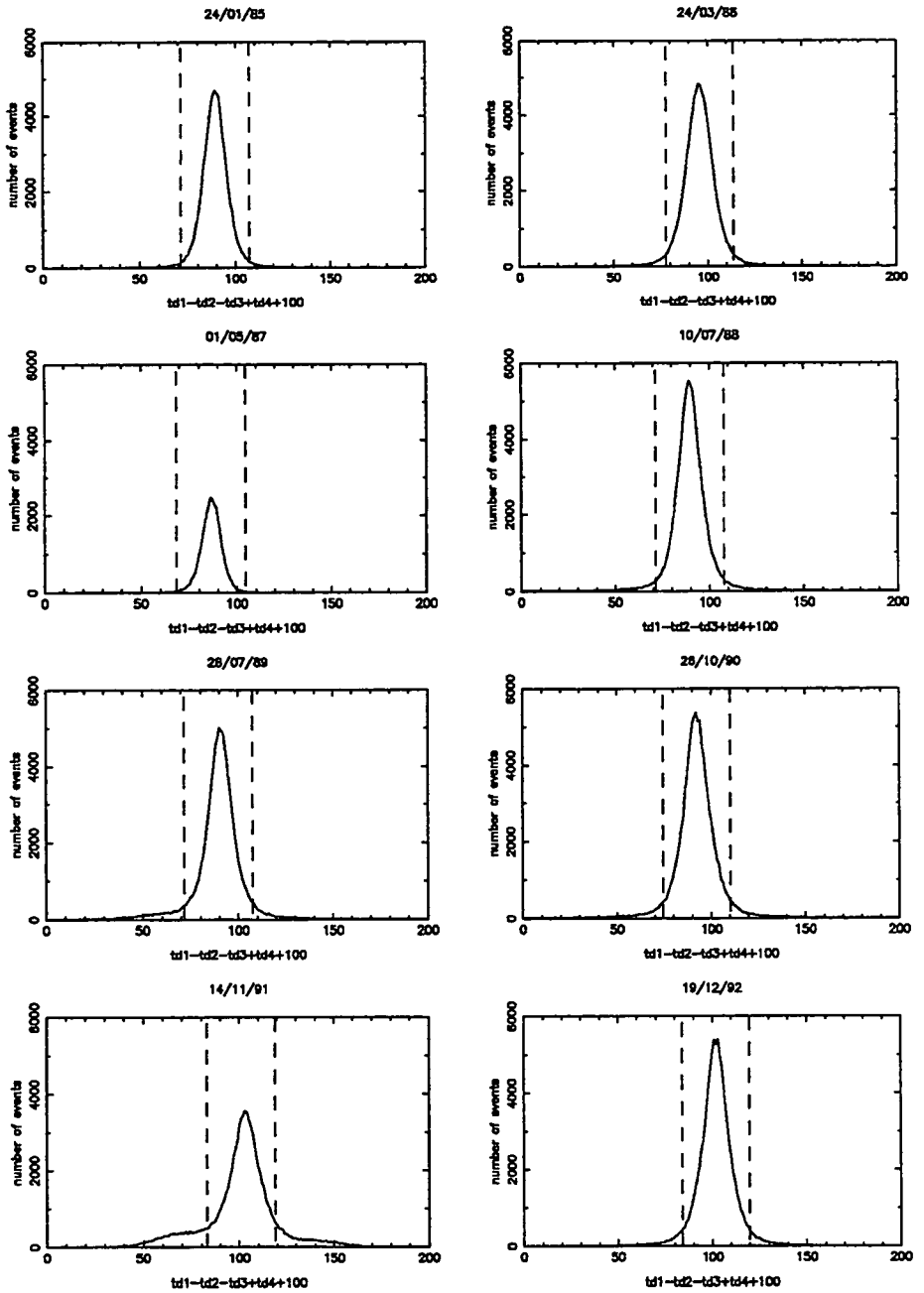

Figure 3.5 The 'difference of difference' distribution for 8 random days in 1985 - 1992. The dotted line in each case shows the ±18ns cut-off.

In practice there will be some variation around a mean value. Evaluating the mean over a 20 minute period showed that a variation about the mean of ± 18ns gave a statistically sound sample. Thus events with this so-called 'difference of differences' > 18ns and < -18ns were rejected. Figure 3.5 show this distribution for one day selected at random from each of the 8 years. The mean value is taken to be the value of the difference of differences for the mean 20 minute time delays. Clearly any events failing the ± 18ns selection criterion are anomalous.

Finally a correction had to be made to some of the event arrival times. Due to an electronic fault the times recorded sometimes had 8 seconds dropped from their value. This could easily be corrected by a code which checked for sequentially increasing arrival times and added 8 seconds to those which dropped behind.

4 SOLAR AND LUNAR SHADOWING

4.1 Introduction

It was as far back as 1957 that Clark first postulated it should be possible to observe a dip in the count of cosmic rays at the position of both the Sun and the Moon (Clark 1957). Both these objects would act as a block to the cosmic rays which otherwise are almost completely isotropic due to their many interactions with the Galactic magnetic field. Certainly the Sun's magnetic field will bend the cosmic rays a little but at the energies discussed in this thesis this effect is negligible compared to the typical angular resolution of an extensive air shower array with which these cosmic rays are measured.

It is only in more recent times with the advent of EAS arrays with improving angular resolution that it has been possible to put theory into practice. It is by no means an easy task. Given that the angular diameter of the Sun and the Moon is only approximately 0.52° the effect is a small one and the data sample needed will be correspondingly high. We are aided to some degree by the fact that the Sun and the Moon have the same apparent angular diameter on the sky and therefore it is possible to combine the data for both objects.

Given that one can observe this dip in count rate it should be possible from this curve to obtain the angular resolution, σ , of the EAS array in question. This is an important parameter since for point sources the signal to background ratio varies as$\frac{1}{\sigma^2}$. It is on this basis that the search area for a point source is decided upon.

The first group to observe this effect was the CYGNUS group (Alexandreas *et al* 1991a, 1991b) Their most recent analysis (Alexandreas *et al* 1993d) using data obtained from 1986-1992 gives approximately 250,000 events within 2.5° of the centre of the Sun or Moon. From this they infer an angular resolution of the array of 0.70° for events with no data cuts imposed upon them. They find that the angular resolution is strongly dependent on the number of particles detected in each event.

The second group to have succeeded is the HEGRA group at La Palma (Karle *et al* 1991). They obtained 54,901 events within 5° of the Moon and 54,656 within 5° of the centre of the Sun. From this dataset they claim to observe a 142 events deficit in a 0.65° bin centred on the Sun compared with a mean count of 1820 corresponding to a 3.3σ effect. This gives an angular resolution of less than 1°. Their background was taken to be the mean count between 1° and 5° of the Sun/Moon. It is worth noting that this effect is only seen when the shower front is fitted with a cone. When a plane wave approximation is used no effect is seen indicative perhaps of the loss of angular resolution that such an approximation necessarily brings.

The EAS-TOP group (Navarra *et al* 1992) claim to have seen the Sun and Moon shadowing at the 2.7σ level giving an angular resolution of 0.83°. The JANZOS group (Allen *et al* 1993) have also observed the Sun/Moon shadow obtaining an angular resolution of better than about 1.2°.

CASA/MIA are the only group so far to have a large enough dataset to observe this effect with the Sun and the Moon separately (Barione *et al* 1993d). From 1990-1992 2.8 million

events passed their selection criteria within $\pm 12°$ of the centre of the Sun or Moon. One of these criteria was that the shower axis must lie within the array boundary. When they looked at only those showers with $N_e > 10^{4.5}$ they observed the Moon at the 5.7σ level and the Sun at the 4.8σ level giving an angular resolution of 0.49° and 0.58° respectively. When no cut was made on shower size they found an angular resolution of 0.77° and 0.89° respectively.

4.2 Data Analysis

The method described above was implemented on the 8 years of data. BASA cannot observe declinations less than about 2° and thus, as events within 5° of the Sun were required, only those days for which the Sun's declination was above 8° were used. In this way equal exposure was given to all parts of the 5° circle. The solar ecliptic coordinates were calculated for the beginning of each day for which an 'accepted' (as described in Chapter 3) data file was present. A list of all events within a 20°x20° RA and δ field were obtained. As a rough cut the daily value of the solar coordinate was used and all events within 25°x25° considered. For these, the exact solar position at the cosmic ray event time was calculated and the 20°x20° field data recorded. Annuli of equal solid angle were obtained centred on the Sun and the events within 5° of the Sun binned into them.

All events were recorded within 5 degrees of the Sun and binned into annuli of equal solid angle for an initial annulus of radius 0.5°.

4.2.1 Solar Coordinates

The RA and δ of the Sun for was calculated from the formulae given in the Astronomical Almanac (C2) (See Figure 4.1). These formulae gave the apparent coordinates of the Sun to a precision of 0.01° - well in excess of what was required here considering the angular resolution of BASA. Parallax corrections were not deemed necessary for such precision. The formulae used were as follows.

$$\begin{aligned} n &= \text{number of days from JD2000.0} \\ &= JD - 245\,1545.0 \\ &= \alpha + \text{day of year} + \text{fraction of day from UT} \end{aligned}$$

YEAR	α
1985	-5479.5
1986	-5114.5
1987	-4749.5
1988	-4384.5
1989	-4018.5
1990	-3653.5
1991	-3288.5
1991	-2923.5

- Mean longitude of the Sun corrected for aberration :

  $L = 280.460° + 0.985\,6474° \times n$

- Mean anomaly :

  $g = 357.528° + 0.985\,6003° \times n$

- L and g are placed in the range 0° - 360°

- Ecliptic longitude:

  $\lambda = L + 1.915° \times \sin(g) - 0.20° \times \sin(2g)$

- Ecliptic latitude:

$$\beta = 0$$

- Obliquity of the ecliptic :

$$\epsilon = 23.439° - 0.000\ 0004° \times n$$

- Right ascension (in the same quadrant as ϵ :

$$\alpha = \tan^{-1}(\cos \epsilon \tan \delta)$$

- Declination :

$$\delta = \sin^{-1} (\sin \epsilon \sin \lambda)$$

4.2.2 Lunar Coordinates

The procedure described above for the Sun was carried out again for the Moon. The lunar ecliptic coordinates were calculated using a sub-routine kindly supplied by the CYGNUS collaboration (Ellsworth R. 1992 private communication) which is based on an algorithm obtained from the U.S. Naval Observatory (See Figure 4.2). Due to the Moon's proximity to the Earth it is necessary to apply parallax corrections to the coordinates obtained in this way. These were based on the standard formulae (eg Duffet-Smith 1981) We allow for the fact that the Earth is not a perfect sphere but is flattened along the line joining the North and South poles. Given that the geocentric coordinates of the Moon at a given time are (α, δ) then its apparent coordinates measured at a given position are (α', δ') where

$$\alpha' = \alpha - \tan^{-1} \frac{\rho \cos\phi' \sin H}{r\cos\delta - \rho\cos\phi' \cos H}$$

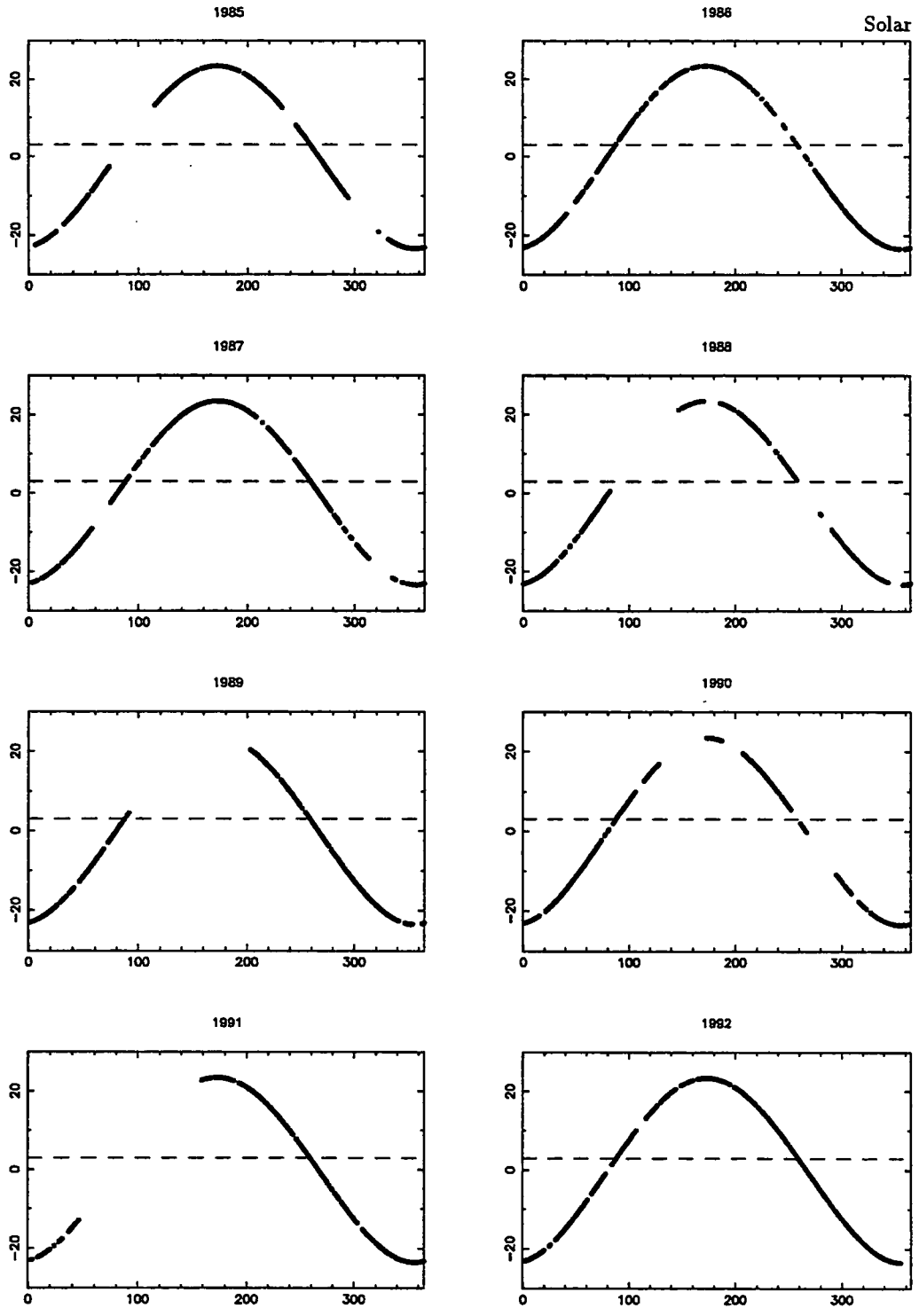

Figure 4.1 The solar declination calculated for each day's data for each of the 8 years analysed. The dashed lines shows the lower declination limit of acceptable data given the latitude of BASA.

$$H' = H + \tan^{-1}\frac{\rho\cos\phi'\sin H}{r\cos\delta - \rho\cos\phi'\cos H}$$

$$\delta' = \tan^{-1}(\cos H'[\frac{r\sin\delta - \rho\sin\phi'}{r\cos\delta\cos H - \rho\cos\phi'}])$$

r = distance of Moon from centre of the Earth in Earth − radii units

ϕ' = the geocentric latitude of the array

In practice we do not obtain the geocentric latitude explicitly but rather implicitly in the expressions $\rho\sin\phi'$ and $\rho\cos\phi$ viz:

$$\rho\sin\phi' = 0.996647\sin u + \frac{h}{6,378,140}\sin\phi$$

$$\rho\cos\phi = \cos u + \frac{h}{6,378,140}\cos\phi$$

where $u = \tan^{-1}(0.996647\tan\phi)$

ϕ = the geographical latitude of the array

h = the height of the array above sea level

4.3 Annuli of Equal Solid Angle

The solid angle limits were calculated as follows. The solid angle of a body of radius R at a distance d from the observer is $\omega = \frac{\pi R^2}{d^2}$. The solid angle between consecutive annuli is:

$$\text{Solid angle} = \int_{\cos\theta_{n-1}}^{\cos\theta_n} d\theta$$
$$= 2\pi(\cos\theta_{n-1} - \cos\theta_n)$$

Thus to obtain annuli of equal solid angle one must set $\cos\theta_{n-1} - \cos\theta_n$ = constant. One must find a value of r1, the initial radius of the bin, which strikes a balance between r1 being sufficiently small for the 0.52° Sun to make a clear impact and r1 being sufficiently

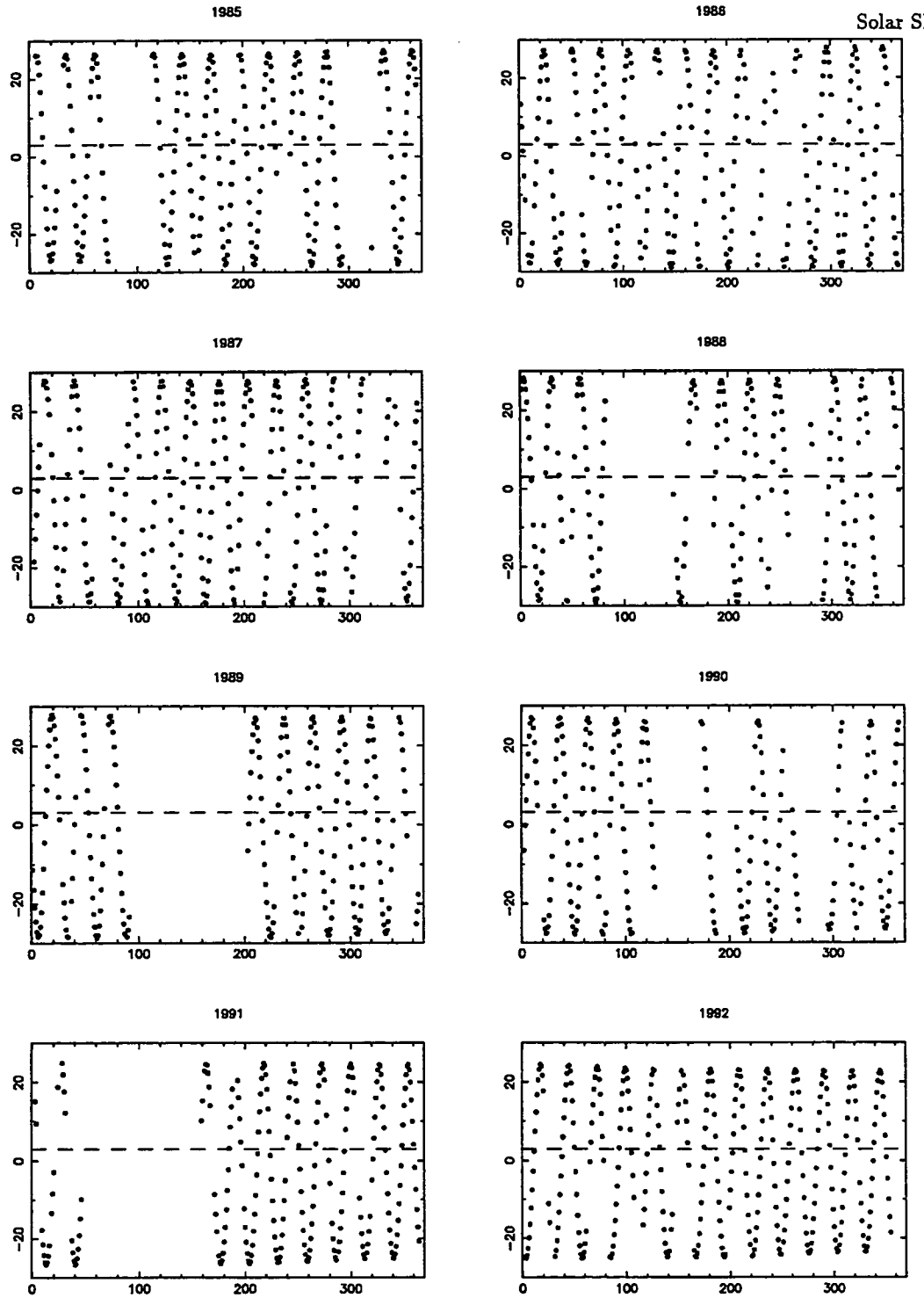

Figure 4.2 The lunar declination (corrected for parallax) calculated for each day's data for each of the 8 years analysed. The dashed lines shows the lower declination limit of acceptable data given the latitude of BASA.

large for there to be a significant number of events in each bin. The latter would not pose a problem if we could obtain a high enough count. Here r1 is taken to be 0.5°.

4.4 Angular Resolution

The importance in obtaining the angular resolution of an array lies in the fact that there is a direct relationship between it and the size of on-source cell which one should choose in the search for point sources in order to optimise the signal to noise ratio. Consider the following. The probability of an event arriving for the hemisphere above the array is set to one and the source direction is set at θ=0°. Because of the angular resolution of the array the point source signal will be smeared to a Gaussian distribution. We assume the distribution to be two dimensional and the width σ to give the angular resolution. Then the probability of observing a signal from θ in dΩ is

$$p(\Omega)d\Omega = \frac{1}{2\pi\sigma^2} exp(^{-\frac{\theta^2}{2\sigma^2}})d\Omega$$

The factor $\frac{1}{2\pi\sigma^2}$ is a normalisation factor resulting from the fact that the probability of an event arriving for the hemisphere above the array is set to one. Consider a cone of radius β around the source position. The number of events from the source is given by

$$\begin{aligned} N_{LS} &= n_0 \int_\Omega p(\Omega)d\Omega \\ &= \frac{n_0}{2\pi\sigma^2} \int_0^{2\pi} d\phi \int_0^{\beta} exp(^{-\frac{\theta^2}{2\sigma^2}}) sin\theta\theta \end{aligned}$$

When β is small then we may approximate sinβ approximately equal to β. In this case

$$N_{LS} = \frac{n_0}{2\pi\sigma^2} 2\pi \int_0^{\beta} exp(^{-\frac{\theta^2}{2\sigma^2}})\theta d\theta$$

Setting x = $\frac{\theta^2}{2}$ we find dx = $\frac{2\theta d\theta}{2} = \theta d\theta$. Thus

$$N_{LS} = \frac{n_0}{2\pi\sigma^2} 2\pi \int_0^{\frac{\beta^2}{2}} exp(^{-\frac{x}{\sigma^2}}) dx$$
$$= n_0(1 - exp(^{-\frac{\beta^2}{2\sigma^2}}))$$

We wish to compare this with an isotropic CR background flux.

$$N_{CR} = n_A \int_\Omega d\Omega$$
$$= n_A \int_0^{2\pi} d\phi \int_0^{\beta} sin\theta d\theta$$
$$= 2\pi n_A(1 - cos\beta)$$

If we assume that the noise on the background is Poissonian then the noise M_{CR} is given by

$$M_{CR} = \sqrt{N_{CR}}$$
$$= \sqrt{(2\pi n_A(1 - cos\beta))}$$

and the signal-noise ratio is given by

$$\frac{N_{LS}}{M_{CR}} = \frac{n_0(1 - exp(^{-\frac{\beta^2}{2\sigma^2}}))}{\sqrt{(2\pi n_A(1 - cos\beta))}}$$

Figure 4.3 shows the function $\alpha = \frac{1-exp(^{-\frac{\beta^2}{2\sigma^2}})}{\sqrt{(1-cos\beta)}}$. The maximum of this function occurs for $\frac{\beta}{\sigma} = 1.6$ and varies only slightly for different σ. Thus to maximise the signal to noise we take the ratio $\frac{\beta}{\sigma}$ to be 1.6.

In this case $N_{LS} = 0.72\ n_0$. So we find that 72% of events from a source will end up in a cell of radius 1.6σ. It is this relation which is used, together with an estimate of the angular resolution, to decide upon what on-source cell size should be chosen.

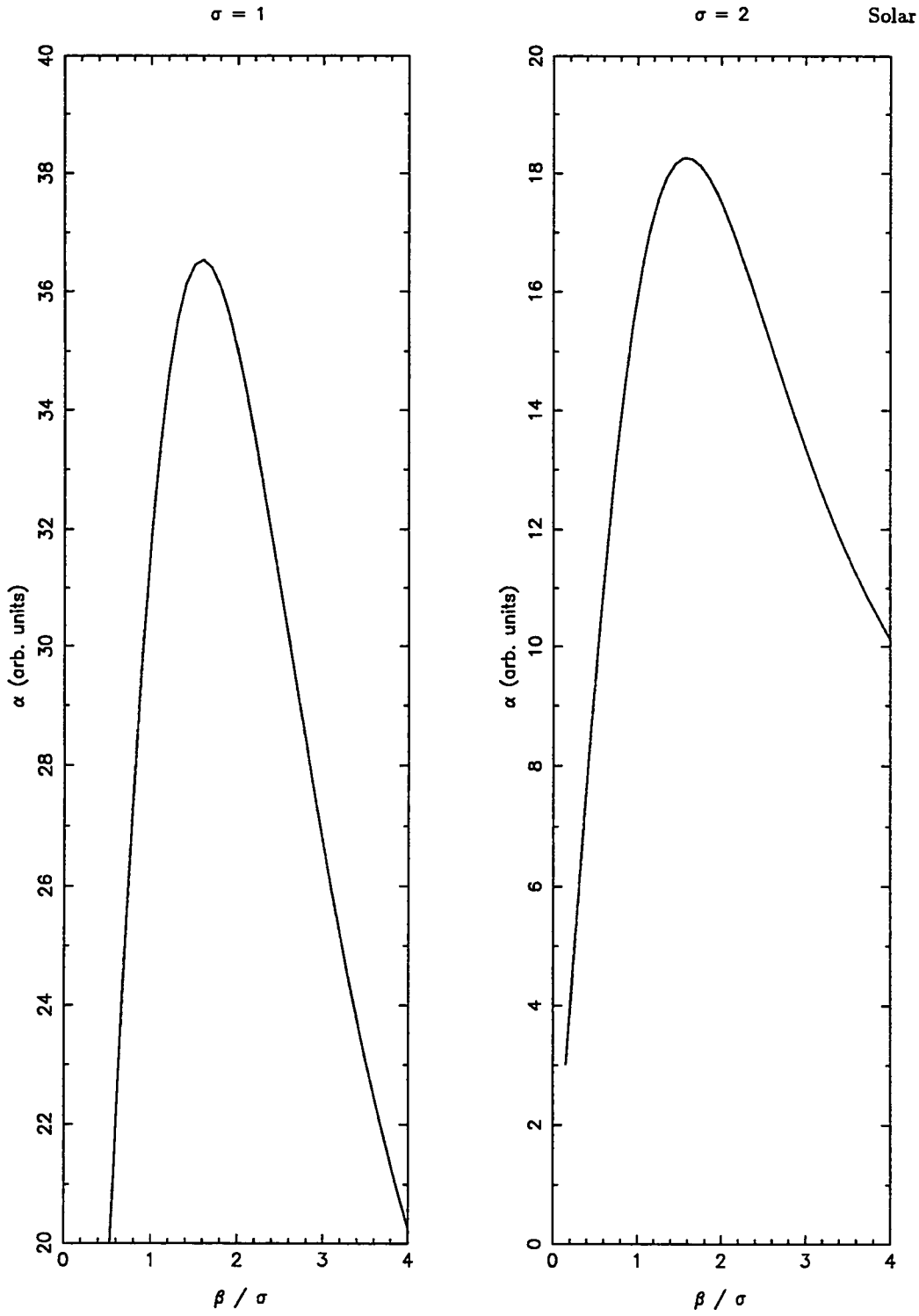

Figure 4.3 The ratio α for varying $\frac{\beta}{\sigma}$. The left hand plot show $\sigma = 1$, the right hand $\sigma = 2$. The maximum of α occurs when $\frac{\beta}{\sigma} \sim 1.6$

4.5 Predicted Distribution For a Given σ

When predicting the distribution of events around the Sun or Moon for a given σ it is necessary to take into account an effect generated by the HA acceptance distribution of the array. Figure 4.4 shows schematically this distribution of events, n , with hour angle, HA. Also shown are $\frac{dn}{dHA}$ and $\frac{d^2n}{dHA^2}$. This shows that $\frac{d^2n}{dHA^2}$ is negative over the most important part of the HA distribution ie the peak where most of the showers come from. This means that one would expect the number of showers to fall off with radial distance from any given point.

To allow for this effect, rather than integrating over an annulus of radius α, we use a simple approximation and take the average of 4 points surrounding a chosen point of HA and declination (h,δ). Thus we find the average number of events $\frac{N(h+\alpha,\delta)+N(h-\alpha,\delta)+N(h,\delta+\alpha)+N(h,\delta-\alpha)}{4}$ to compare with N(h,δ) the number of events at (h,δ). The results are given as a ratio of N(h,δ) to the average value obtained as described.

This was done using HA-δ distributions binned in 2° bins. The cosδ effect could be ignored safely as the maximum declination reached by the Sun is 23°. N(h,δ) was evaluated for each point along a HA strip and compared to the average of its appropriate 4 neighbours. The comparison was made for neighbours at 2°, 4° and 6°. This was then repeated for all declinations. Strictly one should sum the declination sweeps weighted according to the actual declination exposure of the data from 1985-1992 but the value of the comparison ratio did not vary greatly with declination and furthermore most of the events came from the same declination (23°).

The table below shows how the number of showers falls off from any central point. The results show the number of events at a certain distance as a percentage of the number at the central point.

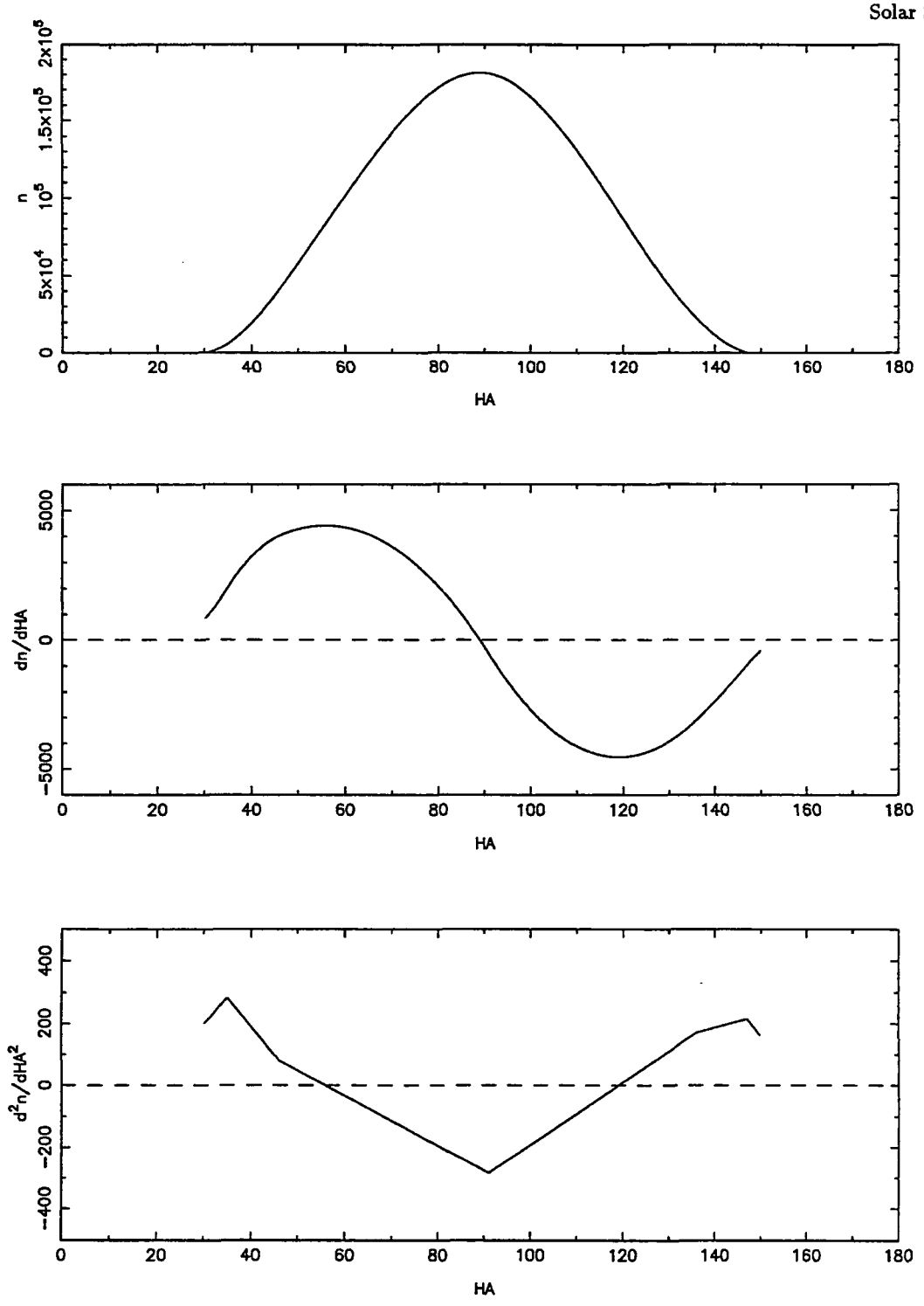

Figure 4.4 The upper figure shows a smoothed HA distribution. The lower two figures show the first and second derivatives respectively. The coarseness of the latter can be attributed to the numerical procedure, noise in the original data and discrete sampling.

Distance	%
0°	100.0
2°	99.89
4°	99.51
6°	97.87

This fall-off effect was then incorporated into the predicted distribution for any given angular resolution. The effect can be represented by a polynomial

$$r = 1 + (13.92x + 8.0x^2 - 1.8958x^3) \times 10^{-4}$$

There will also be an effect from the declination distribution. $\frac{d^2n}{d\delta^2}$ may be negative in places but one would expect this to cancel out with places where it is positive. In any case this is accounted for when one calculates the fall-off effect empirically as has been done here.

4.6 Maximum-Likelihood Method

We follow a similar method to that described by Alexandreas *et al* (1991a) . We assume that the angular resolution function is a 2-d Gaussian distribution. A variable z is used to describe the probability used to construct the likelihood.

$$z = \frac{1 - cos(\beta)}{1 - cos(\beta_{max})}$$

where β is the angle between the shower arrival direction and the sun or the Moon. The distribution of z can be shown to be

$$\frac{dP}{dz} \sim 1 - \frac{\beta_{MS}^2}{2\sigma^2} exp(\frac{-\beta(z)^2}{2\sigma_1^2})$$

where β_{MS} is the angular radius of the Sun or Moon and $\sigma_1 \sim \sigma$, the angular resolution of the array. In fact for $\sigma > 0.5°$ the difference between σ_1 and σ is $< 0.02°$.

The likelihood is the product of the normalised probability $\frac{dP}{dz}$ for each event in the sample. The normalisation of the probability ensures that the likelihood will have a maximum at the correct σ if there is shadowing in the data.

Combining the previously mentioned fall-off effect we calculate

$$F(\beta) = P(\beta)r(\beta) = [1 - \frac{\beta_{MS}^2}{2\sigma^2} exp(\frac{-\beta(z)^2}{2\sigma_1^2})][1 + (13.92\beta + 8.0\beta^2 - 1.8958\beta^3) \times 10^{-4}]$$

.

4.7 Results

In all for the 8 years of data a total of 213,313 events were recorded within 5° of the Sun or Moon. Figures 4.5 shows the number of events within annuli of increasing radius around the Sun and Moon. The different plots show the predicted distributions for various angular resolutions (σ). In all cases the radius of the first annulus is 0.5°. Figure 4.6 shows the same plots for a subset of the data from 1985 - 1992. Here data is only included where the difference of difference distribution width does not fluctuate greatly. In practice this means including only data from 1985 - 1987 and from part of 1990 and 1992. It was not anticipated that there should be marked difference in results but the latter subset would give data of a slightly higher quality. Any increase in data quality is however offset to some extent by a reduction in the statistics - this subset of data consists of 106,862 events within 5° of the Sun or Moon.

We see that the curves are consistent with an angular resolution of approximately 2.5° as previously thought. By eye the fit for 2.5° looks quite good for small β ie within about 1.5° of the Sun. However chi-squared continues to decrease for increasing σ - in fact it

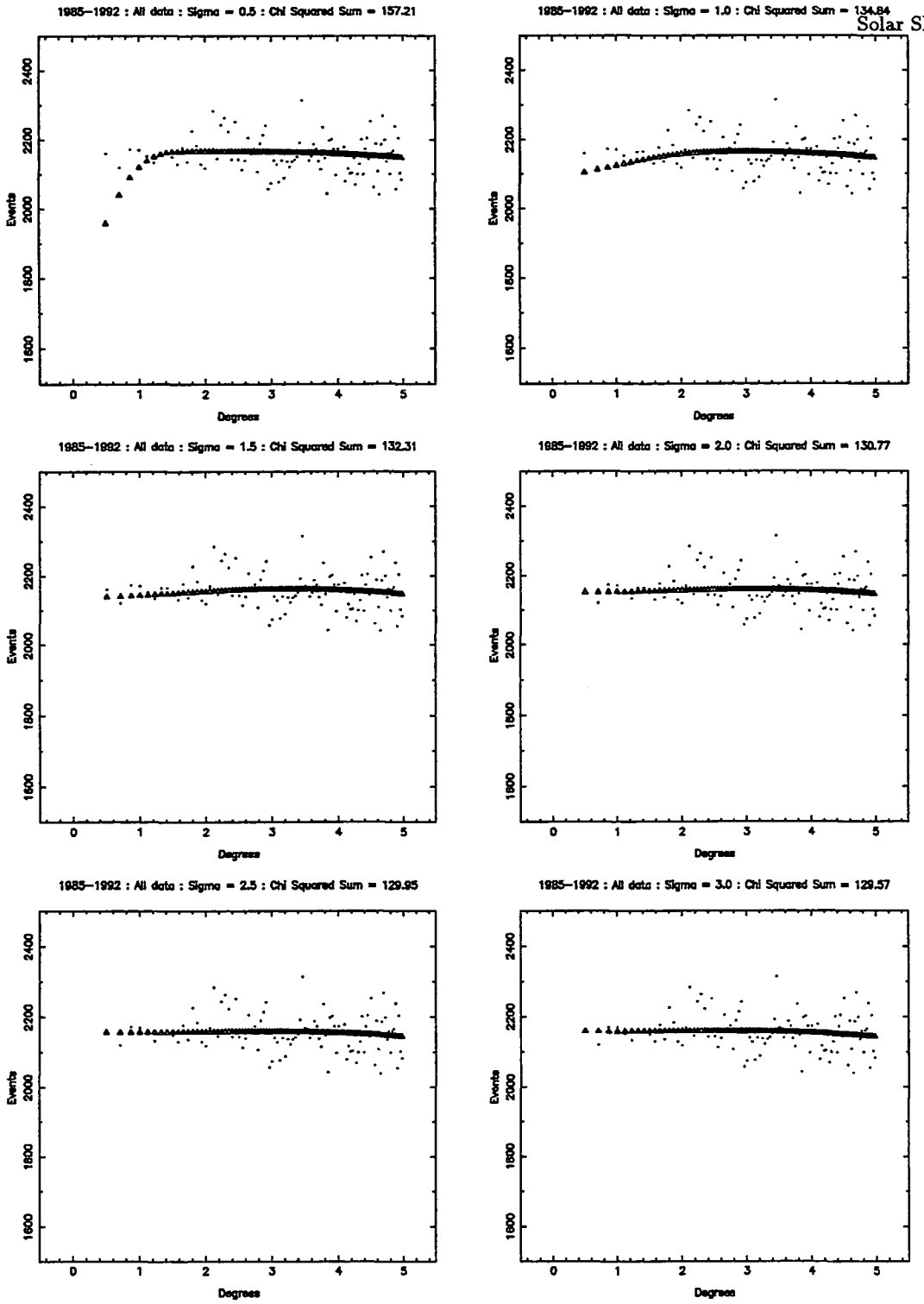

Figure 4.5 The events within 5° degrees of the Sun or Moon for 1985-1992. The triangles show the predicted distributions for angular resolutions 0.5° up to 3.0° in steps of 0.5°.

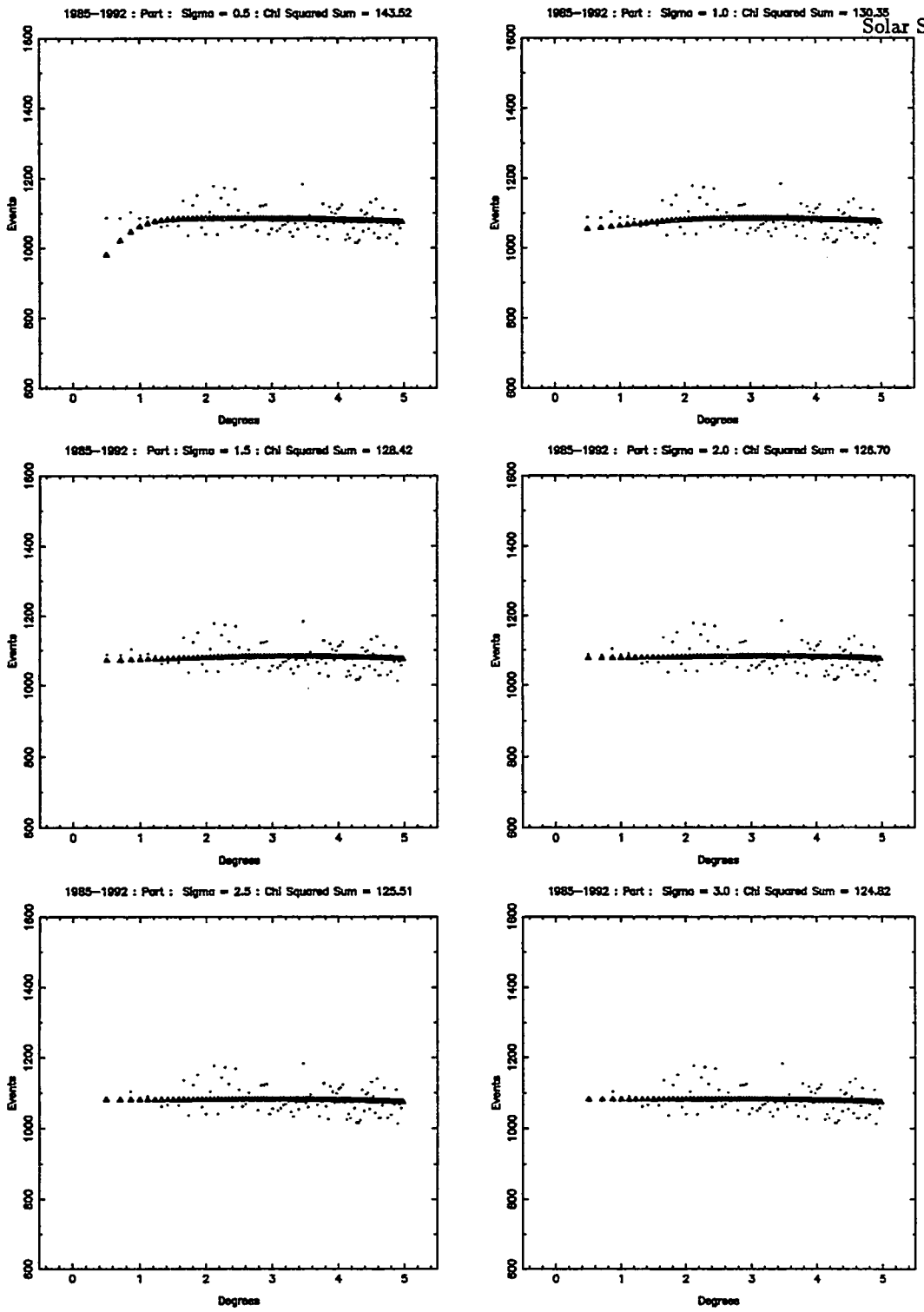

Figure 4.6 The events within 5° degrees of the Sun or Moon for part of 1985-1992. The triangles show the predicted distributions for angular resolutions 0.5° up to 3.0° in steps of 0.5°.

does so up to about σ=6° although the variations get very small and the difference in expected curves are practically negligible when one get to such large σ.

The chi-squared values for the subset of data are slightly smaller but there is not a dramatic difference and the general trends are the same. This might give us some confidence in the quality of the data set as a whole and justify including all the data in the search for point sources. There is one point in particular which has a particularly high chi-squared value of approximately 11 for the whole data set and approximately 9 for the subset of data.

Although we are unable to say we have detected the Sun and the Moon at a particular confidence level as have other groups we can conclude that the angular resolution is about 2.5°-3.0° consistent with the value previously obtained from Monte-Carlo simulations.

4.8 Angular Resolution from Crab Burst

As will be described in Chapter 5, the original analysis of BASA data revealed a burst from the Crab on 23rd February 1989. An excess of 21 events was observed with 55 being observed when 34 were expected from an on-source circle of radius 2.5°. Thus the excess number of events expected in a circle of radius R when the angular resolution is σ is given by

$$f(R,\sigma) = 21 \times (1 - exp(\frac{-R^2}{2\sigma^2})$$

This was calculated for given R for σ = 1°, 1.5° and 2.0°. To obtain the predicted number of events within each circle of radius R for a uniform distribution, the total number of events within a circle of radius 6° was measured. 229 events were found and since an observed excess of 21 events were thought to be from the Crab the remaining 208 events

were distributed uniformly throughout the 6° circle. Then the observed number of counts for a given R were compared to this uniform distribution.

This gave observed excess counts which could be compared with the predictions for various σ. The data seemed to indicate a value of σ somewhere between 1.5° and 2.0° but with the rather small statistics the errors on the observed excesses were high (Lidvansky A.L. private communication).

REFERENCES : CHAPTER 4

Alexandreas D.E. *et al* Phys. Rev. D. **43**, 1735 (1991a)

Alexandreas D.E. *et al* 22^{nd} I.C.R.C. **Vol 2** p672 (1991b)

Alexandreas D.E. *et al* 23^{rd} I.C.R.C. **Vol 1** (1993) p223

Allen W.H. *et al* 23^{rd} I.C.R.C. **Vol 1** (1993) p227

Borione J. *et al* 23^{rd}I.C.R.C. **Vol 1** (1993) p220

Clark G.W. Phys. Rev. **108** , 450 (1957)

Duffet-Smith Practical Astronomy with your Calculator (1981)

Karle A. *et al* AIP Conf Proc Ann Arbor **220** 127 (1990)

Navarra G. *et al* Geneva European Cosmic Ray Conference (1992)

5 POINT SOURCES

5.1 Introduction

In total 8 years of data, 1985 - 1992 , were analysed subject to the selection criteria described in Chapter 3. The initial Russian analysis involved the use of 8 off-source circles in the determination of the background count. For now only the 'hour angle method' (to be described below) is to be utilised.

As with all extensive air shower arrays the number of showers recorded is strongly dependent on the arrival direction. Since Baksan has a latitude of about 40 degrees then the maximum occurs at a declination of about 40 degrees also. Naturally if one is to make an estimate of a background count one must take this angular acceptance of the array into account. This was done empirically by obtaining the distribution of events in hour angle and declination. Due to the large number of showers recorded this distribution was determined with high precision. The acceptance of course is a function of pressure and temperature and will vary from day to day. However for DC effects the average over time will suffice. For the daily results ie the single pass of a source, the limited statistics of counts means that very high precision is not needed. In this case it is sufficient to normalise the distribution to the total number of events in that day.

It was decided to examine this distribution for one year at a time. The 1986 data were split into 3 sections of 4 month duration. Figure 5.1 shows results for Cyg X-3 and 4U0155+63 taken as examples of a medium and high declination source. The results showed that for a given source each section gave a distribution similar enough to the others to indicate that diurnal variations were negligible. Thus evaluating the HA-dec distributions over a whole year to use as a basis for the angular acceptance of the array for that year was valid.

5.2 On Source and Background Evaluation

All events within a circle of radius 2.5° centred on the candidate source position were counted as 'on source'. The choice of 2.5° was prompted by Monte-Carlo simulations of the array's angular resolution. These results indicated that 62% of all source events would fall within such a circle.

For each individual year the procedure was as follows. The HA distribution was obtained for a given declination band (source declination $\pm$ 2.5°). This was then normalised to the total number of events in that declination band and binned in 1° $\times \frac{366.25}{365.25}$ bins to allow for the difference between solar and sidereal time. (The expected number was to be calculated for a 20 minute run in solar time which has 365.25 days in one year and hour angle is measured in sidereal time which had 366.25 days in one year.) Thus each bin of this normalised HA distribution gave the fraction of the total declination band sample expected within those 4 minutes of solar time.

It was now possible to calculate the expected background for each 20 minute run of data. The total number of events in the same declination band were calculated for one run. On finding the Moscow time at which the source transits the meridian for a given day one

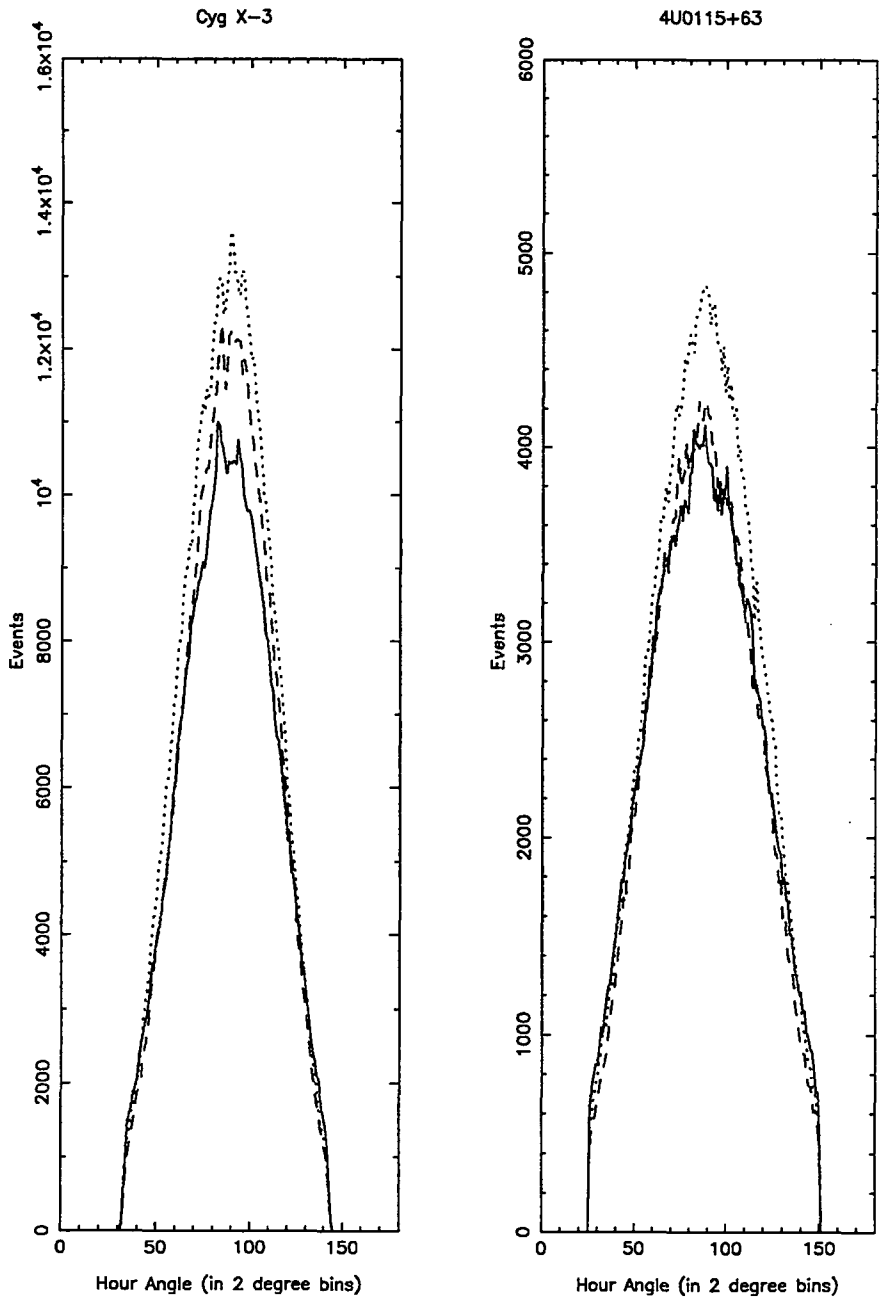

Figure 5.1 The 1986 hour angle distributions for the declination band ± 2.5° from the source position for Cyg X-3 and 4U0115+63. The solid line show data from January-April, the dashed line for May-August and the dotted line for September-December.

could assign the appropriate 5 bins of the HA distribution to each 20 minute run and sum the values therein.

This gave a number related to the fraction of the declination band sample, H , which one expected to come from these 20 minutes of solar time given the source's position in its transit. Effectively we had

$$\mathrm{H} = \frac{\text{no. of events in 20 minutes}}{\text{no. of events in whole distribution}}$$

Thus since 20 minutes is equal to $\frac{1}{72}$ of the 24 hour distribution and we had divided by the total events in the distribution it was necessary to multiply H by 72. This could then be multiplied by the actual number of events N in the declination band in 20 minutes.

Finally this was multiplied by a factor α to allow for the fact that the background was required not for a declination band but for a circle.

$$\alpha = \frac{\text{solid angle of } 2.5^\circ\text{circle}}{\text{solid angle of dec band} \times \frac{366.25}{365.25}} = \frac{\sin 90 - \sin(90 - 2.5)}{\sin(\delta + 2.5) - \sin(\delta - 2.5) \times \frac{366.25}{365.25}}$$

The factor $\frac{366.25}{365.25}$ was required to convert the solid angle of the declination ban for 360° ie one sidereal day to one solar day.

The equation used to evaluate the expected background from a 2.5° circle was :

$$\mathrm{N_{expected}} = \mathrm{H} \times \mathrm{N_{decband}} \times 72 \times \alpha$$

In this way the background count for each run was evaluated. This was compared with the observed 'on source' counts for each pass of the source. On a given solar day there may be counts from parts of two passes for the source. Thus we defined the 'prime' pass as that for which the source crosses the meridian during that day. Results are quoted for the prime pass allowing for the contribution from either the previous or following day as appropriate.

We estimate the upper limit to the flux at the 90% confidence level as follows:

$$F(> E_{th}) = 1.3 \times \frac{\sqrt{\mathrm{N_{off}}}}{\mathrm{N_{off}}} \times I(> E_{th}) \times \Omega_s \times \frac{1}{f}$$

We use here the Hillas cosmic ray spectrum below 2 PeV as suggested by Nagle,Gaisser & Protheroe (1988) that is :

$$I(> E_{th}) = 10^{-10} \times (\frac{E_{th}}{2PeV})^{-1.55}\ cm^{-2}\ s^{-1}\ sr^{-1}$$

$\mathrm{N_{off}}$ is the number of off-source counts, Ω_s is the solid angle on the on source region, in our case a circle of radius 2.5° , and f is the fraction of candidate source events expected to fall within the source region. Following the Monte-Carlo simulations reported in Alexeenko et al (1990) we take f to be 0.62.

5.3 Results

The results from the search for a dc excess for each year are given for each source in Appendix B.There are no significant dc excesses from any of the sources. Also given are a list of days when the excess exceeds 3.0σ. There are 57 such days excluding the 3 which had only one on-source event. Given that we observed 18 sources for,on average, 1,862 days each we would expect about 44 such days. For sources with a known period, a periodicity search was made on the event arrival times.

A search was also made for emission on the timescale of one calendar month. The results for all sources were consistent with background fluctuations. The cumulative results for

1985-1992 with flux limits are shown in Table 5.1 Source coordinates are shown for epoch J2000.

Table 5.1 Upper Limits to Fluxes at 90% Confidence Level.

Source	RA	δ	Days observed	On	$\frac{On}{Off}$	Flux (> 0.2 PeV) $cm^{-2}s^{-1}$
Cyg X-3	308.1	41.0	1,867	188,176	0.9976	$< 1.0 \times 10^{-13}$
Her X-1	254.5	35.3	1,866	170,267	1.0000	$< 1.1 \times 10^{-13}$
4U0115+63	19.7	63.8	1,874	148,173	0.9996	$< 1.2 \times 10^{-13}$
Cyg X-1	299.6	35.2	1,869	168,697	1.0019	$< 1.1 \times 10^{-13}$
1E2259+586	345.3	58.9	1,874	172,274	0.9990	$< 1.1 \times 10^{-13}$
V0332+53	53.7	53.2	1,873	192,101	1.0000	$< 1.0 \times 10^{-13}$
Crab	83.6	22.0	1,836	94,357	1.0027	$< 1.5 \times 10^{-13}$
Geminga	98.5	17.8	1,842	69,352	0.9992	$< 1.7 \times 10^{-13}$
PSR0355+54	59.7	54.2	1,871	188,710	0.9992	$< 1.0 \times 10^{-13}$
PSR0655+64	105.2	64.3	1,869	146,054	0.9983	$< 1.2 \times 10^{-13}$
PSR1913+16	288.9	16.1	1,833	59,971	0.9956	$< 1.8\times 10^{-13}$
PSR1937+21	294.9	21.6	1,849	90,465	1.0002	$< 1.5 \times 10^{-13}$
PSR1953+29	298.9	29.1	1,861	136,875	1.0026	$< 1.2 \times 10^{-13}$
PSR2217+47	335.0	47.9	1,871	200,543	1.0015	$< 1.0 \times 10^{-13}$
Mrk 421	166.1	38.2	1,852	182,611	1.0015	$< 1.0\times 10^{-13}$
M31	10.7	41.3	1,867	190,158	0.9961	$< 1.0 \times 10^{-13}$
GRO J0422+32	65.4	32.9	1,857	158,954	0.9987	$< 1.1 \times 10^{-13}$
GRO J1837+59	279.4	59.2	1,882	169,754	0.9984	$<1.1 \times 10^{-13}$

5.4 Periodicity Analysis

The BASA array data does not provide absolute timing for the arrival time of events. Thus it is not possible to search for a periodic signal over large time scales. However it is thought that the clock is stable enough to allow analysis of data taken from a single pass of the source. It is not however possible to obtain absolute phases and one can only give phases relative to an arbitrary starting point. With this in mind a GPS system has been installed and is described in Chapter 7. None of the data in this thesis however has the benefit of GPS system timing.

In order to eradicate any spurious periodicity the arrival times of the events must be barycentred. This is due to the fact that with respect to a γ-ray source the Baksan detector revolves round the Earth's rotation axis once per day, the Earth-Moon barycentre once per lunar month and the Solar System barycentre once per year (See Figure 5.2).

Each of these motions can introduce a Doppler shifting of the γ-ray arrival times which could either introduce a spurious periodicity or hide a real one. This effect is accounted for by transforming the arrival times to the rest frame of the Solar System barycentre.

The largest of these effects is that due to the Earth's orbital motion. If one regards the source as being infinitely far away then one can treat a single γ-ray pulse as a plane wave crossing the Solar System. In this case the Doppler correction is simply the difference between the arrival time of the wave at the observing site and the Solar System barycentre. The maximum effect occurs for the case when the Sun, observing site and source are aligned in that order. For an observatory on the equator with latitude and longitude of zero this

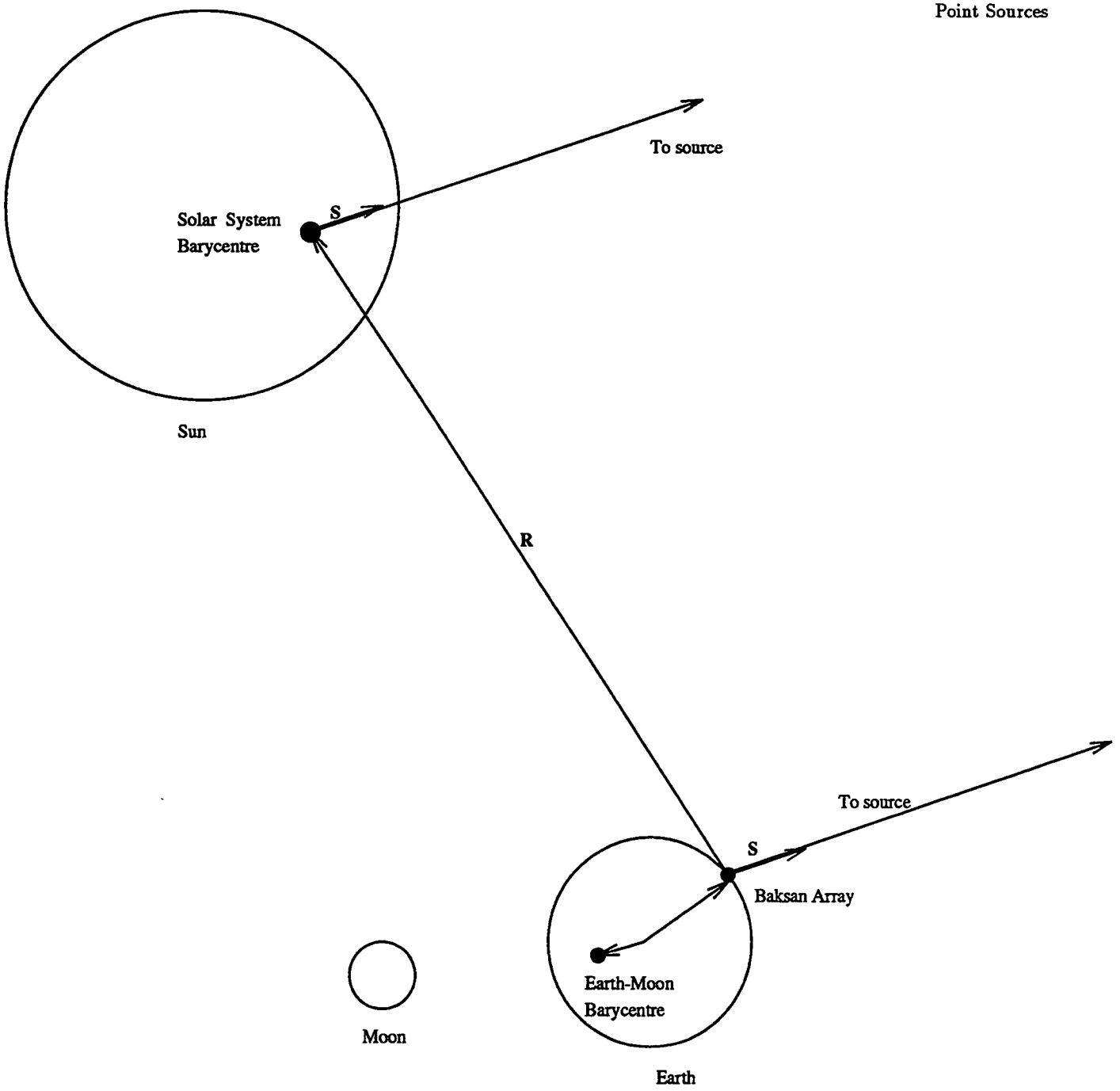

Figure 5.2 A schematic view of the geometry involved for the barycentring procedure of γ-ray arrival times (After Carraminana 1991) .

will occur with a source (δ=0,α=180) transiting at midnight on the equinox (March 21st.) The shift will then be equal to the time taken for light to travel from the observing site to the Solar System barycentre which is approximately 8 minutes. This was used to check the barycentring routine adopted.

The correction for the Earth's rotation is much smaller. The radius of the Earth is approximately 0.021 light-seconds so that the difference in arrival times between events 12 hours apart (ie the time taken for light to travel the diameter of the Earth) can be as much as twice this that is ~40ms. The Earth-Moon barycentre is approximately 0.016 light-seconds from the Earth's centre and hence over half a lunar month arrival times can differ by as much as ~32ms.

The final correction to be applied is a general relativistic correction. This is due to the fact that the Earth's orbit lies deep within the gravitational potential well of the Sun. Time dilation effects mean that the time interval between γ-ray pulses measured at the Earth is greater than measured at a source infinitely far from the effect of the Sun's potential well. If the Earth's orbit were exactly circular this difference would be constant but due to the ellipticity of the orbit it is not and depends on the position of the Earth in its orbit. This could mask a real periodicity or conceivably introduce a spurious periodicity. The maximum effect is ~3ms.

Members of the Durham University VHE γ-ray group kindly used their standard programs to barycentre the arrival times. These use the Jet Propulsion Laboratory DE200 Solar System Ephemeris which provides the relative orientations of the Earth, Moon and Solar System barycentre at time increments of two hours.

Having barycentred the arrival times these were folded with the appropriate period for the given source. Where there were less than 10 events on a given day it was not felt to be worth while performing a periodicity search. The first test applied to the phase data was a

simple χ^2 test comparing the observed number of events in each of 10 phase bins with the mean count in a phase bin. Tables 5.2 and 5.3 show the days in question with the value of χ^2 obtained. For 9 degrees of freedom the value of χ^2 would have to be greater than 16.92 (eg Conover W.J. 1980) for one to be able to say at the 95% confidence level that the data shows any sign of non-uniformity. Figures 5.3 - 5.7 show the results of binning the data in 10 phase bins.

The disadvantage of the χ^2 test is that one has to bin the data. The optimum bin size depends on the size of the peak but this is not well determined and therefore one must choose some *a priori* value for the number of bins which you think is appropriate. Furthermore ideally binning would start so that the pulse lies in the middle of a bin but in practice again it is necessary to simply start at a pre-chosen value. Two tests which do not bin the data are the Rayleigh Test and the Protheroe Test. The former is sensitive to first harmonic variation while the Protheroe Test is more sensitive to a single sharp peak. Tables 5.2 and 5.3 show the probability of the null hypothesis based on the Rayleigh Test and also the value of the Protheroe Test Statistic. Also quoted is the value which this Protheroe statistic must exceed for the data to show non-uniformity at the 95% confidence level. This was evaluated for the appropriate number of events from the interpolation formula given in Protheroe R. 1985.

The values of the various statistics which would indicate non-uniformity at the 95% confidence level are shown in bold. Four sources show non-uniformity at this level in two of the three statistical tests. These are 4U0115+63 on 19.03.89, PSR1953+29 on 12.02.85, 1E2259+586 on 01.08.91 and PSR0655+64 on 12.08.89. In actual fact the χ^2 for 4U0115+63 is just below the 95% confidence level but we include it as it approaches the 95% confidence level and certainly stands out from the other χ^2 values obtained. The quoted statistics are of course for the individual days and no account has been made of the number of days for which a periodicity search was made (2 for 4U0115+63, 5 for

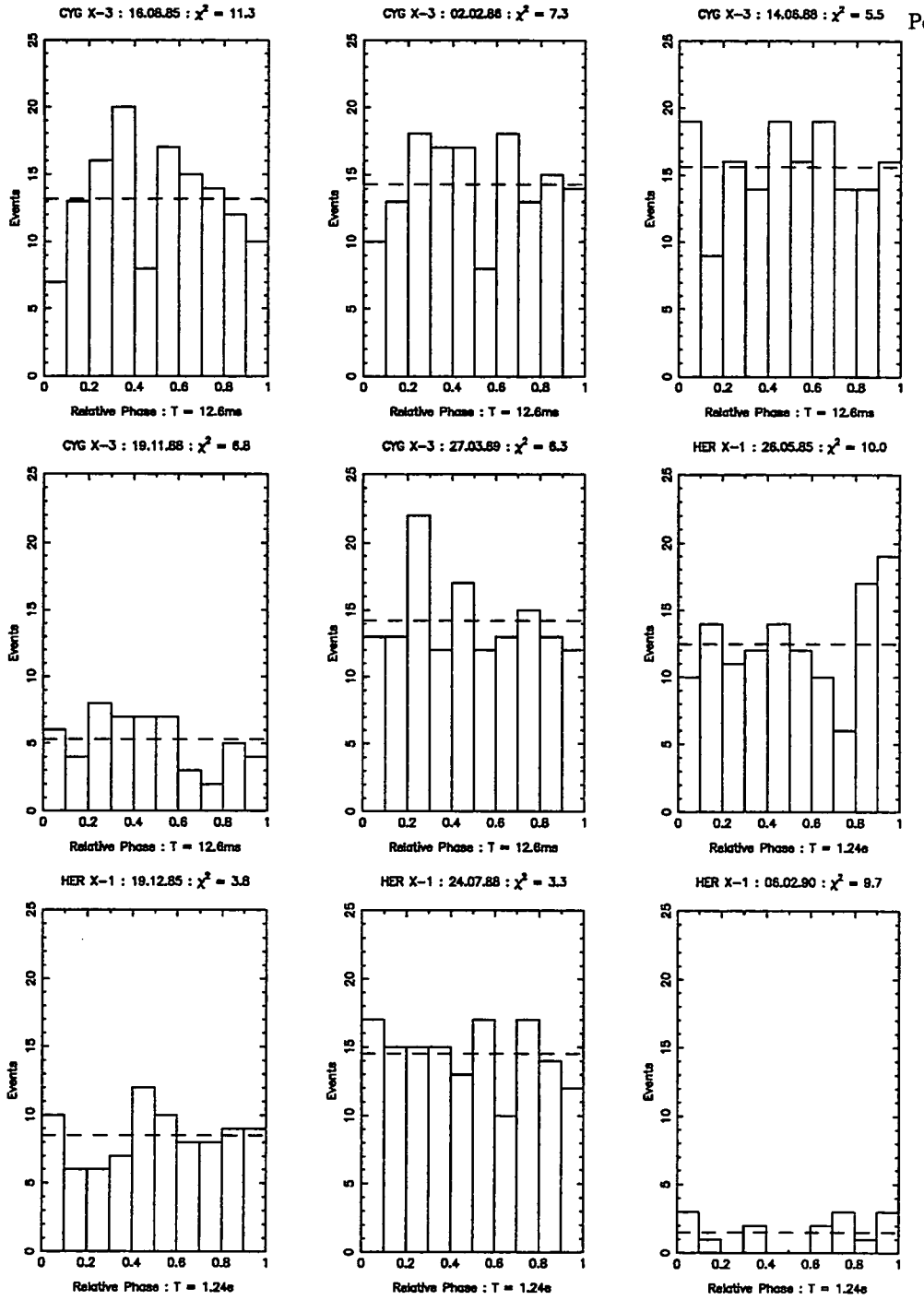

Figure 5.3 The phase diagrams for given days with dc excess $>3\sigma$. The dotted line shows the mean count in each phase bin which is used for the χ^2 test.

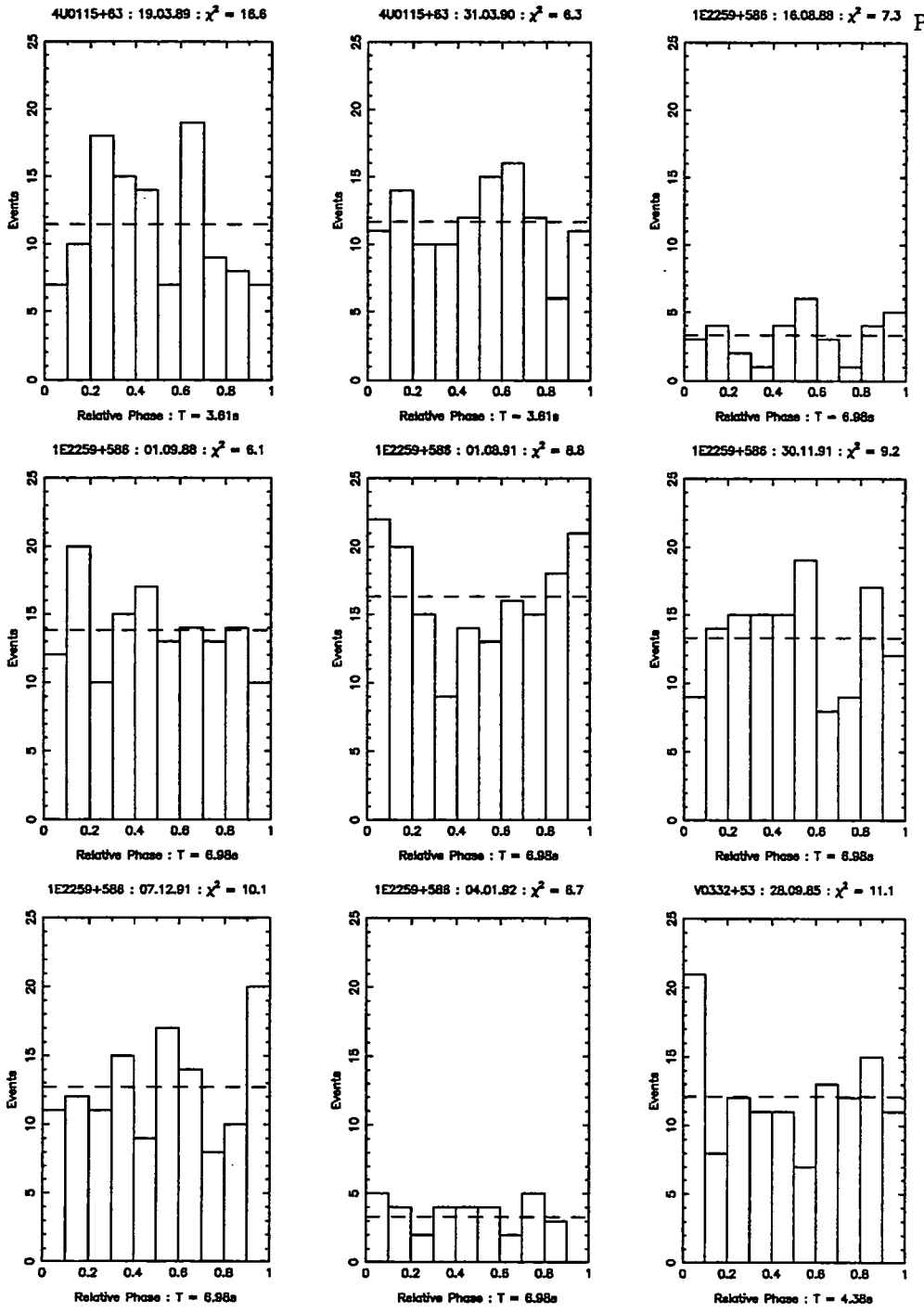

Figure 5.4 The phase diagrams for given days with dc excess $>3\sigma$. The dotted line shows the mean count in each phase bin which is used for the χ^2 test.

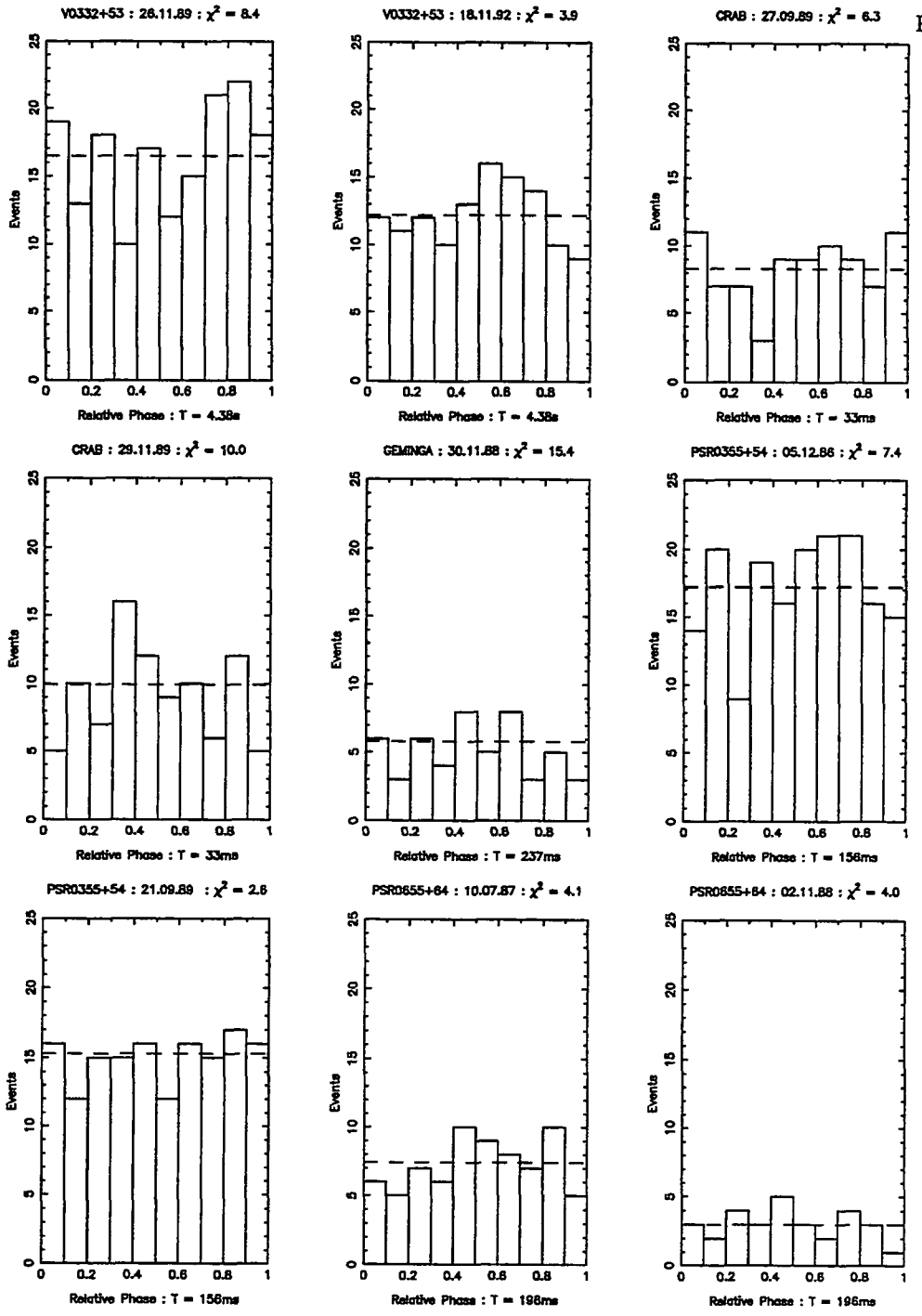

Figure 5.5 The phase diagrams for given days with dc excess $>3\sigma$. The dotted line shows the mean count in each phase bin which is used for the χ^2 test.

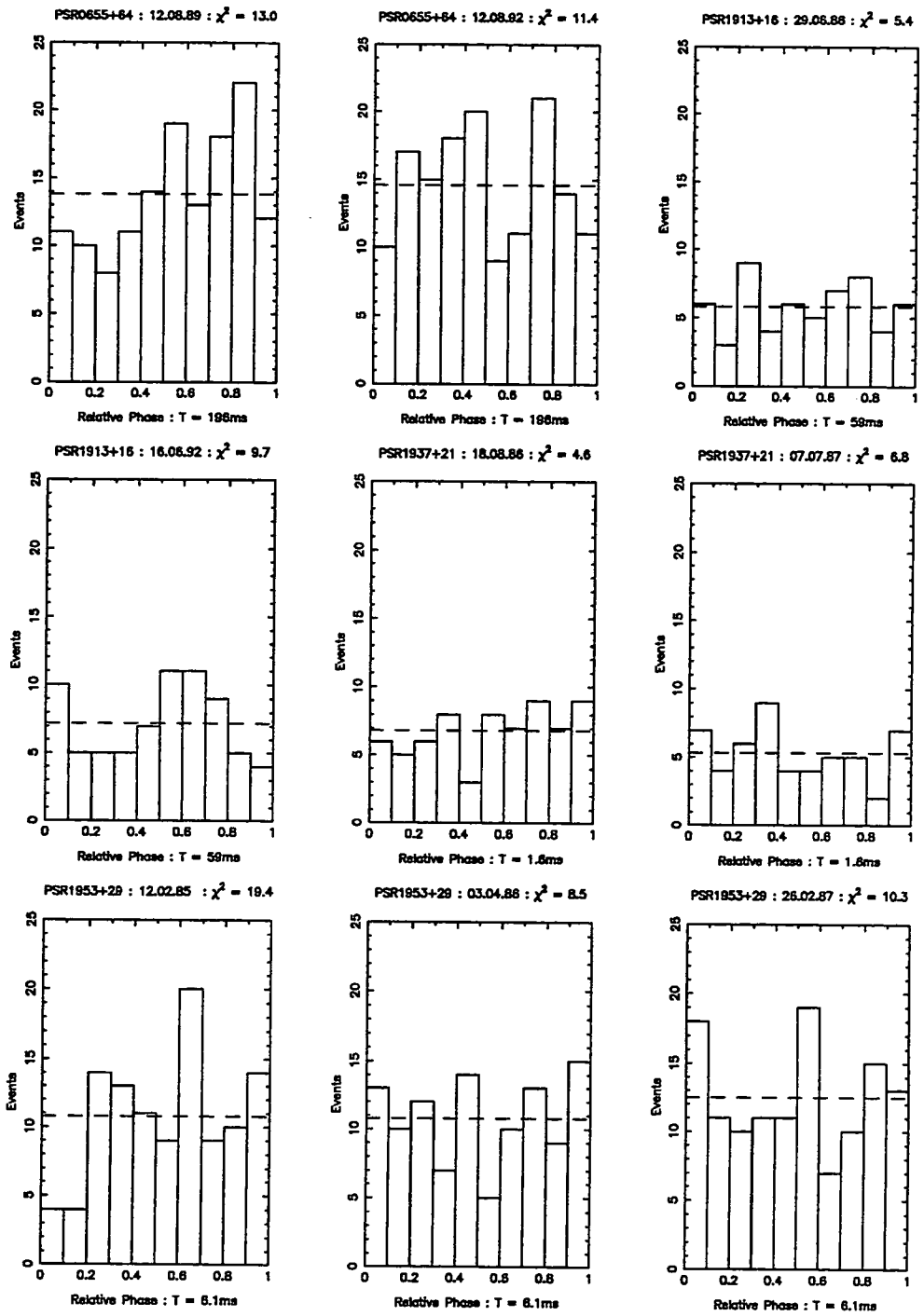

Figure 5.6 The phase diagrams for given days with dc excess $>3\sigma$. The dotted line shows the mean count in each phase bin which is used for the χ^2 test.

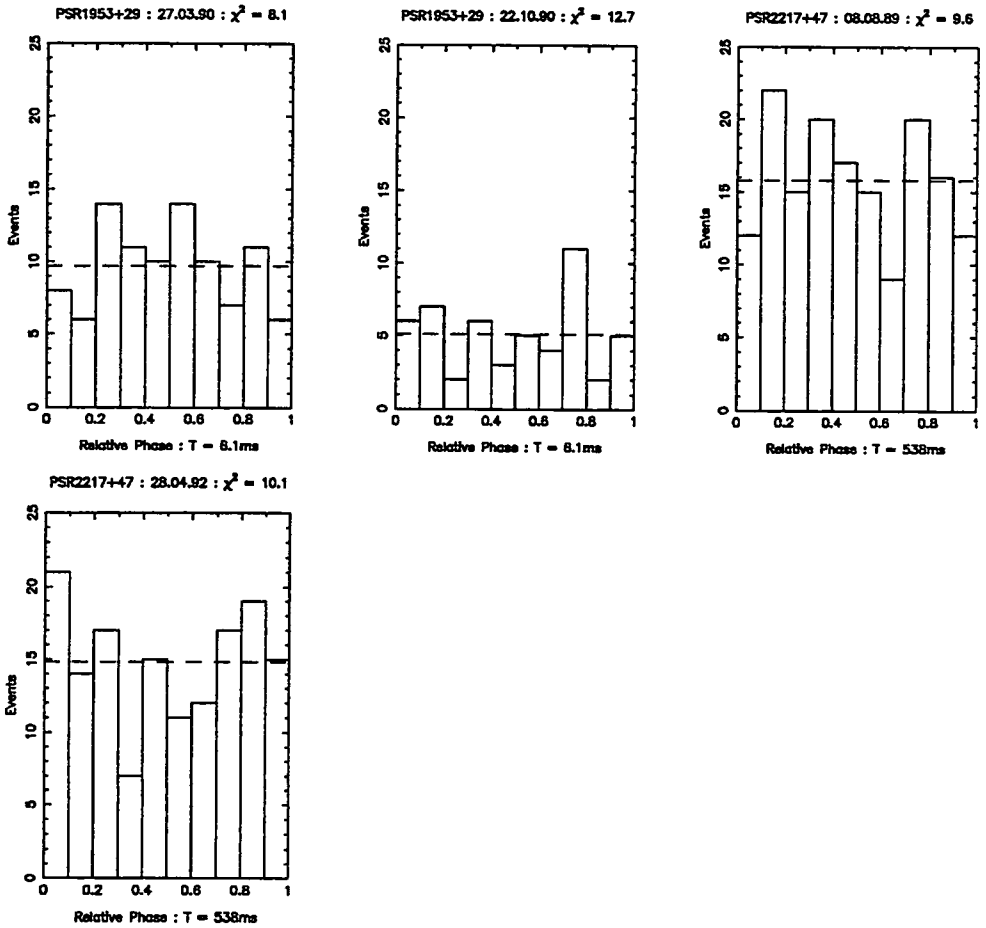

Figure 5.7 The phase diagrams for given days with dc excess $>3\sigma$. The dotted line shows the mean count in each phase bin which is used for the χ^2 test.

PSR1953+29, 6 for 1E2259+586 and 4 for PSR0655+64). It would be interesting to see results from other groups for these days as further positive evidence would add to the significance of the result.

Table 5.2 Periodicity Analysis Results.

Source	Period	Date	Events	Excess (σ)	χ^2	Rayleigh NH Probability	Protheroe Statistic	Protheroe 95%CL
Cyg X-3	12.6ms	16.08.85	132	3.28	11.3	0.1585	**8.74**	8.67
Cyg X-3	12.6ms	02.02.86	143	3.75	7.3	0.7130	8.76	8.82
Cyg X-3	12.6ms	14.06.88	156	3.16	5.5	0.6736	**9.22**	8.98
Cyg X-3	12.6ms	19.11.88	53	3.50	6.8	0.1639	6.58	7.01
Cyg X-3	12.6ms	27.03.89	142	3.13	6.3	0.4360	8.70	8.81
Her X-1	1.24s	26.05.85	125	3.23	10.0	0.4596	8.48	8.57
Her X-1	1.24s	19.12.85	85	3.18	3.8	0.6471	7.76	7.86
Her X-1	1.24s	24.07.88	145	3.12	3.3	0.9781	8.67	8.85
Her X-1	1.24s	06.02.90	15	3.14	9.7	0.1393	4.44	4.81
4U0115+63	3.61s	19.03.89	115	3.24	**16.6**	0.0765	**8.55**	8.42
4U0115+63	3.61s	31.03.90	117	3.33	6.3	0.6070	8.33	8.45
1E2259+586	6.98s	16.08.88	33	4.82	7.3	0.9927	5.57	6.16
1E2259+586	6.98s	01.09.88	138	3.83	6.1	0.7483	8.68	8.75
1E2259+586	6.98s	01.08.91	163	3.68	8.8	**0.0298**	**9.31**	9.06

Table 5.3 Periodicity Analysis Results.

Source	Period	Date	Events	Excess (σ)	χ^2	Rayleigh NH Probability	Protheroe Statistic	Protheroe 95%CL
1E2259+586	6.98s	30.11.91	133	3.33	9.2	0.3732	**8.77**	8.69
1E2256+586	6.98s	07.12.91	127	3.23	10.1	0.9778	8.50	8.60
1E2256+586	6.98s	04.01.92	33	3.27	6.7	0.8120	5.61	6.16
V0322+53	4.38s	28.09.85	121	3.93	11.1	0.1917	**8.61**	8.51
V0322+53	4.38s	26.11.89	165	3.04	8.4	0.1326	**9.26**	9.09
V0322+53	4.38s	18.11.92	122	3.78	3.9	0.2513	8.38	8.53
Crab	33ms	27.09.89	83	3.22	6.3	0.5983	7.62	7.82
Crab	33ms	29.11.89	99	3.62	10.0	0.5776	7.94	8.14
Geminga	237ms	30.11.88	58	3.57	15.4	0.1091	7.09	7.17
PSR0355+54	156ms	05.12.86	172	3.26	7.4	0.2033	**9.61**	9.16
PSR0355+54	156ms	21.09.89	153	3.10	2.6	0.6000	8.82	8.95

Table 5.4 Periodicity Analysis Results.

Source	Period	Date	Events	Excess (σ)	χ^2	Rayleigh NH Probability	Protheroe Statistic	Protheroe 95%CL
PSR0655+64	196ms	10.07.87	74	3.42	4.1	0.2898	7.34	7.61
PSR0655+64	196ms	02.11.88	30	3.12	4.0	0.6393	5.34	5.99
PSR0655+64	196ms	12.08.89	138	3.70	13.0	**0.0170**	**9.00**	8.75
PSR0655+64	196ms	12.08.92	146	3.57	11.4	0.4539	**9.03**	8.86
PSR1913+16	59ms	29.06.86	58	3.07	5.4	0.9755	6.55	7.17
PSR1913+16	59ms	16.06.92	72	3.29	9.7	0.2033	7.28	7.56
PSR1937+21	1.6ms	18.08.86	68	3.36	4.6	0.3855	6.93	7.46
PSR1937+21	1.6ms	07.07.87	53	3.57	6.8	0.5242	6.53	7.01
PSR1953+29	6.1ms	12.02.85	108	3.15	**19.4**	0.1300	**8.40**	8.30
PSR1953+29	6.1ms	03.04.86	108	3.65	8.5	0.4011	8.19	8.30
PSR1953+29	6.1ms	26.02.87	125	3.01	10.3	0.7325	**8.64**	8.57
PSR1953+29	6.1ms	27.03.90	97	3.00	8.1	0.2606	7.93	8.11
PSR1953+29	6.1ms	22.10.90	51	3.31	12.7	0.6966	6.57	6.94
PSR2217+47	538ms	08.08.89	158	3.27	9.6	0.7836	9.34	9.00
PSR2217+47	538ms	28.04.92	148	3.39	10.1	0.1267	8.85	8.88

5.5 Cyg X-3 Radio Bursts

As has been mentioned Cygnus X-3 can produce some very strong radio bursts during which the radio flux can rise to up to 10^3 times its quiescent value. It is possible that the trigger for such a radio flare could trigger a burst of VHE or UHE γ-ray emission. Therefore it should be instructive to monitor the γ-ray signals around such times. Below are the dates of known radio flares of Cyg X-3 with any corresponding γ-ray observations.

03.10.85 On this day BASA observed 85 events from the direction of Cyg X-3 when 84 were expected amounting to only a 0.12σ excess. For the month of October as a whole BASA observed 1665 events where 1612 were expected which constitutes a 1.3σ excess which was the 6th highest of the 90 monthly excesses obtained for Cyg X-3. Using the previous 'off-source circle' method analysis previous work on BASA data found a 3.3σ excess from Cyg X-3 on the 14th and 1.8σ on each of the next two subsequent days (Alexeenko V.V. *et al* 1987). Phase analysis of the data from these three days showed no evidence of pulsed emission. Using the present analysis the results give 1.99σ, 0.35σ and 0.99σ respectively.

The Haverah Park group reported an excess of events at orbital phase 0.25 during the month of October (Eames P.J.V. *et al* 1987). The Soudan group reported a μ burst during this radio flare (Marshak M.L. *et al* 1987). They observed a μ excess between September 24 and October 7th. However the Frejus group reported no excess (Berger Ch. *et al* 1986) and Kamiokande also observed no statistically significant signal (Kifune T *et al* 1987).

02-07.06.89

Ohya observed 3 days above 3σ during June of this year (Muraki Y. *et al* 1993). BASA was not operational in June of 1989.

The Soudan detector observed no excess of μ from Cyg X-3 during this time (Thomson M. *et al* 1991). The CYGNUS collaboration found no evidence for either pulsed or unpulsed emission in the week following the flare (Alexandreas D.E. *et al* 1990). The IMB-3 μ-detector also failed to find any signal during this flare (Becker-Szendy R. *et al* 1991) as did the Utah-Michigan group (Cassidy G.L. *et al* 1989). **21-29.07.89**

Ohya observed one excess above 3σ during July (Muraki Y. *et al* 1993). The Soudan detector observed no excess of μ from Cyg X-3 during this time (Thomson M. *et al* 1991). The CYGNUS collaboration found no evidence for either pulsed or unpulsed emission in the week following the flare (Alexandreas D.E. *et al* 1990) however on the 23rd of July they did observe 104 events when 77.3 were expected. These events were concentrated in a 2 hour period of the day. Once more the IMB-3 μ-detector failed to detect a signal during this flare (Becker-Szendy R. *et al* 1991) as did the Utah-Michigan array (Cassidy G.L. *et al* 1989).

During the above dates BASA observed 797 events from the source direction when 828 were expected giving a deficit of -1.1σ and there were no daily excesses exceeding 2.0σ during this time. For the month of July as a whole 997 events were observed where 1042 were expected.

12-25.08.90

Ohya observed a 3.2σ excess on the 1st of August and a 2.3σ excess on the 16th (Muraki Y. *et al* 1991). Akeno saw nothing on the 15th which was the time of the peak of the flare (Hayashida N. *et al* 1991). BASA observed 1103 events in this time form Cyg X-3's direction when 1092 were expected giving a 0.34σ excess. No daily excesses exceeding 2.0σ were observed by BASA during these two dates and a deficit of events was observed on the 1st,15th and 16th . The monthly total gave 2991 events observed when 2984 were expected.

04-15.10.90

Ohya saw one 4σ excess in October (Muraki Y. *et al* 1993) and Akeno saw nothing on the 6th which was the peak of the flare (Hayashida N. *et al* 1991). The Soudan detector observed no excess of μ from Cyg X-3 during this time (Thomson M. *et al* 1991). BASA has no data between these two dates. For October as a whole 959 events were observed where 948 were expected.

18-25.01.91

Ohya observed a 4.1σ excess on the 17th of January (Muraki Y. *et al* 1991). They also observed four successive 2σ excess in January. Akeno measured a 3.6σ excess in the 7 days following the radio peak on 21st and a 4.0σ excess in the 50 following days (Hayashida N. *et al* 1991) while Tibet EAS array saw no excess on the 21st or any cumulative excess for the next 50 days (Amenomori M. *et al* 1991). HEGRA saw a 4.6σ excess on January 20th when they considered showers with log (Ne) > 4.6. However they felt that when they considered that their data sample consisted of looking at 30 sources for a total of 3 years this was not beyond the level one might expect from chance (Merck M *et al* 1993). From data taken with the Soudan 2 (Thomson M. *et al* 1991) detector from January 1989 - February 1991 two days stood out as having a large excess of muons. On January 20th 16 μ were observed when 5.3 were expected and on January 23rd 16 μ were observed when 6.1 were expected. When these 32 μ were folded with the orbital period the results were consistent with no orbital modulation.

Between the 18th - 25th BASA observed 481 events compared to an expected value of 480 and there were no daily excesses exceeding 2.0σ between these two dates. BASA has no data for the 17th or 21st and observed a deficit of events from Cyg X-3 on the 20th. For the whole of January BASA observed 1854 compared to an expected 1837.

July 91

Ohya observed a 4.1σ excess on the 13th of July and a 3.5σ excess on the 27th (Muraki Y. *et al* 1991). Akeno saw nothing on the day of the peak of the radio flare which was the 26th (Hayashida N. *et al* 1991). BASA observed a deficit of events from Cyg X-3 on the 13th, 26th and 27th. On the 5th of July a 2.5σ excess was observed and on the 18th a 2.1σ excess. BASA observed 2805 events from Cyg X-3 in July of this year compared to an expected value of 2695.001. This constitutes a 2.1σ excess which is the highest of any of the 90 months between 1985 and 1992 during which Cyg X-3 was observed.

12.10.91

Ohya observed a 5σ excess during this month (Muraki Y. *et al* 1993). During this month Baksan observed 2612 events from Cyg X-3 when 2692 were expected and there were no days above 3σ. On the 12th itself 96 events were observed when 106 were expected.

5.6 The Crab Burst of 1989

As mentioned previously the initial Russian point source analysis took as its background count the mean value of the counts from 8 circles surrounding the on source circle of radius 2.5° . These off-source circles, also of radius 2.5°, were shifted by zero or $\pm$ 5° in declination and by zero or $\pm \frac{5}{(\cos\delta)}$ in RA to allow for the curvature of the field. To the mean background a correction had to be made for the gradient in the declination distribution of events due to the zenith angle dependence of the array already mentioned. As this was of the order of 1% such a correction is practically negligible when considering the counts from a single day.

When the 1985 - 1989 data was analysed in this way (using Russian selection on which days to include) the highest excess from any of the 1256 days during which the Crab was observed occurred on February 23rd 1989 (Alexeenko V.V. *et al* 1989,1991,1992) . Initially an excess $>4\sigma$ was claimed however following certain corrections this was lowered somewhat. The detector positions were remeasured more accurately and a correction made to the sidereal time calculation the latter resulting in a shift of all the events by approximately 1° in RA. The initial 4σ claim prompted other groups to check their data for an excess on this day also. KGF were the first to confirm the burst (Acharya B.S. *et al* 1990) followed by Tien Shan (Nesterova N.M. private communication) and 2 independent results from the EAS-TOP group (Aglietta M. *et al* 1991). These and the final Baksan result are shown in Table 5.2

Table 5.5 Positive Observations of The Crab on February 23rd 1989

Array	On	Off	σ (Li-Ma)
KGF	35	17.8	3.4
Tien Shan	6	1.6	2.6
Baksan	55	34.1	3.1
EAS-TOP	38	25.5	2.1
	403	378.3	1.2

Akeno observed no excess on this date (Rao. M.V.S. & Sreekantan B.V. 1992). Ohya saw no excess in their μ-poor data (Muraki Y. *et al* 1990) nor did Hegra (Rao. M.V.S. & Sreekantan B.V. 1992). The CYGNUS array saw no evidence for emission around this time (Alexandreas D.E. *et al* 1993a). The CASA/MIA installation was not operational during the burst (Cronin J.W. *et al* 1992).

A rather worrying feature of the Baksan result is that it is very dependent on the precise details of the analysis performed. The data for this day was analysed using various methods and the results found to be quite different for each. Within the 8 circles method itself there are a number of alterations which can be made. The initial detection was made using the time delays averaged over 20 minutes but it is also possible to use the delays averaged over 24 hours. Further as described in Chapter 3 there is a 'difference of differences' cut imposed on the time delays. The data was analysed using various permutations of the above. Also rather than a 2.5° radius circle as on-source a $10° \times 10°$ on-source region with the background being obtained from the average count from 12 similar off-source boxes was tried. The results are shown in Table 5.3 Also shown are the results from the standard hour angle method used in this thesis.

Clearly the inclusion of events failing the difference of difference cut degrades any signal seen. Experimentally the distribution of time delays was found to have non-gaussian tails. However at some times in 1989 and in particular on the day in question these tails were distorted indicative of some electronic instability. The time delays in channel 2 were particularly anomalous. As for the hour angle method, it has already been stated that the background for this method has much higher statistics than the 8 circle method. It is not perhaps then surprising that the latter method is prone to greater daily fluctuations which could result in false detections. One further difference between the two methods is that the 8 circle method only utilised events where all 6 outer channels were triggered (about 60% of the total number) and the hour angle method utilised 4 and 5 fold events also ie those which failed to trigger either channel 5 and/or channel 6.

Table 5.6 Effect of different analysis methods.

8 Circle Method : Six Folds Only				
	Events	Predicted	σ	Method
	55	34.1	3.57	20 min tds, δt cut
2.5° radius circle	53	44.5	1.27	20 min tds, no cut
	48	34.1	2.37	24 hr tds, δt cut
	50	43.1	1.05	24 hr tds, no cut

12 box method : Six Folds Only				
	Events	Predicted	σ	Method
10°×10° box	206	162.7	3.40	20 min tds, δt cut
	236	207.4	1.98	20 min tds, no cut

Hour angle method : All Folds				
	Events	Predicted	σ	Method
2.5° radius circle	67	51.786	2.11	20 min tds, δt cut

The shifts in arrival directions of events due to the differing procedures are in fact small (less than $\sim$ 1°). Thus for an on-source region of a circle of radius 2.5° one would not expect large discrepencies between the methods. However the peak of events observed for the Crab burst is rather unusual in that it is surrounded by regions of low flux rather than by a fairly flat background as would be expected. This clustering of events can lead to a

larger change to the number of events falling in the on-source and off-source regions than would be expected due to such small shifts in arrival directions.

Some weight is added to the detection by the periodicity analysis on the arrival times of the on-source events obtained for the standard 2.5° radius circle using the 20 minute mean time delays and employing the difference of differences cut.

The barycentred times were then folded with the Crab 33ms period and binned in 10 phase bins. The values of P and P(dot) were taken from the Jodrell Bank Crab ephemeris. BASA did not have any accurate absolute timing measurements and so the resulting phase shown is relative to an arbitrary point in the Crab cycle. However it is interesting to see that there is a sharp peak in the 9th phase bin amounting to 16 of the 55 events. Furthermore 8 of these 16 events all occurred in the same 20 minute run (see Figure 5.8).

The KGF array also found some evidence of pulsed emission at the pulsar period (Sinha S *et al* 1990). There was a 5.7σ excess in the first half of the period which includes the main pulse at 0 and the interpulse at 0.42 phase observed at other frequencies. The μ-content and shower size of these events were no different to the background showers.

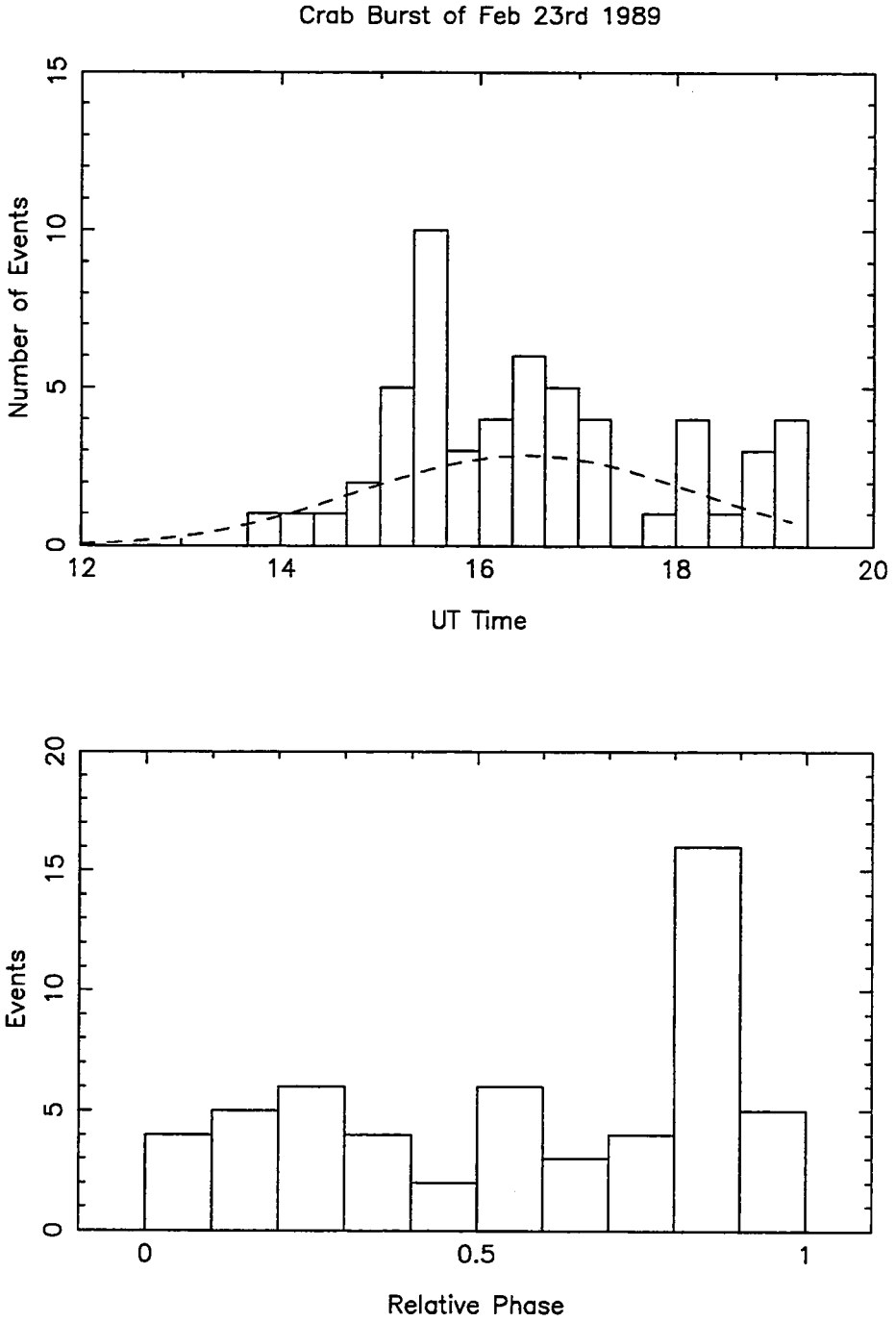

Figure 5.8 The top graph shows the arrival times in UT of the 6-fold on source events within 2.5° of the Crab The dashed line shows the expected background calculated from the average of 8 off-source circles. The lower graph shows the relative phase distribution of these 55 events after the arrival times have been barycentred and folded with the Crab period.

REFERENCES : CHAPTER 5

Acharya B.S. *et al* Nature **347** 364 (1990)

Aglietta M. *et al* Europhys. Lett. **15** 81 (1991)

Alexandreas D.E. *et al* Phys Rev Lett **64** 2973 (1990)

Alexandreas D.E. *et al* Ap J **405** 353 (1993)

Alexeenko V.V. *et al* 20^{th}I.C.R.C. **Vol 1** 229 (1987)

Alexeenko V.V. *et al* Proc. of Int. Workshop on VHE Gamma Ray Astronomy ed A.A. Stepanyan *et al* 187 (1989)

Alexeenko V.V. *et al* 22^{nd}I.C.R.C. **Vol 1** 293 (1991)

Alexeenko V.V. *et al* J. Phys. G: Nucl. Part. Phys. **18** L83 (1992)

Amenomori M. *et al* 22^{nd}I.C.R.C. **Vol 1** 444 (1991)

Becker-Szendy R. *et al* Phys Rev D **43** 1413 (1991)

Cassidy G.L. *et al* Phys Rev Lett **63** 2329 (1989)

Conover W.J. Practical Nonparemetric Statistics (1980)

Cronin J.W. *et al* Phys Rev D **45** 12 4385 (1992)

Hayashida N. *et al* 22^{nd}I.C.R.C. **Vol 1** 309 (1991)

Merck M. *et al* 23^{rd}I.C.R.C. **Vol 1** 361 (1993)

Muraki Y. *et al* 21^{st}I.C.R.C. **2** 212 (1990)

Muraki Y. *et al* 22^{nd}I.C.R.C. **Vol 1** 317 (1991)

Muraki Y. *et al* 23^{rd}I.C.R.C. **Vol 1** 380 (1993)

Protheroe R. 19^{th}I.C.R.C. **Vol 3** 485 (1985)

Rao. M.V.S. & Sreekantan B.V. Current Sci. **62** 617 (1992)

Sinha S. *et al* 21^{st}I.C.R.C. **2** 366 (1990)

Thompson M. *et al* Preprint Submitted to Phys Lett B (1991)

6 COSMIC RAY ANISOTROPY

6.1 Introduction

A fundamental question in cosmic ray physics is whether CR are of Galactic or extra-Galactic (EG) origin. The answer to this seems to depend upon which energy band one is considering.

It is generally accepted that up to approximately 10^{14}eV or 10^{15}eV, the so-called 'knee' of the CR spectrum, CR are of Galactic origin. Shocks due to SNR are favoured as a possible source mechanism. At the highest energies, $> 10^{19}$eV, it seems likely that the CR are of EG origin. If such highly energetic particles were of Galactic origin their large gyroradii in the interstellar magnetic field would make it unlikely, even for the heavier species, for them to be retained in the Galaxy for long. Possible EG source candidates include shocks in the lobes of radio galaxies with AGN.

In the intermediate range there is less certainty although a Galactic origin is again favoured to minimise the total energy of CR in the Universe. It may be however that there is some superposition of a Galactic and EG source composition in this region. (Wolfendale 1989, Axford 1994)

It must be borne in mind of course that because CR are charged particles they are affected by the magnetic fields permeating the Galaxy. In such a field the radius of gyration may be estimated by $r = \frac{E}{Z.B}$ where r is in pc, E in 10^{15}eV, B in μ-Gauss and Z is the charge. Only above $\sim 10^{18}$eV where the gyroradius becomes comparable with the galactic dimensions can the arrival direction be directly related to source direction. Thus for all but the most energetic sources the CR arrival directions are indicative not only of source distribution but also of the local magnetic field.

The question remains - how to differentiate between Galactic and EG CR? There are various possibilities.

6.1.1 Galactic Plane Enhancement

CR, regardless of their origin, will interact with matter, radiation and magnetic fields. Such interactions can produce γ-rays. The 3 dominant interactions are bremsstrahlung collisions between CR and matter (dominating $<$ 70MeV), nuclear interactions between CR and matter (dominating $>$ 70MeV) and inverse compton scattering of electrons with low energy photons (this requires very energetic electrons.) Both a Galactic and EG origin yield a component of diffuse γ-ray flux $\sim 10^5$ times smaller than the CR flux at 100TeV. The main difference is in the anisotropy of this flux.

If the CR are truly EG then the flux should be completely isotropic. If, however, the CR are Galactic then one would expect the CR sources to follow the matter distribution in the Galaxy ie be concentrated in the disk (this is true for SNR and PSR). In this case one would expect the resulting γ-rays to be concentrated in the region of the plane. In fact SAS-2 and COS-B results show that at 100MeV the dominant feature in the γ-ray sky is the Galactic Plane. Thus looking for an enhanced signal in EAS data from the plane would shed some light on the picture. As mentioned previously, however, the level of anisotropy

is expected to be small. The predicted value of $\frac{I_\gamma}{I_{CR}}$ is 7×10^{-5} at 2×10^{14}eV (Berezinsky & Kudryavtsev 1990, Matthews 1990) and so a large data sample will be required to detect such an effect. Wolfendale and Wdowczyk believe there to be a significant contribution from discrete sources and put a much lower value to this figure. The CR energy spectrum has a slope of $\sim$ -2.6 up to $\sim3\times10^{15}$eV and even steeper at higher energies ($\sim$ -3.1). If the γ-ray exponent ($\sim$ -2.0) continues to much higher energies than several GeV where it is presently measured then it is expected that the ratio $\frac{I_\gamma}{I_{CR}}$ will increase with increasing energy.

The Galactic Plane Drift Scan Experiment consists of four 1.5m aperture reflectors which are operated in parallel and is specifically designed to search for an excess from the Plane. Data from 1988-1989 showed no apparent broad excess around the plane setting an upper limit of $\frac{I_\gamma}{I_{CR}} < 9.0\times10^{-3}$ at $\sim 3\times10^{12}$eV (Reynolds *et al* 1990).

The Utah-Michigan array have searched for such a flux of γ-rays in data covering 1988 - 1990 and comprising 1.9×10^7 events above 2×10^{14}eV. They assume that γ-ray initiated showers are μ-poor and decide a shower is γ-ray initiated rather than hadron initiated when then μ content is $<\frac{1}{10}$ that of the mean value for all the showers. In the direction of the plane ($|b| < 10°$) they find an upper limit of $\frac{I_\gamma}{I_{CR}} < 8.0\times10^{-5}$ above 2×10^{14}ev and similar values for higher energies (Matthews 1990)

Data from the 40m^2 μ-detector at GREX was used to search for an enhanced signal from the Galactic Plane at $\sim10^{15}$eV. Data covered the period 1988-1989 and comprised 2 sets of data each with 3.5×10^5 events. Data from within $|b| < 10°$ gave minimal evidence for a Galactic Plane excess and no enhancement was brought about by using only μ-poor showers (Blake *et al* 1991). This was confirmed with later data up to 1990 from the same group (Blake *et al* 1993). The data were consistent with a Galactic Plane enhancement factor of zero and direct observations of events with $|b|$ <10° showed minimal evidence

for any enhancement either with or without selections made based on μ-content. With no cut on events they found an upper limit of $\frac{I_\gamma}{I_{CR}} < 1.1\times10^{-3}$ and when selecting μ-poor showers they found an upper limit of $\frac{I_\gamma}{I_{CR}} < 8.7\times10^{-4}$. Using Hillas cosmic ray spectrum below 2 PeV as suggested by Nagle,Gaisser & Protheroe (1988) that is :

$$I_{CR}(> E_{th}) = 10^{-10} \times (\frac{E_{th}}{2PeV})^{-1.55}\ cm^{-2}\ s^{-1}\ sr^{-1}$$

this corresponds to an upper limit to the γ-ray flux of 1.4×10^{-12}cm^{-2}s^{-1}sr^{-1} above 3.3×10^{14}eV.

Low μ-content showers were analysed from Mt. Chacaltaya data covering 1987-1989 (Yoshii H *et al* 1991). Using

$$I_{CR}(> E_{th}) = 3.3 \times 10^{15} \times (E_{th})^{-1.7}\ cm^{-2}\ s^{-1}\ sr^{-1}$$

they found an upper limit of 1.18×10^{-11}cm^{-2}s^{-1}sr^{-1} above 1.8×10^{14}eV for the γ-ray flux from a region with $\alpha = 180°$ - $210°$. This corresponds to an upper limit of $\frac{I_\gamma}{I_{CR}} < 6.13\times10^{-3}$ at $\sim 1.8\times10^{14}$eV. Had they used the Hillas spectrum the upper limit for the flux would have been 2.27×10^{-11}cm^{-2}s^{-1}sr^{-1}.

Wdowczyk & Wolfendale define a Galactic Plane enhancement factor f_E given by

$$I(b) = I_o(1 - f_E(E)) + f_E(E)exp(-b^2)$$

where b = galactic latitude in radians and f_E(E) is this energy dependent parameter characterising the magnitude of the excess (eg Wdowczyk 1986).

Above 10^{18}eV data has been analysed from Haverah Park, Sydney and Yakutsk (Wdowczyk J. & Wolfendale A.W. 1989). The authors concluded that the Galactic Plane enhancement seems to increase with energy. This would be expected if the particles were of Galactic origin because the sources are largely along the Plane. They also noted a sharp

decrease in the enhancement as these sources switch off at about 10^{19}eV pointing to an EG origin for such particles.

Buckland Park data (Clay R.W. 1984) shows an upper limit of $\frac{I_\gamma}{I_{CR}} < 1.3\times10^{-2}$ at 10^{15}eV-10^{16}eV. Data taken with the Akeno array (1984-1990) and AGASA (1990-1991) shows that f_E is approximately zero from 10^{16}eV-10^{18}eV and increases above approximately $10^{18.5}$eV although the effect is not very significant (Hayashida N *et al* 1991). At 10^{17}eV-$10^{17.5}$eV they find the contribution of Galactic γ-rays to be $< 5\times10^{-3}$ the total CR flux.

6.1.2 Sidereal Anisotropy

If most of the UHE CR originate in the Galaxy their arrival directions should reflect the anisotropy of the Galactic magnetic field and/or the anisotropy of the CR source distribution. Most models for CR origin predict a rising anisotropy for increasing energy. Results suggest that there is a near constancy in the amplitude and phase of the 1st harmonic up to $\sim10^{14}$eV where it is $\sim 1\times10^{-3}$ with phase 1-3hr. Beyond here there seems to be a rising amplitude to tens of percent at 10^{19}eV although the Griesen effect comes in to play - that is the number of events (and hence statistical accuracy) falls rapidly with energy. In fact $>10^{15}$eV many of the anisotropies are upper limits.

The two most obvious features of the CR energy spectrum, the knee near 10^{15}eV and ankle near 10^{19}eV appear to be associated with changes in anisotropy - at 10^{15}eV there seems to be a more rapid increase in the amplitude of anisotropy than at lower energies and the onset of very large anisotropies occur at 10^{19}eV where the spectrum flattens.

The Galactic Plane crosses the field of view of most northern detectors at $\sim$6h and $\sim$20h but one would expect a stronger signal from the latter because of the proximity of the Galactic centre.

Let us look more closely at the data which has provided these broad results. The data is summarised in Table 6.1.

Above 10^{11}eV the Poatina muon telescopes detected a 1st harmonic of $4.3\pm1.8\times10^{-4}$ at 2.6±1.7hr and a 2nd harmonic of $1.2\pm1.8\times10^{-4}$ at 2.5hr (Fenton & Fenton 1976). This was after the data had been corrected with a pressure correction coefficient of -0.057% per mb.

The Ottawa μ-detector operating from 1976-1990 found the amplitude of the first harmonic to increase monotonically with energy from $<1\times10^{-4}$ at 10^{11}eV to $7.2\pm1.6\times10^{-4}$ at 9.6×10^{11}eV. The phase of this was 3.4h (Berkovitch & Agrawal 1981). Data taken between 1972 and 1978 with the Holborn μ-detector (Davis *et al* 1979) was corrected for pressure effects and gave a sidereal first harmonic of $4.8\pm1.0\times10^{-4}$ at 2.7hr for 5×10^{11}eV.

The Utah μ-detector found after correction for solar motion a first harmonic of $(4.9\pm^{1.4}_{0.9})\times10^{-4}$ at 2.8±1.2hr and a second harmonic of $(3.8\pm^{1.4}_{0.9})\times10^{-4}$ at 9.8±1.2hr for their data at 1.5×10^{12}eV (Bergeson *et al* 1979). The Musala EAS array data was corrected for pressure and temperature effects and for an energy of 6×10^{13}eV a first harmonic of $7.3\pm2.1\times10^{-4}$ at 1.7±1.1hr and a 2nd harmonic of $5.5\pm2.1\times10^{-4}$ at 5.0±0.8hr (Gombosi *et al* 1977).

The Mt. Norikura experiment (Sakakibara *et al* 1976) found in data from 1973-1976 a first harmonic amplitude of $5.7\pm2.0\times10^{-4}$ at 1.0±1.6hr and a 2nd harmonic of $3.7\pm1.0\times10^{-4}$ at 7.4±0.6hr for energies in the range 3-5×10^{13}eV.

Combining results from 1951-1965 Linsley finds that at 3×10^{14}eV there is a significant anisotropy of amplitude $7.5\pm2.0\times10^{-4}$ at phase 20.1±1.3hr. (Linsley J. 1977)

The Akeno array has data at 2×10^{14}eV taken from 1984-1988 (Murakami K *et al* 1990). A pressure correction is applied with a barometric coefficient of -0.79% per mb. The

Table 6.1 Harmonic Results.

Array	Energy (eV)	Harmonic	Amplitude ($/10^{-4}$)	Phase (hr)
Poatina	$>10^{11}$eV	1st	4.3±1.8	2.6±1.7
		2nd	1.2±1.8	2.5
Ottawa	10^{11}eV	1st	<1	3.4
	9.6× 10^{11}eV	1st	7.2±1.6	3.4
Holborn	5× 10^{11}eV	1st	4.8±1.0	2.7
Utah	1.5×10^{12}eV	1st	$4.9^{+1.4}_{-0.9}$	2.8±1.2
		2nd	$3.8^{+1.4}_{-0.9}$	9.8±1.2
Musala	6×10^{13}eV	1st	7.3±2.1	1.7±1.1
		2nd	5.5±2.1	5.0±0.8
Combined data	3×10^{14}eV	1st	7.5±2.0	20.1±1.3
Akeno	2×10^{14}eV	1st	6.0	3
Mt. Norikura	1.5×10^{13}eV	1st	6.0±0.3	0.8±0.3
EAS-TOP	6×10^{13}eV	1st	6.5±0.9	2.6±0.5
Liawanee	7×10^{13}eV	1st	2.0	-
Chacaltaya	10^{17}eV-10^{18}eV	1st	2.9±1.3	15.5±1.6
	10^{18}eV-10^{19}eV	2nd	9.0±5.0	7.4±1.9
Haverah Park	0.5-4×10^{18}eV	1st	340±150	2.9±5.1
HP, Yakutsk,Sidney	$>10^{19}$eV	1st	7600±1000	10.1±1.1
Yakutsk	8-10×10^{18}eV	1st	4160±1170	2.3±1.0
	$10^{18.7}$eV-$10^{19.7}$eV	1st	1400±410	1.3±1.1
		2nd	430	0.8

Compton-Getting effect of the Earth around the Sun is 4.0×10^{-4} at 35° and after this is corrected for the resulting vector has an amplitude of 6.0×10^{-4} at 3hr. They find this however not to be very significant but point out that they do not as yet have particularly good statistics.

The Mt. Norikura array (Nagashima K. *et al* 1990) has data from 1973-1987. A pressure correction with barometric coefficient $\sim$ -0.7% per mb was applied and the temperature effect found to be negligible. A significant 1st harmonic of amplitude $6.0\pm0.3\times10^{-4}$ was found at phase 0.8±0.3 hr LST for median energy 1.5×10^{13}eV. They found the anisotropy to be *falling* with energy as they found no significant sidereal variation for median energy 2.0×10^{14}eV.

EAS-TOP data covering 1990-1992 was corrected for pressure with a barometric coefficient of -0.66% per mb. At 6×10^{13}eV a significant 1st harmonic of $6.5\pm0.9\times10^{-4}$ was detected at phase $2.6^{\pm}0.5$hr LST. No significant second harmonic was seen. For increasing declination this anisotropy was seen to have constant phase and increasing amplitude as would be expected for a cosδ behaviour of a vectorial anisotropy. (Aglietta M *et al* 1993) .

In the Southern hemisphere the Liawenee array data from 1982-1988 taken with a median energy 7×10^{13}eV was corrected for pressure, temperature and a Compton-Getting effect caused by the Earth's motion round the Sun. The resulting sidereal vector had an amplitude of 2.0×10^{-4} (Fenton A.G. *et al* 1990).

Data taken with the Chacaltaya array from 1964 - 1979 indicate that in the region 10^{17}eV-10^{18}eV the first harmonic dominates and has amplitude $2.9\pm1.3\times10^{-2}$ and phase 15.5±1.6hr while in the region 10^{18}eV-10^{19}eV (1972 - 1979) the second harmonic is seen to dominate with amplitude $9.0\pm5.0\times10^{-2}$ and phase 7.4±1.9hr. (Anda R. *et al* 1981). Haverah Park found in their data from 1963-1980 that $>3\times10^{19}$eV showers arrived preferentially from high Galactic latitudes while below this energy there was a preference for low

Galactic latitudes. They also found evidence of increasing enhancement from below the plane over the energy region 5×10^{17}eV to 10^{19}eV. Between 0.5-4×10^{18}eV they found a first harmonic of amplitude $3.4\pm1.5\times10^{-2}$ and phase 2.9±5.1hr (Astley S.M. *et al* 1981.) 313 EAS events $>10^{19}$eV were combined from Haverah Park, Yakutsk, Sydney and Volcano Ranch and an anisotropy of 7.6×10^{-1} was found in direction 10.1±1.1hr. Clearly however at such high energies the statistics are very poor and significance has to be accordingly low. Temperature and pressure corrections were applied to data taken from the Yakutsk array. A first harmonic amplitude of $4.16\pm1.17\times10^{-1}$ was found with phase 2.3±1.0hr in the energy region 8-10×10^{18}eV however no significant anisotropy was seen $>10^{19}$eV.

Data from Yakutsk (Egorov T.A. *et al* 1991) in the region 10^{17}eV-10^{20}eV taken between 1974 and 1991 was analysed and no statistically significant amplitude in harmonics found. However $>10^{18.25}$eV the phase is in the direction of the plane. Selecting the energy region $10^{18.7}$eV-$10^{19.7}$eV they found a significant anisotropy with a 1st harmonic of amplitude $(1.40\pm0.41)\times10^{-1}$ with phase 1.3±1.1hr and 2nd harmonic amplitude 4.3×10^{-2} and phase 0.8hr.

SUGAR (Bray *et al* 1981) found no significant 1st, 2nd or 3rd harmonics in data covering 1967 - 1979 at 10^{16}eV-10^{21}eV. Also the Fly's Eye ($>10^{17}$eV experiment with data taken from 1981-1988 found no evidence of any significant anisotropy (Cassiday G.L. *et al* 1990). Data taken $>10^{16}$eV with the Akeno array (1984-1990) and AGASA (1990-1991) show no significant first or second harmonics in sidereal time. (Hayashida N *et al* 1991).

6.1.3 The Magellanic Clouds

Alternatively Ginzburg proposed , about 20 years ago,looking to the Magellanic Clouds for a possible answer to the question of the origin of CR (Ginzburg 1972). The amount of interstellar matter in the clouds has been calculated by radio measurements of neutral

hydrogen. Ginzburg used this to calculate the expected flux of CR from the clouds for the cases of the CR being a) Galactic and b) EG. If the former is the case then Ginzburg calculated that the flux of γ-rays should be approximately one third that if the latter is true. Also if the CR are of Galactic origin then there should be a significantly different output form each of the clouds.

The Compton GRO took 6 weeks worth of data from the SMC (Streekumar *et al* 1993) and observed 0.5×10^{-7} photons cm^{-2} sec^{-1}. When one compares this with the flux expected if the CR are EG, $(2.4\pm0.5)\times10^{-7}$ photons cm^{-2} sec^{-1} then this clearly points towards a Galactic origin for the CR. Chi et al (1993) put an upper limit of 11% on the contribution of EG CR to the flux seen at Earth in the region 10^9eV - 10^{10}eV.

6.2 Origin of Solar and Sidereal Variations

At the energies discussed in this thesis solar modulation can be neglected as this effect ceases to be important above $\sim10^{12}$eV. One can ignore the effects of the interplanetary magnetic field and solar wind. However there are certain effects which can produce spurious anisotropies and distort any real Galactic anisotropy. In general these occur in solar time but can generate spurious sidereal anisotropies. Such effects can be divided into two main categories: a) those occurring outside the atmosphere and b) those occurring within the Earth's atmosphere.

6.2.1 Anisotropy from Beyond the Earth's Atmosphere

The Compton-Getting effect arises from the relative motion between an observer and the isotropic CR flux (Compton A.H. & Getting I.A. 1935). The maximum flux is expected

in the direction in which the observer is moving and the minimum in the diametrically opposite direction. The amplitude of this effect can be given by $\delta = \frac{(2+\gamma).v}{c}$ where $\delta = \frac{(I_{max}-I_{min})}{(I_{max}+I_{min})}$ and γ is the exponent of the differential rigidity spectrum. Taking γ=2.6 we find the effect for the Earth's motion round the Sun to give an anisotropy amplitude of 4.6×10^{-4} with a phase of $\sim$ 06hr since v$\sim$30kms^{-1} (eg Thambyahpillai T. 1975). For Baksan at latitude of 43° the effect is $4.6\times\cos(43)\times10^{-4}=3.4\times10^{-4}$. This effect is energy independent. Another Compton-Getting effect is that caused by the motion of the solar magnetic field with respect to the Earth. This effect is however energy dependent and can be neglected at the energies discussed in this thesis.

6.2.2 Anisotropies from Within the Earth's Atmosphere

Both atmospheric temperature and barometric pressure effects can produce anisotropies in solar time. These affect the production of secondary particles in the cosmic ray shower because temperature and pressure variations will affect the number density of particles in the atmosphere and hence the probability of an interaction with a cosmic ray. This can be compensated for by assuming a linear relationship between the pressure and count rate and finding the correlation coefficient. To some extent pressure and temperature are interelated and so one would not want to find a separate correlation for temperature and then correct separately. Here we find a barometric coefficient, correct that data using this and then assume any residual harmonic in solar time is due to a temperature effect.

6.3 Harmonic Analysis

It was in 1954 that Farley and Storey first applied the known theory of radio communications to the problem of probing the cosmic ray anisotropy by means of harmonic analysis

(Farley & Storey 1954). It is assumed that any genuine anisotropy in the arrival directions of cosmic rays would manifest itself as an intensity wave in sidereal time , say

$$I(t) = I_o + i \cos[2\pi(N+1)t - \theta]$$

where I = the mean annual rate in sidereal time

N + 1 = is the number of solar days in a year (366)

t = the time in years

i , θ = the relative amplitude and phase of the sidereal variation.

It is known that effects such as diurnal temperature changes can produce a similar wave in solar time. The problem arises from the fact that such a solar wave can produce spurious sidereal variations also. Consider such a solar wave to have the form

$$S(t) = S_o + S \cos(2\pi Nt - \alpha)$$

where S = the mean annual rate in solar time

N = is the number of solar days in a year (365)

t = the time in years

S , α = the relative amplitude and phase of the solar variation.

It is quite possible that such a variation should not be constant throughout the year. Suppose that the amplitude S itself undergoes an annual modulation of amplitude A and phase β

$$S(t) = S\,[\,1 + A \cos(2\pi Nt - \beta)]$$

The case of the phase being modulated shall be discussed later.

Then the overall solar variation would have the form

$$S(t) = S_o + S + (S\,A\cos[2\pi(t-\beta)]\cos(2\pi Nt-\alpha)$$
$$= S_o + S\cos(2\pi Nt-\alpha) + S\,A\cos[2\pi(t-\beta)]\cos(2\pi Nt-\alpha)$$

Using the cosine identity we find

$$\cos(2\pi Nt-\alpha)\cos[2\pi(t-\beta)] = \frac{1}{2}[\cos(2\pi Nt-\alpha+2\pi(t-\beta)+\cos(2\pi Nt-\alpha-2\pi(t-\beta)]$$
$$= \frac{1}{2}[\cos(2\pi t(N+1)-\alpha-2\pi\beta] + \frac{1}{2}[\cos(2\pi t(N-1)-\alpha+2\pi\beta]$$

So that

$$S(t) = S_o + (S\cos(2\pi Nt-\alpha) + \frac{SA}{2}[\cos(2\pi t(N+1)-\alpha-2\pi\beta] + \frac{SA}{2}[\cos(2\pi t(N-1)-\alpha+2\pi\beta]$$

Clearly the second term in the expression will give a spurious sidereal component there being N + 1 sidereal days in a year. Then the observed sidereal variation would be

$$i'\cos(2\pi(N+1)t)+\theta' = i\cos[2\pi(N+1)t-\theta] + + \frac{SA}{2}[\cos(2\pi t(N+1)-\alpha-2\pi\beta]$$

Here t is zero at 0.0 on September the 22nd when solar and sidereal time coincide. Thus one would detect a sidereal amplitude and phase of i' and θ' as opposed to the true i and θ.

The N - 1 term would cause a spurious component in what was termed anti-sidereal time there being N - 1 antisidereal days in a year. This is a mathematically rather than physically motivated time coming out simply due to the expansion of the cosine term. However it does provide a useful tool in determining the real sidereal variation. It can be seen that the sidereal and antisidereal components have the same amplitude $\frac{SA}{2}$ and

are symmetric about the solar vector which has phase α the sidereal component having phase α - $2\pi\beta$ and the antisidereal component having phase α + $2\pi\beta$. Provided that data is taken for complete years to avoid spurious variations at other frequencies then it is possible to extract the real sidereal variation by a method of vector subtraction. The spurious sidereal variation will be equal to the reflection in the solar vector of the antisidereal variation both of which are measurable. This reflection is then subtracted from the observed sidereal variation to remove the spurious and leave the real sidereal variation free from solar variation effects.

Figure 6.1 shows a harmonic dial with a schematic representation of the situation. The length of the vector shows the amplitude of the harmonic and the direction shows the phase. Because the solar clock loses $\sim$ 4 minutes per day with respect to the sidereal clock (that is approximately 2 hours per month) the vectors plotted in sidereal time for successive months will rotate anticlockwise. If the amplitude of the solar vector is constant as is the phase then vectors 6 months apart will cancel as they have equal amplitude and are diametrically opposite. However if the amplitude and/or phase of the solar vector varies then the sidereal vectors will not reduce to zero. In this way a variation in solar time can cause spurious sidereal variations.

In the Figure 6.1, vector S represents the solar vector. Vector SpS+Si shows the measured sidereal vector which is a combination of a genuine sidereal vector and a spurious sidereal vector generated by the solar vector. Vector SpA shows the measurable spurious anti-sidereal vector generated by the solar vector and SpS shows the spurious sidereal vector generated by the solar vector which can be calculated as it is a 'mirror reflection' of SpA through S.

Here we have assumed only a modulation of the amplitude and found that 2 spurious sidebands result. If however the phase is allowed to vary also then the situation is very

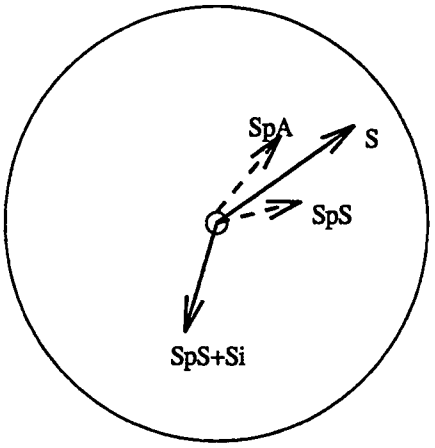

Figure 6.1 A harmonic dial showing the Farley-Story technique.

complex with many sidebands resulting and little hope of retrieving the original sidereal variation. In order to proceed we assume no phase modulation.

6.4 Anisotropy Analysis

6.4.1 Data Selection

In an attempt to keep the non-uniformity of sidereal exposure to a minimum the following selection criteria were applied to the raw data:

- all runs for which the counts deviated by more than 4σ from the daily mean were excluded
- after this 4σ cut all days with less than 70 runs left were excluded
- as noted earlier the count rate fell drastically for a large part of 1987 and some of 1988. None of the data for this period was included
- any event with a zero time delay for any of channel 1 - 4 was excluded It should be noted that with the emphasis changing from discrete sources to large scale structure it was no longer felt necessary to impose a zenith cut of 40° or a difference of differences cut (See Chapter 3). Following these selection criteria the data from 1985 - 1992 comprised of 66.97 $\times 10^6$ events. In actual fact, for practical reasons,the data was processed not in 8 separate years but as 1985-1986 together, 1987-1989 together and then each of 1990 - 1992 individually. Rather than display each set of results individually we show the combined results for 1985-1989 and 1990-1992 which show the characteristics of the each data set. We also show the final results for the whole dataset covering 1985-1992.

6.4.2 Observed Maps

The RA-dec and HA-dec distributions from 0° - 360° and 0° - 90° were obtained and binned in 2° bins. The hour angle distributions of summed data from 1985-1989 and 1990-1992 are shown in Figure 6.2

6.4.3 Pressure and Temperature Effects

A pressure correcting wave was obtained for each month of the year based on the average of the 1980 - 1985 data (unfortunately the barometer at Baksan broke in 1985 and was no pressure data was available until the upgrade of 1991). For each month there are 6 harmonics. The barometric coefficient was found empirically to be -1.17 % per mm Hg.

The temperature effect can be a combination of atmospheric effects on the actual shower itself and an effect due to the efficiency of the detectors themselves.

6.4.4 Predicted Maps

The non-uniformity of exposure in sidereal time is accounted for by obtaining a map of what an isotropic flux would look like subject to the same non-uniformity. The procedure is as follows. First the data on the number of events per run is binned as a function of solar, sidereal and anti-sidereal time with and without the pressure wave being applied. The pressure corrected and uncorrected values are compared for solar, sidereal and anti-sidereal time. The pressure wave is expected to manifest itself as a solar wave and one would thus expect the greatest difference in pressure-corrected and raw data to be in solar time. This is indeed the case and although the pressure wave was obtained for 1980 - 1985 data it does seem to flatten the solar wave as would be expected for the data covering 1985 - 1992. (See Figures 6.3 - 6.5)

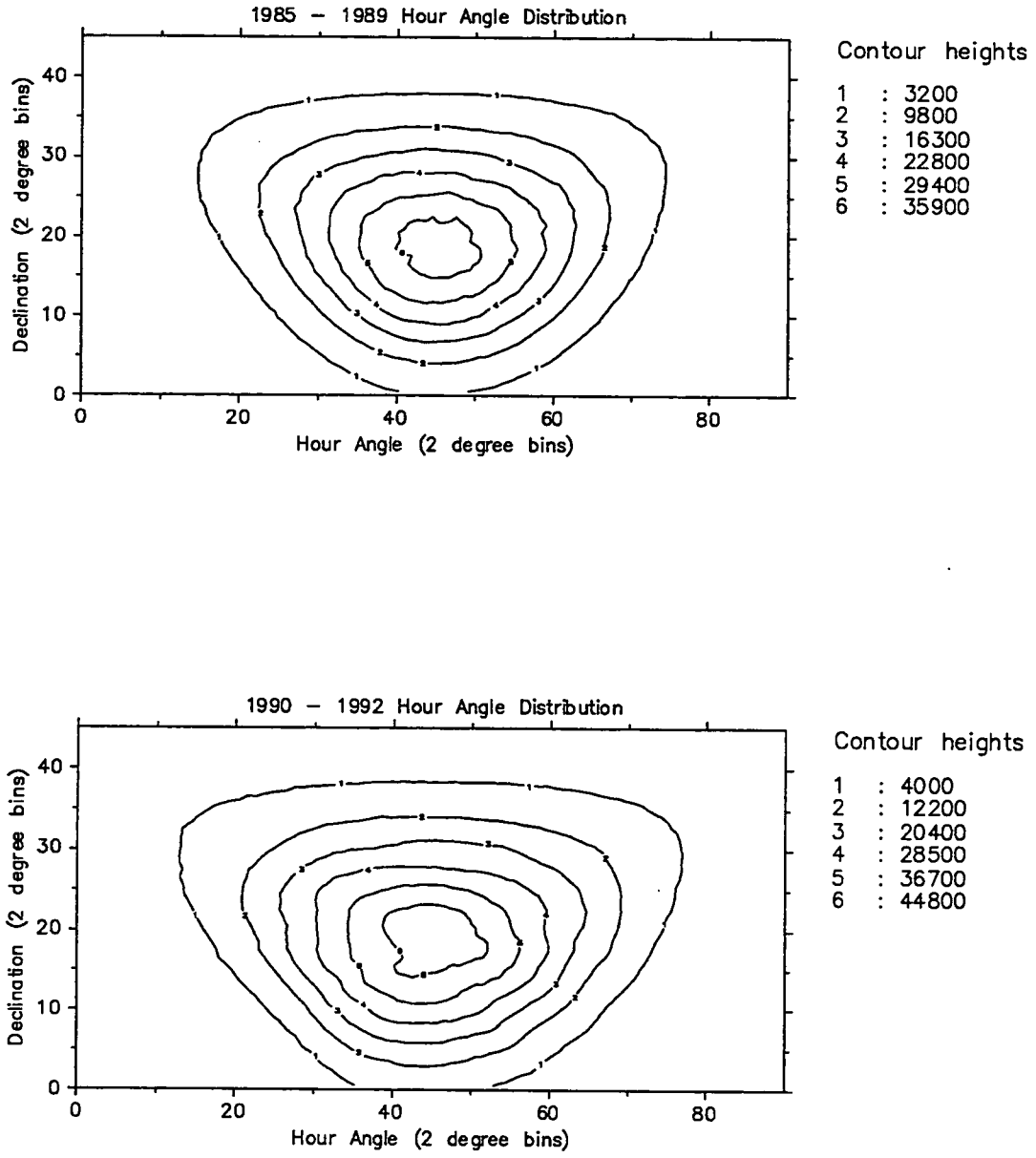

Figure 6.2 The hour angle distributions for 1985-1989 and 1990-1992.

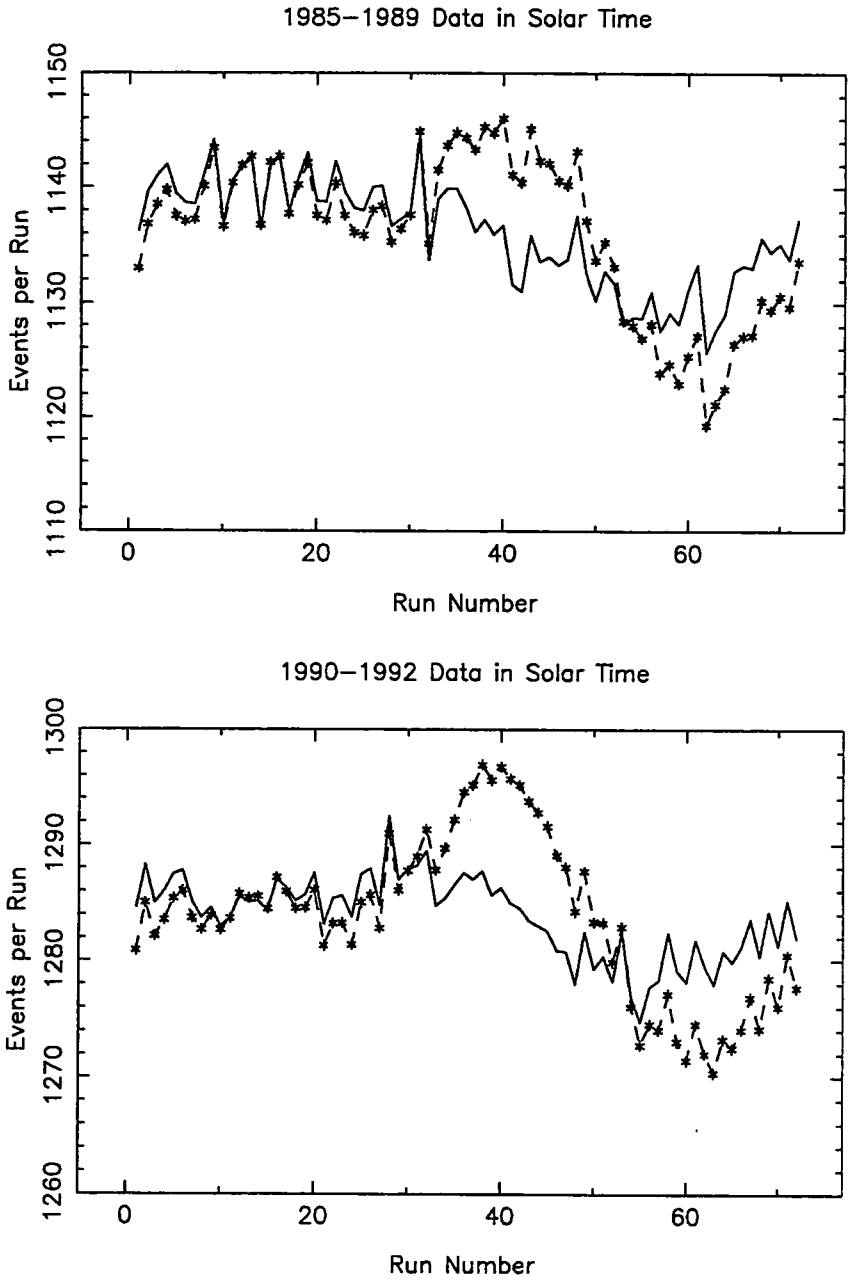

Figure 6.3 Data for 1985-1989 and 1990-1992 binned in solar time. The dotted lines shows the raw data and the solid lines the pressure corrected data.

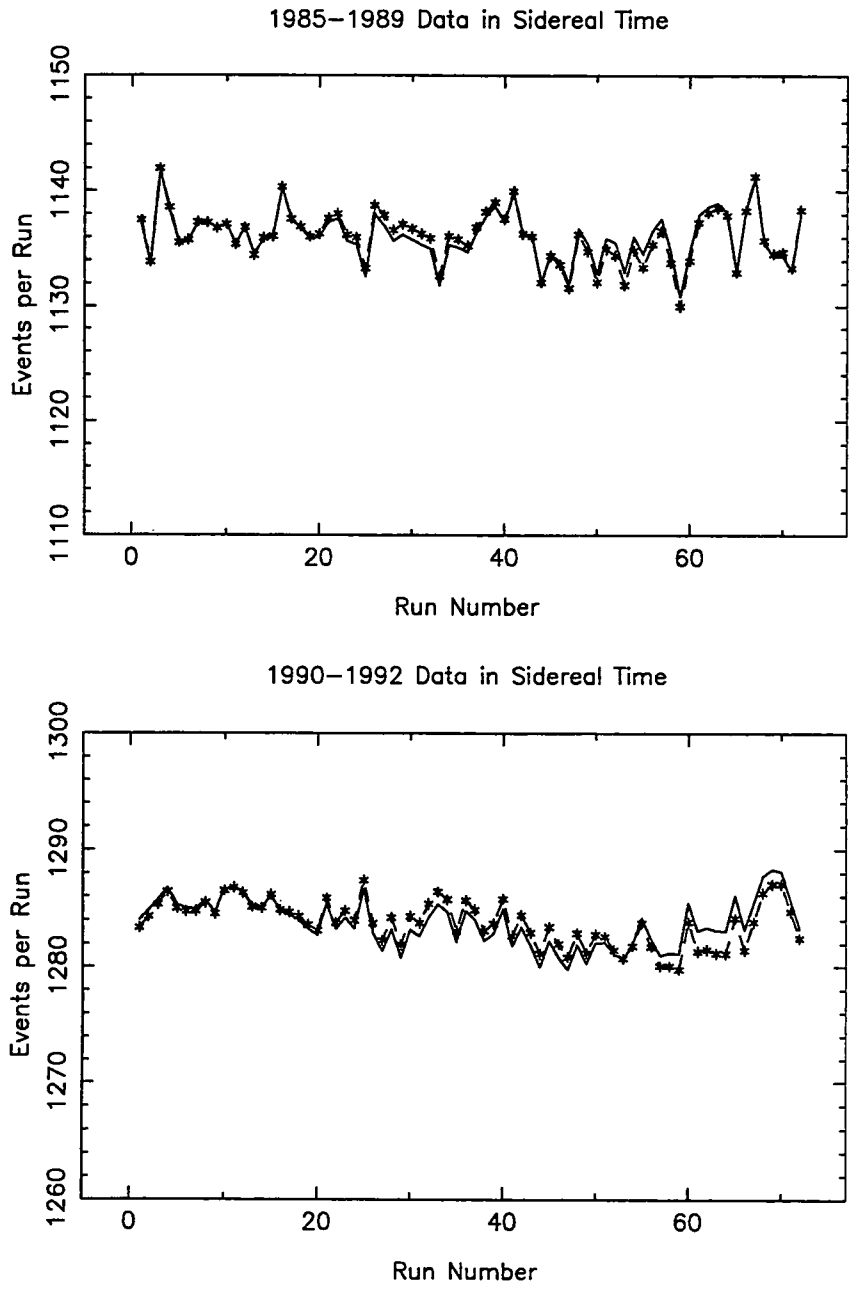

Figure 6.4 Data for 1985-1989 and 1990-1992 binned in sidereal time. The dotted lines shows the raw data and the solid lines the pressure corrected data.

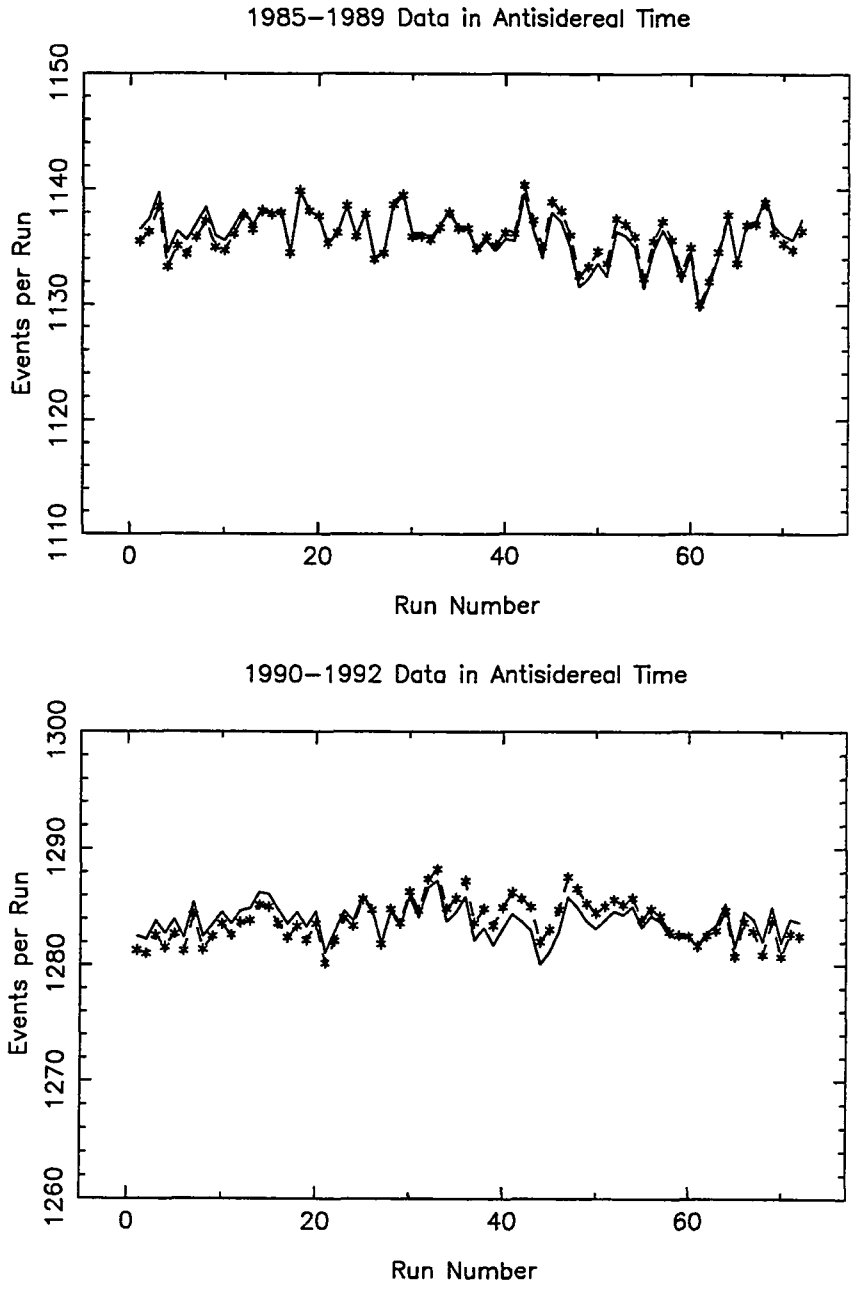

Figure 6.5 Data for 1985-1989 and 1990-1992 binned in antisidereal time. The dotted lines shows the raw data and the solid lines the pressure corrected data.

A harmonic analysis was then performed on the 3 times pressure-corrected data and 1st, 2nd and 3rd harmonic amplitude and phases found for each. Any residual solar wave left after pressure correction is thought to be due to the temperature effect. The 1985 - 1989 solar time data had a 1st harmonic amplitude of 4.7×10^{-3}. For 1990 - 1992 this dropped by approximately half following measures to improve the stability of the detectors by controlling their temperature to some degree. (See Table 6.2)

From the solar and anti-sidereal 1st harmonic vectors it was possible to obtain the spurious sidereal vector generated by the solar wave ie the reflection of the anti-sidereal wave in the solar wave. This vector clearly has the same amplitude as the anti-sidereal one but differs in phase.

The exposure distribution was then obtained. The events per run were binned in 180 2° bins of sidereal time having been corrected for pressure, a solar wave and a spurious sidereal wave. The pressure wave had 6 harmonics, the solar 3 and the spurious sidereal 1. Prior to binning, the exposure distribution was normalised by the total number of events in the observed map.

This exposure was then folded in with the HA-dec distribution to allow for the angular acceptance of the array. In this way a map was obtained which would correspond to an isotropic incident flux of cosmic rays as seen by our detector.

6.4.5 Comparison of the predicted map with those observed

A final map was produced by comparing the values in corresponding bins of the observed RA-dec distribution and the predicted RA-dec distribution. The results were output as $\frac{on-off}{\sqrt{off}}$. For each year section all bins where the excess was greater than 3σ were noted to see if any persisted throughout. No such bins were immediately apparent. (See Figure 6.6)

Table 6.2 Solar, Sidereal and Antisidereal Harmonics.

Years	Time Binning	Harmonic	Amplitude $/10^{-4}$	Phase (RA) hours
1985 - 1989	Solar	1	47.6±0.5	6.1±0.1
		2	15.0±0.9	3.2±0.3
		3	44.1±1.7	2.2±1.3
1990 - 1992		1	28.9±0.5	7.3±0.1
		2	15.0±0.7	23.9±0.2
		3	00.0±1.9	4.5±4.1
1985 - 1989	Sidereal	1	6.8±1.4	2.7±0.7
1990 - 1992		1	14.8±0.7	2.7±0.2
1985 - 1989	Antisidereal	1	13.4±1.0	5.8±0.3
1990 - 1992		1	4.2±1.2	7.9±1.1

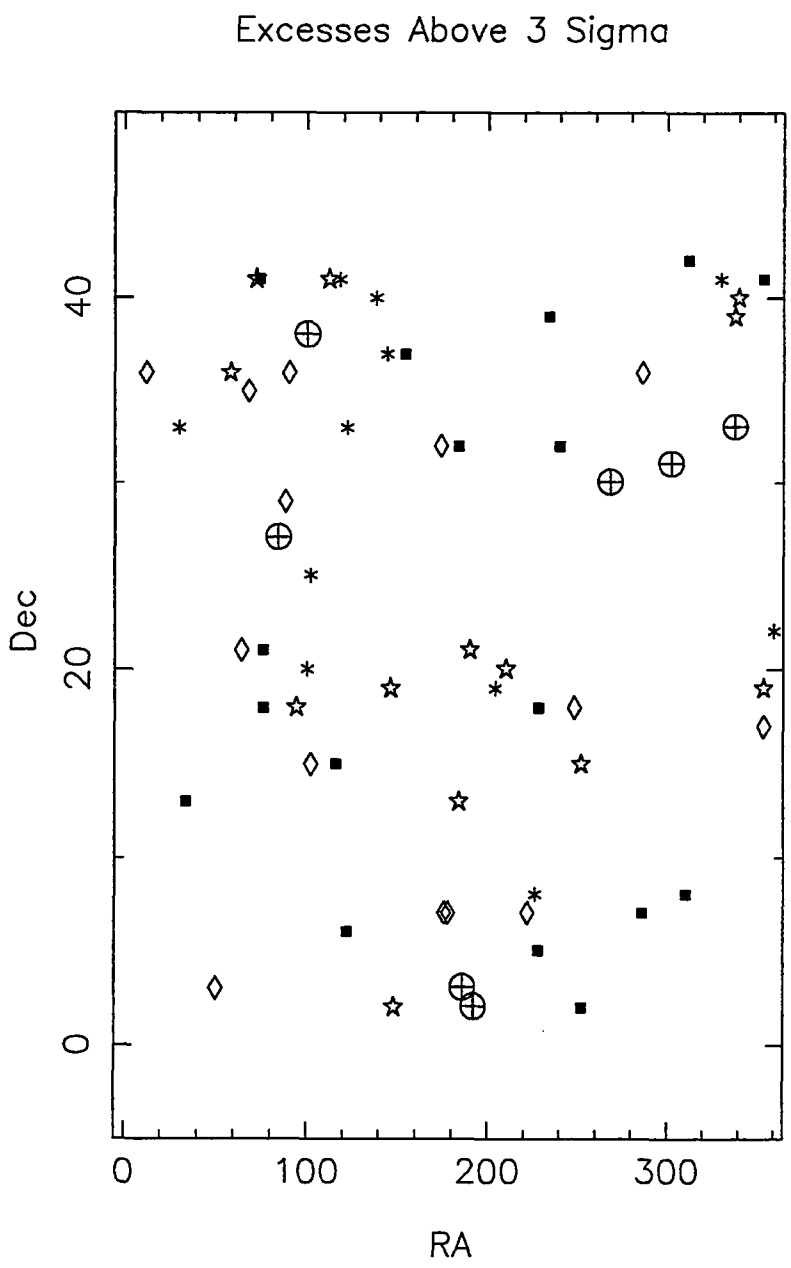

Figure 6.6 The bins showing $> 3\sigma$ excess over the expected number of counts are shown with different symbols for each of the 8 years.

In order to see any large scale features this resulting map was smoothed with a Gaussian smoothing function with σ equal to 5 pixels or 10 degrees. The box for smoothing was taken out to $\pm$ 3σ. Naturally such a smoothing procedure incurs some edge effects. In order to eradicate these the unsmoothed map was duplicated on the left and right of the original and this 3 times larger map was smoothed. The two extra right and left hand maps were then removed to leave a map smoothed with no left or right hand side edge effects. In order to remove the edge effects at the top and bottom of this smoothed map it was decided simply to cut the map from 0° - 90° to 10° - 70° in declination. In fact the statistics in these excluded regions were poor in any case. Figure 6.7 shows the resultant maps for 1985 - 1989 , 1990 - 1992 and finally 1985 - 1992.

6.4.6 Harmonic Analysis

The observed data and the predicted data were summed separately over declination and then the former divided by the latter. In this way it was possible to apply a harmonic analysis and see if there were any true sidereal wave.

The 1985 - 1989 and the 1990 - 1992 data have 1st harmonics which agree well in phase and amplitude. Both sets of data also show negligible 2nd and 3rd harmonics. This fact is quite reassuring given the difference in the exposure of both sets of data and the fact that the former had a solar wave amplitude approximately twice the latter. It seems we are then justified in combining both sets of data and obtaining an overall value for this time. The combined data again shows negligible evidence of 2nd or 3rd harmonic but gives a 1st harmonic amplitude and phase of $(12.7 \pm 1.2) \times 10^{-4}$ at 23.1$\pm$0.3hr consistent with the two individual data set values.

Note that this value takes no account of any possible cosδ effect on the sidereal anisotropy. In order to compare anisotropies from similar experiments in a similar energy region it

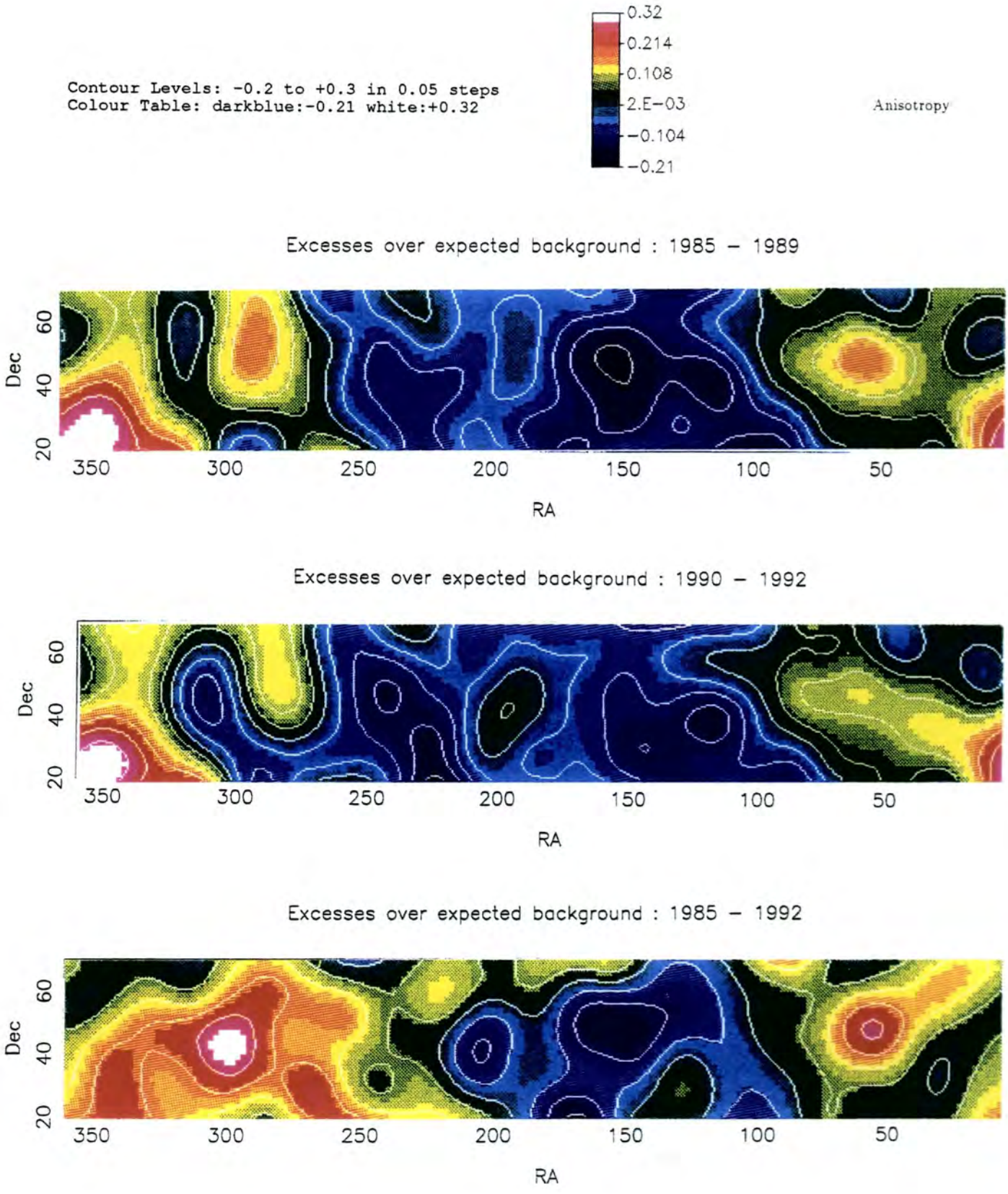

Figure 6.7 The smoothed sky maps from 10° - 70° in declination for the three data sets.

Table 6.3 Final Results of Harmonic Analysis.

Years	No. of Showers /10^6	Harmonic	Amplitude /10^{-4}	Phase (RA) hours
1985-89	27.92	1	12.8 ± 2.5	21.6 ± 0.7
		2	3.6 ± 3.9	—
		3	0.0 ± 0.5	—
1990-92	39.04	1	13.5 ± 1.7	0.1 ± 0.5
		2	2.8 ± 3.1	—
		3	1.7 ± 3.3	—
1985-92	66.97	1	12.7 ± 1.2	23.1 ± 0.3
		2	0.0 ± 3.1	—
		3	2.9 ± 2.0	14.1 ± 2.2

is worthwhile taking account of this by dividing by cosλ where λ is the latitude of the observatory.

Previous work using the Baksan neutrino observatory data from 1982-1986 gives a first harmonic of $(10.3\pm1.1)\times10^{-4}$ at a phase of (1.9±0.4)hr - the amplitude has been extrapolated to $\delta = 0°$ and a similar Farley and Storey analysis performed (Andreyev Yu.M. *et al* 1987). Data at approximately 10^{13}eV from the central carpet area only was analysed (Alexeenko V.V. *et al* 1981) covering 1980-1981 was analysed and a pressure correction applied. A first harmonic amplitude of 0.057±0.004 was found at phase 1.4±0.3hr and a second harmonic of 0.019±0.004 at 6.2±0.4hr. Extrapolated to $\delta = 0°$ these amplitudes become 0.078±0.005 and 0.026±0.005 respectively. Further analysis (Alexeenko V.V. & Navarra G 1985) showed a first harmonic amplitude of 0.058±0.003 was found at phase 1.2±0.2hr and a second harmonic of 0.016±0.004 at 6.1±0.5hr for 10^{13}eV-10^{14}eV. Extrapolated to $\delta = 0°$ these amplitudes become 0.079±0.004 and 0.022±0.005 respectively.

In comparing results from other experiments it is worth noting which corrections have been applied. All the following results, apart from the composite 1951-1965 results have had some form of pressure correction applied. The Akeno and Liawenee data have also had a correction for the Compton-Getting effect of the Earth's motion around the Sun.

While the Baksan value seems to be quite large compared to similar experiments one can take some confidence in it due to its consistency throughout the years from 1985-1992 as can be seen from the separate results from 1985-1989 and 1990-1992. The Baksan experiment is also the only one of those above to have employed the Farley-Storey method to eradicate spurious sidereal variations and no correction for the Compton-Getting effect has been made explicitly.

Table 6.4 Comparison of Sidereal First Harmonic .

Array	Energy (eV)	Data Period	Correction	Amplitude	Phase (hr)
Mt. Norikura (36°N)	1.5×10^{13}	1973-1987	pressure	$7.4\pm0.1\times10^{4}$	0.8 ± 0.3
EAS-TOP (42°N)	6×10^{13}	1990-1992	pressure	$8.8\pm1.2\times10^{4}$	2.6 ± 0.5
Liawenee (42°S)	7×10^{13}	1982-1988	pressure,CG	2.7×10^{4}	?
Mt. Norikura (36°N)	2×10^{14}	1973-1987	pressure	-	-
Akeno (35°N)	2×10^{14}	1984-1988	pressure,CG	7.3×10^{4}	0.8 ± 0.3
Baksan (43°N)	2×10^{14}	1985-1992	pressure,F-S	$17.4\pm1.6\times10^{4}$	23.1 ± 0.7
Composite	3×10^{14}	1951-1965	-	$7.5\pm2.0\times10^{4}$	20.1 ± 1.3

6.4.7 Galactic Plane Enhancement.

To investigate, qualitatively at any rate, any possible correlation between our final map of excesses and the distribution of the neutral hydrogen in the Galaxy use is made of a map of the HI density binned into 2° bins. This is then weighted according to the exposure and folded in to the predicted event distribution to give a simulated map with an enhanced component from the plane (as HI basically traces the Galactic Plane). This would be the case either if the discrete source distribution followed the distribution of gas or if the cosmic rays were interacting with the gas directly and producing a diffuse component to the γ-ray flux.

To show how well an actual Galactic Plane enhancement would be seen following such a treatment of the data we show simulated data with the same total number of events subjected to the same smoothing procedure. A model with a component from the plane of 6×10^{-3} of the cosmic ray particle flux per 10^{22} atoms of HI gives a similar level of anisotropy to that observed. We apply random Poisson fluctuations to the predicted number of events in each $2^\circ\times2^\circ$ bin. Figure 6.8 shows firstly the resultant HI map and secondly the final observed map for 1985 - 1992 with the contoured HI map superimposed on top. Certainly the simulated and observed maps agreed to the extent that they both had minima at high Galactic latitude but the Galactic plane did not show up well in the observed data with a local minimum falling at the place of a peak on the HI Galactic Plane.

The number of events within a given distance of the Galactic Plane were compared for the observed and predicted maps. Within 10° of the Galactic Plane there is a 4×10^{-4} fractional excess over expectation amounting to a 1.5σ effect. However this excess persists if one continues out to within 35° of the plane and is probably due simply to the coincidence of a minimum in the cosmic ray 1st harmonic with the region of high Galactic latitude.

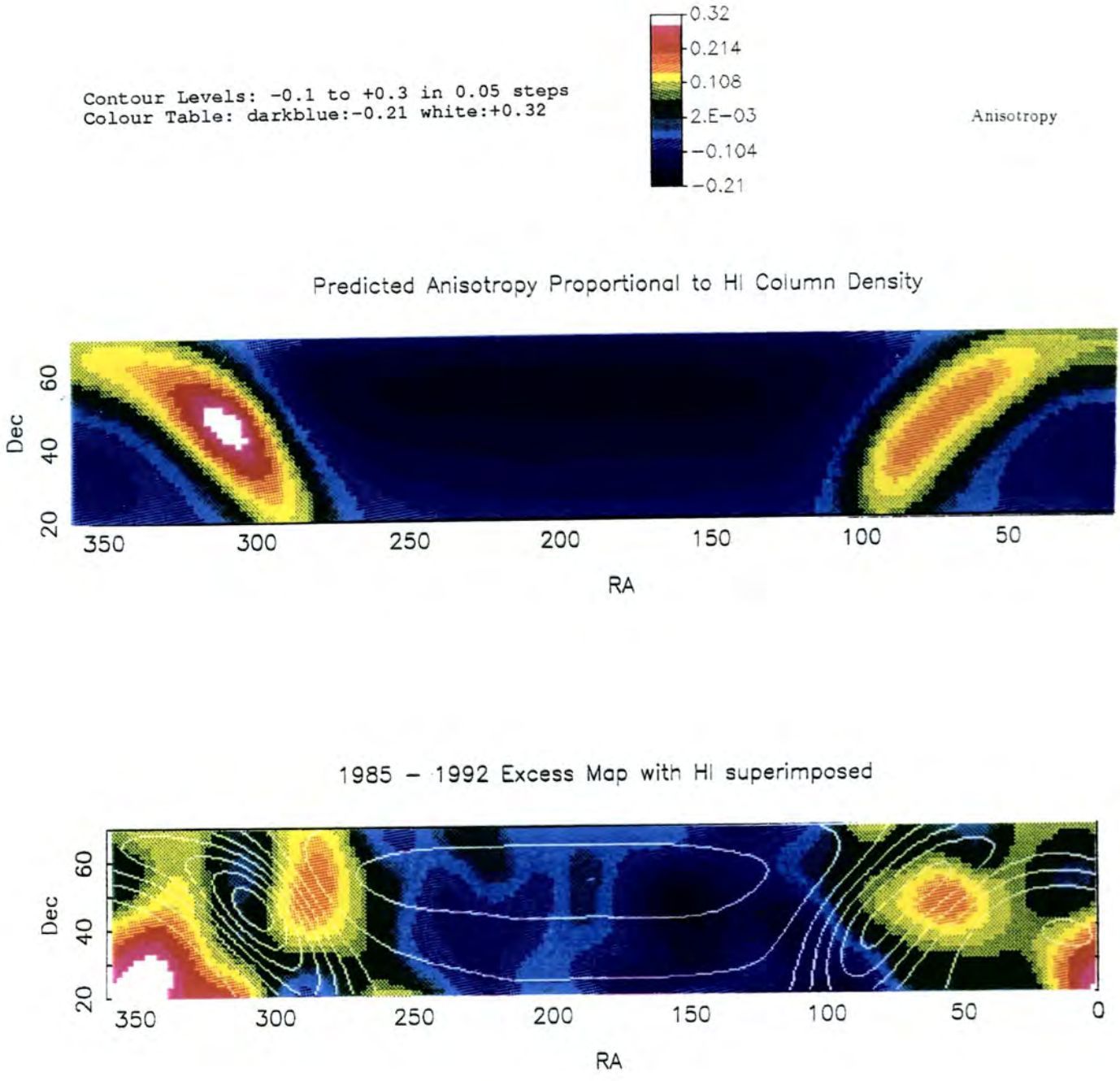

Figure 6.8 The top figure shows the predicted map based on the HI distribution and the lower figure superimposes the contours from this on to the observed map for 1985-1992.

However this figure of 4×10^{-4} can be regarded as an upper limit to the ratio of flux of γ-rays from the plane to the flux of cosmic rays. Thus we find an upper limit of $\frac{I_\gamma}{I_{CR}} < 4\times10^{-4}$ at $\sim$ 0.2PeV. This upper limit is higher than that obtained by the CASA/MIA collaboration. It does not however make any assumptions on the μ-content.

In order to calculate an upper limit to the γ-ray flux at 2×10^{14}eV we again use the Hillas cosmic ray spectrum below 2 PeV as suggested by Nagle,Gaisser & Protheroe (1988) that is :

$$I_{CR}(> E_{th}) = 10^{-10} \times (\frac{E_{th}}{2PeV})^{-1.55}\ cm^{-2}\ s^{-1}\ sr^{-1}$$

which gives I_{CR} ($> 2\times10^{14}$eV) = $3.55\times10^{-9}\ cm^{-2}\ s^{-1}\ sr^{-1}$. Then using $\frac{I_\gamma}{I_{CR}} < 4\times10^{-4}$ we find an upper limit to the γ-ray flux of I_γ ($> 2\times10^{14}$eV) $< 1.4\times10^{-12}\ cm^{-2}\ s^{-1}\ sr^{-1}$.

This is not inconsistent with the predicted value of $6.6\times10^{-13}\ cm^{-2}\ s^{-1}\ sr^{-1}$. $> 10^{14}$eV from the Galactic Centre (Berezinsky & Kudryavtsev 1990, Ticona R. *et al* 1993).

REFERENCES : CHAPTER 6

Aglietta M. *et al* Nuclear Physics B (Proc Suppl) 33A,B (1993)

Anda R. *et al* 17^{th}I.C.R.C. **2** 164 (1981)

Andreyev Yu.M. *et al* 20^{th}I.C.R.C. **2** 22 (1987)

Astley S.M. *et al* 17^{th}I.C.R.C. **2** 156 (1981)

Axford W.I. Ap. J. Suppl. Ser. **90** 937 (1994)

Berezinsky V.S. & Kudryavtsev V.A. Ap.J. **349** 620 (1990)

Bergeson *et al* 16^{th}I.C.R.C. 4 188 (1979)

Berkovitch & Agrawal 17^{th}I.C.R.C. **10** 246 (1981)

Blake P.R. *et al* 22^{nd}I.C.R.C. **2** 133 (1991)

Blake P.R. *et al* 23^{rd}I.C.R.C. **1** 471 (1993)

Cassiday G.L. *et al* Ap. J. **351** 454 (1990)

Chi X. *et al* J. Phys. G:Nucl. Part. Phys. **19** 795 (1993)

Clay R.W. *et al* Nature **309** 687 (1984)

Compton A.H. & Getting I.A. Phys. Rev. **47** 11 87 (1935)

Davis *et al* 16^{th}I.C.R.C. 4 210 (1979)

Egorov T.A. *et al* 22^{nd}I.C.R.C. **2** 121 (1991)

Fenton A.G. *et al* 21^{st}I.C.R.C. **3** 177 (1990)

Fenton & Fenton Proc International CR Symp. on High Energy CR Modulation Tokyo 313 (1976)

Ginzburg V.L. Nature Physical Science **239** 8 (1972)

Gombosi *et al* 15^{th}I.C.R.C. **11** 109 (1977)

Hayashida N. *et al* 22^{nd}I.C.R.C. **2** 117 (1991)

Linsley J. 15^{th}I.C.R.C. **12** 203 (1977)

Matthews J AIP Conf Proc Ann Arbor **220** (1990)

Murakami K *et al* 21^{st}I.C.R.C. **3** 177 (1990)

Nagashima K. *et al* 21^{st}I.C.R.C. **3** 180 (1990)

Reynolds P.T. *et al* 21^{st}I.C.R.C. **2** 383 (1990)

Sakakibara *et al* Proc International CR Symp. on High Energy CR Modulation Tokyo 316 (1976)

Streekumar P. *et al* Phys. Rev. Lett. **70** 127 (1993)

Thambyahpillai T. Origin of Cosmic Rays 37 Eds. J.L. Osborne & A.W. Wolfendale (1975)

Ticona R. *et al* 23^{rd}I.C.R.C. **1** 475 (1993)

Wdowczyk J. Cosmic Radiation in Contemporary Astrophysics 149 Ed. M.M. Shapiro Erice (1986)

Wdowczyk J. % Wolfendale A.W. Ann. Rev. Nucl. Part. Sci **39** 43 (1989)

Yoshii H. *et al* 22^{nd}I.C.R.C. **2** 391 (1991)

7 CONCLUSIONS

7.1 Synopsis of Results

7.1.1 Angular Resolution

We have attempted to determine the angular resolution of the Baksan Air Shower Array using the CR shadow of the Sun and the Moon. Using 8 years of data a total of 213,313 events were recorded within 5° of the Sun or Moon. Although we are unable to say we have detected the Sun and the Moon at a particular confidence level as have other groups we can conclude that the angular resolution is about 2.5°-3.0° consistent with the value previously obtained from Monte-Carlo simulations. This is considerably larger than that of newer installations such as CASA/MIA and CYGNUS which can claim angular resolutions of <1° (Alexandreas *et al* 1993, Borione *et al* 1993d).

7.1.2 Point Sources

Using BASA we have looked at 18 candidate sources of UHE γ-rays. We have used an 'hour angle' method of calculating the expected number of events which has better statistics than the previous 8 off-source method used in the initial Russian analysis. In

each case we find only upper limits to the flux above 0.2PeV for DC emission from 1985-1992 (cf CASA/MIA flux limits). This reflects the general trend in the results coming from the newer and larger installations eg CYGNUS and CASA/MIA who both report only upper limits from candidate sources. The latest CASA/MIA flux limits (Borione *et al* 1993a,b,c) are of the order of 3 times smaller than BASA limits when they consider all events. When considering μ-poor events only this upper limit lowers to $\sim 1\times10^{-14}$ $cm^{-2}s^{-1}$. It should be noted that these limits are for 1990-1992 and BASA data covers 1985-1992.

There are 57 days where the excess for a single transit of a particular source is above 3σ. Given that we have searched for 18 sources for,on average, 1,862 days each we would expect about 44 such days. We find the distribution of daily excesses above 3σ to be consistent with a random distribution. The results of a periodicity analysis on such days points to 4 possible observations of pulsed emission at the 95% confidence level. These are 4U0115+63 on 19.03.89, PSR1953+29 on 12.02.85, 1E2259+586 on 01.08.91 and PSR0655+64 on 12.08.89. Without confirmation from other groups however the findings are not significant enough to stand alone.

7.1.3 Cosmic Ray Anisotropy

We have employed a Farley and Storey harmonic analysis (Farley & Storey 1954) to the 8 years worth of data comprising 66.97 $\times10^6$ events. In this way we hope to eliminate any spurious sidereal variations arising from modulated variations in solar time. These variations could occur naturally from eg changes in pressure and temperature.

When pressure corrections have been made and the Farley and Storey harmonic analysis performed we find negligible evidence of 2nd or 3rd harmonic but a 1st harmonic amplitude and phase of (12.7 $\pm$1.2) $\times$ 10^{-4} at 23.1° $\pm$ 0.3hr. When one takes into account the

$\cos\delta$ effect on the sidereal anisotropy this value becomes $17.4\pm1.6\times10^{-4}$. This value, while larger than some recently quoted eg (Fenton & Fenton 1976, Sakakibara *et al* 1976, Linsley J. 1977, Murakami K *et al* 1990, Nagashima K. *et al* 1990, Aglietta M *et al* 1993), is not inconsistent with the expected anisotropy of $\sim$1% expected at this energy range. Furthermore when one splits the data set into 1985-1989 and 1990-1992 one obtains consistent results.

We have also searched for a Galactic Plane enhancement which would occur if γ-rays were produced by interactions of cosmic rays near their sources (which are expected to be concentrated in the plane.) We find an upper limit of $\frac{I_\gamma}{I_{CR}} < 4\times10^{-4}$ at $\sim$ 0.2PeV and while this limit is higher than that obtained by CASA/MIA of $\frac{I_\gamma}{I_{CR}} < 8.0\times10^{-5}$ above 2×10^{14}ev (Matthew 1990) it does not make any assumptions on the μ-content of γ-ray initiated showers. Both upper limits are not inconsistent with the predicted value of $\sim7.0\times10^{-5}$ (Berezinsky & Kudryavtsev 1990).

7.2 Future Developments at BASA

7.2.1 Detector Temperature

With the upgrade in 1991 there was some attempt to control the temperature of the detectors. This involved a heater under the array of scintillators connected to a temperature probe. Results showed that these measures reduced the effect of outside temperature variations from about 4°C to about 1.5°C. The success of this could be seen in the large scale anisotropy analysis when it was found that once corrected for pressure the 1985-1989 data had a solar harmonic amplitude almost twice that of the 1990-1992 data (it is expected

that any solar harmonic variation remaining after the effect of pressure is removed is due to temperature effects). It is thought that the main effect is due to sunlight and there are plans to whitewash the outer detector buildings and perhaps install a permanent heater to raise the temperature to about 20°C so that a 1.5°C change would be less significant.

7.2.2 Pressure Data

The pressure wave which was used as a correction factor in the large scale anisotropy analysis was based on 5 years of data from 1981-1985. Although it did manifest itself primarily in solar time and did seem to flatten the count rate for 1985-1992 in solar time as it should this is of course not an ideal situation. The barometer used for pressure measurements was out of action between 1985 and 1991. However pressure data is now being successfully recorded every 20 minutes. It is expected, although this has not yet been checked, that this new data will give a very similar wave to that calculated for 1981-1985.

7.2.3 Particle Densities

As mentioned previously, up until now in the reconstruction of the arrival direction of events we have been limited to approximating the shower front to a plane wave. It is known however that actually the shower front is curved and such a plane front approximation is detrimental to the angular resolution of the array (the notable case is that of HEGRA who claim to observe solar/lunar shadowing when they adopt a curved front and not when they adopt a plane one). The reason that we have had no choice but to use a plane front is that there were no measurements of the particle densities at each detector. Thus it was not possible to locate the shower core and apply an appropriate correction to each of the detector's time delays dependant on that detector's distance from the shower axis. However in mid 1991 an upgrade in the detector meant that just such information was now

available. There have been some slight problems with the recording of these amplitudes primarily with the cables connecting the detectors to the main processing area. However once these are ironed out it will be possible to use the amplitude data in order to use a more accurate curved shower front fit and thereby improve the array's angular resolution.

7.2.4 GPS System

A major limitation of BASA up until now has been that there is no absolute timing system, The clock measuring arrival times with millisecond accuracy was thought to have a drift rate of 3-5 milliseconds per day but details of when the clock was reset and suchlike were scant. Furthermore the absence of absolute timing meant that any phase analysis could only be referred to an arbitrary point in the period with no possibility of finding the absolute phase of any possible emission seen. Since mid May of 1993 a GPS (Global Positioning System) receiver has been in operation at BASA. This allows absolute timing of arrival events and a very accurate measurement of the array position coordinates in real time. This should allow the accurate measurement of arrival times which, once barycentred, can be used confidently even for periodicity searches in fast millisecond pulsars.

7.2.5 Muon Detector

The main development at BASA involves the construction of a complementary muon detector. It is planned that the final detector will have an area of $700m^2$ with dimensions approximately 18m×39m. This is to be constructed in 3 sections each of dimension approximately 6m×39m. The first of these is already under construction and it is hoped that this first third will be completed by the end of 1993. The muon detectors are to be under approximately 1-1.3m of rock and the threshold energy will be 500MeV. The location will be as shown in Figure 7.2. A 6m×6m prototype has been in operation since June 1993

but there have been initial problems in reading out the amplitude and timing data from the computer. Although this is just a minor teething problem there is no data available as yet. When the muon detector is operational however it will be a major improvement to the array. For the first time it should be possible to measure the muon content of the showers coming from a particular source direction. As has been mentioned before, despite the theoretical predictions that γ-induced showers should have a muon content an order of magnitude less than hadron- initiated showers there have been notable instances of signals from potential sources having close to background muon content. Any further measurements of muon content of showers from candidate sources can only be for the good. If it were found that the signals from candidate sources were muon-poor then this could be used as a further a priori selection cut to enhance the signal of γ-rays for analysis.

REFERENCES : CHAPTER 7

Aglietta M. *et al* Nuclear Physics B (Proc Suppl) 33A,B (1993)

Alexandreas D.E. *et al* 23^{rd} I.C.R.C. **Vol 1** (1993) p223

Berezinsky V.S. & Kudryavtsev V.A. Ap.J. **349** 620 (1990)

Borione A. *et al* 23^{rd} I.C.R.C. **1** 286 (1993a)

Borione A. *et al* 23^{rd} I.C.R.C. **1** 385 (1993b)

Borione A. *et al* 23^{rd} I.C.R.C. **1** 425 (1993c)

Borione A. *et al* 23^{rd} I.C.R.C. **1** 220 (1993d)

Farley F.S.M. & Storey J.R. Proc Phys Soc **A67** 996 (1954)

Fenton & Fenton Proc International CR Symp. on High Energy CR Modulation Tokyo 313 (1976)

Linsley J. 15^{th}I.C.R.C. **12** 203 (1977)

Matthews J AIP Conf Proc Ann Arbor **220** (1990)

Murakami K *et al* 21^{st}I.C.R.C. **3** 177 (1990)

Nagashima K. *et al* 21^{st}I.C.R.C. **3** 180 (1990)

Sakakibara *et al* Proc International CR Symp. on High Energy CR Modulation Tokyo 316 (1976)

1 Appendix 1

We show here the data excluded on the grounds of anomalous time delays. (See Figures 1.2 - 1.12). The mean time delays over 24 hours were evaluated for each of the 6 detector channels. Zero time delays in channels 5 or 6 are perfectly acceptable as event arrival direction reconstruction is still then possible. Recall that as a rough guide to the order of magnitude of step change to be excluded the change in arrival direction of a given event for different time delays was calculated where the separation between events with RA and dec (α_1, δ_1) and (α_2, δ_2) is

$$\cos^{-1}(\cos\delta_1 \cos\delta_2 \cos(\alpha_1 - \alpha_2) + \sin\delta_1 \sin\delta_2)$$

This indicated that a difference of 1° was not exceeded provided the time delay increment was

- $\leq$ 4ns for channel 1 (and therefore presumably 2, 3, 4 also.)
- $\leq$ 6ns for channel 6 (this simply being indicative of the fact that channels 5 and 6 are $\frac{3}{2}$ times as far as the other channels, hence their time delays are larger and a given increment will have less effect.

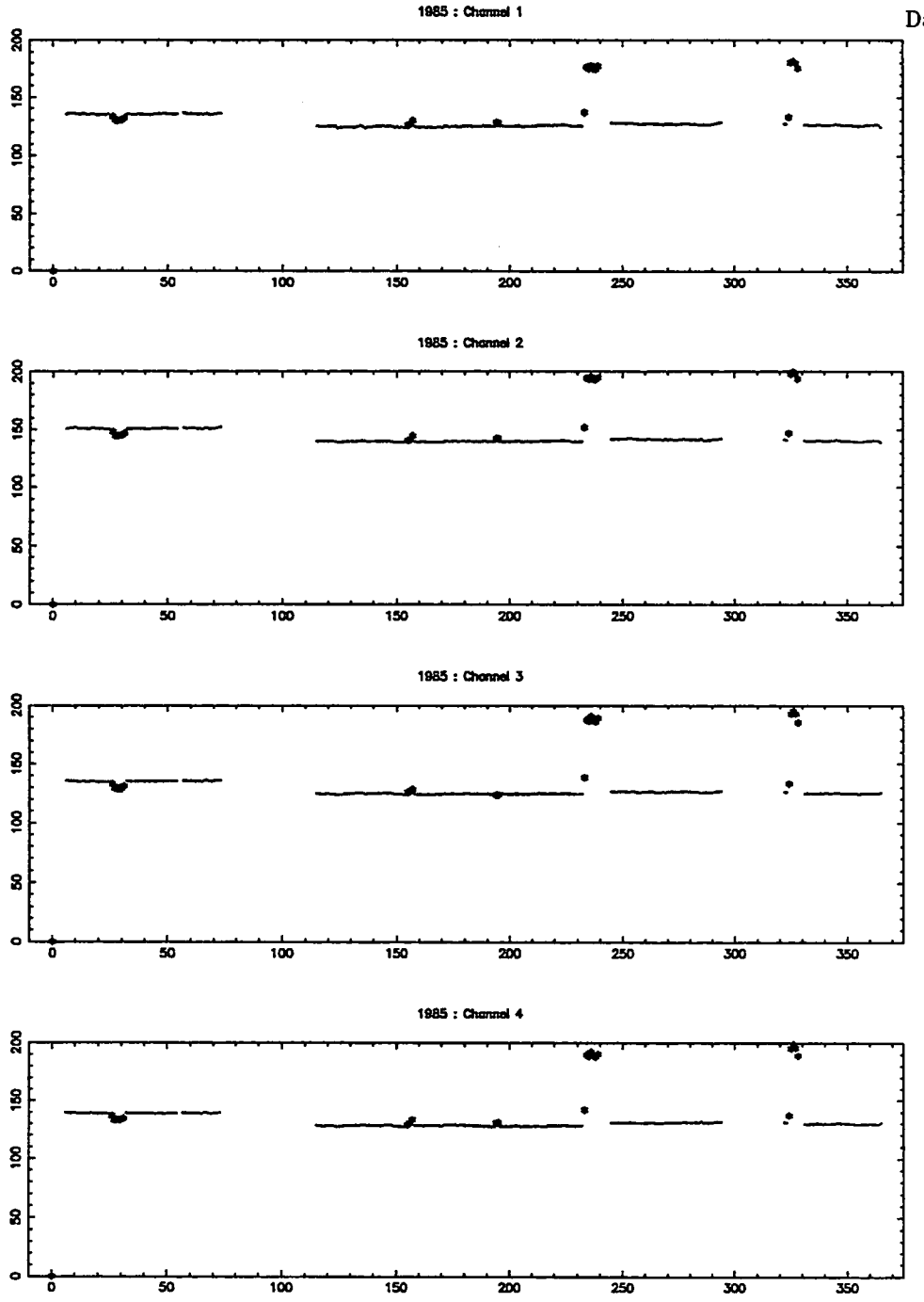

Figure 1.1 The mean time delays for channels 1 - 4 for each day of 1985. The day number starting from the 1st of January is plotted on the x-axis and the corresponding time delay is on the y-axis. The filled stars denote days excluded due to anomalous time delays.

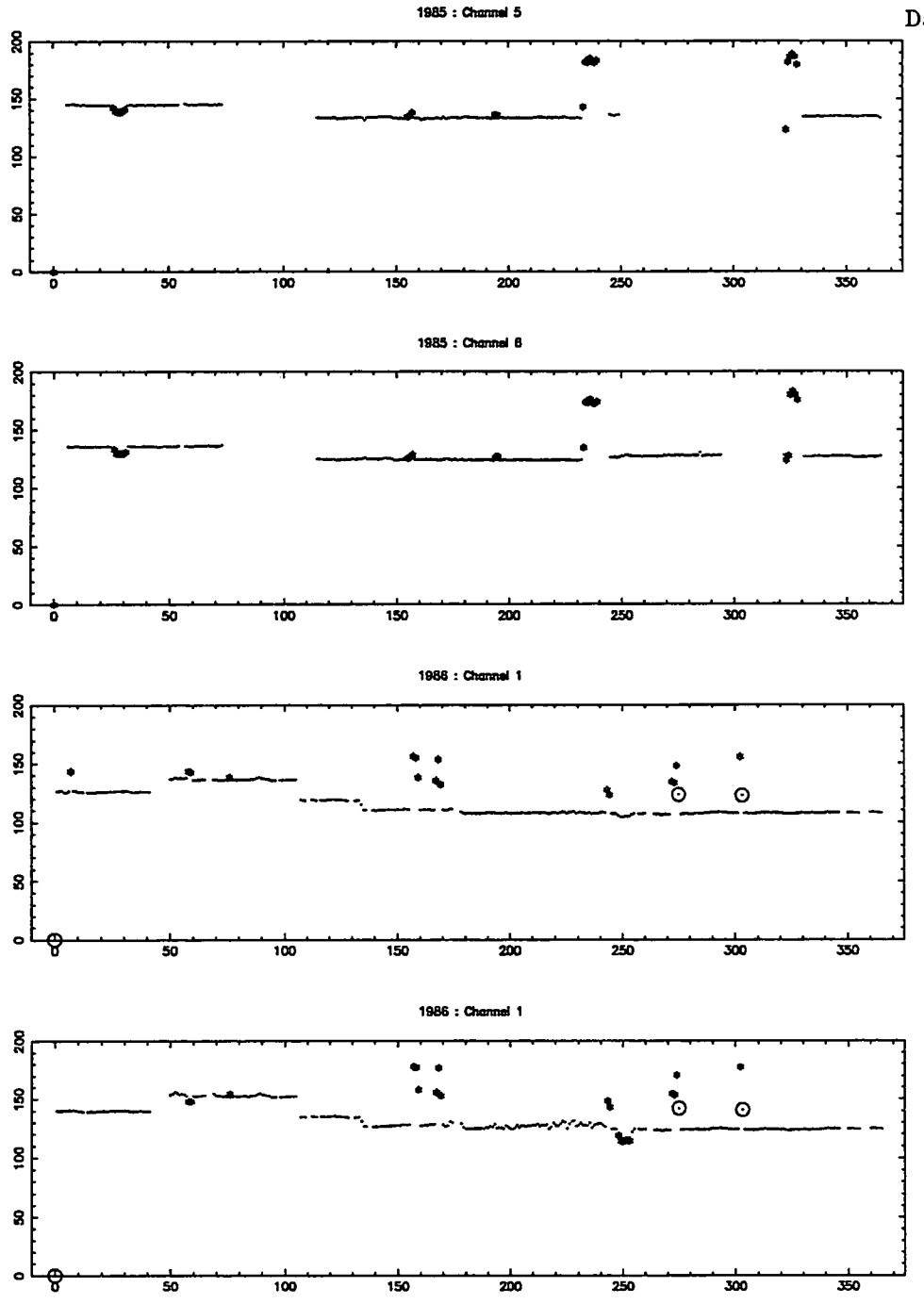

Figure 1.2 The mean time delays for channels 5 - 6 for each day of 1985 and channels 1 - 2 for 1986. The day number starting from the 1st of January is plotted on the x-axis and the corresponding time delay is on the y-axis. The filled stars denote days excluded due to anomalous time delays and the open circles denote days where the exclusion of certain runs permitted the inclusion of the rest of the day.

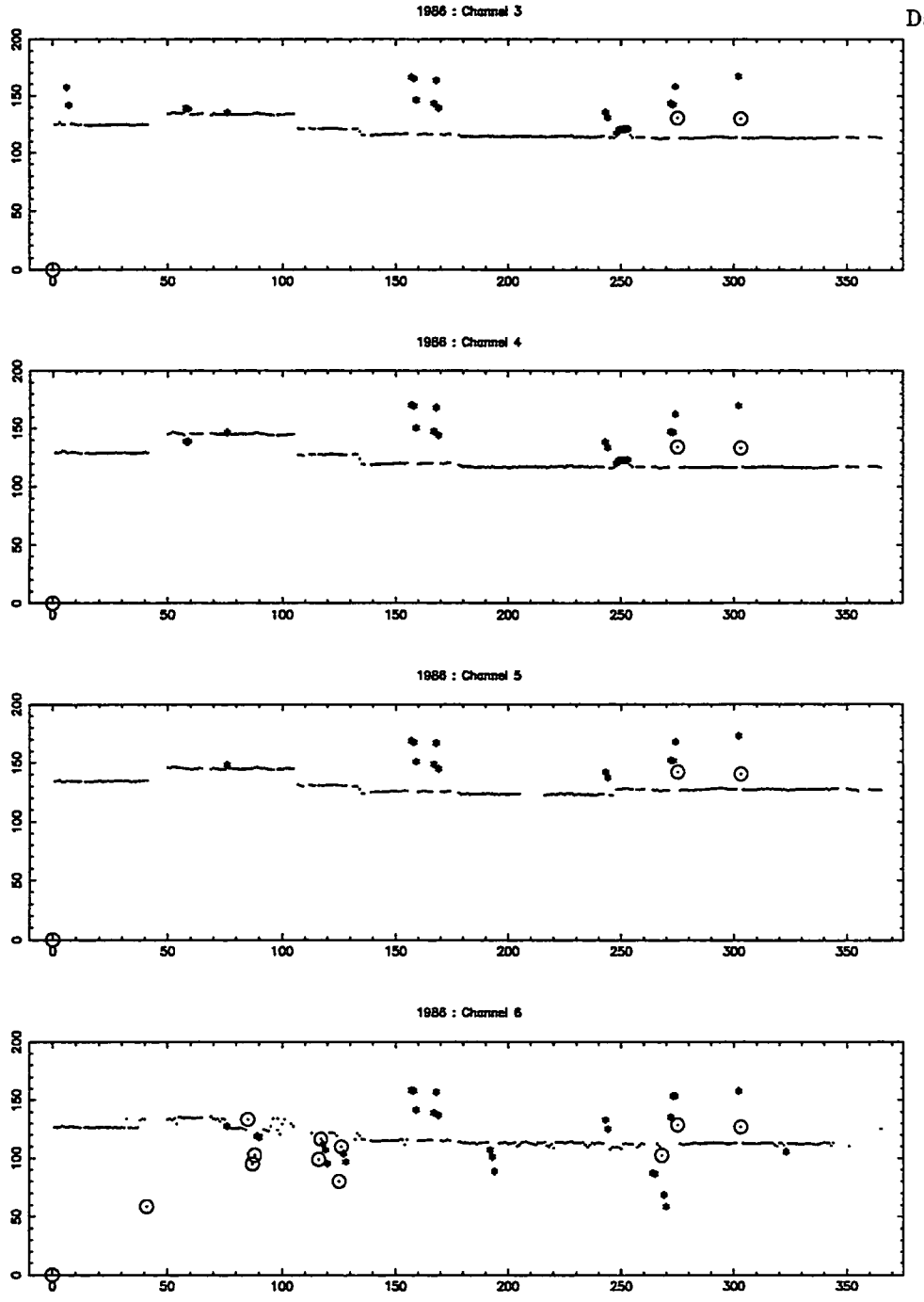

Figure 1.3 The mean time delays for channels 3 - 6 for each day of 1986. The day number starting from the 1st of January is plotted on the x-axis and the corresponding time delay is on the y-axis. The filled stars denote days excluded due to anomalous time delays and the open circles denote days where the exclusion of certain runs permitted the inclusion of the rest of the day.

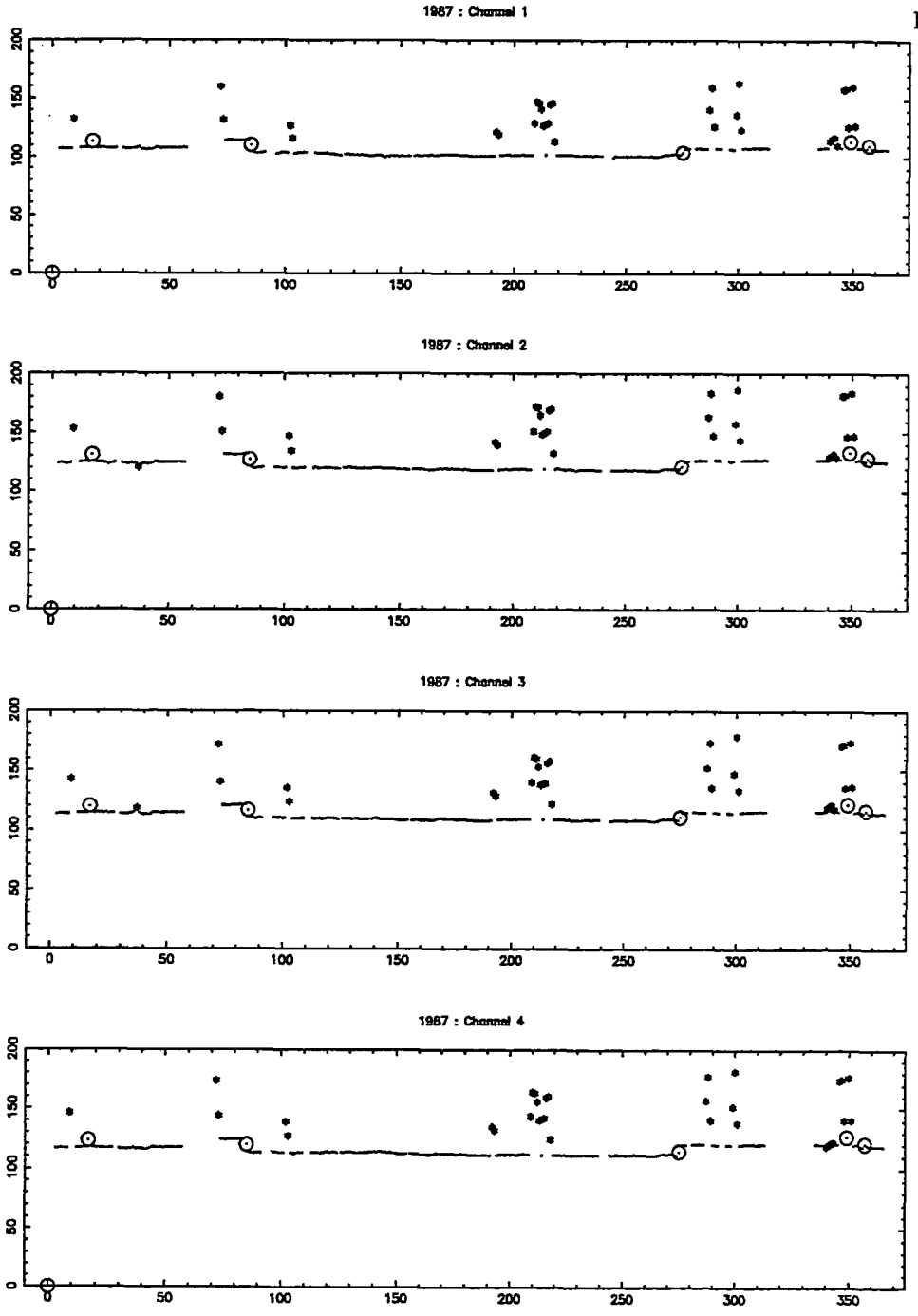

Figure 1.4 The mean time delays for channels 1 - 4 for each day of 1987. The day number starting from the 1st of January is plotted on the x-axis and the corresponding time delay is on the y-axis. The filled stars denote days excluded due to anomalous time delays and the open circles denote days where the exclusion of certain runs permitted the inclusion of the rest of the day.

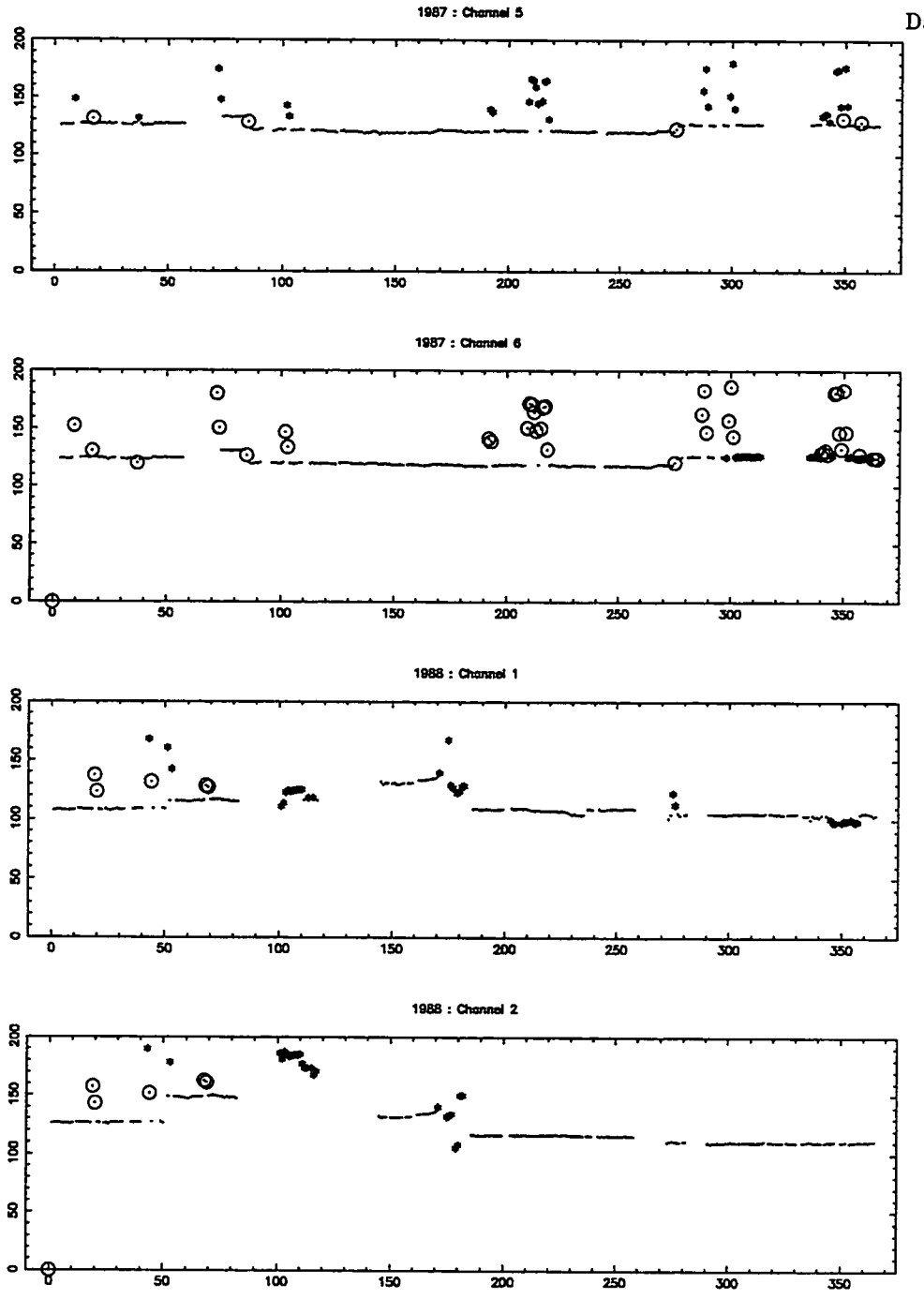

Figure 1.5 The mean time delays for channels 5 - 6 for each day of 1987 and channels 1 - 2 for 1988. The day number starting from the 1st of January is plotted on the x-axis and the corresponding time delay is on the y-axis. The filled stars denote days excluded due to anomalous time delays and the open circles denote days where the exclusion of certain runs permitted the inclusion of the rest of the day.

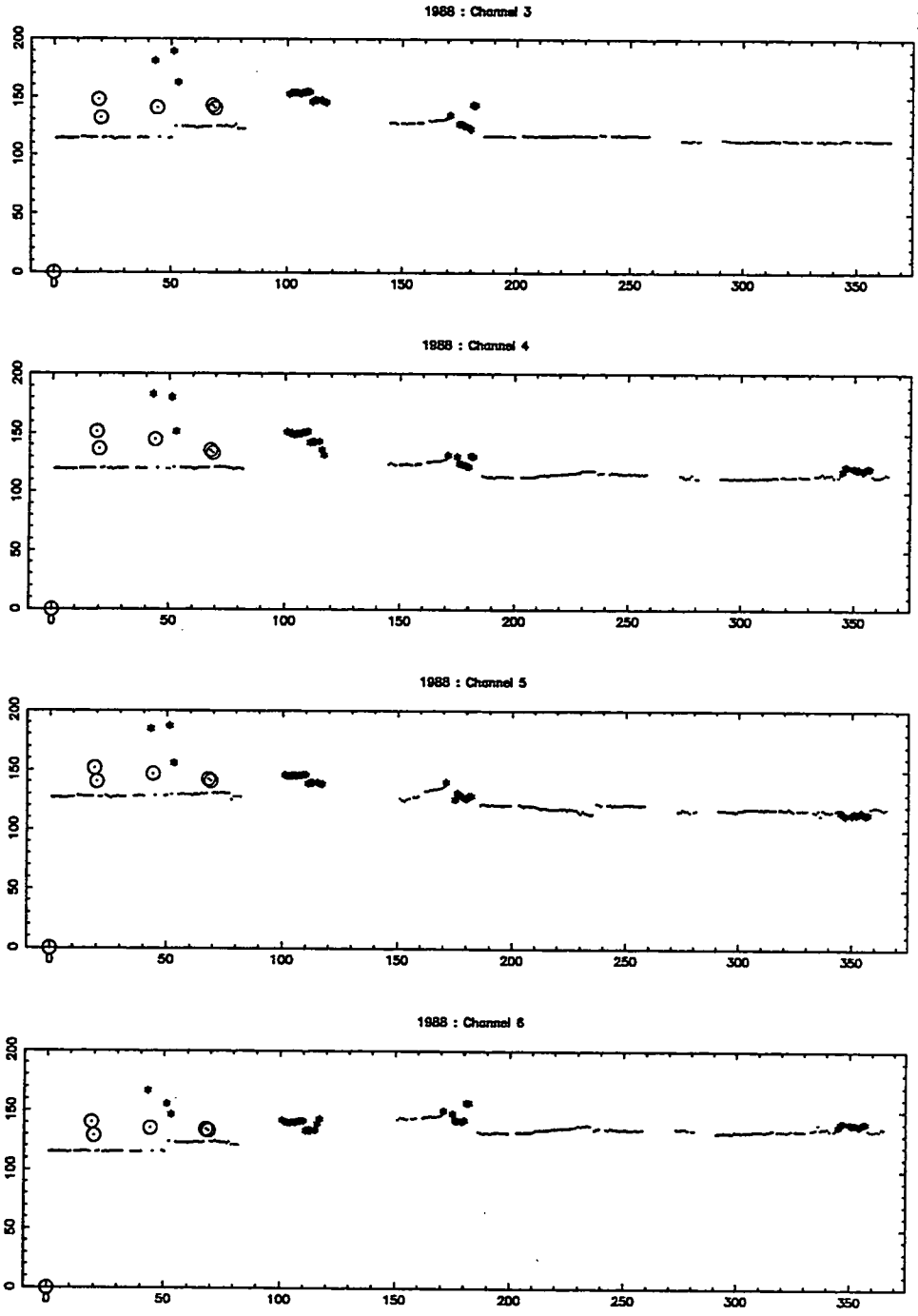

Figure 1.6 The mean time delays for channels 3 - 6 for each day of 1988. The day number starting from the 1st of January is plotted on the x-axis and the corresponding time delay is on the y-axis. The filled stars denote days excluded due to anomalous time delays and the open circles denote days where the exclusion of certain runs permitted the inclusion of the rest of the day.

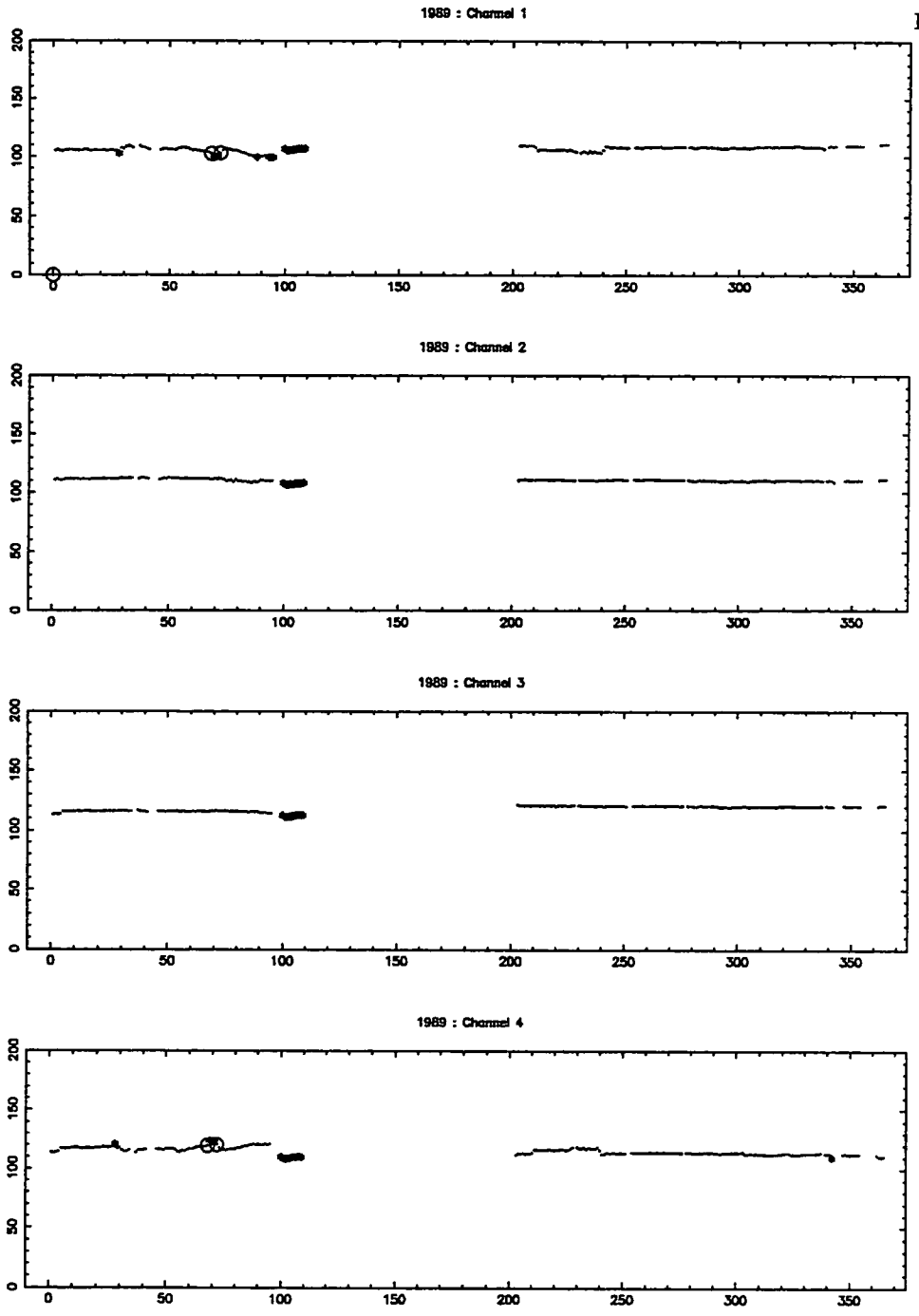

Figure 1.7 The mean time delays for channels 1 - 4 for each day of 1989. The day number starting from the 1st of January is plotted on the x-axis and the corresponding time delay is on the y-axis. The filled stars denote days excluded due to anomalous time delays and the open circles denote days where the exclusion of certain runs permitted the inclusion of the rest of the day.

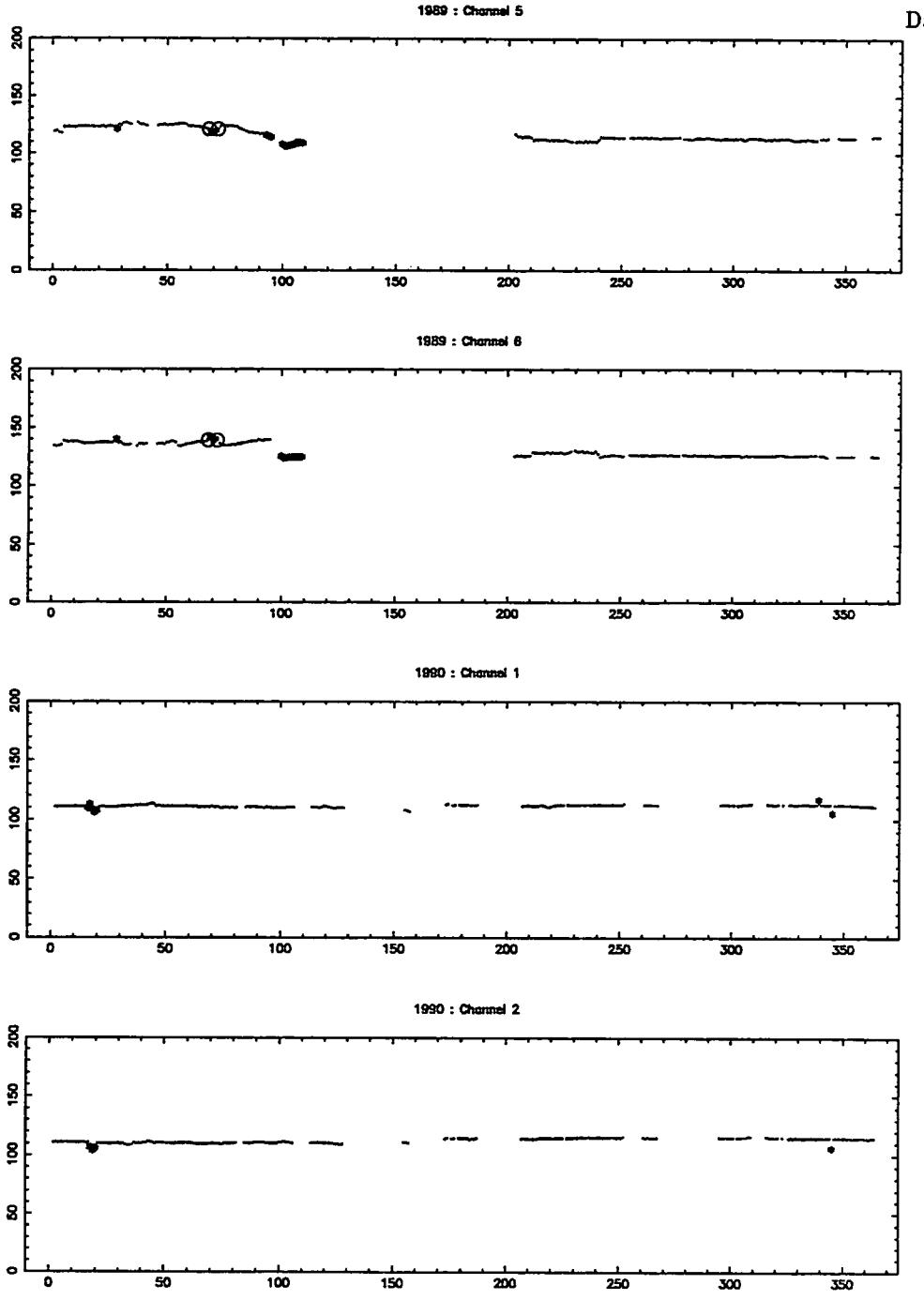

Figure 1.8 The mean time delays for channels 5 - 6 for each day of 1989 and channels 1 - 2 for 1990. The day number starting from the 1st of January is plotted on the x-axis and the corresponding time delay is on the y-axis. The filled stars denote days excluded due to anomalous time delays and the open circles denote days where the exclusion of certain runs permitted the inclusion of the rest of the day.

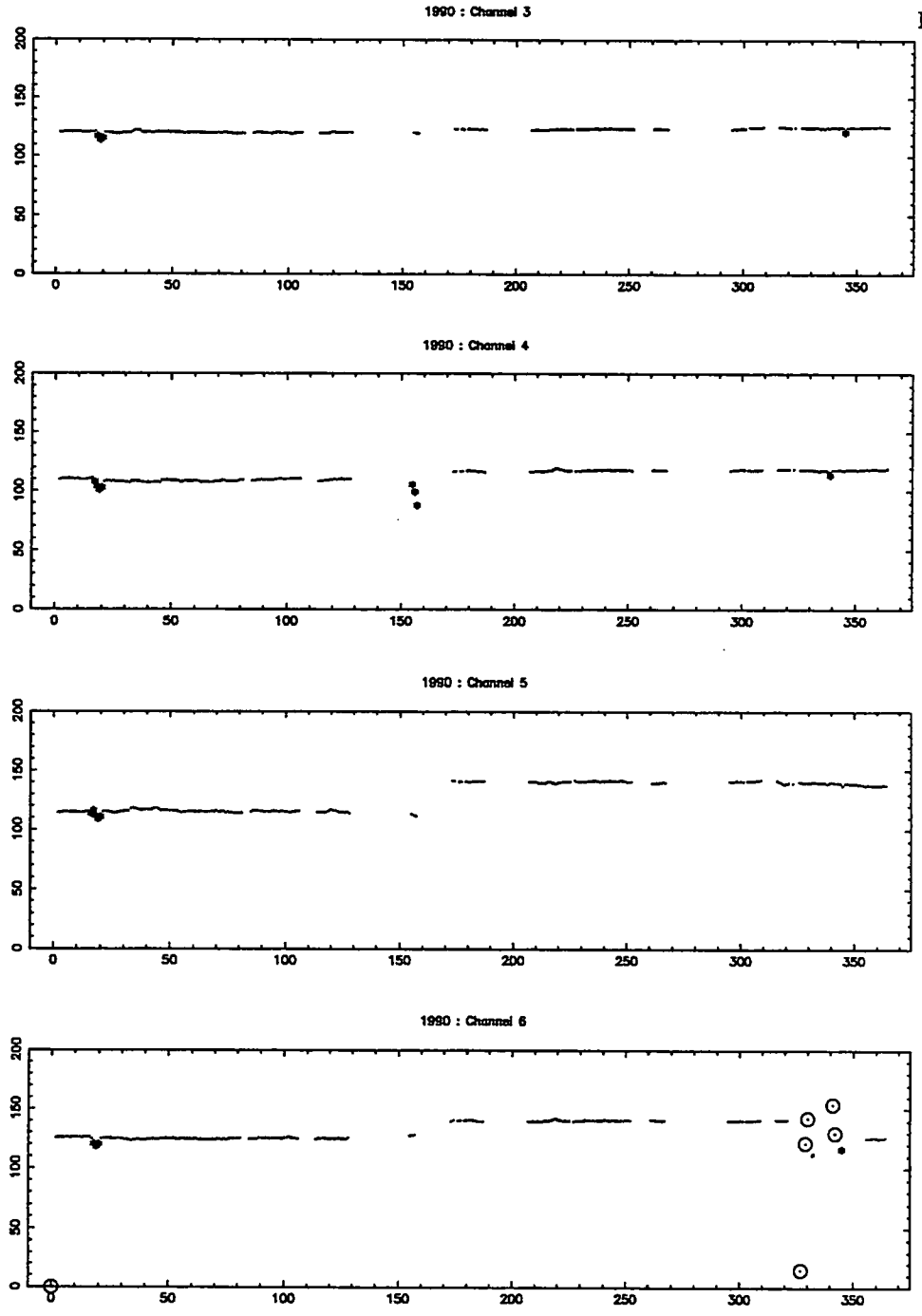

Figure 1.9 The mean time delays for channels 3 - 6 for each day of 1990. The day number starting from the 1st of January is plotted on the x-axis and the corresponding time delay is on the y-axis. The filled stars denote days excluded due to anomalous time delays and the open circles denote days where the exclusion of certain runs permitted the inclusion of the rest of the day.

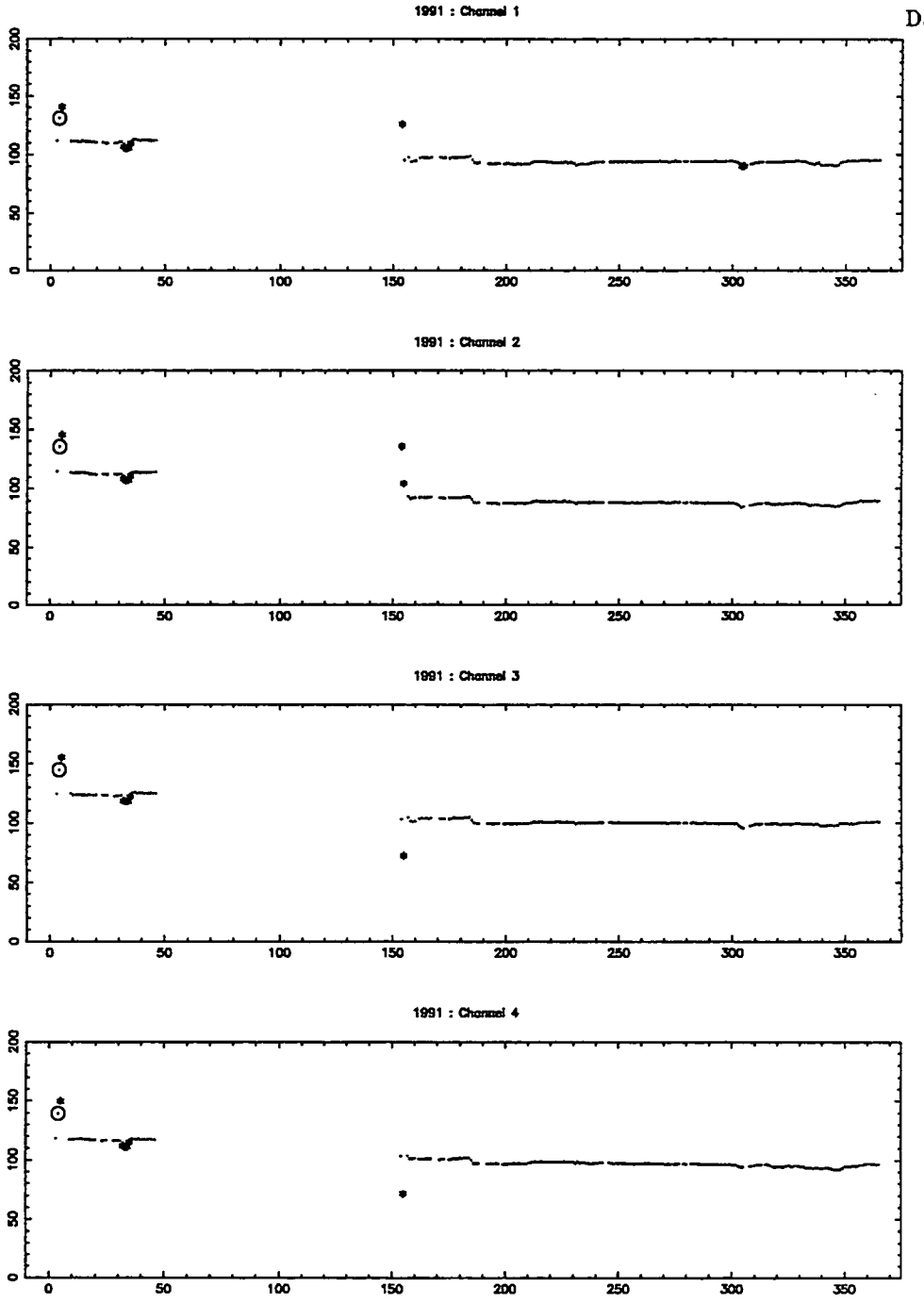

Figure 1.10 The mean time delays for channels 1 - 4 for each day of 1991. The day number starting from the 1st of January is plotted on the x-axis and the corresponding time delay is on the y-axis. The filled stars denote days excluded due to anomalous time delays and the open circles denote days where the exclusion of certain runs permitted the inclusion of the rest of the day.

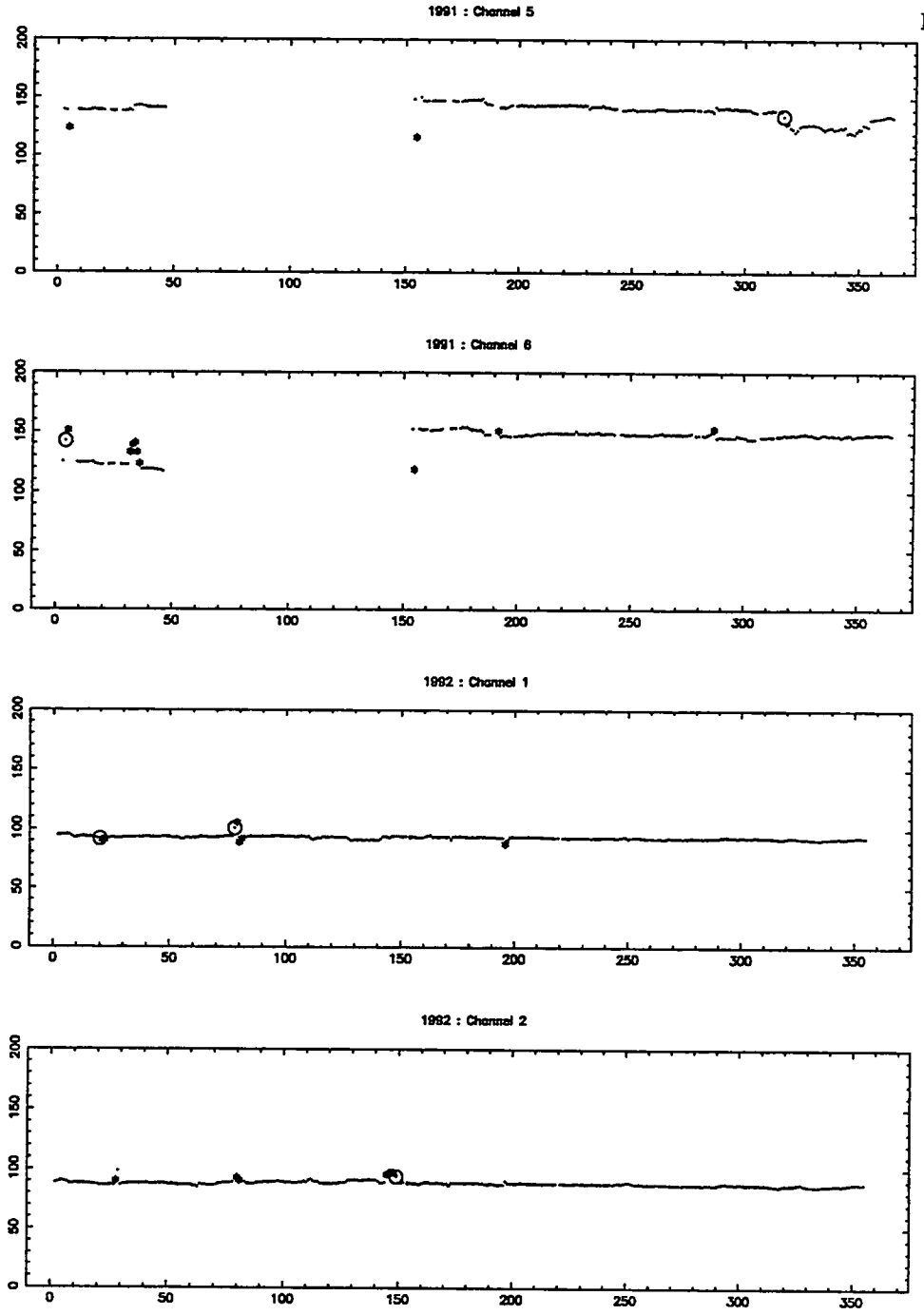

Figure 1.11 The mean time delays for channels 5 - 6 for each day of 1991 and channels 1 - 2 for 1992. The day number starting from the 1st of January is plotted on the x-axis and the corresponding time delay is on the y-axis. The filled stars denote days excluded due to anomalous time delays and the open circles denote days where the exclusion of certain runs permitted the inclusion of the rest of the day.

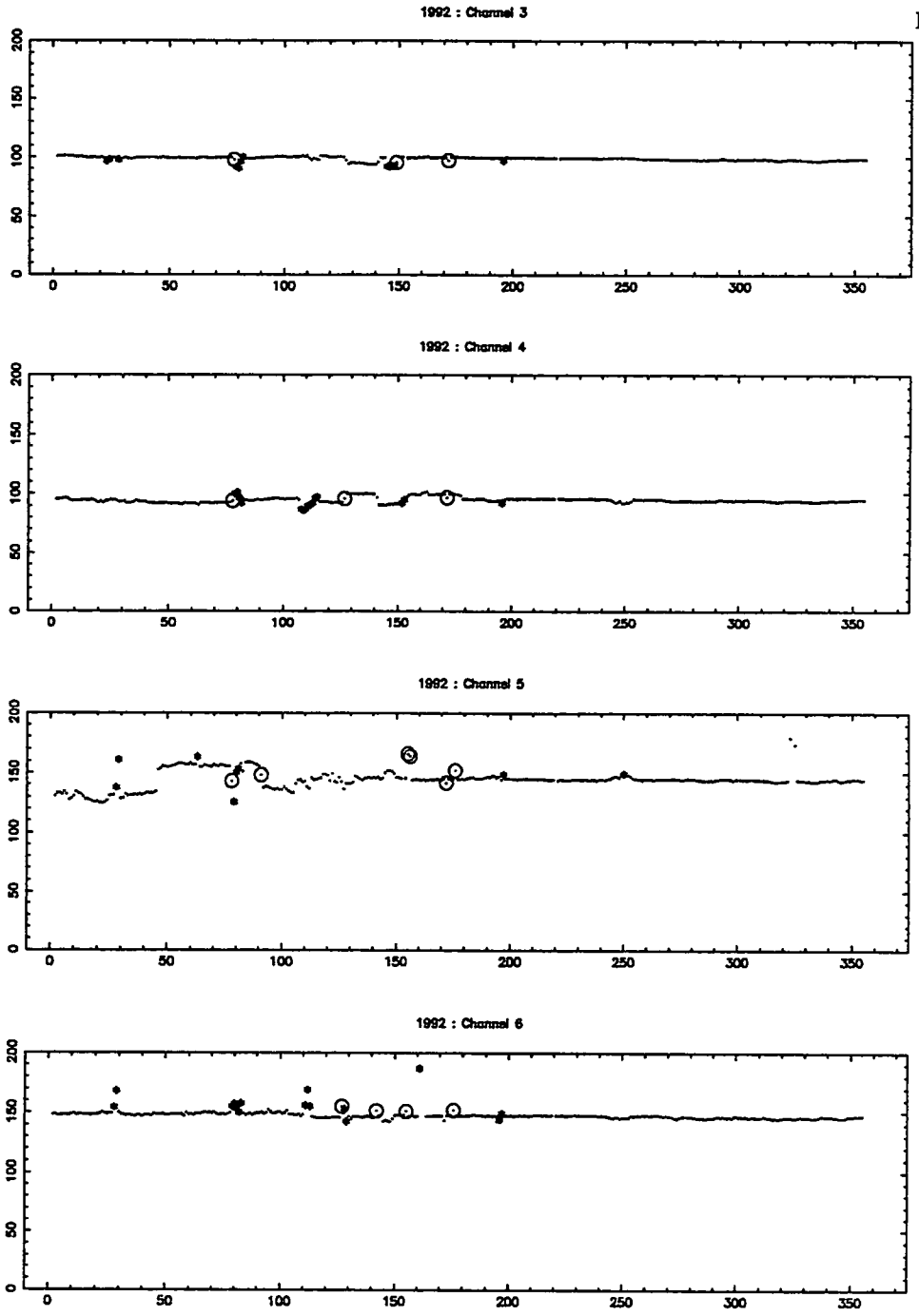

Figure 1.12 The mean time delays for channels 3 - 6 for each day of 1992. The day number starting from the 1st of January is plotted on the x-axis and the corresponding time delay is on the y-axis. The filled stars denote days excluded due to anomalous time delays and the open circles denote days where the exclusion of certain runs permitted the inclusion of the rest of the day.

2 APPENDIX 2

Here we give the results of the search for dc or sporadic emission from 18 candidate sources. The dc results are stated for each source for each year separately and cumulatively also. A list of days is given for each source where the daily excess exceeds 3σ. There were approximately 3 days which met this criterion where the observed number of events was 1. For these cases obviously the expected number was some fraction of one event and thus the result was not thought to be significant. Such days have been omitted from the list.

Table 2.1 Observations of Cyg X-3 1985 - 1992.

Year	Days Observed	On	Off	$\frac{(On-Off)}{\sqrt{Off}}$	$\frac{On}{Off}$
1985	242	23,805	23,798.452	0.04	1.0003
1986	257	32,568	32,315.483	1.40	1.0078
1987	258	17,416	17,617.746	-1.52	0.9885
1988	183	15,855	15,824.962	0.24	1.0019
1989	204	20,832	21,080.871	-1.71	0.9882
1990	214	22,799	22,983.534	-1.22	0.9920
1991	201	21,274	21,285.771	-0.08	0.9994
1992	308	33,627	33,717.072	-0.49	0.9973
1985-1989	1144	110,476	110,637.514	-0.49	0.9985
1990-1992	723	77,700	77,986.377	-1.03	0.9963
1985-1992	1867	188,176	188,623.891	-1.03	0.9976

Daily	Excesses	Exceeding	3.0σ
Date	On	Off	$\frac{On}{Off}$
16.08.85	132	99.310	3.28
02.02.86	143	104.610	3.75
14.06.88	156	121.212	3.16
19.11.88	53	32.905	3.50
27.03.89	142	109.311	3.13

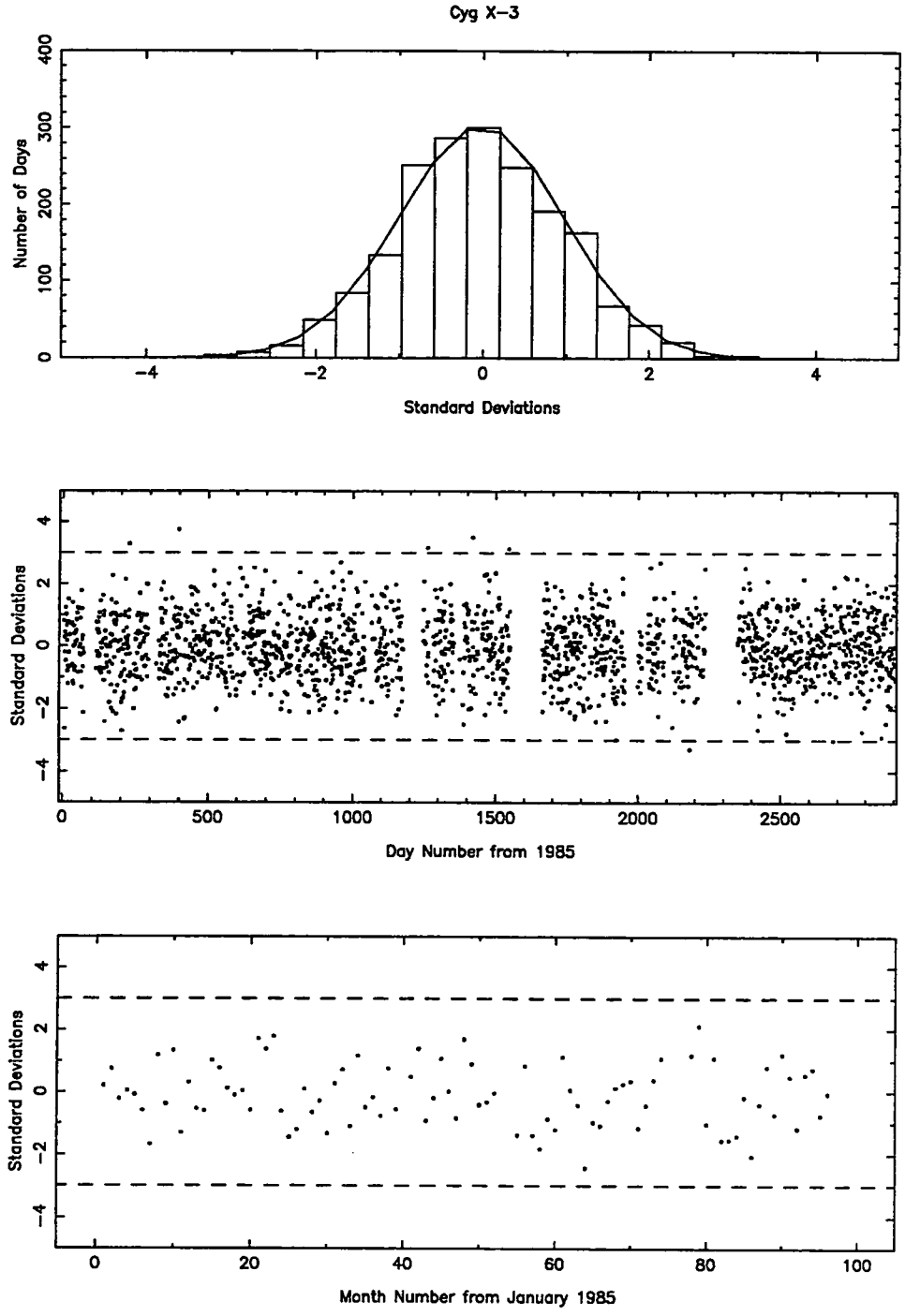

Figure 2.1 Distribution of daily excesses for Cyg X-3. The top graph shows the distribution binned in 0.4 σ bins and compared to a normalised Gaussian centred on zero.

Table 2.2 Observations of Her X-1 1985 - 1992.

Year	Days Observed	On	Off	$\frac{(On-Off)}{\sqrt{Off}}$	$\frac{On}{Off}$
1985	241	21,051	21,226.084	-1.20	0.9918
1986	258	28,575	28,635.853	-0.36	0.9979
1987	253	15,592	15,698.022	-0.85	0.9932
1988	186	14,715	14,620.417	0.78	1.0065
1989	206	19,095	19,174.570	-0.57	0.9959
1990	212	20,694	20,561.404	0.92	1.0064
1991	202	19,596	19,567.393	0.20	1.0015
1992	308	30,949	30,778.211	0.97	1.0055
1985-1989	1144	99,028	99,354.945	-1.04	0.9967
1990-1992	722	71,239	70,907.008	1.25	1.0047
1985-1992	1866	170,267	170,261.953	0.01	1.0000

Daily	Excesses	Exceeding	3.0σ
Date	On	Off	$\frac{On}{Off}$
26.05.85	125	93.707	3.23
19.12.85	85	60.315	3.18
24.07.88	145	119.961	3.12
06.02.90	15	6.800	3.14

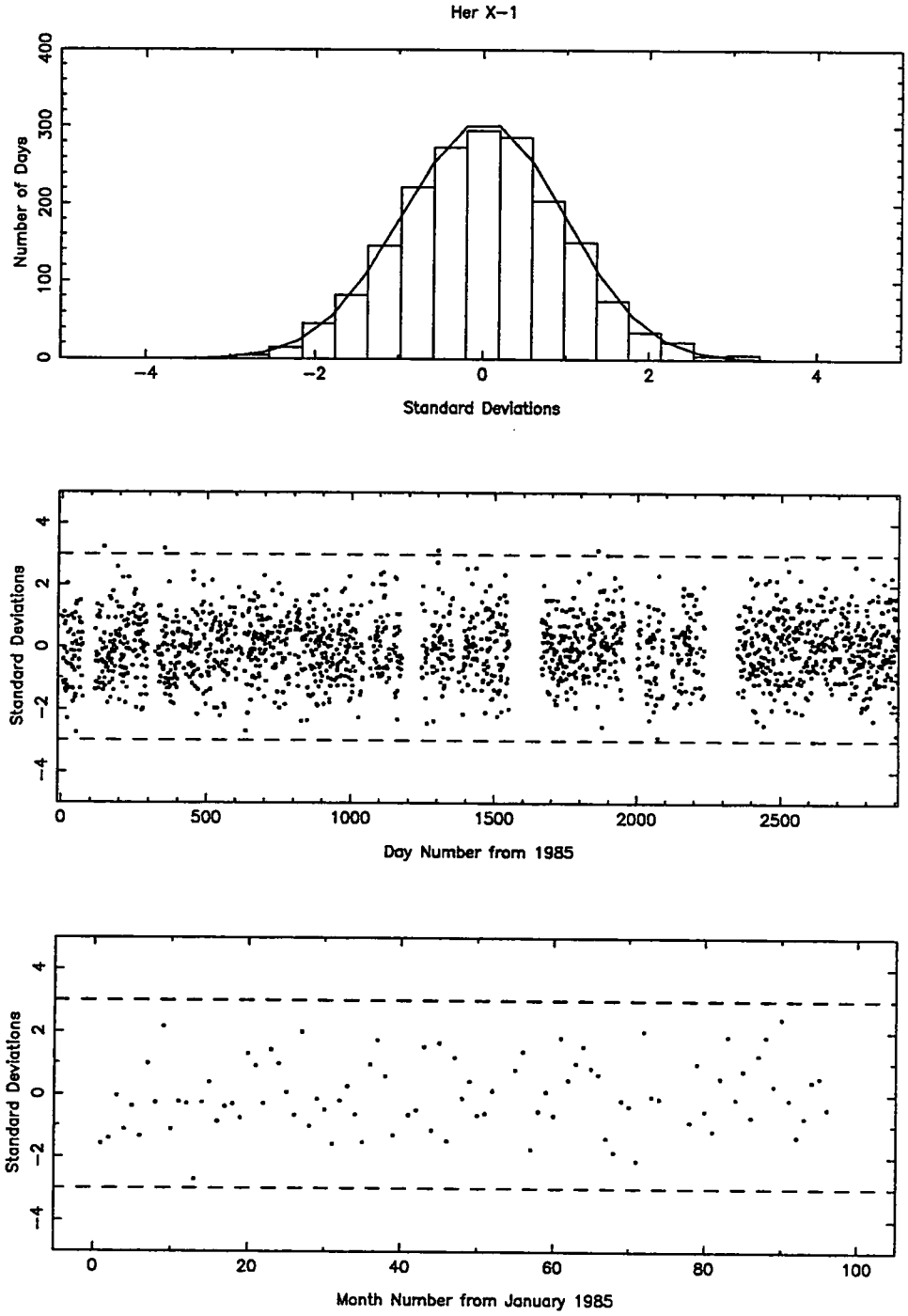

Figure 2.2 Distribution of daily excesses for Her X-1. The top graph shows the distribution binned in 0.4 σ bins and compared to a normalised Gaussian centred on zero. The middle graph shows the daily excesses as a function of time and the bottom graph shows the monthly excesses.

Table 2.3 Observations of 4U 0115+63 1985 - 1992.

Year	Days Observed	On	Off	$\frac{(On-Off)}{\sqrt{Off}}$	$\frac{On}{Off}$
1985	246	19,399	19,404.575	-0.04	0.9997
1986	259	24,176	24,030.722	0.94	1.0060
1987	258	13,250	13,223.657	0.23	1.0020
1988	181	11,911	11,987.221	-0.70	0.9936
1989	207	17,277	17,333.661	-0.43	0.9967
1990	213	17,027	17,016.110	0.08	1.0006
1991	200	17,579	17,580.354	-0.01	0.9999
1992	310	27,554	27,662.230	-0.65	0.9961
1985-1989	1151	86,013	85,979.835	0.11	1.0004
1990-1992	723	62,160	62,258.694	-0.40	0.9984
1985-1992	1874	148,173	148,238.528	-0.17	0.9996

Daily	Excesses	Exceeding	3.0σ
Date	On	Off	$\frac{On}{Off}$
19.03.89	115	85.108	3.24
31.03.90	117	86.105	3.33
28.05.92	8	2.520	3.45

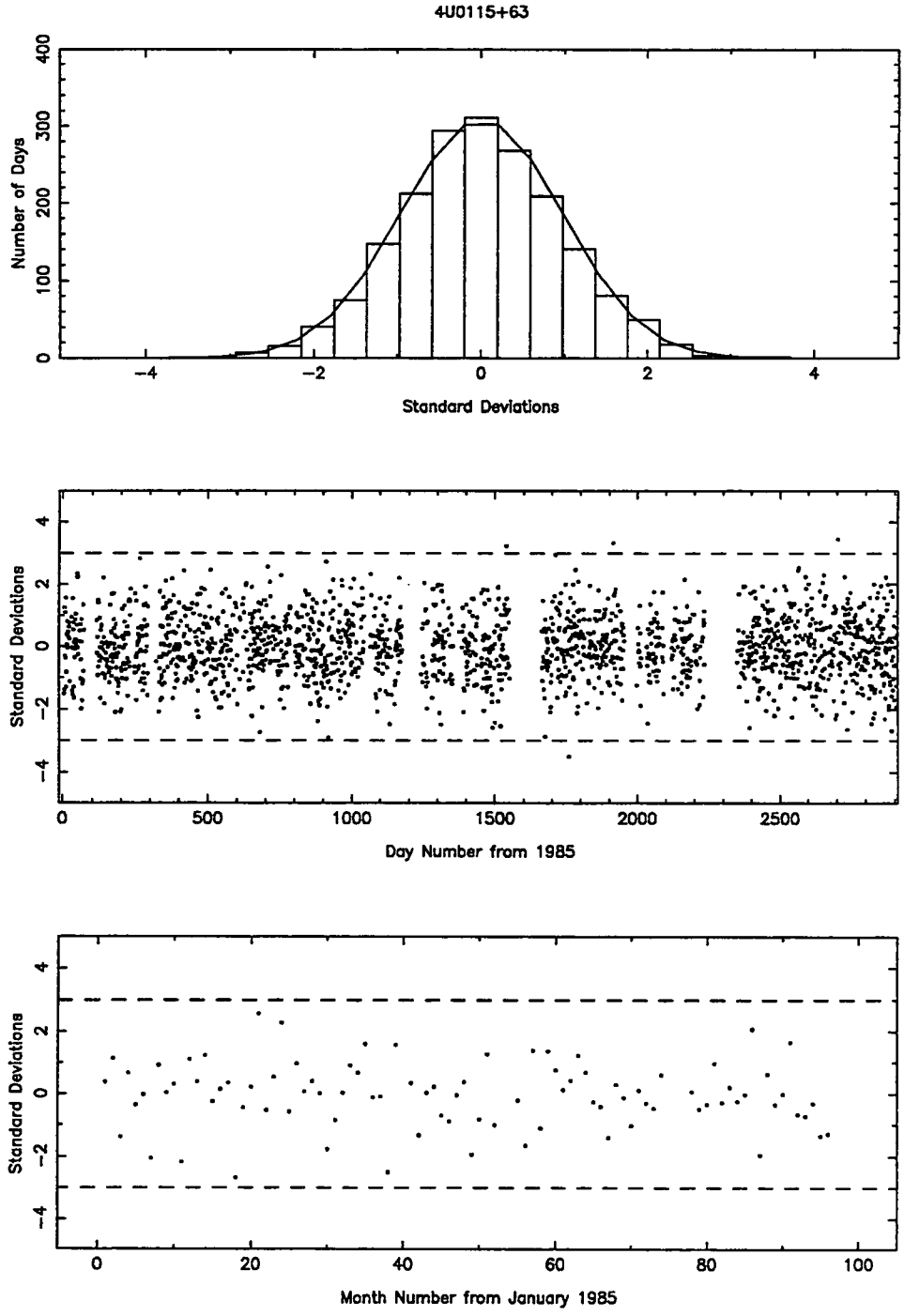

Figure 2.3 Distribution of daily excesses for 4U 0115+63. The top graph shows the distribution binned in 0.4 σ bins and compared to a normalised Gaussian centred on zero. The middle graph shows the daily excesses as a function of time and the bottom graph shows the monthly excesses.

Table 2.4 Observations of Cyg X-1 1985 - 1992.

Year	Days Observed	On	Off	$\frac{(On-Off)}{\sqrt{Off}}$	$\frac{On}{Off}$
1985	243	21,567	21,474.492	0.63	1.0043
1986	257	28,810	28,865.420	-0.33	0.9981
1987	256	15,683	15,477.334	1.65	1.0133
1988	181	14,245	14,128.264	0.98	1.0083
1989	204	18,941	18,747.110	1.42	1.0103
1990	217	20,264	20,431.933	-1.17	0.9918
1991	202	19,069	19,015.104	0.39	1.0028
1992	309	30,118	30,233.766	-0.67	0.9962
1985-1989	1141	99,246	98,692.620	1.76	1.0056
1990-1992	728	69,451	69,680.803	-0.87	0.9967
1985-1992	1869	168,697	168,373.423	0.79	1.0019

Daily	Excesses	Exceeding	3.0σ
Date	On	Off	$\frac{On}{Off}$
29.04.85	97	68.887	3.39
02.01.86	143	111.225	3.01
23.09.89	120	89.558	3.22
01.12.90	48	28.046	3.77
26.07.92	152	116.614	3.28

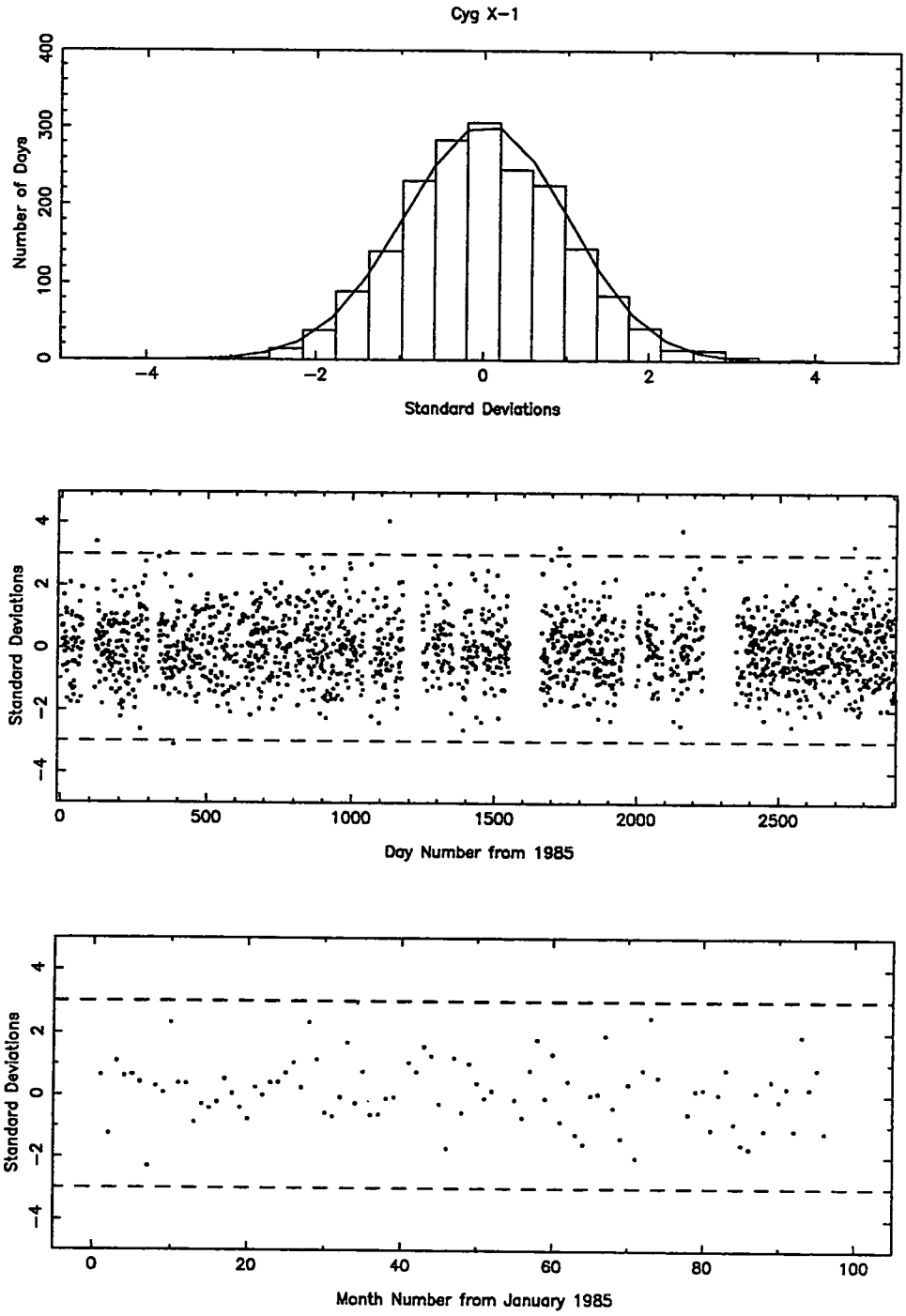

Figure 2.4 Distribution of daily excesses for Cyg X-1. The top graph shows the distribution binned in 0.4 σ bins and compared to a normalised Gaussian centred on zero. The middle graph shows the daily excesses as a function of time and the bottom graph shows the monthly excesses.

Table 2.5 Observations of 1E2259+586 1985 - 1992.

Year	Days Observed	On	Off	$\frac{(On-Off)}{\sqrt{Off}}$	$\frac{On}{Off}$
1985	242	22,139	22,216.323	-0.52	0.9965
1986	262	28,700	28,584.332	0.68	1.0040
1987	260	15,902	15,982.082	-0.63	0.9950
1988	178	14,625	14,350.523	2.29	1.0191
1989	210	19,654	19,939.353	-2.02	0.9857
1990	216	20,546	20,594.985	-0.34	0.9976
1991	198	19,767	19,846.278	-0.56	0.9960
1992	308	30,941	30,929.200	0.07	1.0004
1985-1989	1,152	101,020	101,072.613	-0.17	0.9995
1990-1992	722	71,254	71,370.463	-0.44	0.9984
1985-1992	1,874	172,274	172,443.076	-0.41	0.9990

Daily	Excesses	Exceeding	3.0σ
Date	On	Off	$\frac{On}{Off}$
16.08.88	33	14.581	4.82
01.09.88	138	99.746	3.83
01.08.91	163	122.317	3.68
30.11.91	133	99.742	3.33
07.12.91	127	95.429	3.23
04.01.92	33	18.813	3.27

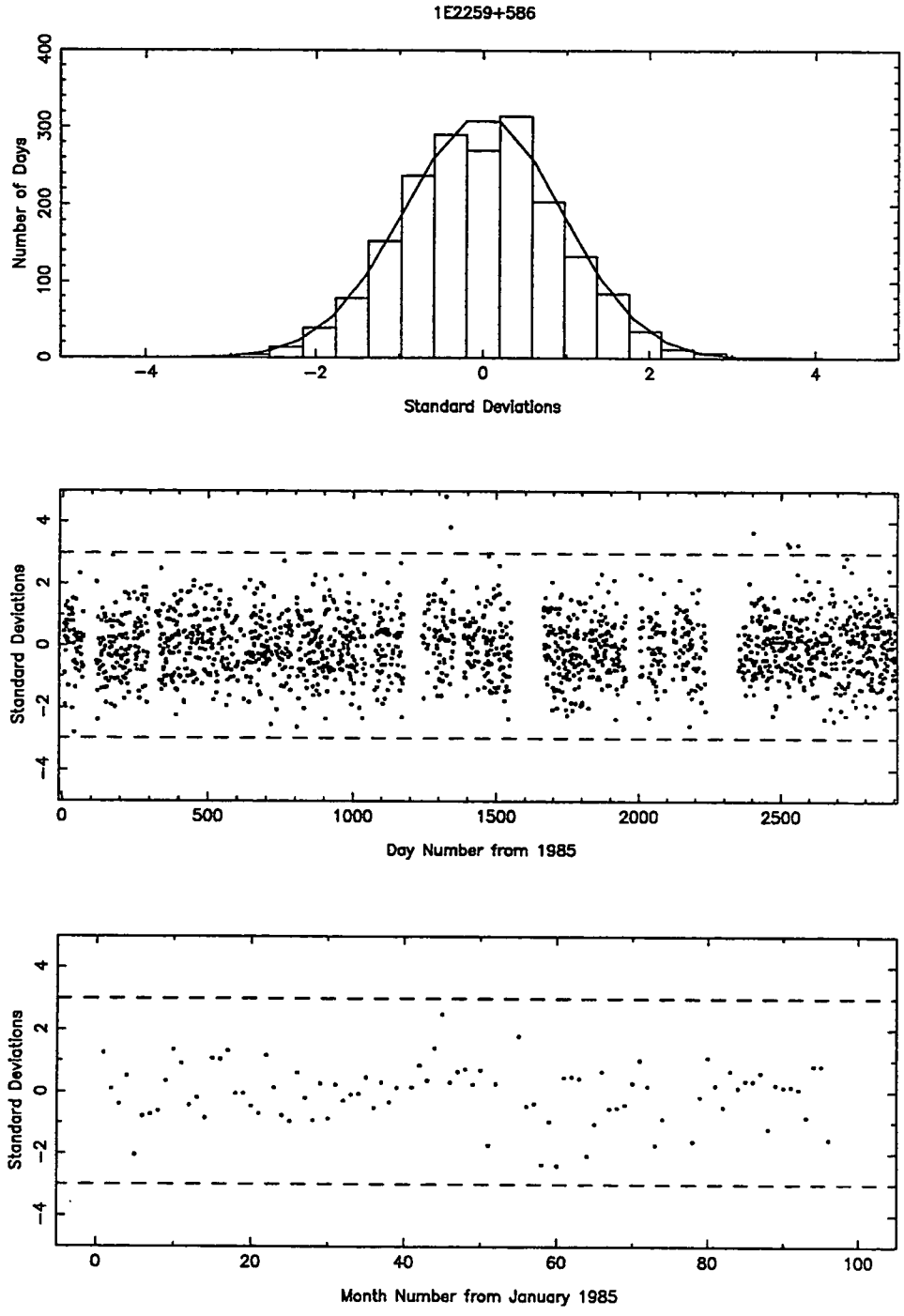

Figure 2.5 Distribution of daily excesses for 1E2259+586. The top graph shows the distribution binned in 0.4 σ bins and compared to a normalised Gaussian centred on zero. The middle graph shows the daily excesses as a function of time and the bottom graph shows the monthly excesses.

Table 2.6 Observations of V0332+53 1985 - 1992.

Year	Days Observed	On	Off	$\frac{(On-Off)}{\sqrt{Off}}$	$\frac{On}{Off}$
1985	247	24,417	24,220.967	1.26	1.0081
1986	260	31,068	31,305.393	-1.34	0.9924
1987	258	18,188	18,051.464	1.02	1.0076
1988	182	15,539	15,614.094	-0.60	0.9952
1989	208	23,352	23,285.502	0.44	1.0029
1990	210	22,901	22,904.973	-0.03	0.9998
1991	200	21,697	21,863.946	-1.13	0.9924
1992	308	34,939	34,848.755	0.48	1.0026
1985-1989	1,115	112,564	112,477.420	0.26	1.0008
1990-1992	718	79,537	79,617.674	-0.29	0.9990
1985-1992	1,873	192,101	192,095.094	0.01	1.0000

Daily	Excesses	Exceeding	3.0σ
Date	On	Off	$\frac{On}{Off}$
28.09.85	121	84.836	3.93
26.11.89	165	130.294	3.04
18.11.92	122	86.774	3.78

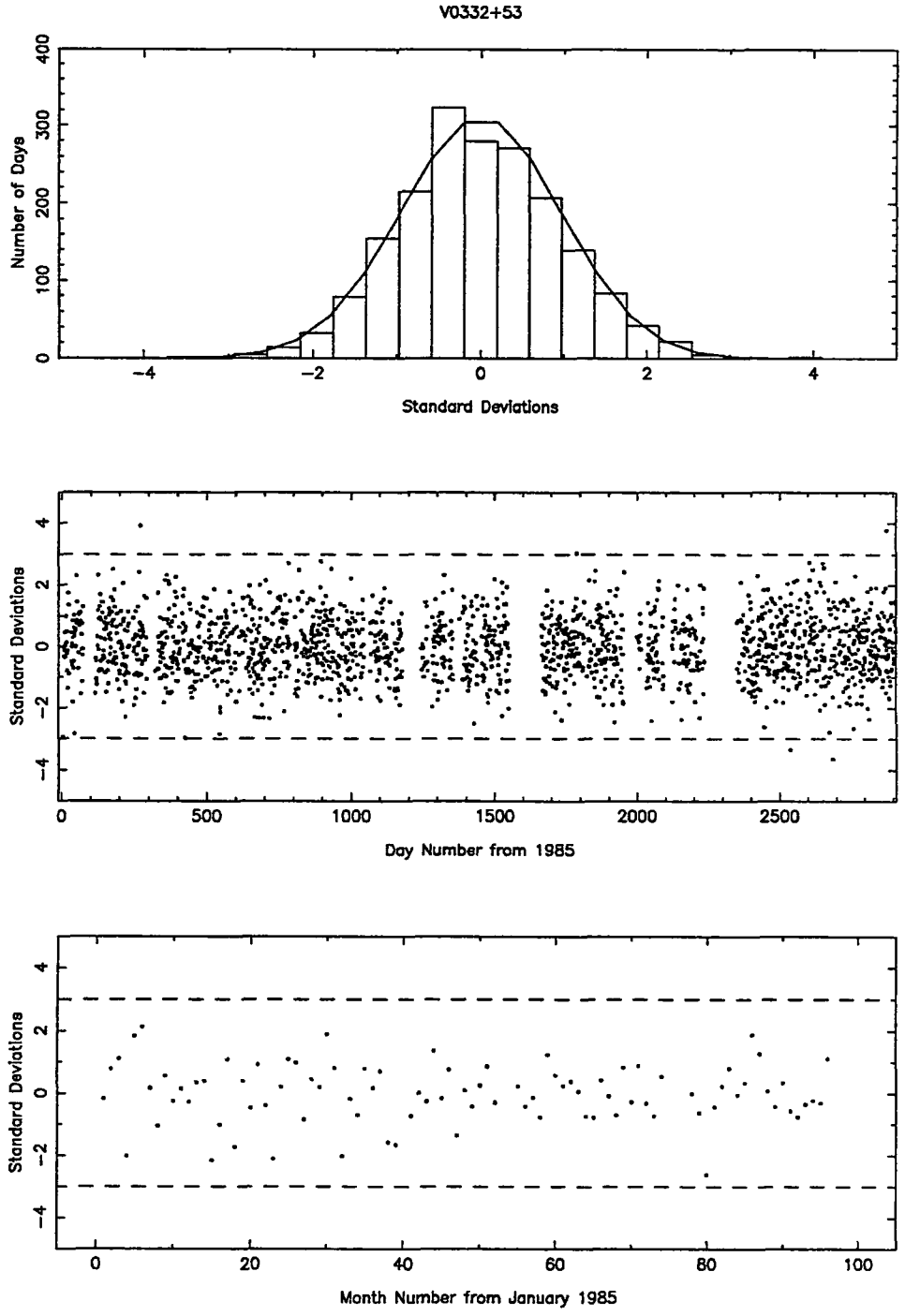

Figure 2.6 Distribution of daily excesses for V0332+53. The top graph shows the distribution binned in 0.4 σ bins and compared to a normalised Gaussian centred on zero. The middle graph shows the daily excesses as a function of time and the bottom graph shows the monthly excesses.

Table 2.7 Observations of the Crab 1985 - 1992.

Year	Days Observed	On	Off	$\frac{(On-Off)}{\sqrt{Off}}$	$\frac{On}{Off}$
1985	239	12,163	12,071.737	0.83	1.0076
1986	252	14,750	14,735.096	0.12	1.0010
1987	253	8,380	8,474.200	-1.02	0.9889
1988	174	7,462	7,514.600	-0.61	0.9930
1989	204	11,134	11,037.464	0.92	1.0087
1990	209	11,175	11,179.438	-0.04	0.9996
1991	199	11,576	11,465.068	1.04	1.0097
1992	306	17,717	17,622.644	0.71	1.0054
1985-1989	1122	53,889	53,833.097	0.24	1.0010
1990-1992	714	40,468	40,267.151	1.00	1.0050
1985-1992	1836	94,357	94,100.247	0.84	1.0027

Daily	Excesses	Exceeding	3.0σ
Date	On	Off	$\frac{On}{Off}$
27.09.89	83	58.398	3.22
29.11.89	99	68.912	3.62

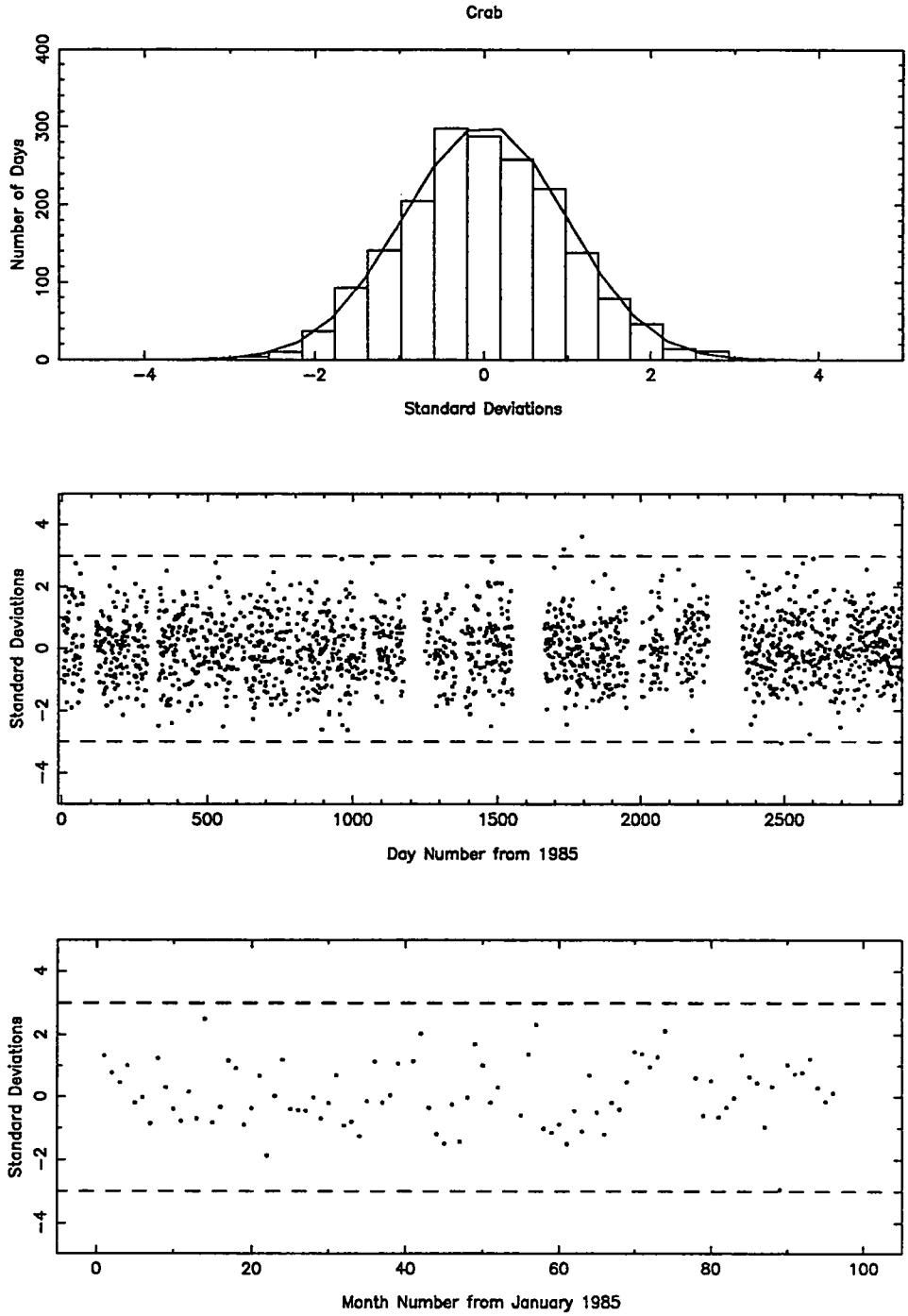

Figure 2.7 Distribution of daily excesses for the Crab. The top graph shows the distribution binned in 0.4 σ bins and compared to a normalised Gaussian centred on zero. The middle graph shows the daily excesses as a function of time and the bottom graph shows the monthly excesses.

Table 2.8 Observations of Geminga 1985 - 1992.

Year	Days Observed	On	Off	$\frac{(On-Off)}{\sqrt{Off}}$	$\frac{On}{Off}$
1985	241	8,847	8,935.625	-0.94	0.9901
1986	252	10,492	10,490.543	0.01	1.0001
1987	255	6,051	6,033.603	0.22	1.0029
1988	173	5,447	5,533.878	-1.17	0.9843
1989	207	7,924	8020.710	-1.08	0.9879
1990	208	8,316	8,238.439	0.85	1.0094
1991	200	8,869	8,722.585	1.57	1.0168
1992	306	13,406	13,428.725	-0.20	0.9983
1985-1989	1128	38,761	39,014.359	-1.28	0.9935
1990-1992	714	30,591	30,389.749	1.15	1.0066
1985-1992	1842	69,352	69,404.108	-0.20	0.9992

Daily	Excesses	Exceeding	3.0σ
Date	On	Off	$\frac{On}{Off}$
30.11.88	58	36.442	3.57

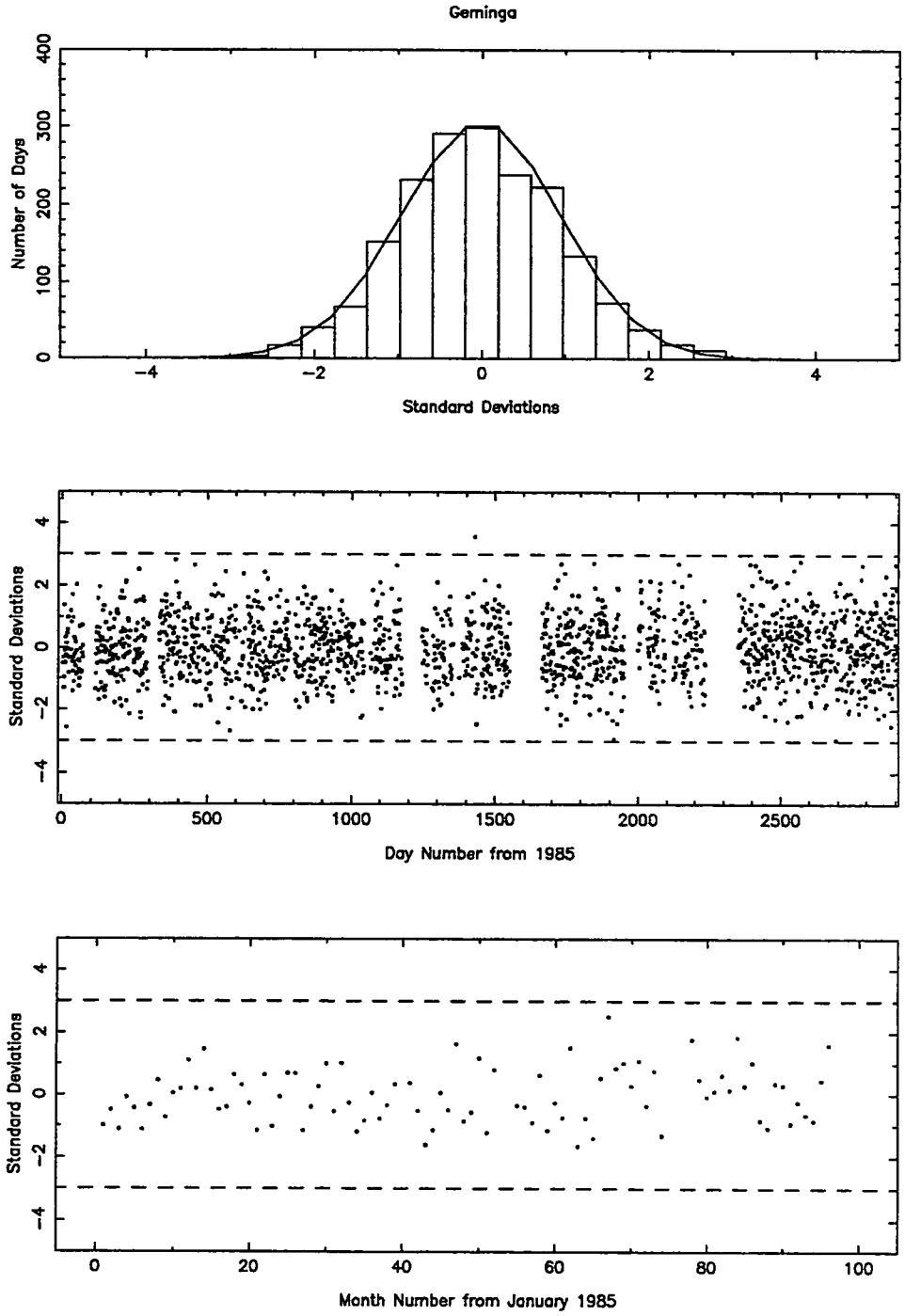

Figure 2.8 Distribution of daily excesses for Geminga. The top graph shows the distribution binned in 0.4 σ bins and compared to a normalised Gaussian centred on zero. The middle graph shows the daily excesses as a function of time and the bottom graph shows the monthly excesses.

Table 2.9 Observations of PSR0355+54 1985 - 1992.

Year	Days Observed	On	Off	$\frac{(On-Off)}{\sqrt{Off}}$	$\frac{On}{Off}$
1985	245	24,027	23,961.137	0.43	1.0027
1986	259	30,720	30,819.193	-0.57	0.9968
1987	257	17,730	17,719.032	0.08	1.0006
1988	182	15,401	15,379.129	0.18	1.0014
1989	210	22,851	22,854.617	-0.02	0.9998
1990	209	22,646	22,465.359	1.21	1.0080
1991	201	21,419	21,557.979	-0.95	0.9936
1992	308	33,916	34,096.427	-0.98	0.9947
1985-1989	1,153	110,729	110,733.108	-0.01	1.0000
1990-1992	718	77,981	78,119.765	-0.50	0.9982
1985-1992	1,871	188,710	188,852.873	-0.33	0.9992

Daily	Excesses	Exceeding	3.0σ
Date	On	Off	$\frac{On}{Off}$
05.12.86	172	134.186	3.26
21.09.89	153	119.206	3.10
28.05.92	11	4.339	3.20

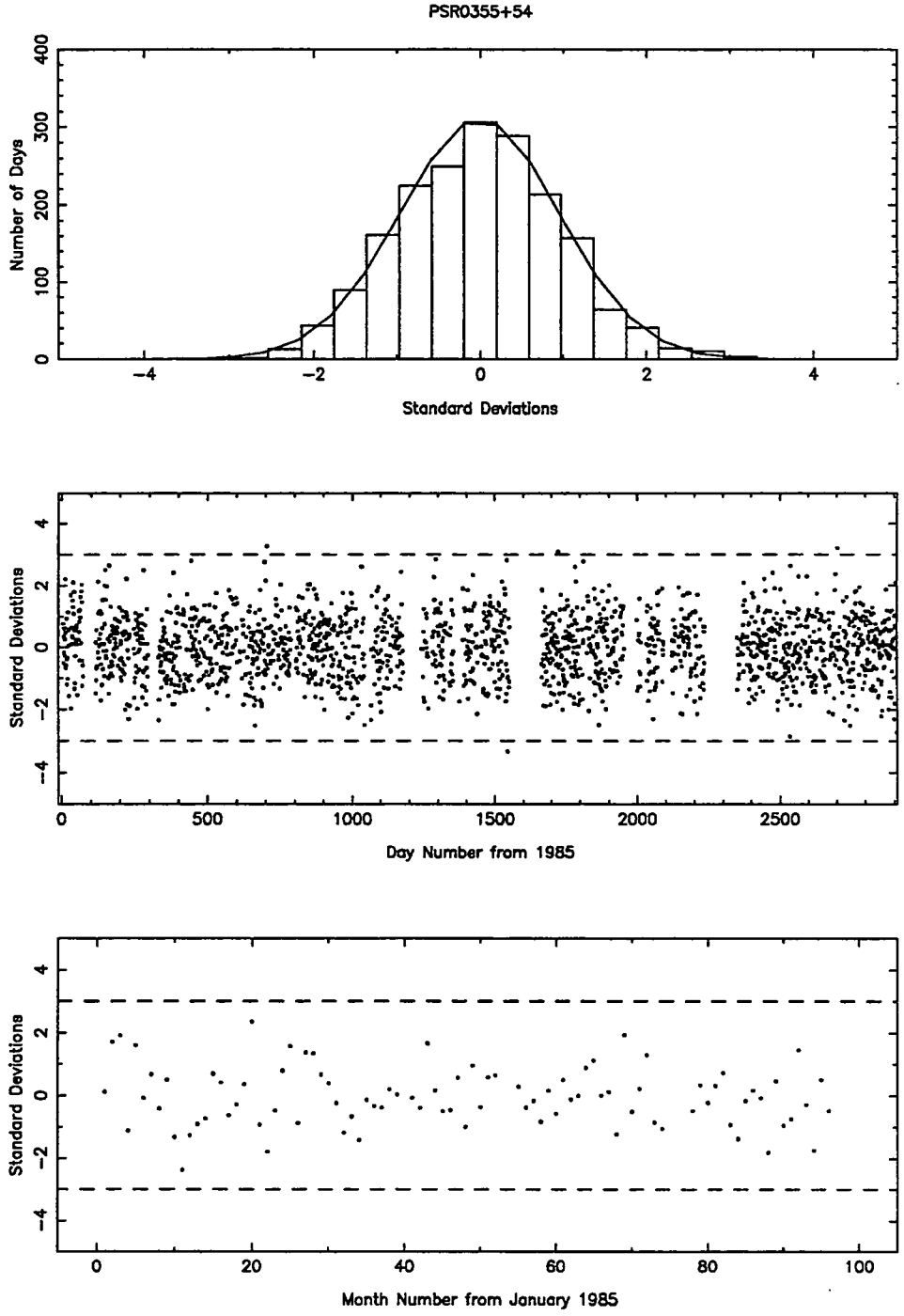

Figure 2.9 Distribution of daily excesses for PSR0355+54. The top graph shows the distribution binned in 0.4 σ bins and compared to a normalised Gaussian centred on zero. The middle graph shows the daily excesses as a function of time and the bottom graph shows the monthly excesses.

Table 2.10 Observations of PSR0655+64 1985 - 1992.

Year	Days Observed	On	Off	$\frac{(On-Off)}{\sqrt{Off}}$	$\frac{On}{Off}$
1985	243	19,271	19,143.917	0.92	1.0066
1986	256	23,105	23,195.627	-0.60	0.9961
1987	255	13,162	13,121.155	0.36	1.0031
1988	187	11,996	12,015.710	-0.18	0.9984
1989	210	17,142	17,323.689	-1.38	0.9895
1990	210	16,905	16,968.641	-0.49	0.9962
1991	201	17,862	17,855.125	0.05	1.0004
1992	307	26,611	26,680.361	-0.42	0.9974
1985-1989	1,151	84,676	84,800.098	-0.43	0.9985
1990-1992	718	61,378	61,504.128	-0.51	0.9979
1985-1992	1,869	146,054	146,304.226	-0.65	0.9983

Daily	Excesses	Exceeding	3.0σ
Date	On	Off	$\frac{On}{Off}$
10.07.87	74	49.856	3.42
02.11.88	30	17.100	3.12
12.08.89	138	100.872	3.70
12.08.92	146	108.757	3.57

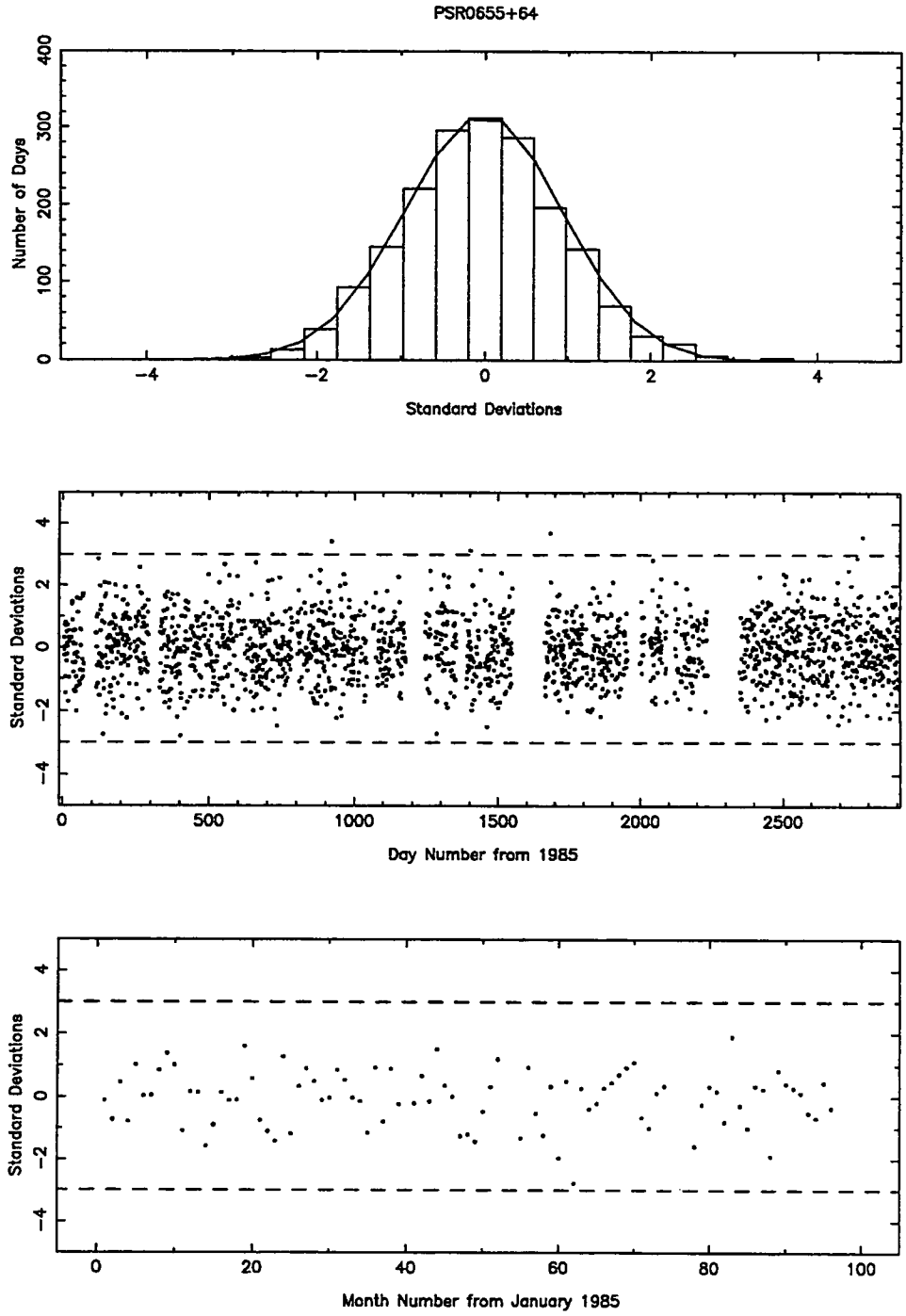

Figure 2.10 Distribution of daily excesses for PSR0655+64. The top graph shows the distribution binned in 0.4 σ bins and compared to a normalised Gaussian centred on zero. The middle graph shows the daily excesses as a function of time and the bottom graph shows the monthly excesses.

Table 2.11 Observations of PSR1913+16 1985 - 1992.

Year	Days Observed	On	Off	$\frac{(On-Off)}{\sqrt{Off}}$	$\frac{On}{Off}$
1985	236	7,586	7,546.499	0.45	1.0052
1986	254	8,906	8,994.569	-0.93	0.9902
1987	252	5,110	5,137.913	-0.39	0.9946
1988	180	5,194	5,087.592	1.49	1.0209
1989	199	6,620	6,653.057	-0.41	0.9950
1990	204	6,993	6,969.925	0.28	1.0033
1991	198	7,365	7,568.0800	-2.33	0.9732
1992	310	12,197	12,279.228	-0.74	0.9933
1985-1989	1,121	33,416	33,419.630	-0.02	0.9999
1990-1992	712	26,555	26,817.233	-1.60	0.9902
1985-1992	1,833	59,971	60,236.863	-1.08	0.9956

Daily	Excesses	Exceeding	3.0σ
Date	On	Off	$\frac{On}{Off}$
29.06.86	58	38.850	3.07
16.06.92	72	48.990	3.29

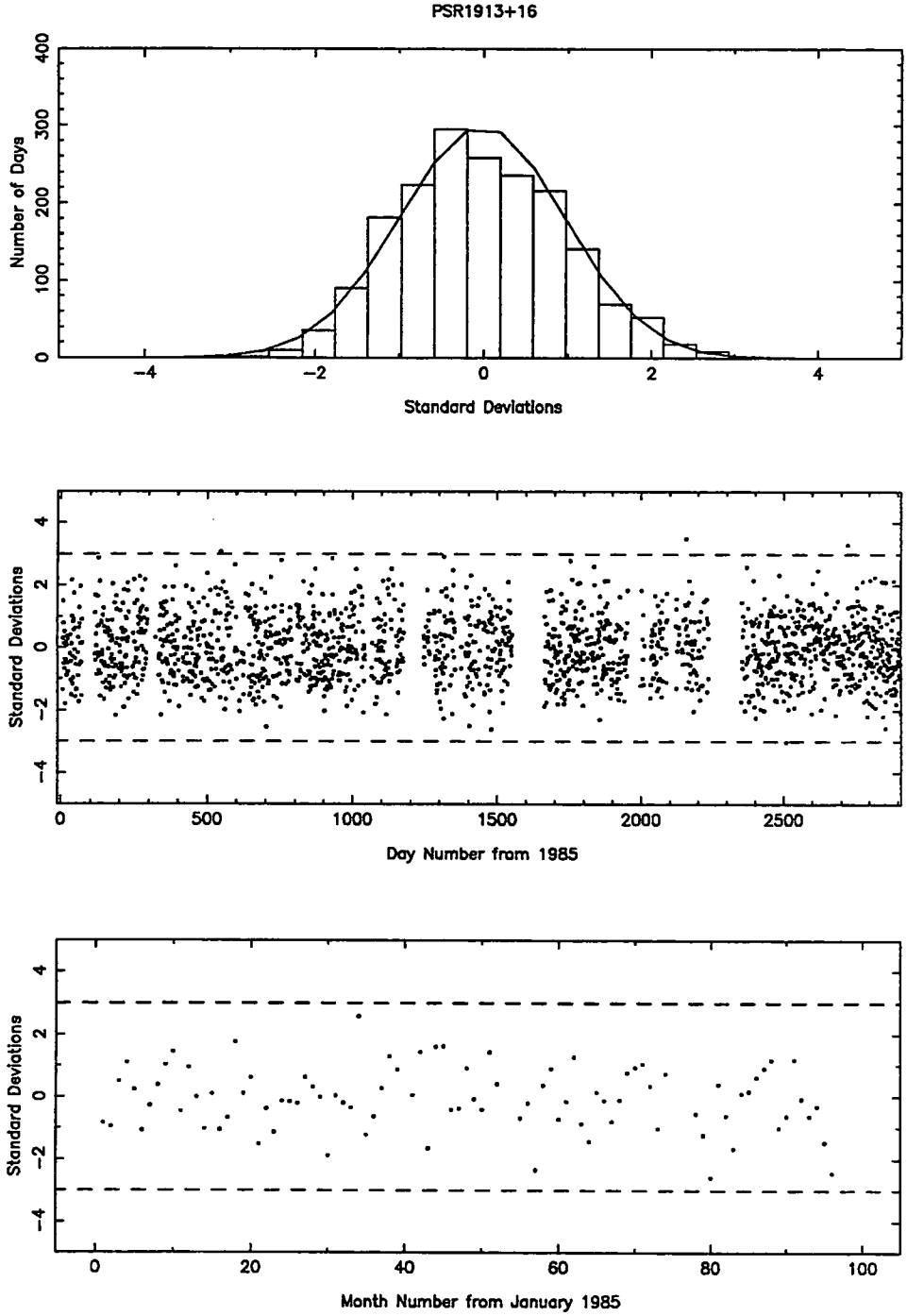

Figure 2.11 Distribution of daily excesses for PSR1913+16. The top graph shows the distribution binned in 0.4 σ bins and compared to a normalised Gaussian centred on zero. The middle graph shows the daily excesses as a function of time and the bottom graph shows the monthly excesses.

Table 2.12 Observations of PSR 1937+21 1985 - 1992.

Year	Days Observed	On	Off	$\frac{(On-Off)}{\sqrt{Off}}$	$\frac{On}{Off}$
1985	240	11,424	11,414.392	0.09	1.0008
1986	254	14,763	14,775.496	-0.10	0.9992
1987	254	8,131	8,000.335	1.46	1.0163
1988	179	7,691	7,639.488	0.59	1.0067
1989	205	9,957	9,894.334	0.63	1.0063
1990	212	10,647	10,758.552	-1.08	0.9896
1991	200	10,860	10,841.810	0.17	1.0017
1992	305	16,992	17,120.827	-0.98	0.9925
1985-1989	1132	51,966	51,724.045	1.06	1.0047
1990-1992	717	38,499	38,721.188	-1.13	0.9943
1985-1992	1849	90,465	90,445.233	0.07	1.0002

Daily	Excesses	Exceeding	3.0σ
Date	On	Off	$\frac{On}{Off}$
18.08.86	68	45.382	3.36
14.04.87	12	5.090	3.06
07.07.87	53	32.617	3.57

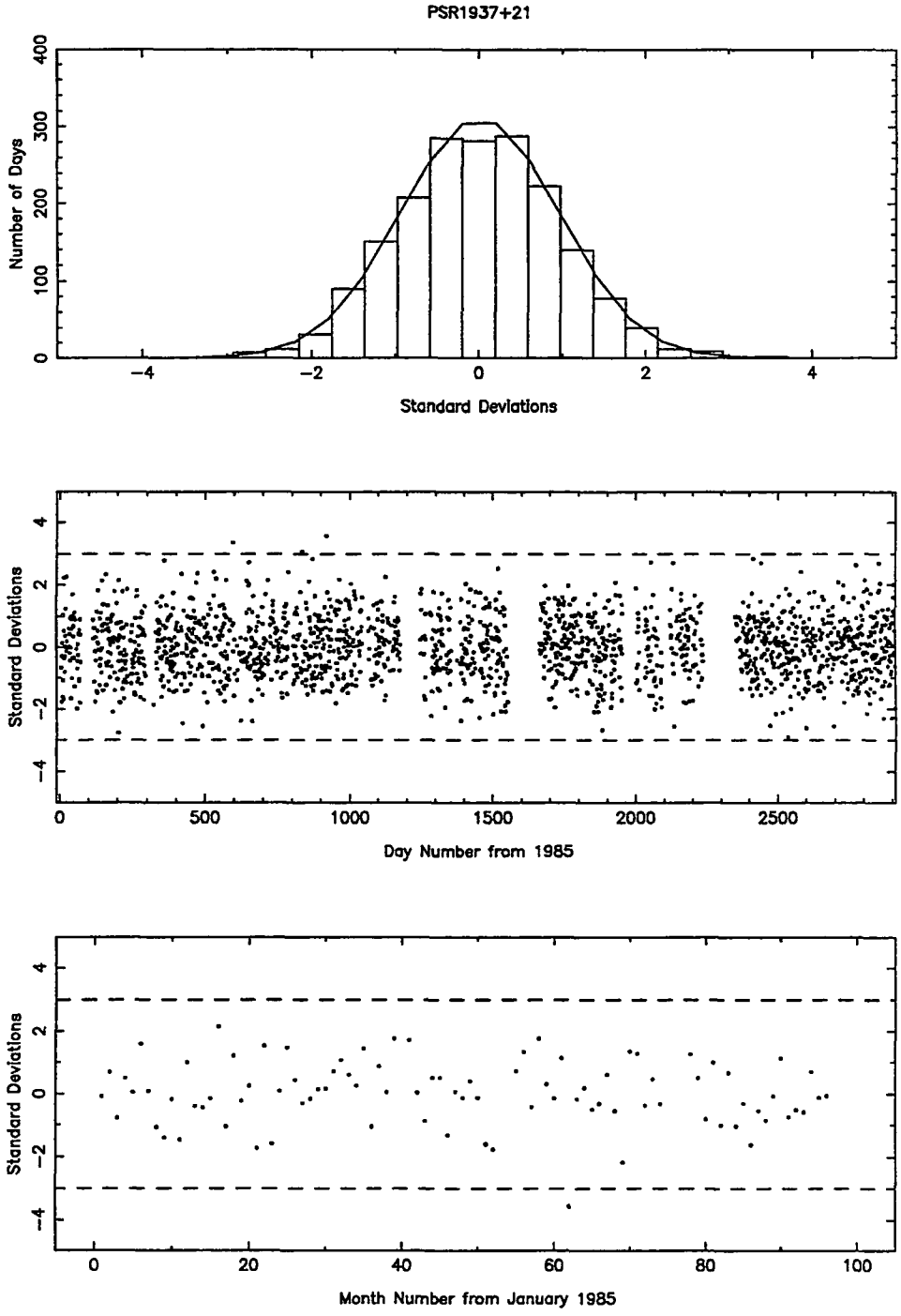

Figure 2.12 Distribution of daily excesses for PSR 1937+21. The top graph shows the distribution binned in 0.4 σ bins and compared to a normalised Gaussian centred on zero. The middle graph shows the daily excesses as a function of time and the bottom graph shows the monthly excesses.

Table 2.13 Observations of PSR 1953+29 1985 - 1992.

Year	Days Observed	On	Off	$\frac{(On-Off)}{\sqrt{Off}}$	$\frac{On}{Off}$
1985	243	17,485	17,430.020	0.42	1.0032
1986	257	23,219	22,962.455	1.69	1.0112
1987	254	12,454	12,362.781	0.82	1.0074
1988	179	11,549	11,491.010	0.54	1.0050
1989	204	15,249	15,150.182	0.80	1.0065
1990	216	16,477	16,485.970	-0.07	0.9995
1991	200	15,770	15,737.339	0.26	1.0021
1992	308	24,672	24,900.623	-1.45	0.9908
1985-1989	1137	79,956	79,396.447	1.99	1.0070
1990-1992	724	56,919	57,123.932	-0.86	0.9964
1985-1992	1861	136,875	136,520.379	0.96	1.0026

Daily	Excesses	Exceeding	3.0σ
Date	On	Off	$\frac{On}{Off}$
12.02.85	108	79.884	3.15
03.04.86	108	76.156	3.65
26.02.87	125	95.614	3.01
07.06.88	8	2.879	3.02
27.03.90	97	71.595	3.00
22.10.90	51	32.211	3.31
21.12.90	4	0.929	3.19

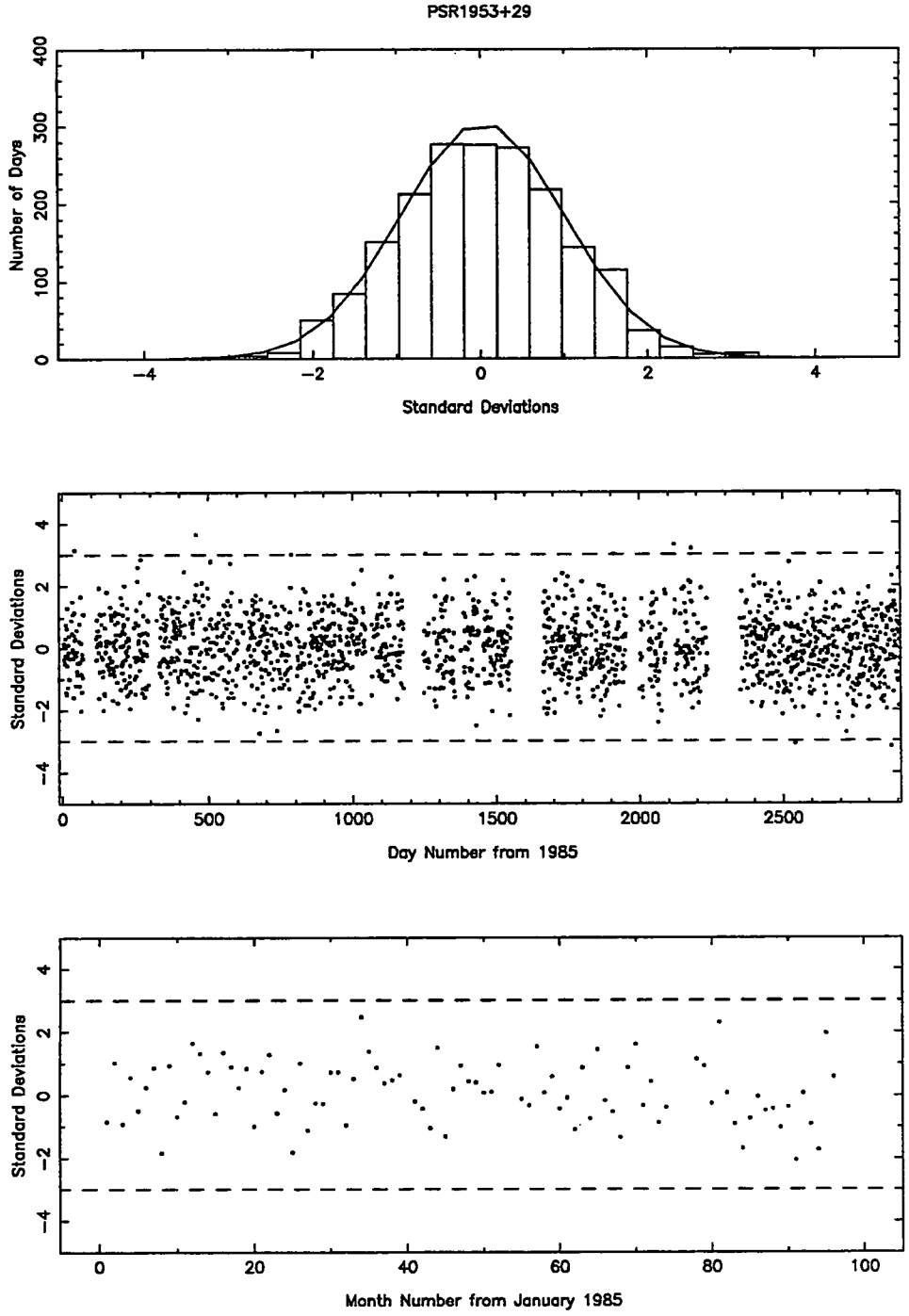

Figure 2.13 Distribution of daily excesses for PSR 1953+29. The top graph shows the distribution binned in 0.4 σ bins and compared to a normalised Gaussian centred on zero. The middle graph shows the daily excesses as a function of time and the bottom graph shows the monthly excesses.

Table 2.14 Observations of PSR2217+47 1985 - 1992.

Year	Days Observed	On	Off	$\frac{(On-Off)}{\sqrt{Off}}$	$\frac{On}{Off}$
1985	242	24,715	24,610.428	0.67	1.0042
1986	261	33,265	33,131.565	0.73	1.0040
1987	260	18,698	18,725.332	-0.20	0.9985
1988	180	16,649	16,901.186	-1.94	0.9851
1989	208	23,159	23,237.309	-0.51	0.9966
1990	214	25,056	24,871.898	1.17	1.0074
1991	198	22,571	22,403.959	1.12	1.0075
1992	308	36,430	36,355.206	0.39	1.0021
1985-1989	1,151	116,486	116,605.820	-0.35	0.9990
1990-1992	720	84,057	83,631.063	1.47	1.0051
1985-1992	1,871	200,543	200,236.884	0.68	1.0015

Daily	Excesses	Exceeding	3.0σ
Date	On	Off	$\frac{On}{Off}$
08.08.89	158	121.928	3.27
28.04.92	148	112.079	3.39

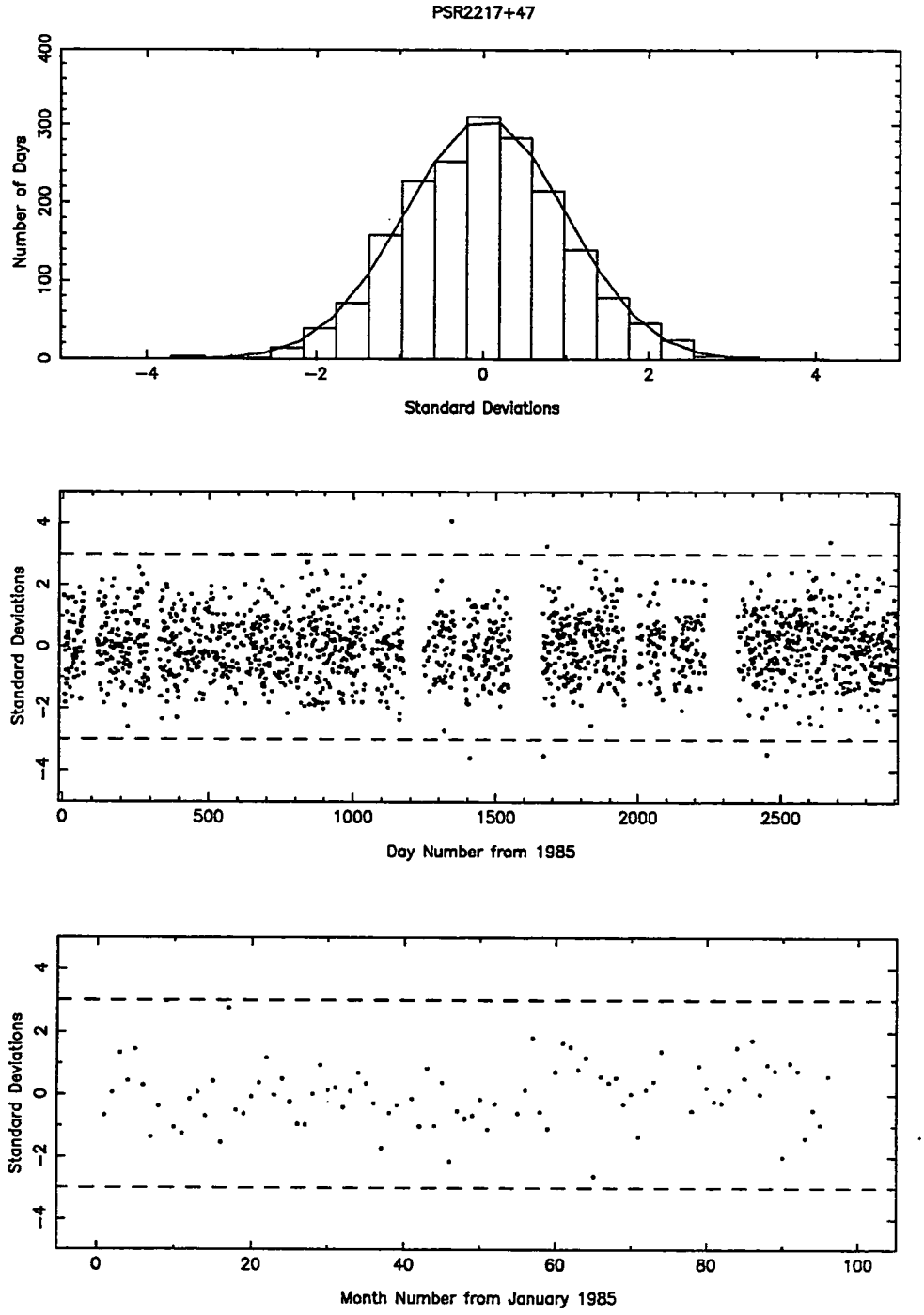

Figure 2.14 Distribution of daily excesses for PSR2217+47. The top graph shows the distribution binned in 0.4 σ bins and compared to a normalised Gaussian centred on zero. The middle graph shows the daily excesses as a function of time and the bottom graph shows the monthly excesses.

Table 2.15 Observations of Markarian 421 1985 - 1992.

Year	Days Observed	On	Off	$\frac{(On-Off)}{\sqrt{Off}}$	$\frac{On}{Off}$
1985	244	23,246	23,051.812	1.28	1.0084
1986	257	29,920	29,904.105	0.09	1.0005
1987	256	17,207	17,075.398	1.01	1.0077
1988	175	15,620	15,655.324	-0.28	0.9977
1989	203	21,151	21,319.699	-1.16	0.9921
1990	211	21,924	21,995.431	-0.48	0.9968
1991	199	21,028	20,969.837	0.40	1.0028
1992	307	32,515	32,357.185	0.88	1.0049
1985-1989	1,135	107,144	107,006.338	0.42	1.0013
1990-1992	717	75,467	75,322.452	0.53	1.0019
1985-1992	1,852	182,611	182,328.789	0.66	1.0015

Daily	Excesses	Exceeding	3.0σ
Date	On	Off	$\frac{On}{Off}$
09.03.92	63	42.552	3.13

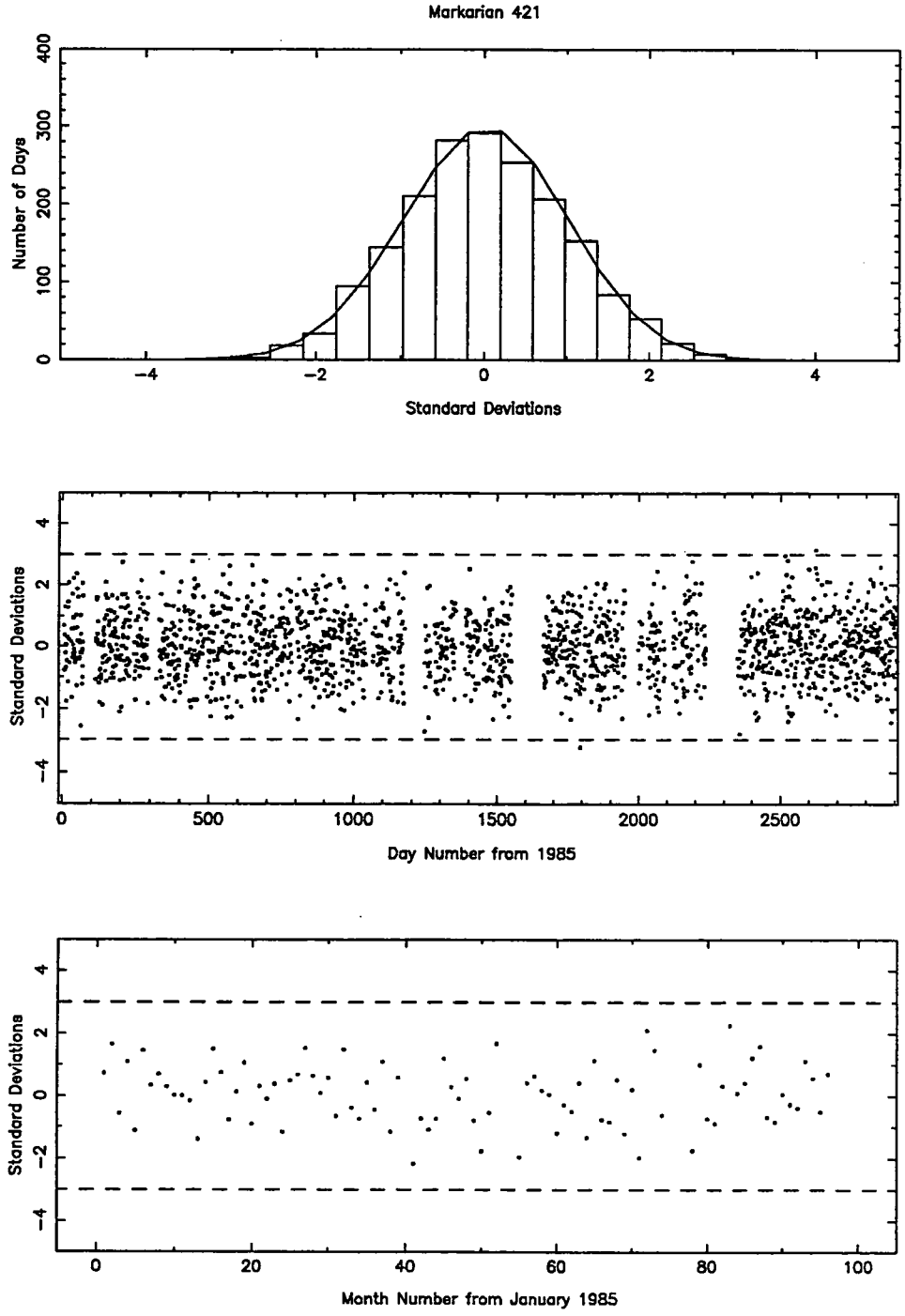

Figure 2.15 Distribution of daily excesses for Markarian 421. The top graph shows the distribution binned in 0.4 σ bins and compared to a normalised Gaussian centred on zero. The middle graph shows the daily excesses as a function of time and the bottom graph shows the monthly excesses.

Table 2.16 Observations of M31 1985 - 1992.

Year	Days Observed	On	Off	$\frac{(On-Off)}{\sqrt{Off}}$	$\frac{On}{Off}$
1985	244	23,946	23,922.762	0.15	1.0010
1986	259	32,005	32,300.612	-1.64	0.9908
1987	258	17,918	17,974.021	-0.42	0.9969
1988	176	15,509	15,457.863	0.41	1.0033
1989	208	22,115	22,372.298	-1.72	0.9885
1990	213	23,326	23,236.180	0.59	1.0039
1991	199	21,088	21,221.636	-0.92	0.9937
1992	310	34,251	34,423.262	-0.93	0.9950
1985-1989	1,145	111,493	112,027.555	-1.60	0.9952
1990-1992	722	78,665	78,881.078	-0.77	0.9973
1985-1992	1,867	190,158	190,908.634	-1.72	0.9961

Daily	Excesses	Exceeding	3.0σ
Date	On	Off	$\frac{On}{Off}$
01.06.85	146	110.327	3.40
04.12.90	64	43.985	3.02
01.12.92	156	121.850	3.09

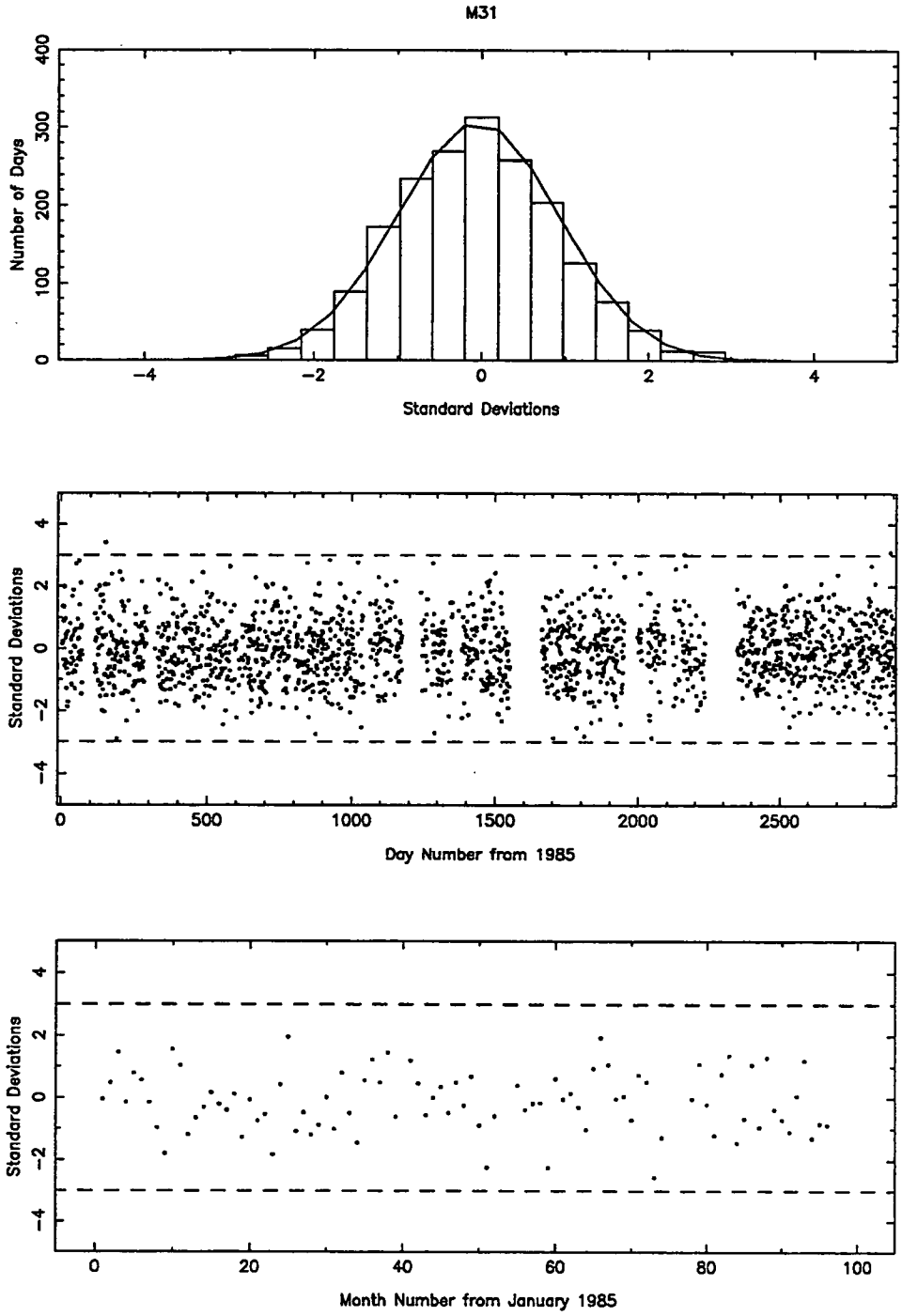

Figure 2.16 Distribution of daily excesses for M31. The top graph shows the distribution binned in 0.4 σ bins and compared to a normalised Gaussian centred on zero. The middle graph shows the daily excesses as a function of time and the bottom graph shows the monthly excesses.

Table 2.17 Observations of GRO J0422+32 1985 - 1992.

Year	Days Observed	On	Off	$\frac{(On-Off)}{\sqrt{Off}}$	$\frac{On}{Off}$
1985	244	20,268	20,316.636	-0.34	0.9976
1986	255	26,387	26,204.355	1.13	1.0070
1987	256	14,704	14,757.144	-0.44	0.9964
1988	177	12,797	12,722.514	0.66	1.0059
1989	209	18,977	18,977.037	-0.00	1.0000
1990	209	18,900	18,980.037	-0.58	0.9958
1991	199	17,865	18,155.914	-2.16	0.9840
1992	308	29,056	29,043.457	0.07	1.0004
1985-1989	1,141	93,133	92,977.686	0.51	1.0017
1990-1992	716	65,821	66,179.409	-1.39	0.9946
1985-1992	1,857	158,954	159,157.095	-0.51	0.9987

Daily	Excesses	Exceeding	3.0σ
Date	On	Off	$\frac{On}{Off}$
30.07.92	149	115.338	3.13

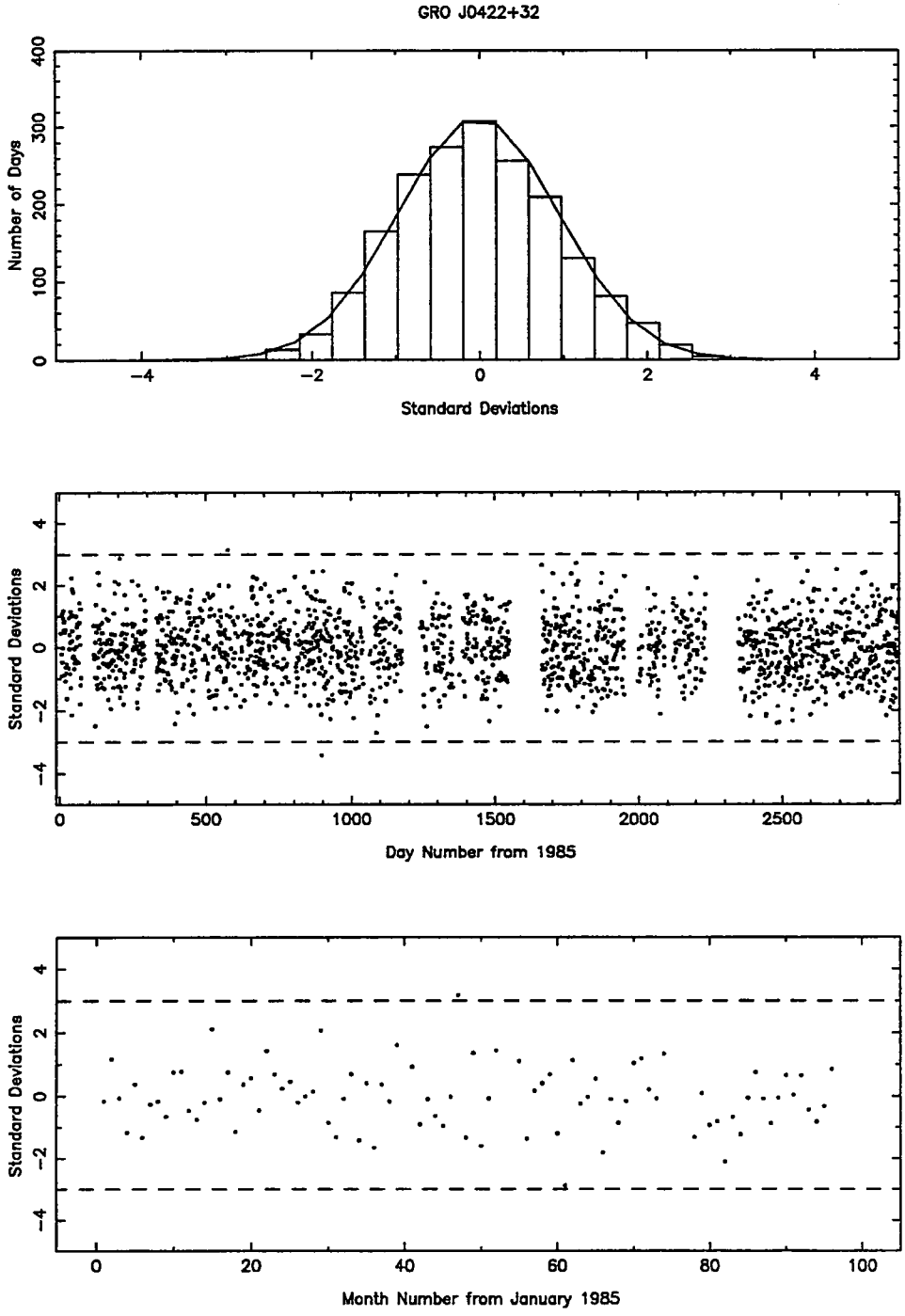

Figure 2.1 Distribution of daily excesses for GRO J0422+32. The top graph shows the distribution binned in 0.4 σ bins and compared to a normalised Gaussian centred on zero. The middle graph shows the daily excesses as a function of time and the bottom graph shows the monthly excesses.

Table 2.1 Observations of GRO J1837+59 1985 - 1992.

Year	Days Observed	On	Off	$\frac{(On-Off)}{\sqrt{Off}}$	$\frac{On}{Off}$
1985	244	21,849	21,750.171	0.67	1.0045
1986	259	28,184	28,257.780	-0.44	0.9974
1987	257	15,635	15,539.751	0.76	1.0061
1988	186	14,767	14,739.603	0.23	1.0019
1989	208	19,057	19,249.848	-1.39	0.9900
1990	217	20,250	20,172.256	0.55	1.0039
1991	202	19,749	19,938.557	-1.34	0.9905
1992	309	30,263	30,374.046	-0.64	0.9963
1985-1989	1,154	99,492	99,537.153	-0.14	0.9995
1990-1992	728	70,262	70,484.859	-0.84	0.9968
1985-1992	1,882	169,754	170,022.012	-0.65	0.9984

Daily	Excesses	Exceeding	3.0σ
Date	On	Off	$\frac{On}{Off}$
11.10.85	106	78.653	3.08
04.01.92	21	10.759	3.12

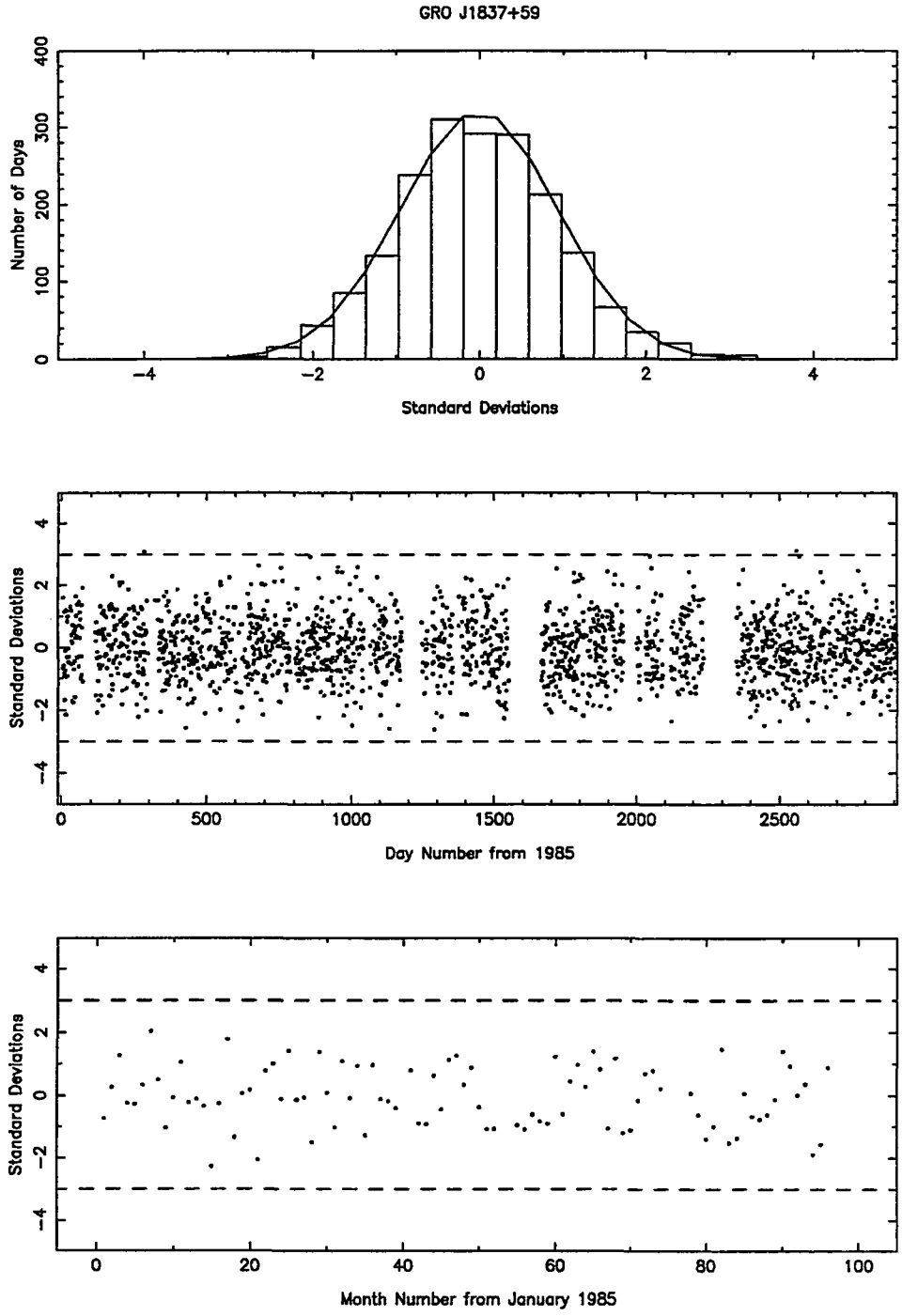

Figure 2.2 Distribution of daily excesses for GRO J1837+59. The top graph shows the distribution binned in 0.4 σ bins and compared to a normalised Gaussian centred on zero. The middle graph shows the daily excesses as a function of time and the bottom graph shows the monthly excesses.